



SAPIENZA
UNIVERSITÀ DI ROMA

Facoltà di Scienze Matematiche, Fisiche e Naturali
Dipartimento di Biologia e Biotecnologie “C. Darwin”

Dottorato in Biologia Ambientale ed Evoluzionistica
Curriculum Biologia Animale (XXXIV Ciclo)

Macroevolutionary trends and ecological correlates in the craniomandibular complex of carnivorans

Dottorando

Davide Tamagnini
Matricola: 1841930

Tutor

Prof. Luigi Maiorano

Anno Accademico 2021/2022

Preface

I owe my family and friends a huge thank you for all the support received throughout these years. I am also grateful to any colleague, researcher, and supervisor who helped me with my research project. I sincerely hope that this work might represent a promising starting point for further multidisciplinary and wide-ranging studies in macroevolution, hopefully involving people from all over the world.

The theory of evolution is quite rightly called the greatest unifying theory in biology.

— Ernst Mayr

Index

Preface	2
Extended abstract	4
Introduction	10
Section 1	13
• Chapter 1 - New avenues for old travellers: phenotypic evolutionary trends meet morphodynamics, and both enter the global change biology era	15
Section 2	31
• Chapter 2 - A new, fast method to search for morphological convergence with shape data	33
• Chapter 3 - A method for mapping morphological convergence on three-dimensional digital models: the case of the mammalian sabre-tooth	54
• Chapter 4 - Ancestral state estimation with phylogenetic ridge regression	67
Section 3	81
• Chapter 5 - Testing the occurrence of convergence in the craniomandibular shape evolution of living carnivorans	83
• Chapter 6 - Macroevolutionary ecomorphology of the Carnivora skull: adaptations and constraints in the extant species	99
• Chapter 7 - Purrs, roars, and claws: Do conical and sabertoothed cats represent an exception to craniofacial evolutionary allometry?	115
Conclusions	166
References	168
Appendix 1	173
Appendix 2	176

Extended abstract

Chapter 1

Evolutionary trends (ETs) are traditionally defined as persistent and directional changes in the state of one or more quantitative traits, resulting in substantial changes through time and representing the primary phenomenon characterising evolution at high taxonomic levels and over long-time scales. The first groundbreaking investigations concerning phenotypic directional evolution led to the description of iconic and pervasive trends throughout the history of a single clade, frequently relying on the evidence available from fossil record (e.g., increasing hypsodonty and gradual acquisition of the monodactyl posture in equids caused by the spread of grasslands). Then, the formulation of the so-called ‘biological rules’ extended the definition of ETs to include directional responses to ecological, climatic or biological gradients, with several clades being simultaneously analysed obtaining the same evolutionary pattern (e.g., latitudinal or elevation gradients, like in Allen’s or Bergmann’s rules). ETs constitute an ideal case study to describe and separate *tempo* and *mode* in evolution, and their mutually independent variations. The strength of an ET can be quantified as the magnitude of a vector, providing a practical way of representing the speed (or *tempo*) of evolution. The direction of the same vector represents the *mode* of evolution (i.e., observed pattern of variation). Phenotypic ETs were frequently found as the resulting evolutionary outcome in studies about the controversial field of evolutionary predictability, that focuses on the occurrence of repetitive and foreseeable patterns in evolution under specific conditions (e.g., recurrent patterns in insular systems). Although the search for new ETs and the validation of the existing ones remain central topics in evolutionary biology, the formulation of a well-supported and operative definition of ET remains an unsolved issue. After introducing a new operative definition of ETs, the main goal of this Chapter was to propose a modern theoretical framework for the study of phenotypic ETs, based on Seilacher’s theory of morphodynamics, that explored the interactions between ETs and the main evolutionary factors involved in their occurrence (i.e., phylogenetic history, developmental constraints, environment, and biological function).

The proposed operative definition of ET was a macroevolutionary transposition of the concept of ‘(non) parallel evolution’ (i.e., continuum from convergent through parallel to divergent evolution) that was originally suggested in order to describe the independent evolution of replicate populations, in reference to bacterial cultures of laboratory experiments. Four possible classes of ETs (i.e., simple trend, parallel evolution, convergence, and divergent evolution) are conceivable from this perspective. The criterion of distinction between them relies on the orientation of the evolutionary trajectories in the multivariate trait space shown by the single clades. Therefore, parallelism is the resulting outcome when evolutionary trajectories point in the same direction, otherwise, a condition of convergence or divergent evolution occurs, depending on whether trajectories respectively point ‘at’ or ‘away from’ a region of the trait space. According to our definition of ETs, parallel evolution, convergence, and divergent evolution can be considered as patterns produced whenever, analysing multiple clades at the same time, a portion of the

groups undergoes an episode of directional evolution, whereas other groups are subject to a different evolutionary regime.

Research on ETs would take a major step forward if a pattern-based approach, like the one described above (that can only validate or disprove the presence of a pattern), was systematically accompanied by multifactorial analyses. These analyses would also allow researchers to take into account data relative to underpinning dynamics leading to the occurrence of directional evolution (e.g., ecological variables or life-history traits). When it comes to evolutionary dynamics occurring in phenotypic evolution, the tangled nature of interactions between the factors underpinning morphological evolution has already been explored by the theory of morphodynamics, concluding that four components have a predominant role: phylogenetic history, evo-devo constraints, environment, and biological function. As anticipated above, in this Chapter we explored the interactions between phenotypic ETs and these evolutionary factors (starting with evo-devo constraints and environment, then shifting onto phylogeny and finally focusing on biological function in the light of new perspectives in morphological quantification), also mentioning applications or methodological approaches that can be used in these contexts. For instance, when it comes to ecomorphological studies on ETs, we suggested that the inclusion of spatially structured variation in evolutionary models (i.e., Wrightian view of evolution) would allow considering metapopulations composed by interacting demes characterised by different trait values: this would enable the distinction between patterns produced by spatial processes, like drift and habitat-specific selection, and ETs associated with non-neutral and directional evolutionary regimes. We also discussed how assemblage-based studies on ETs struggle to describe evolutionary dynamism over large spatial and/or temporal scales (e.g., inconsistent presence of Bergmann's rule in different assemblages of the mammalian order Carnivora), suggesting to always adopt a phylogenetically-informed approach for the study of macroevolutionary patterns and processes, specifically relying on phylogenetic comparative methods (i.e., statistical models that estimate the evolutionary regime that best approximates the tempo and mode of evolution acting on the considered traits, allowing researchers to correct for biases due to the non-independence of sampled observations in macroevolutionary samples). Finally, we described an intriguing new frontier of macroevolution that is represented by the possibility to perform research on ETs in the presence of extreme environmental shifts, like those resulting from the current phase of climate change, allowing biologists to refine predictions of future or hypothetical evolutionary outcomes and potentially leading to indirect implications in climate change and conservation biology.

Chapter 2

Currently available methods to explore evolutionary convergence either rely on the analysis of the phenotypic resemblance between sister clades as compared to their ancestor, fit different evolutionary regimes to different parts of the tree to see whether the same regime explains phenotypic evolution in phylogenetically distant clades or assess deviations from the congruence between phylogenetic and phenotypic distances. The new R function *search.conv* allows researchers to test for the occurrence of

morphological convergence in multivariate shape data working with either ultrametric or non-ultrametric phylogenies. It relies on θ , that is the average angle between the phenotypic vectors of putatively convergent species in the multivariate shape space (i.e., a measure of the resemblance between the phenotypes), whose cosine represents the correlation coefficient between these vectors. The simulations performed on this R function correctly identified convergent morphological evolution in 95% of the cases and type I error rate was inferior to 6%. Among the considered real case-studies, convergence tests performed on mandibular shape data of fossil and living felids and barbourofelids using the R function *search.conv* confirmed that “true” sabertooths (i.e., Homotheriini and Smilodontini) independently converged on barbourofelids in their mandible morphology, whereas Metailurini (i.e., “false” sabertooths) were not found to converge on barbourofelids, as expected.

Chapter 3

The graphical representation of evolutionary trends might be a crucial tool for improving their description and comparing the outcomes of different studies in this evolutionary field. The new R function *conv.map* allows researchers to visualise the regions of 3D model that underwent convergent evolution and assesses convergence by testing whether phenotypes in distant clades in a phylogenetic tree are more similar to each other than expected from their phylogenetic distance (i.e., adopting a method similar the one used in the R function *search.conv*). Cranial 3D models belonging to different metatherian and placental clades including sabertoothed species (e.g., felids, barbourofelids, dasyuromorphians) were compared using the R function *conv.map* in order to validate the presence of convergent evolution and graphically visualise the convergent morphological regions of their crania. Our results revealed a range of shared anatomical features in the premaxillary area, the carnassial region, and in the occipital region around the nuchal crest, which were common to all sabertooth carnivores despite considerable phylogenetic distances. This strongly suggests that, despite some anatomical differences and possible functional diversification within sabertooths, their morphotype universally confers a broadly comparable capacity to hunt and rapidly kill relatively large prey by applying a stabbing bite to the throat assisted by powerful neck muscles, although this specialization may have led to their extinction at different times and locations when large prey became less abundant.

Chapter 4

The reconstruction of ancestral states is a fundamental step for macroevolutionary analyses and it is a required step for applying phylogenetic comparative methods. The inclusion of fossil phenotypes as ancestral character values at nodes in phylogenetic trees is known to increase both the power and reliability of phylogenetic comparative methods applications. A new implementation of the R function *RRphylo* (named *RRphylonoder*), that is based on phylogenetic ridge regression, enabled the possibility to integrate fossil phenotypic information as ancestral character values in morphological analyses. Results from simulated data proved *RRphylo-noder* to be slightly more accurate and sensibly faster than Bayesian approaches, and the least sensitive to the kind of phenotypic pattern simulated. Furthermore, the use of fossil phenotypes as

ancestral character values noticeably increased the probability to find a phenotypic trend through time when it applies to either the entire tree or just to specific clades within it. Then, *RRphylo-noder* was used on real case-studies, including the evolution of body size (i.e., validation of the evolutionary trend known as Cope's rule) in caniform carnivores. By regressing *RRphylo-noder* ancestral estimates against their age our results found moderate evidence in favour of Cope's rule in caniforms. Although this result is not a robust indication of Cope's rule *per se*, it is interesting that the pattern appears even at the level of ancestors with *RRphylo-noder*.

Chapter 5

Analyses performed in order to test for the presence of convergent evolution in the crania and mandibles of living carnivorans pointed out that this phenomenon appears to be rare within this clade. In particular, almost none of the tested dietary categories reached statistical significance, indicating that the mere influence of diet is unlikely to produce convergent patterns in the cranio-mandibular shape evolution of carnivorans. By contrast, a limited number of cases concerning either ecologically equivalent species or ecologically similar species of different body sizes (i.e., red fox vs Malayan civet, giant panda vs red panda, and raccoon dog vs raccoon) were found to have convergent cranio-mandibular shapes, potentially suggesting the occurrence of a complex interplay of one-to-many, many-to-one, and many-to-many relationships taking place between ecology, biomechanics, and morphology. The analytical framework relying on multiple convergence metrics with different biological meaning (i.e., C1, θ , and Wheatsheaf index) also allowed to discriminate between episodes of convergence and cases of evolutionary conservatism (i.e., closely related species more similar than would be expected based on their phylogenetic relationships). In particular, our results supported the presence of conservatism within omnivore carnivorans. This pattern derives, in all probability, from the existence of an omnivore adaptive zone in the craniomandibular shape evolution of living carnivorans, with other specialized species emerging from this region of the multivariate shape space.

Chapter 6

Ecomorphological analyses were performed on 2D cranio-mandibular size and shape data of living carnivorans in order to clarify the impact of multiple ecological factors (e.g., diet, aquatic vs terrestrial habitat) on morphological evolution within this clade. To do so, complex simulations were implemented in order to estimate the evolutionary scenario that best reflects the evolutionary history of the carnivoran cranio-mandibular complex, and to assess potential biases resulting from the estimation of the best model of evolution. Our simulations confirmed the need to exercise caution in the estimation of the best evolutionary model for highly dimensional shape data (i.e., few species and many variables) since in these cases the adopted model selection criteria might erroneously prefer the most complex models. Our results clearly highlighted that the invasion of aquatic niches produced a trend towards larger cranial dimensions, with pinnipeds being consistently larger than terrestrial carnivorans due to thermoregulation, basal metabolic costs, and food intake functions imposed by the aquatic environment. When dietary categories were

concerned, highly demanding feeding imposed by the consumption of molluscs resulted in exceptionally high disparity and evolutionary rate for both cranial and mandibular shape, whereas the other aquatic diets equally showed higher levels of disparities, but relatively slower evolutionary rates.

Chapter 7

CRaniofacial Evolutionary Allometry (CREA) is a recently formulated evolutionary trend proposing that, among closely related species, the smaller sized of the group would appear paedomorphic with proportionally smaller rostra and larger braincases. Analyses performed on living and fossil felids and relying on 3D geometric morphometrics, together with phylogenetic comparative methods, pointed out that sabertoothed cats (i.e., Machairodontinae) and big conical-toothed cats (i.e., Pantherinae) represent exceptions to this biological rule since they show a decoupling of the allometry-driven pattern of morphological integration between the rostrum and braincase typical of CREA. By contrast, allometric tests performed within either small conical-toothed cats (i.e., Felinae) or the whole family Felidae reached statistical significance, clearly indicating the occurrence of CREA within these groups. Overall, the adoption of different landmark configurations, phylogenetic hypotheses, and corrections for phylogenetic effect had a limited impact on CREA pattern recognition within felids. These findings disprove the hypothesis that the cranial shape evolution of sabertoothed cats results from a mere case of cooptation and extension of the allometric trend observed in conical-toothed cats. More importantly, these results also suggest that the acquisition of extreme features concerning evo-devo constraints, biomechanics, and/or ecology (e.g., adapting biomechanically demanding structures such as sabertoothed upper canines, occupying extremely narrow and specialised ecological niches) is likely to represent a preferential way to escape from common evolutionary patterns of morphological variation such as CREA, but this is likely to be frequently achieved at the cost of higher extinction rates as also suggested by the absence of CREA in many extinct lineages of non-mammalian synapsids.

Conclusions

The present Thesis confirms that carnivorans represent an ideal case study for analyses concerning morphological directional evolution and phenotypic evolutionary trends in general. The inclusion of fossil morphologies constitutes one of the most valuable addition to many of the analytical frameworks adopted in the previous Chapters and strongly impacts the results concerning the presence and strength of evolutionary trends in morphological data. Similarly, the high taxonomic coverage that characterise many of the morphological samples used in the present Thesis is likely to have greatly improved the ability to validate/confute the occurrence of evolutionary trends within the considered samples. Future advances in research on phenotypic evolutionary trends, and macroevolutionary pattern in general, are expected from the implementation of a complex ecological modelling in the study of morphological evolution. Linking these biological fields is also suggested to potentially provide useful information for investigations on conservation prioritization, phenotypic diversity, and predictability of evolution in the near future. Similarly, combining

modern techniques of morphological quantification (e.g., geometric morphometrics and finite element analysis) with advanced methods in ecological niche evaluation (e.g., species distribution modelling) is supposed to be a promising way to bring deep insights in the understanding of ecomorphological pattern and processes. Hopefully, the operative definition of evolutionary trend provided in Chapter 1 and the analytical approaches adopted throughout the present Thesis will represent a good starting point for future pattern-based studies on carnivoran evolution, and macroevolution in general, enabling in such a fascinating topic of evolutionary biology, figuratively speaking, “new avenues for old travellers”.

Introduction

Evolutionary trends (i.e., persistent and directional changes in the state of one or more quantitative traits, resulting in substantial changes through time) are a fascinating and highly controversial topic in evolutionary biology. In fact, they were reported as one of the most important concepts in the study of evolution by many authors in the past decades (e.g., McKinney 1990; Alroy 2000), but at the same time aberrant (and now completely confuted) evolutionary theories heavily relied in the past on evidences concerning the presence of directional patterns in evolution (e.g., considerations made in support of orthogenesis deriving from the description of increasing complexity of horns in brontotheres – Osborn 1929; Muhlbachler 2008). Despite evolutionary trends had a central role in many groundbreaking works in evolutionary biology (e.g., formulation of the so-called biological rules, like Bergmann's or Allen's rules - Allen 1877; Bergmann 1847), the lack of a broadly accepted operative definition of this phenomenon prevented evolutionary biologists from unanimously pinpointing the requirements needed for its detection and validation and limited research performed on evolutionary trends in the last few years (Stayton 2015 a, b). The present Thesis aims to restore centrality to this evolutionary phenomenon by introducing a new operative definition of “evolutionary trend” and by testing for the presence of different morphological trends in the craniomandibular evolution of the order Carnivora, even investigating, whenever possible, the ecological influences on the resulting outcomes.

In the present Thesis, morphological evolution is investigated by means of modern techniques of morphological quantification that are commonly known as geometric morphometrics (Adams et al. 2004, 2013). These methods have their roots into the pioneering work of (D'Arcy) Thompson (i.e., Cartesian grids used in his “theory of transformations” to formulate hypotheses concerning the phenotypic evolution of organisms - Thompson 1917; Arthur 2006) and rely on the use of landmarks (i.e., anatomically corresponding points that are digitised on every specimen included in the morphological sample) in order to extract morphological data and obtain size and shape variables. Geometric morphometrics is particularly indicated for pattern-based analyses as those included in the present Thesis and can be easily combined with phylogenetic comparative methods (i.e., statistical models that estimate the evolutionary regime that best approximates the tempo and mode of evolution acting on the considered traits, allowing researchers to correct for biases due to the non-independence of sampled observations in macroevolutionary samples) in order to detect episodes of directional evolution in the morphological evolution of a clade.

Ecomorphological studies typically aims to estimate the impact of qualitative ecological variables on morphology (e.g., dietary categories; types of locomotion - Meloro et al. 2015; Dumont et al. 2016; Michaud et al. 2018). In other cases, researchers try to make ecological inferences by comparing the morphologies of enigmatic fossil species with those of living species whose ecology is known (e.g., approaches that rely on the spatial distribution of observations in the trait space; discriminant function analysis - Figueirido and Soibelzon 2010; van Heteren et al. 2016). Although new methods of morphological quantification (e.g., geometric morphometrics) paved the way to new multidisciplinary analyses in many fields of evolutionary

biology (e.g., evo-devo research concerning phenotypic integration and modularity – Klingenberg 2013; Adams 2016), a proper integration between recently developed techniques in ecological and morphological fields is still lacking in modern ecomorphology. In this sense, morphofunctional analyses represent a reference point since several state-of-art approaches have already been proposed in order to combine data describing morphological traits with evidence deriving from biomechanics (e.g., combination of geometric morphometrics with finite element analysis - O'Higgins et al. 2011; Polly et al. 2016). The present Thesis aims to apply modern ecomorphological methods in order to validate/dispute hypotheses concerning morphological evolutionary trends within carnivorans, potentially paving the way for further improvements in the study of directional evolution in the eco-evolutionary field in the near future.

The craniomandibular complex is a multifunctional biological structure frequently investigated in ecomorphological studies in order to estimate the impact of a multitude of ecological and environmental variables on vertebrate morphological evolution (e.g., resource use patterns, data from stable isotope analyses, evidences concerning diet or locomotion – Moss and Young 1960; Terhune et al. 2015; Evans et al. 2019; Watanabe et al. 2019; Chemisquy et al. 2020). In particular, the mandible is mainly used as a case study in research concerning the role of food capturing and processing, or biomechanical constraints linked with diet in general, on size and shape evolution (e.g., Meloro and O'Higgins 2011; Serrano-Fochs et al. 2015; Marcé-Nogué et al. 2017). By contrast, the cranium is a more functionally complex structure, that is involved in feeding and agonistic behavior, brain protection, and sensory perception: for this reason, several cranial studies have already been performed to test for the influence of these factors on its morphology and for potential interactions with environmental variations (e.g., Hipsley and Müller 2017; Tseng and Flynn 2018; Watanabe et al. 2019). Thus, cranium and mandible represent two functionally and anatomically integrated, yet distinct, structures that respond differently to evolutionary pressures, with the cranium being potentially subject to a higher number of structural and functional constraints than the mandible. This makes, as anticipated above, the craniomandibular complex an ideal case study for ecomorphological analyses as those included in the present Thesis.

The order Carnivora represents a suitable clade for ecomorphological research thanks to the great amount of phenotypic variability and flexibility of ecological adaptations shown by its members, paired with a high variability of evolutionary conditions among the families of this group (Ewer 1973; Gittleman 1986). This produces peculiar scenarios that constitute extremely informative ecomorphological case studies. For example, the order Carnivora includes taxa characterised by narrow ecological niches (e.g., felids and pinnipeds) that forced some of their members to evolve peculiar cranial adaptations (e.g., sabertoothed canines and homodont dentition, respectively - Piras et al. 2018; Berta et al. 2018). By contrast, other families stand out for the variety of diets of their members (e.g., ursids), which, for instance, include bamboo-feeders (e.g., giant pandas), hypercarnivores (e.g., polar bears), and generalist species (e.g., brown bears and the extinct short-faced bears - Figueirido et al. 2009). Furthermore, living and fossil carnivorans include families currently characterised by reduced morphological disparity and species diversity that experienced major radiations of different morphotypes throughout their evolutionary history (e.g., hyaenids -

Stynder et al. 2012). The present Thesis aims to investigate the presence of directional evolution within carnivorans, following a long tradition of research on morphological evolutionary trends performed on living and extant carnivorans in the previous decades (e.g., studies concerning Bergmann's rule, Cope's rule, and convergent evolution – Radinsky 1981a, b, 1982; Finarelli and Flynn 2006; Diniz-Filho et al. 2007, 2009; Figueirido et al. 2010, 2013; Meloro et al. 2015).

Therefore, as anticipated above, the present Thesis is focused on the detection of morphological evolutionary trends in living and fossil carnivorans (using the craniomandibular complex as an ideal case study) and particularly on the following topics:

- Chapter 1: A new operative definition of (phenotypic) evolutionary trend in order to clarify the steps required to validate their presence in morphological evolution and a new theoretical framework, based on Seilacher's theory of morphodynamics, in order to allow researchers to study the interactions between evolutionary trends and the evolutionary dynamics underpinning their occurrence, even testing hypotheses concerning the predictability of evolution.
- Chapter 2: A new pattern-based metric for testing the presence and strength of convergent evolution in morphological data and the use of this tool on real case studies like the mandibular shape evolution of felids and barbourofelids.
- Chapter 3: A new R function to visualise the regions of a 3D structure (i.e., cranium) that underwent convergent evolution and the use of this tool on cranial similarities in sabertoothed clades of carnivorans and metatherian mammals.
- Chapter 4: A new technique for the reconstruction of ancestral states in morphological data, which allows users to integrate fossil phenotypic information as ancestral character values and the use of this method on real case studies like size evolution in caniforms in order to validate/confute the occurrence of Cope's rule within this clade.
- Chapter 5: The assessment of the occurrence of convergent evolution in the craniomandibular shape evolution of living carnivorans by considering multiple dietary categories or textbook examples taken from the literature and by adopting three different pattern-based convergence metrics.
- Chapter 6: The measurement of the impact of different ecological factors (e.g., diet, aquatic vs terrestrial habitat) on the craniomandibular shape evolution of living carnivorans in order to detect patterns of covariation and directional responses.
- Chapter 7: The validation of the occurrence of a recently proposed evolutionary trend, known as craniofacial evolutionary allometry, in living and fossil felids (i.e., conical and sabertoothed cats).

Section 1

The Chapter included in this Section (Chapter 1) illustrates the common thread underpinning the present Thesis by providing an operative definition of phenotypic evolutionary trends in macroevolution and debating the interactions between evolutionary trends and the main factors that influence their occurrence and strength (i.e., evo-devo constraints, environment, biological function, and phylogeny). In particular, the impact of ecological factors on morphological trends (e.g., convergence, directional evolution, craniofacial evolutionary allometry) within carnivorans will be the central topic of many Chapters included in the next Sections. Chapter 1 also describes several textbook examples of morphological evolutionary trends in vertebrate evolution (e.g., acquisition of the monodactyl posture in equids, divergent evolution in the morphology of Darwin's finches, Allen's rule in the body shape of ursids and canids) and suggests a potentially relevant use of research on phenotypic evolutionary trends induced by anthropogenic climate change as an ideal arena for the validation of hypotheses concerning the predictability of evolution.

Chapter 1 - New avenues for old travellers: phenotypic evolutionary trends meet morphodynamics, and both enter the global change biology era



New Avenues for Old Travellers: Phenotypic Evolutionary Trends Meet Morphodynamics, and Both Enter the Global Change Biology Era

Davide Tamagnini^{1,2} · Daniele Canestrelli³ · Carlo Meloro⁴ · Pasquale Raia⁵ · Luigi Maiorano^{1,2}

Received: 25 January 2021 / Accepted: 22 July 2021
© The Author(s) 2021

Abstract

Evolutionary trends (ETs) are traditionally defined as substantial changes in the state of traits through time produced by a persistent condition of directional evolution. ETs might also include directional responses to ecological, climatic or biological gradients and represent the primary evolutionary pattern at high taxonomic levels and over long-time scales. The absence of a well-supported operative definition of ETs blurred the definition of conceptual differences between ETs and other key concepts in evolution such as convergence, parallel evolution, and divergence. Also, it prevented the formulation of modern guidelines for studying ETs and evolutionary dynamics related to them. In phenotypic evolution, the theory of morphodynamics states that the interplay between evolutionary factors such as phylogeny, evo-devo constraints, environment, and biological function determines morphological evolution. After introducing a new operative definition, here we provide a morphodynamics-based framework for studying phenotypic ETs, discussing how understanding the impact of these factors on ETs improves the explanation of links between biological patterns and processes underpinning directional evolution. We envisage that adopting a quantitative, pattern-based, and multifactorial approach will pave the way to new potential applications for this field of evolutionary biology. In this framework, by exploiting the catalysing effect of climate change on evolution, research on ETs induced by global change might represent an ideal arena for validating hypotheses about the predictability of evolution.

Keyword Biological rule · Non-Brownian evolution · Phenotype · Climate change biology · Ecomorphology

History and Future of Evolutionary Trends

Evolutionary trends (ETs) are traditionally defined as persistent and directional changes in the state of one or more quantitative traits, resulting in substantial changes through

time and representing the primary phenomenon characterising evolution at high taxonomic levels and over long-time scales (Gould, 2002; McNamara, 2006; McShea, 2005). Alroy (2000) described the study of ETs as “one of the oldest and more intriguing topics in evolutionary biology”, agreeing with McKinney (1990), who indicated the concept of ET as “arguably the single most important in the study of evolution”.

The quest for ETs started early in macroevolution and quickly assumed crucial importance in phenotypic evolution and many other fields of evolutionary biology. The first groundbreaking investigations concerning phenotypic directional evolution led to the description of iconic and pervasive trends throughout the history of a single clade, frequently relying on the evidence available from fossil record (e.g., increasing hypsodonty and gradual acquisition of the monodactyl posture in equids caused by the spread of grasslands – Kowalewsky, 1874). Then, the formulation of the so-called ‘biological rules’ extended the definition of ETs to include directional responses to ecological, climatic

✉ Davide Tamagnini
davide.tamagnini@uniroma1.it

¹ Department of Biology and Biotechnologies “Charles Darwin”, University of Rome “La Sapienza”, Rome, Italy

² Museum of Zoology, Sapienza Museum Centre, University of Rome “La Sapienza”, Building, Viale dell’Università 32, 00185 Rome, Italy

³ Department of Ecological and Biological Science, University of Tuscia, Viterbo, Italy

⁴ Research Centre in Evolutionary Anthropology and Palaeoecology, School of Biological and Environmental Sciences, Liverpool John Moores University, Liverpool, UK

⁵ Department of Earth, Environmental and Resources Sciences, University of Naples “Federico II”, Napoli, Italy

or biological gradients, with several clades being simultaneously analysed obtaining the same evolutionary pattern (e.g., latitudinal or elevation gradients, like in Allen's or Bergmann's rules – Allen, 1877; Bergmann, 1847).

During the second half of the twentieth century, an animated debate rose regarding how to identify an ET. In particular, a key point in this debate was whether to find out a directional pattern in evolution suffices to establish the presence of an ET, or if an explanation about the underpinning biological mechanisms is needed (Dayan & Simberloff, 1998; Mayr, 1956; Meiri, 2011). Further theoretical battlegrounds concerned erroneous interpretations of processes involved in the occurrence of directional evolution. In the past, these misinterpretations led to gross oversimplifications of the complexity of evolutionary dynamics and produced “common portrayals of evolution in non-academic settings including outright notions of ‘advancement’, that held sway within evolutionary biology as well” (Gregory, 2008, p. 259). For example, Edward D. Cope based his concept of kinetogenesis (i.e., theory stating that movements of animals aided in the alteration and development of moving parts of the body) on the idea that key evolutionary novelties originate from generalized phenotypes, in keeping with Lamarck's view of evolution as possessing intrinsic directionality (Bowler, 1977). Whereas kinetogenesis (and its allied concept of orthogenesis) became extinct, the idea that evolution may possess a weak form of directionality (i.e., in contrast to old views of evolution as a movement towards ‘perfection of life’) in specific circumstances recently found support (Raia & Fortelius, 2013; Raia et al., 2016). This vision relies on the concept that specialisation and adaptation towards optimal phenotypes can only occur after the birth of clades, for example, originating directional trends through time (Ayala, 1988; Gould, 1988a; Raia & Fortelius, 2013; Raia et al., 2016; Rosenzweig & McCord, 1991). Similar weak forms of directionality were suggested to occur in specific fields of evolutionary biology, such as the evolution of organismal diversity and complexity. For example, the zero-force evolutionary law (McShea & Brandon, 2010; McShea et al., 2019) stated that “in any evolutionary system in which there is variation and heredity, there is a tendency for diversity and complexity to increase, one that is always present but may be opposed or augmented by natural selection, other forces or constraints acting on diversity or complexity” (McShea et al., 2019, p. 1103).

Although the search for new ETs and the validation of the existing ones remain central topics in evolutionary biology (Cardini, 2019; Cardini & Polly, 2013), the formulation of a well-supported and operative definition of ET remains an unsolved issue. The lack of a broadly accepted operative definition prevented evolutionary biologists from unanimously pinpointing the requirements needed for detecting and validating ETs and blurred the definition of

conceptual differences between ETs and other independent/nested key concepts in evolution, whose operative definition had already been formulated (e.g., convergence – Stayton, 2015a, 2015b).

The pivotal importance of ETs in evolutionary biology can be understood by considering many possible contexts in which they represent a central tenet. For instance, ETs constitute an ideal case study to describe and separate the two components of evolution proposed by Simpson (1944), the *tempo* and *mode* in evolution, and their mutually independent variations (Felice et al., 2018; Michaud et al., 2018). The strength of an ET can be quantified as the magnitude of a vector, providing a practical way of representing the speed (or *tempo*) of evolution. The direction of the same vector represents the *mode* of evolution (i.e., observed pattern of variation). Phenotypic ETs can also be investigated in the framework of evolutionary landscapes, accounting for variations in evolutionary constraints affecting a clade through time or in response to environmental shifts. Phenotypic ETs were frequently found as the resulting evolutionary outcome in studies about the controversial field of evolutionary predictability, that focuses on the occurrence of repetitive and foreseeable patterns in evolution under specific conditions (e.g., recurrent patterns in insular systems—de Visser & Krug, 2014; Whittaker et al., 2017). For instance, directional evolution towards a relative reduction of flight muscles in insular colonies of birds was found to be a predictable and frequent phenotypic specialization produced by an ecological release from mammalian predators (Wright et al., 2016). And it is specialisation that was suggested by recent conservation studies to serve as a fundamental proxy for vulnerability and extinction rate increases of species in future or hypothetical scenarios, supporting the idea that research on phenotypic ETs is conceivable to become additional topics included in the future scientific debate on climate change and conservation biology (Gallagher et al., 2015).

Our main goal is to propose a modern theoretical framework for the study of phenotypic ETs, based on Seilacher's theory of morphodynamics (Briggs, 2017; Seilacher & Gishlick, 2015), that explores the interactions between ETs and the main evolutionary factors involved in their occurrence. The theory of morphodynamics can be visually represented with a tetrahedron whose nodes correspond to the main evolutionary factors influencing morphological evolution: phylogenetic history, developmental constraints, environment, and biological function (Briggs, 2017). Thanks to the inclusion of the environmental component, morphodynamics might be considered an expansion of the concept of ‘constructional morphology’ proposed by Seilacher (1970, 1991), which considered the role of phylogenetic history, developmental constraints, and biological function in determining morphological evolution of organisms. Both morphodynamics and constructional morphology “replace

the idealistic concept of ‘bauplan’, in which the concept of organisms as integrated, functional machines was substituted for the sterile notion of organisms as systems of pure morphological form” (Bock, 1991, p. 27).

In order to achieve our goal, after introducing a new operative definition of ETs, our discussion will start by investigating the influence of environment and evo-devo constraints on phenotypic ETs, focusing on the benefits resulting from the adoption of spatially-explicit models and on the role played by the plasticity-first evolution model. Then, we will elaborate on the importance of including phylogenetic information by adopting phylogenetic comparative methods to evaluate evolutionary patterns. Finally, we will describe how recent advances in morphological quantification can be applied to investigate the relationship between (directional) morphological evolution and biological function. In order to suggest new frontiers of research, in the last section we will discuss how, by exploiting the catalysing effect of climate change on evolution, research on directional evolution induced by global change might represent an ideal arena for the validation of hypotheses about the predictability of evolution.

Geometric Definition and Classification of Evolutionary Trends

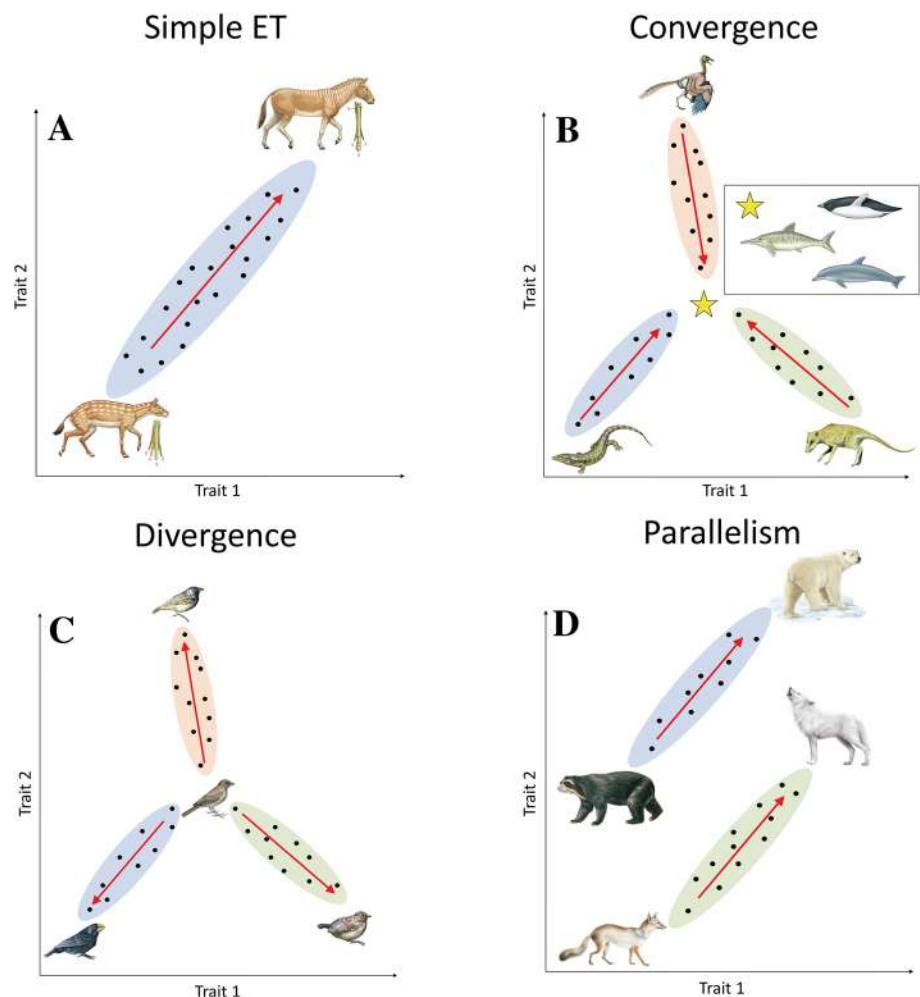
The description of an ET, traditionally considered as an unambiguous phenomenon, has often been limited to anecdotal lists including self-evident examples, without any further quantitative consideration (Stayton, 2015b). The absence of a widely-supported operative definition led to the formulation of multiple (and partially overlapping or conflicting) theoretical definitions. Furthermore, this absence contributed to generate confusion about the relationship between evolutionary concepts like ETs, convergence, divergent evolution, and parallelism, that were considered nested or independent evolutionary cases according to different authors (Manceau et al., 2010; Scotland, 2011).

The concept of ‘(non) parallel evolution’ (i.e., continuum from convergent through parallel to divergent evolution) was recently proposed by Bolnick et al. (2018) to describe the independent evolution of replicate populations, in reference to bacterial cultures of laboratory experiments. The aim of this term is to adopt a pattern-based (Box 1), geometric, and quantitative definition to include in a single concept all classes of evolutionary patterns existing whenever two or more replicates evolving toward a constant direction in a trait space are taken into account. According to this approach, the distinction between parallelism, convergence, and divergent evolution entirely relies on the amplitude of the angles among these evolutionary trajectories, represented as vectors in the trait space. The transposition of (non) parallel

evolution to the macroevolutionary scale (Fig. 1) represents a perfect geometric definition of ETs. This definition constitutes a key innovation to solve the main theoretical issue related to the study of ETs, that is the description of the existing classes of ETs (and their relationships) occurring whenever multiple clades are simultaneously considered (Stayton, 2015a). Three possible classes (i.e., parallel, convergent, and divergent evolution) are conceivable from this perspective. The criterion of distinction between them relies, even in this case, on the orientation of the evolutionary trajectories shown by the single groups (Fig. 1B–D). Therefore, parallelism will be the resulting outcome when evolutionary trajectories point in the same direction, otherwise, a condition of convergence or divergent evolution will occur, depending on whether trajectories respectively point ‘at’ or ‘away from’ a region of the trait space.

This operative definition of ETs is in line with the idea of ‘directional evolution’ provided by Hunt and Carrano (2010). The authors described directional evolution, Brownian Motion (BM) evolution, and stasis as the most relevant models in long-term (i.e., paleontological) macroevolutionary studies, even stating that only mean and variance of the distribution of trait values matter over paleontological temporal scales. In particular, Hunt and Carrano (2010) distinguished between directional and BM evolution arguing that whenever deviations from the mean of this distribution occur, the resulting model will be defined as directional evolution; otherwise, we will be in presence of BM evolution. Coherently with this distinction, several methods using BM as a null hypothesis were proposed in order to detect specific ETs, such as convergent evolution (e.g., Wheatsheaf, C1 and θ metrics—Arbuckle et al., 2014; Stayton, 2015a; Castiglione et al., 2019a) and directional trends through time (e.g., Castiglione et al., 2019b; Sherratt et al., 2016). Nevertheless, in the presence of constraints, BM-like diffusions might result in a directional pattern of evolution determined by the position of constraints in the trait space (Fisher, 1986). For example, the presence of a lower boundary in size evolution has been supposed to be the mechanism that accounts for Cope’s rule (i.e., tendency for clades to increase their size through time – Stanley, 1973). According to this vision, Cope’s rule is simply produced by an increase in size variance through time (Gould, 1988b). Based on these considerations, McShea (1994, p. 1747) distinguished between passive and driven ETs, stating that, “in a driven trend, the distribution mean increases on account of a force (which may manifest itself as a bias in the direction of change) that acts on lineages throughout the trait space in which diversification occurs. In a passive system, no pervasive force or bias exists, but the mean increases because change in one direction is blocked by a boundary, or other inhomogeneity, in some limited region of the trait space”. McShea also validated the occurrence of driven and passive ETs in the

Fig. 1 Scatterplots resulting from the occurrence of any possible class of ETs considering species (black dots) belonging to one (A) or multiple (B–D) clades (ellipses) at the same time and relative examples from the literature. (A) Directionality in limb evolution of fossil equids. (B) Convergent evolution in body shapes of marine vertebrates, such as penguins, dolphins, and ichthyosaurs. (C) Divergent evolution in morphology of Darwin’s finches. (D) Parallel evolution produced by the occurrence of Allen’s rule in body shape of ursids and canids. Evolutionary trajectories are represented as vectors (red arrows) in the trait space (Color figure online)



evolution of horses, brachiopods, and rodents, and tried to classify as driven or passive trends several other live hypotheses, such as trends through time in size, complexity, and energy intensiveness (McShea, 1998). Our operative definition of ETs can be applied to both passive and driven ETs.

According to our definition of ETs, parallel evolution, convergence, and divergent evolution can be considered as patterns produced whenever, analysing multiple clades at the same time, a portion of the groups undergoes an episode of directional evolution, whereas other groups are subject to a different evolutionary regime. The adoption of a multi-scale approach is therefore recommended to recognise these classes of ETs. Performing evolutionary analyses at different taxonomic levels has also been suggested as a promising avenue to define the evolutionary boundaries acting on a clade more rigorously and the relationships between morphology, evolutionary *tempo*, and ecological divergence in a broad comparative context (Tamagnini et al., 2017). In this sense, research on ETs would take a major step forward if a pattern-based approach, like the one described above (that can only validate or disprove the presence of a pattern),

was systematically accompanied by multifactorial analyses. These analyses would also allow researchers to take into account data relative to underpinning dynamics leading to the occurrence of directional evolution (e.g., ecological variables or life-history traits). When it comes to evolutionary dynamics occurring in phenotypic evolution, the tangled nature of interactions between the factors underpinning morphological evolution has already been explored by the theory of morphodynamics (Briggs, 2017, pp. 203–204), concluding that four components have a predominant role: phylogenetic history, developmental constraints, environment, and biological function. However, the central role of genetic constraints (e.g., scarce genetic variation, low mutation rate, and multivariate genetic correlations) was subsequently recognized as a limiting factor for phenotypic evolution (Futuyma, 2010). Given the role of evo-devo processes as a bridge between genetic and developmental constraints (Müller, 2007), it is in our opinion advisable to adopt them as the fourth factor included in the present theoretical framework (Fig. 2), replacing the factor ‘developmental constraints’ originally included in the theory of morphodynamics. In

the next sections, we will explore the interactions between phenotypic ETs and these evolutionary factors (starting with evo-devo constraints and environment, then shifting onto phylogeny and finally focusing on biological function in the light of new perspectives in morphological quantification), also mentioning applications or methodological approaches that can be used in these contexts.

Box 1

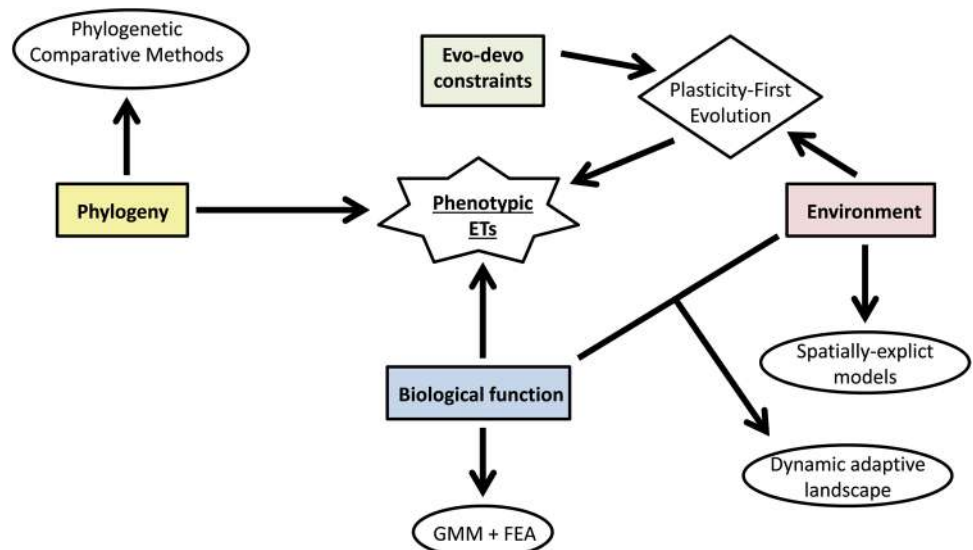
Process-Based Versus Pattern-Based Approaches and Implications with Evo-Devo Mechanisms

The necessity to identify an underpinning evolutionary process to validate the presence of evolutionary patterns has been criticised and gave rise to a long-standing debate in the history of evolutionary biology (Mayr, 1956). When it comes to ETs, the emerging solutions to this dispute are all stemming from two alternative approaches to individuate the presence of a phenomenon that led to the formulation of process-based and pattern-based definitions. Process-based definitions require the *a priori* demonstration that a common mechanism is acting in response to the same evolutionary conditions in all considered groups. By contrast, pattern-based definitions bind the validation of an evolutionary pattern to the mere fulfilment of mathematical or geometrical criteria, generally based on ratios or angular values: it follows that this type of approach is always coupled with quantitative measures and null models (Rosenblum et al., 2014; Stayton, 2015a).

The improved understanding of the functioning of evo-devo mechanisms under different evolutionary conditions initiated an identification process of the linkage between

phenotypic variation and specific evo-devo constraints. For instance, Felice and colleagues (2018) hypothesised that phenotypic integration and modularity act as a bridge between developmental, genetic, and functional levels of trait associations, influencing the morphology of organisms, even catalyzing the evolution and the production of biodiversity. Under suitable conditions, phenotypic integration canalises trait variations along limited evolutionary directions, meeting one of the preconditions to the rise of an ET (Goswami et al., 2014; Wagner & Zhang, 2011). Variations in consolidated patterns of integration between morphological modules were also observed to play an essential role in the iterative occurrence of extreme phenotypes, like the skull of saber-toothed cats, classifiable as episodes of convergent evolution (Meloro & Slater, 2012). The recent advances in mechanism investigation might tempt evolutionary biologists to adopt process-based definitions of ETs in every situation, formulating a developmental or physiological explanation for an observed directionality simply assuming its validity on the basis of different and previously observed case studies. However, despite this type of definitions frequently represents the optimal choice in microevolution, the validity of evo-devo processes in broad comparative data still has to be extensively proved, and process-based approaches were frequently demonstrated to produce contradictions or misinterpretations in the explanation of evolutionary patterns when considering large taxonomic scales (Felice et al., 2018; Meiri, 2011; Stayton, 2015a). Furthermore, process-based definitions systematically fail to categorize the occurrence of a specific pattern, like the presence of directionality, whenever an evolutionary mechanism in place cannot be easily found (e.g., Collar et al., 2014).

Fig. 2 Visualisation of the theoretical framework for the study of phenotypic ETs, including the main evolutionary factors (rectangles), processes (rhombi), methods (ellipses), and respective interactions (arrows) described in the present work. Coloured elements represent the key elements of morphodynamics (Color figure online)



The advantage of adopting pattern-based definitions in macroevolution partially resides in their extreme flexibility, allowing researchers to accommodate additional modifiers easily and clearly define nested cases within an evolutionary phenomenon (Stayton, 2015a). But more importantly, pattern-based validations are suitable for making inferences about different systems in broad comparative data and can serve to steer *post hoc* studies on the mechanisms responsible for the observed patterns. Inferences based on a process-based approach would require, by contrast, an *a priori* validation of the putatively involved mechanism for each different system, unless resulting in gross extrapolations beyond the conditions of the system (e.g., Menge, 1992). Obtaining this sort of process corroboration is challenging due to its experimental nature, which limits the number and the scale of analysable samples. The necessity to shift from small scale understanding to large scale predictions is shared in other fields of evolutionary biology, like macroecology, where there is an increasing demand to identify general, predictive, and empirical relationships in natural systems (Currie, 2019).

The Role of Evo-Devo Constraints and Environment in Shaping Directional Macroevolutionary Patterns and Processes: Plasticity-First Evolution and Spatially-Explicit Models

Investigating the interconnection between evo-devo constraints, environment, and phenotypic variations is crucial for better understanding macroevolutionary processes and improving the prediction of patterns produced by evolutionary directionality. The recent formulation of the evolutionary mechanism named plasticity-first evolution (PFE) model (Levis & Pfennig, 2016) has emphasised the influence of environment and its interactions with evo-devo constraints in shaping phenotypes. According to the PFE model, the environmentally initiated phenotypic change, known as phenotypic plasticity, acts as a precursor of evolutionary adaptation. The environmental variability uncovers the cryptic genetic variation shaping the extant phenotypic plasticity. Then, genetic accommodation leads to the adaptive refinement of favoured phenotypes whenever a condition of diffused polyphenism (i.e., condition where different phenotypes can easily coexist) is not favoured by selection. Shifting the focus on the resulting macroevolutionary effects, directional and persistent environmental stimuli might underpin the rise of an ET acting on pre-existing phenotypic plasticity. Despite concerns regarding the PFE model being raised due to its (at least apparently)

partial inconsistency with the modern synthesis of evolutionary biology (i.e., phenotypic plasticity acting in specific cases as a precursor of evolutionary adaptation), leading to define it as a mere artefact of lab studies (Ho & Zhang, 2018), Levis and colleagues (2018) recently validated the presence of PFE in North American spadefoot toads of the genus *Spea* demonstrating that a persistent environmental stimulus (i.e., presence of different preys and competitors) caused the evolution of intraspecific diet-induced plasticity into fixed morphs within the genus.

Leaving aside the uncertainties relative to the underlying evolutionary mechanisms, the focus on geographical and ecological information in a theoretical model of directional evolutionary patterns recently became a central topic in macroevolution. For instance, Polly (2018) highlighted that existing statistical models used to study evolutionary patterns rely on a Fisherian view of evolution, whereby species are considered single panmictic populations (i.e., populations in which all individuals are potential partners) whose traits are the same regardless of spatial and environmental influences (Fisher, 1930). According to this vision, evolutionary outcomes disregard drift and habitat-specific selection (and are likely to be affected by a misjudgement of the impact of sexual selection). However, both drift and habitat-specific selection might produce, under neutral evolution, phenotypic paths of evolution similar to those resulting from the occurrence of directionality under Fisherian conditions, like the rise of morphological gradients along species distribution ranges (e.g., cranial shape evolution of European common shrews—Polly, 2018). To this aim, Polly also used computational modelling to produce simulations, supporting the idea that drift and habitat-specific selection represent a potential source of misinterpretations in macroevolution. The inclusion of spatially structured variation in evolutionary models (i.e., Wrightian view of evolution) would allow considering metapopulations composed by interacting demes characterised by different trait values: this would enable the distinction between patterns produced by spatial processes, like drift and habitat-specific selection, and ETs associated with non-neutral and directional evolutionary regimes (Hanski, 1999). A potential solution would be the development of individual-based macroevolutionary models. However, a major obstacle to go in this direction is the discrepancy between the lineage-based focus, typical of evolutionary theories, and the attention for individual organisms and their interactions over timescales of a few generations, which often belongs to ecology (Rosindell et al., 2015). In spite of the temporary absence of available spatially explicit models to distinguish between Fisherian and Wrightian trait evolution, ecological models based on the neutral theory of biodiversity represents a key tool to bridge the gap between individual-based ecology and macroevolution, as well as the inclusion

of spatial gradients of selection, metacommunity spatial dynamics, and trait distributions of fossil record (Badgley & Finarelli, 2013; Lyons & Smith, 2013; Maestri et al., 2018; Polly, 2018).

Phylogenetic Comparative Methods and the Necessity to Adopt a Phylogenetically-Informed Approach for the Study of Phenotypic ETs

Macroevolutionary datasets should be collected following a rigorous sampling design. However, evolutionary biologists face issues related to accessibility, incompleteness or sample size, often leading to the implementation of simplified sampling designs that suffer from unknown biases (Albert et al., 2010). Considering taxonomically related groups of species that occur together in space, instead of exclusively analysing monophyletic groups, is often referred to as assemblage approach and is a widespread practice in evolutionary biology, specifically for the study of phenotypic ETs (Meiri, 2011; Stroud et al., 2015). This approach shows, whenever applied to evolutionary biology, the same shortcomings occurring in its original field of application, ecology. For instance, Mittelbach and Schemske (2015) highlighted that assemblage-based analyses can be misleading without a preliminary recognition of the dynamic nature of species pools and the processes underlying species pool formation. The resulting almost inevitable ineffectiveness to describe evolutionary dynamism over large spatial and/or temporal scales originates discrepancies frequently found in assemblage-based studies on ETs (e.g., inconsistent presence of Bergmann's rule in different assemblages of the mammalian order Carnivora—Diniz-Filho et al. 2007, 2009) and suggests to always adopt a phylogenetically-informed approach for the study of macroevolutionary patterns and processes, specifically relying on phylogenetic comparative methods (PCMs).

PCMs are statistical models that estimate the evolutionary regime that best approximates the *tempo* and *mode* of evolution acting on the considered traits, allowing researchers to correct for biases due to the non-independence of sampled observations in macroevolutionary samples (i.e., phylogenetic relationships – Felsenstein, 1985; Venditti et al., 2011). Although discussing existing PCMs and their assumptions is beyond the aim of the present work, the existing literature about this topic is already impressive (e.g., Adams & Collyer, 2019; Cooper et al., 2016 and references therein). Taking into account paleontological data, the possibility to include the available fossil evidence in phylogenetic reconstructions was recently proved to improve estimations of the best model

of evolution, facilitating the detection of changes in *tempo* and *mode* of evolution and the reconstruction of the ancestral states, preventing, therefore, erroneous inferences and increasing the statistical power of PCMs (Mitchell et al., 2019; Schnitzler et al., 2017). The inclusion of paleontological datasets in complex modelling of temporal and spatial evolutionary patterns and the application of PCMs to ecological information represent a promising way to proceed for evolutionary biologists in the foreseeable future and would facilitate the detection of ETs and their variations in strength and direction through time (Castiglione et al., 2019a, 2019b; Maestri et al., 2018).

New Perspectives in Morphological Quantification: Evolutionary Landscapes, Geometric Morphometrics, and Finite Element Analysis

The tangled interactions between variations in selective advantage deriving from biological function and phenotypic or genotypic responses have been traditionally rendered using evolutionary landscapes since this type of graph is meant to show differences in the level of selective advantage intrinsic to a specific set of trait values (Arnold et al., 2001; Wright, 1932). Nowadays, several versions of evolutionary landscapes are available in phenotypic evolution to investigate these interactions both at clade and single-lineage level, enabling, for instance, to recognize the occurrence of evolution driven by ecological opportunity (Hunt et al., 2015; Caetano and Harmon, 2017; Voje, 2020). Regardless of the adopted version of landscape, these graphs are particularly indicated for the visual detection of ETs, since their conformation is likely to reflect the acting evolutionary pattern. For instance, in the absence of boundaries (i.e., driven ETs *sensu* McShea, 1994), favoured phenotypes are distributed along a linear line whenever directionality is common to the entire sample. The resulting evolutionary landscape is a rectilinear ridge (Fig. 3A). Parallelism, convergence and divergent evolution originate a series of parallel ridges, a peak or a depression into the landscapes (Fig. 3B–D), respectively. By contrast, non-directional evolution, as in the case of BM evolution, is likely to generate a flat surface (Fig. 3E). In the presence of boundaries (i.e., passive ETs *sensu* McShea, 1994), their position in the evolutionary landscape contributes to determining the resulting evolutionary pattern.

Recently developed techniques of morphological quantifications (like geometric morphometrics—GMM—and finite element analysis—FEA) allow researchers to quantitatively describe different aspects of phenotypic variation such as size, shape, and functional performance. However, these techniques produce highly multivariate data generally difficult to be implemented for an adequate evolutionary landscape or to

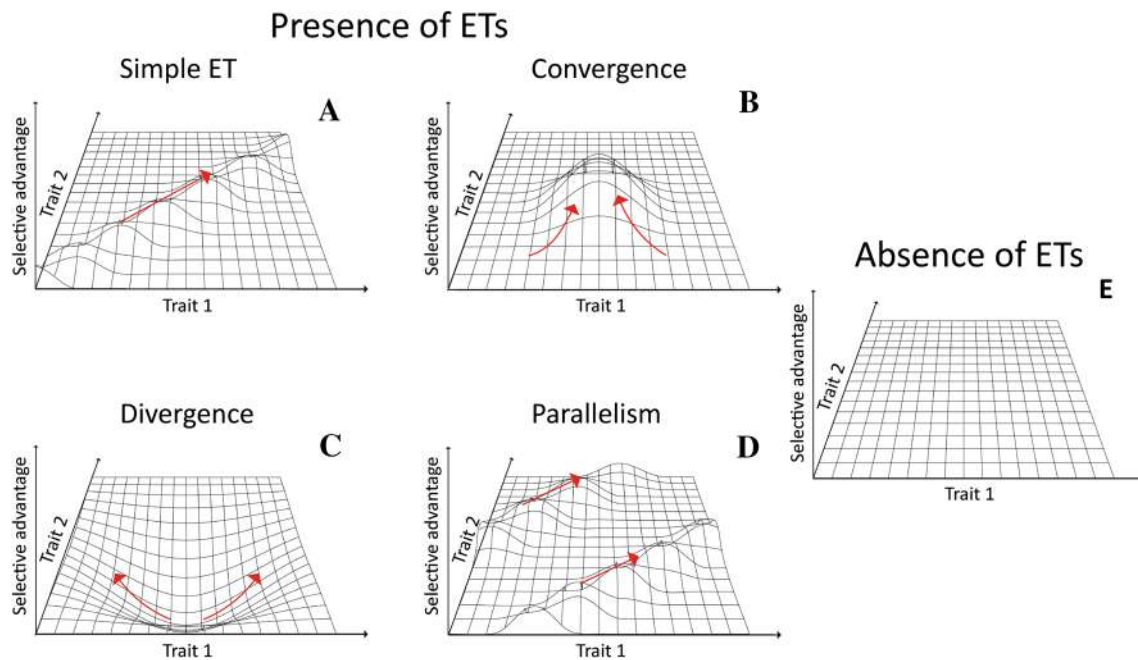


Fig. 3 Examples of evolutionary landscapes resulting, in the absence of boundaries, from the presence of ETs in one (A) or multiple (B–D) clades or from the absence of ETs (E). Simple ETs are linked to a rectilinear ridge configuration (A). Convergent evolution is associated with a peak in the landscape (B), whereas divergence and parallel-

ism are linked to depressions (C) and parallel ridges (D), respectively. Flat surfaces (E) are a typical landscape configuration representing the absence of ETs, as in case of Brownian Motion evolution. Red arrows represent most likely trajectories of directional evolution (Color figure online)

be corrected applying PCMs. For instance, Adams and Collyer (2018a) recently demonstrated that the most common methods (i.e., log-likelihood or AIC score-based techniques) used to estimate the best evolutionary model in multivariate GMM analyses become more ill-conditioned as the ratio between considered morphological traits and sampled species increases or as considered models become more complex. Furthermore, paleomorphological studies have to face issues linked to the scarcity and the fragmented nature of preserved material, plus distortions of fossils produced by taphonomic processes (Arbour & Currie, 2012). To overcome these issues, a new generation of PCMs is rising in GMM, allowing operators to ground estimations of the best model and its parameters on methods unbiased by an increase in trait dimensionality (i.e., statistical tests relying on traces of covariance matrices—Adams & Collyer, 2018a), to adopt innovative techniques of randomizing residuals in phylogenetic ANOVAs and regression models (Adams & Collyer, 2018b) or to graphically visualise potential trends in phylogenetic signal (i.e., phylogenetically aligned component analysis—Collyer & Adams, 2020). Furthermore, recent studies demonstrated how FEA analyses can be employed, relying on trait spaces derived from GMM, to obtain quantitative surfaces describing the performances of different morphologies (O’Higgins et al., 2011; Polly et al., 2016). The combination of multiple performance surfaces (e.g., optimisation concepts such as Pareto front) represents

an informative tool for the construction of phenotypic evolutionary landscapes that show optimal morphologies able to temporarily carry out all functions associated with the selected performances (see Jones et al., 2021 for a worked example about the synapsid-mammal locomotor transition). Combining these techniques of morphological quantification was also proved to be useful for retrodeforming altered fossil specimens or reconstructing damaged remains, as well as for hypothesising and analysing non-available intermediate morphologies (Gunz et al., 2009; Schlager et al., 2018; Tseng, 2013). The possibility to consider non-preserved or purely hypothetical evolutionary forms allows researchers to investigate the occurrence of phenotypic ETs filling unexplored regions of morphological trait spaces, obtaining highly detailed landscapes and characterising the response of functional performance produced by different types of continuous variables, ranging from ecological to physiological ones. A further step forward in eco-evolution is the concept of dynamic adaptive landscape proposed by Laughlin and Messier (2015), whose primary focus is detecting changes occurring in an evolutionary landscape along environmental gradients. This technique uses multivariate trait distributions to determine functional trade-offs at different taxonomic scales, improving the understanding of functional trait evolution and its link to the environmental conditions, and therefore represents a powerful tool for studying the interactions between

biological function and environment. Adopting a dynamic version of phenotypic evolutionary landscapes (potentially also including paleontological evidence) seems to be a promising target, on the one hand, to visualize selective advantage variations along stratigraphic sequences and, on the other, to graphically show the initial outbreak, the constant transformations, and the final weakening of an ET through time (Fig. 4).

The Search for Phenotypic Evolutionary Trends in Climate Change Scenarios as a Tool for Understanding the Predictability of Evolution

As discussed above, pattern-based methods accompanied by multifactorial approaches deriving from a morphodynamics-based theoretical framework will pave the way to new potential applications for studies on phenotypic ETs. Research on ETs in the context of global changes can represent a timely and promising endeavour, particularly considering the predictability of evolution.

Clarifying under what conditions evolution proceeds along predictable pathways would enable researchers to increase and refine the use of evolutionary biology in several applied contexts, for instance, providing tools for

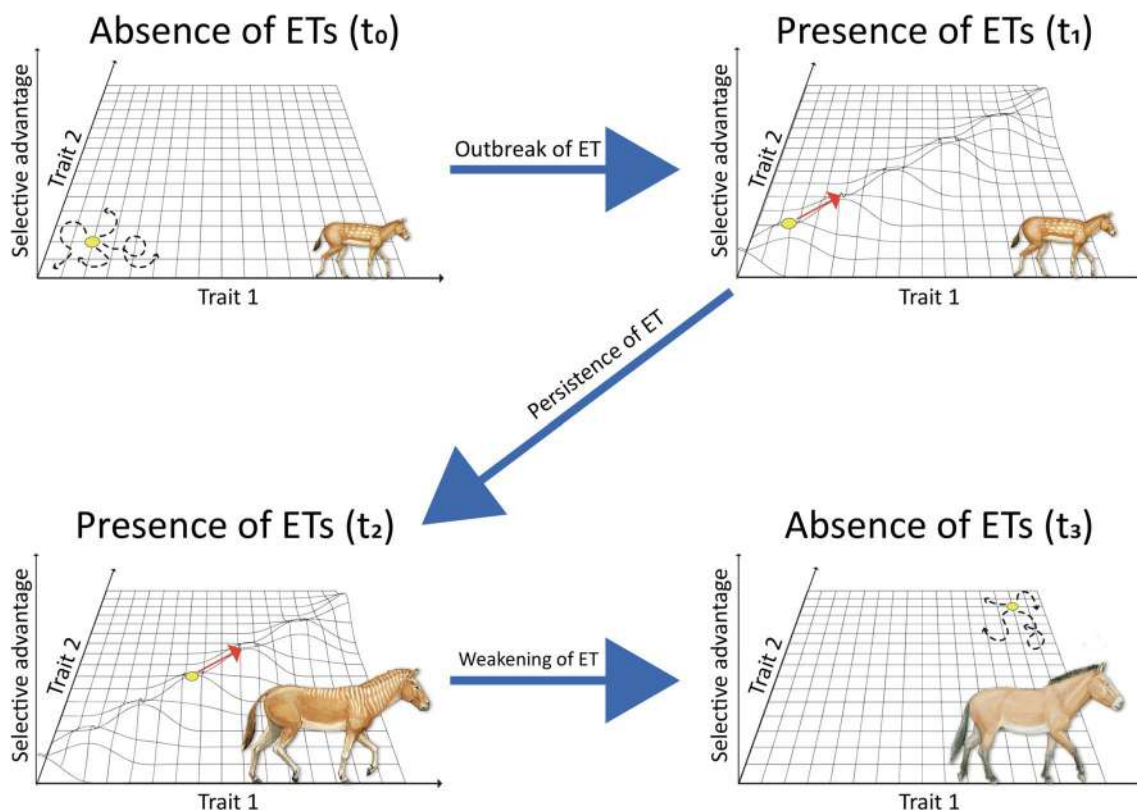


Fig. 4 Example of dynamic evolutionary landscape including the case study of fossil and living equids. A typical scenario for the occurrence of ETs is represented by an initial condition of null selective advantage differences within a given trait space (that is likely to result in Brownian Motion evolution and a flat evolutionary landscape— t_0) that is disrupted by variations in an external factor (e.g., environmental changes). These variations might lead to a temporary phase of directional evolution (potentially reflected by changes in the configuration of the evolutionary landscape— t_1 and t_2). The disappearance of the external forcing can terminate this phase (e.g., end of environmental changes and return of a flat evolutionary land-

scape configuration— t_3). A similar evolutionary scenario might have occurred in limb evolution of equids: the environmental transition from forests to grasslands started during the late Oligocene is likely to have induced an event of directional evolution towards the acquisition of the monodactyl posture within this clade. Before and after this phase, the absence of ETs (e.g., Brownian Motion evolution) can be considered a likely evolutionary outcome, even in the light of the presence of more stable environmental conditions. Yellow dots represent different species of equids that occurred at different (Color figure online)

sustainability assessments and reproducibility of laboratory experiments (Rego-Costa et al., 2018). The first pioneering research in this field found strong sources of stochasticity, as erratic fluctuations of the environment or genetic drift, as limiting factors of evolutionary predictability (Sæther & Engen, 2015). By contrast, investigating the importance of deterministic chaos under simulated repetitive evolutionary conditions, Rego-Costa and colleagues (2018) recently pointed out that a strong forcing by a changing environment (e.g., rapid shifts in selective optima) can improve the predictability of eco-evolutionary dynamics, otherwise resulting in a chaotic scenario under constant evolutionary conditions. It follows that climate change events, whenever causing directional shifts of selective conditions, might represent an enhancer of evolutionary predictability.

The current phase of anthropogenic climate change, resulting in a pattern of diffused global warming, is threatening the existing biodiversity and is potentially leading the entire planet towards a sixth mass extinction that might require millions of years to restore comparable levels of species richness (Barnosky et al., 2011; Davis et al., 2018; Rosenzweig et al., 2008). These environmental changes force species to shift their geographical distribution, change their phenology or alternatively develop adaptations in their morphology and/or physiology relying on an admixture of genetic change and plasticity (Bellard et al., 2012; Hoffmann & Sgrò, 2011). The rise of a phenotypic ET, frequently regarding variations in organism size or shape and changes in the integration between biological modules, constitutes a frequent and highly repeatable event induced by climate change, probably because reflecting a phenotypic response to a constant and directional change in the environment that fits a linear model (MacLean et al., 2018 and references therein). For this reason, research on the occurrence of phenotypic ETs in currently changing environments has the potential to become, in the near future, an indispensable tool for clarifying the dynamics underpinning evolutionary predictability, allowing researchers to verify hypotheses (by the exploitation of the catalysing effect of climate change on evolution) that would otherwise require geological times to be empirically validated in more stable environments. For this purpose, metrics measuring evolvability (i.e., capacity of a system to produce evolutionary adaptations – Colegrave & Collins, 2008; Kirschner & Gerhart, 1998) might be used to assess the likelihood of a clade to develop phenotypic ETs in changing environments. An investigation of morphological integration in the cranium of the mammalian order Carnivora revealed, for instance, that canids possess a higher amount of phenotypic evolvability if compared to other carnivorans. This outcome is mainly produced by an elevated incidence of pure repetitive sequences, promoting new genetic variants by duplication (Laidlaw et al., 2007; Machado et al., 2018). The conspicuous evolvability of this

family was suggested to have underpinned several episodes of directionality in cranial evolution of canids associated with dietary shifts (e.g., increase in relative brachyrostry in hypercarnivore species—Machado et al., 2018). Recent macroevolutionary analyses performed on avian morphology suggest the presence of strong form-function associations that channel phenotypic variation enhancing evolvability towards specific directions of the trait space and produce repeated patterns of morphological convergence that result in highly predictable phenotypes (Felice et al., 2018; Pigot et al., 2020). This evidence seems to confirm the potential that studies on phenotypic ETs in climate change contexts might have for understanding the dynamics underpinning the predictability of evolution. Such studies might open the way for innovative approaches that might improve several inferences about patterns and processes in macroevolution, even producing indirect repercussions in climate change and conservation biology.

Concluding Remarks and Future Directions

ETs channel trait variations and often occur in the presence of directional shifts of selective conditions. Relying on the orientation of evolutionary trajectories in trait spaces, ETs involving multiple clades can be seen as a continuum that goes from convergent through parallel to divergent evolution, making multiscale analyses necessary to distinguish these classes.

Since phylogenetic history, evo-devo constraints, environment, and biological function all play a fundamental role in the occurrence of phenotypic ETs, adopting a morphodynamics-based approach to research on ETs in phenotypic evolution represent a pivotal step forward to fully understand the dynamics that produce this type of evolutionary patterns. Therefore, using methods to assess the influence of each of these factors taken individually, or even performing multifactorial analyses, is of vital importance to shed light on this field (Fig. 5). The possibility to incorporate spatially structured variations, together with the inclusion of fossil record in already existing modelling of evolution, is expected to produce the next major breakthroughs, in terms of analyses on phenotypic ETs, that are likely to be designed in the foreseeable future. An intriguing new frontier of macroevolution is represented by the possibility to perform research on ETs in the presence of extreme environmental shifts, like those resulting from the current phase of climate change. Such research might be crucial for refining predictions of future or hypothetical evolutionary outcomes and might lead to indirect implications in climate change and conservation biology.

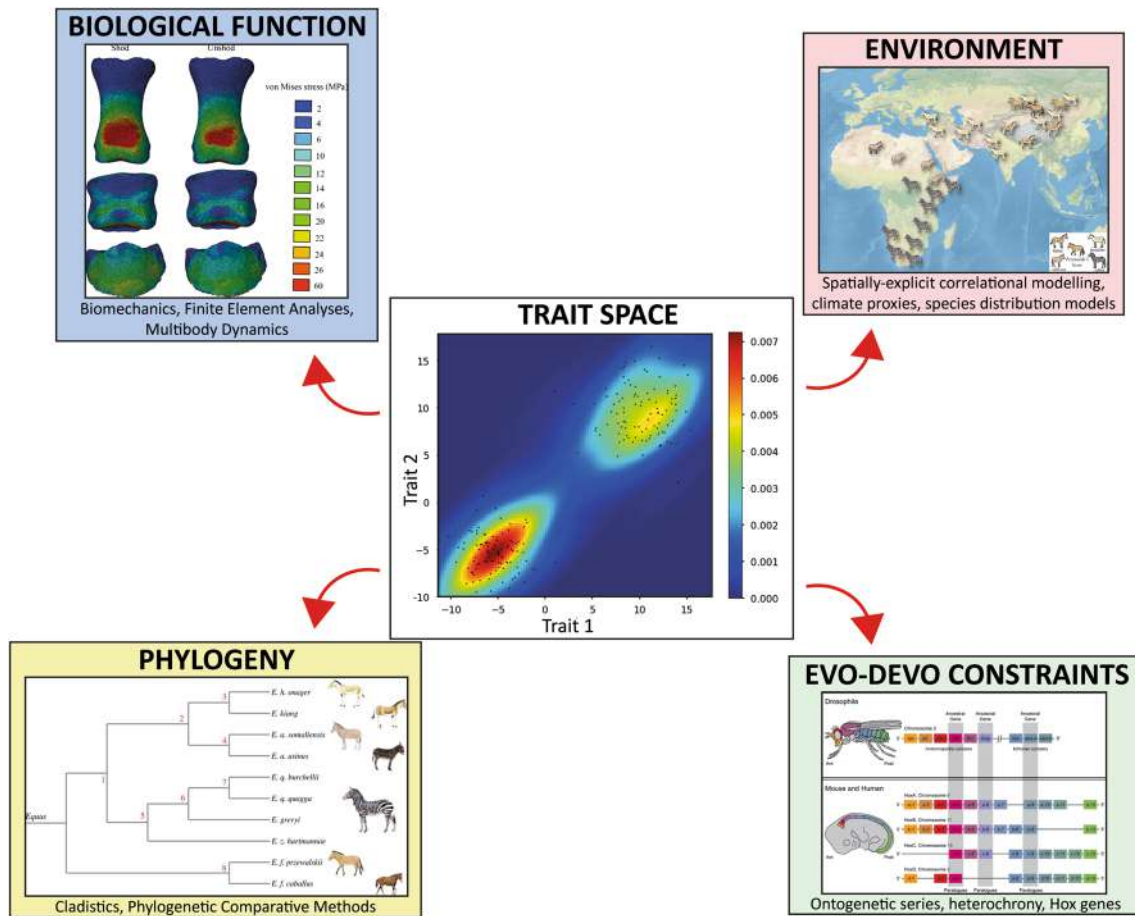


Fig. 5 Operational framework to investigate ETs using morphodynamics. Any trend observed plotting phenotypic traits in a trait space can be investigated in the light of four factors (i.e., phylogeny, evo-devo constraints, environment, and biological function). The impact of each factor is mapped back into the trait space to quantify the amount of selective advantage variation explained over the phenotypic distribution. Optimisation concepts such as Pareto front can be employed to account for multiple constraints and functions within the same surface. Pareto front was applied to phenotypic evolution mainly to investigate the limits of biological function. Typical examples can be found in Shoval et al. (2012), where the authors demonstrated that phenotypic distribution over a morphological trait space generally falls within a triangle whose vertices represent the archetype (i.e., optimal morphological solution for a particular task). Sho-

val et al. also demonstrated that this concept can be applied to gene expression in the bacterium *E. coli*. Other recent examples still cover constraints in biological function, such as Polly et al. (2016), Dickson and Pierce (2019), and Jones et al. (2021). Interestingly, Polly (2020) demonstrated that functional optimization can also be interpreted applying PCMs, thus covering both biological function and phylogeny within the same framework. The visualisation of horse FEA (light blue box) was modified from Panagiotopoulou et al. (2016), both the spatial distribution plot and the phylogeny of extant equids (pink and yellow boxes, respectively) were modified from Cucchi et al. (2017), and the visualisation of Hox genes in *Drosophila*, mice, and humans (green box) was modified from Pang and Thompson (2011). Trait space plot (white box) was produced following <http://qingkaikong.blogspot.com/2018/05/> (Color figure online)

Glossary

Morphodynamics Conceptual framework used to describe all processes influencing a morphology during its evolutionary and developmental histories, including also the impact of external environment.

Evolutionary developmental biology (Evo-devo)

Scientific discipline investigating the mechanistic interactions occurring between phenotypic variation and individual development during evolution. Central questions in evo-devo researches often concern key concepts like integration, modularity, plasticity, and biological innovations.

Modularity	Condition where a biological structure is subdivided into units (i.e., modules) that possess a strong internal covariation but weakly interact with the other units. In morphology, a classic example of modular structure is the mammalian skull, traditionally subdivided into facial and neurocranial modules.
Integration	Tendency of multiple traits to covary throughout a biological structure.
Cryptic genetic variation	Alternative developmental variants uncovering genetic variations that have negligible effects on phenotypic variations except under atypical conditions.
Genetic accommodation	Evolutionary process that refines a phenotype towards an adaptive condition through selection driving quantitative genetic changes.
Ecological opportunity	Condition where a lineage or a clade can suddenly occupy a new niche space with a wide range of underexploited resources. The sudden disappearance of competitors, the access to new environments or the appearance of key innovations are some of the most common triggers producing ecological opportunity.
Geometric Morphometrics (GMM)	Technique of morphological quantification able to extract (and separate) size and shape data from a biological structure, relying on the Cartesian coordinates of corresponding anatomical points, known as landmarks, placed on every specimen of the analysed sample.
Finite Element Analysis (FEA)	Engineering approach frequently employed to quantify the morphological function of a biological structure. The results, expressed in terms of stress and strain, allow estimating the effects produced by applying different loads to the structure and the resulting deformation.
Deterministic chaos	Dependency of the dynamics of a system on its initial conditions.
Phenology	Timing of life cycle events of a species, such as flowering, fruiting, and seasonal migrations.

Acknowledgements We are deeply grateful to David Polly and Markus Bastir for their feedback about preliminary versions or presentations regarding this work. This research received support from the SYNTHESYS programme (ES-TAF-2750 awarded to DT) and the “Avvio alla Ricerca” funds provided by the University of Rome “La Sapienza” (awarded to DT). The research was also supported by a grant from the Italian Ministry of Education, University and Research (PRIN project 2017KLZ3MA) to LM and DC.

Funding Open access funding provided by Università degli Studi di Roma La Sapienza within the CRUI-CARE Agreement. This research received support from the SYNTHESYS programme (ES-TAF-2750 awarded to DT) and the “Avvio alla Ricerca” funds provided by the University of Rome “La Sapienza” (awarded to DT). The research was also supported by a grant from the Italian Ministry of Education, University and Research (PRIN project 2017KLZ3MA) to LM and DT.

Data availability Not applicable.

Code availability Not applicable.

Declarations

Conflict of interest The authors declare that they have no conflict of interest.

Open Access This article is licensed under a Creative Commons Attribution 4.0 International License, which permits use, sharing, adaptation, distribution and reproduction in any medium or format, as long as you give appropriate credit to the original author(s) and the source, provide a link to the Creative Commons licence, and indicate if changes were made. The images or other third party material in this article are included in the article's Creative Commons licence, unless indicated otherwise in a credit line to the material. If material is not included in the article's Creative Commons licence and your intended use is not permitted by statutory regulation or exceeds the permitted use, you will need to obtain permission directly from the copyright holder. To view a copy of this licence, visit <http://creativecommons.org/licenses/by/4.0/>.

References

- Adams, D. C., & Collyer, M. L. (2018a). Multivariate phylogenetic comparative methods: Evaluations, comparisons, and recommendations. *Systematic Biology*, 67(1), 14–31.
- Adams, D. C., & Collyer, M. L. (2018b). Phylogenetic ANOVA: Group-clade aggregation, biological challenges, and a refined permutation procedure. *Evolution*, 72(6), 1204–1215.
- Adams, D. C., & Collyer, M. L. (2019). Phylogenetic comparative methods and the evolution of multivariate phenotypes. *Annual Review of Ecology, Evolution, and Systematics*, 50(1), 405–425.
- Albert, C. H., Yoccoz, N. G., Edwards, T. C., Graham, C. H., Zimmermann, N. E., & Thuiller, W. (2010). Sampling in ecology and evolution – bridging the gap between theory and practice. *Ecography*, 33(6), 1028–1037.
- Allen, J. A. (1877). *The Influence of physical conditions in the genesis of species*.
- Alroy, J. (2000). Understanding the dynamics of trends within evolving lineages. *Paleobiology*, 26(3), 319–329.
- Arbour, V. M., & Currie, P. J. (2012). Analyzing taphonomic deformation of ankylosaur skulls using retrodeformation and finite element analysis. *PLoS ONE*, 7(6), e39323.

- Arbuckle, K., Bennett, C. M., & Speed, M. P. (2014). A simple measure of the strength of convergent evolution. *Methods in Ecology and Evolution*, 5(7), 685–693.
- Arnold, S. J., Pfrender, M. E., & Jones, A. G. (2001). The adaptive landscape as a conceptual bridge between micro- and macroevolution. *Genetica*, 112(1), 9–32.
- Ayala, F. J. (1988). Can ‘progress’ be defined as a biological concept? In M. H. Nitecki (Ed.), *Evolutionary progress* (pp. 75–96). University of Chicago Press.
- Badgley, C., & Finarelli, J. A. (2013). Diversity dynamics of mammals in relation to tectonic and climatic history: Comparison of three Neogene records from North America. *Paleobiology*, 39(3), 373–399.
- Barnosky, A. D., Matzke, N., Tomiya, S., Wogan, G. O. U., Swartz, B., Quental, T. B., Marshall, C., McGuire, J. L., Lindsey, E. L., Maguire, K. C., Mersey, B., & Ferrer, E. A. (2011). Has the Earth’s sixth mass extinction already arrived? *Nature*, 471(7336), 51–57.
- Ballard, C., Bertelsmeier, C., Leadley, P., Thuiller, W., & Courchamp, F. (2012). Impacts of climate change on the future of biodiversity. *Ecology Letters*, 15(4), 365–377.
- Bergmann, C. (1847). *Über die verhältnisse der wärmeökonomie der thiere zu ihrer größe*.
- Bock, W. J. (1991). Explanations in Konstruktionsmorphologie and evolutionary morphology. In N. Schmidt-Kittler & K. Vogel (Eds.), *Constructional morphology and evolution* (pp. 9–29). Springer.
- Bolnick, D. I., Barrett, R. D. H., Oke, K. B., Rennison, D. J., & Stuart, Y. E. (2018). (Non)parallel evolution. *Annual Review of Ecology, Evolution, and Systematics*, 49(1), 303–330.
- Bowler, P. J. (1977). Edward drinker cope and the changing structure of evolutionary theory. *Isis*, 68(2), 249–265.
- Briggs, D. E. G. (2017). Seilacher, konstruktions-morphologie, morphodynamics, and the evolution of form. *Journal of Experimental Zoology Part B: Molecular and Developmental Evolution*, 328(3), 197–206.
- Caetano, D. S., & Harmon, L. J. (2017). Ratematrix: An R package for studying evolutionary integration among several traits on phylogenetic trees. *Methods in Ecology and Evolution*, 1920–1927.
- Cardini, A. (2019). Craniofacial allometry is a rule in evolutionary radiations of placentals. *Evolutionary Biology*, 46(3), 239–248.
- Cardini, A., & Polly, P. D. (2013). Larger mammals have longer faces because of size-related constraints on skull form. *Nature Communications*, 4(1), 1–7.
- Castiglione, S., Serio, C., Tamagnini, D., Melchionna, M., Mondanaro, A., Febraro, M. D., Profico, A., Piras, P., Barattolo, F., & Raia, P. (2019). A new, fast method to search for morphological convergence with shape data. *PLoS One*, 14(12), e0226949.
- Castiglione, S., Serio, C., Mondanaro, A., Febraro, M. D., Profico, A., Girardi, G., & Raia, P. (2019). Simultaneous detection of macroevolutionary patterns in phenotypic means and rate of change with and within phylogenetic trees including extinct species. *PLoS One*, 14(1), e0210101.
- Colegrave, N., & Collins, S. (2008). Experimental evolution: Experimental evolution and evolvability. *Heredity*, 100(5), 464–470.
- Collar, D. C., Reece, J. S., Alfaro, M. E., Wainwright, P. C., & Mehta, R. S. (2014). Imperfect morphological convergence: Variable changes in cranial structures underlie transitions to durophagy in moray eels. *The American Naturalist*, 183(6), E168–E184.
- Collyer, M. L., & Adams, D. C. (2020). Phylogenetically aligned component analysis. *Methods in Ecology and Evolution*, 12(2), 359–372.
- Cooper, N., Thomas, G. H., & FitzJohn, R. G. (2016). Shedding light on the ‘dark side’ of phylogenetic comparative methods. *Methods in Ecology and Evolution*, 7(6), 693–699.
- Cucchi, T., Mohaseb, A., Peigné, S., Debue, K., Orlando, L., & Mashkour, M. (2017). Detecting taxonomic and phylogenetic signals in equid cheek teeth: Towards new palaeontological and archaeological proxies. *Royal Society Open Science*, 4(4), 160997.
- Currie, D. J. (2019). Where Newton might have taken ecology. *Global Ecology and Biogeography*, 28(1), 18–27.
- Davis, M., Faurby, S., & Svenning, J.-C. (2018). Mammal diversity will take millions of years to recover from the current biodiversity crisis. *Proceedings of the National Academy of Sciences*, 115(44), 11262–11267.
- Dayan, T., & Simberloff, D. (1998). Size patterns among competitors: Ecological character displacement and character release in mammals, with special reference to island populations. *Mammal Review*, 28(3), 99–124.
- de Visser, J. A. G. M., & Krug, J. (2014). Empirical fitness landscapes and the predictability of evolution. *Nature Reviews Genetics*, 15(7), 480–490.
- Dickson, B. V., & Pierce, S. E. (2019). Functional performance of turtle humerus shape across an ecological adaptive landscape. *Evolution*, 73(6), 1265–1277.
- Diniz-Filho, J. A. F., Bini, L. M., Rodríguez, M. Á., Rangel, T. F. L. V. B., & Hawkins, B. A. (2007). Seeing the forest for the trees: Partitioning ecological and phylogenetic components of Bergmann’s rule in European Carnivora. *Ecography*, 30(4), 598–608.
- Diniz-Filho, J. A. F., Rodríguez, M. Á., Bini, L. M., Olalla-Tarraga, M. Á., Cardillo, M., Nabout, J. C., Hortal, J.-N., & Hawkins, B. A. (2009). Climate history, human impacts and global body size of Carnivora (Mammalia: Eutheria) at multiple evolutionary scales. *Journal of Biogeography*, 36(12), 2222–2236.
- Felice, R. N., Randau, M., & Goswami, A. (2018). A fly in a tube: Macroevolutionary expectations for integrated phenotypes. *Evolution*, 72(12), 2580–2594.
- Felsenstein, J. (1985). Phylogenies and the comparative method. *The American Naturalist*, 125(1), 1–15.
- Fisher, R. A. (1930). *The genetical theory of natural selection*. Clarendon Press.
- Fisher, D. C. (1986). Progress in organismal design. In D. M. Raup & D. Jablonski (Eds.), *Patterns and processes in the history of life* (pp. 99–117). Springer.
- Futuyma, D. J. (2010). Evolutionary constraint and ecological consequences. *Evolution*, 64(7), 1865–1884.
- Gallagher, A. J., Hammerschlag, N., Cooke, S. J., Costa, D. P., & Irschick, D. J. (2015). Evolutionary theory as a tool for predicting extinction risk. *Trends in Ecology and Evolution*, 30(2), 61–65.
- Goswami, A., Smaers, J. B., Soligo, C., & Polly, P. D. (2014). The macroevolutionary consequences of phenotypic integration: From development to deep time. *Philosophical Transactions of the Royal Society B: Biological Sciences*, 369(1649), 20130254.
- Gould, S. J. (1988a). On replacing the idea of progress with an operational notion of directionality. In M. H. Nitecki (Ed.), *Evolutionary progress* (pp. 319–338). University of Chicago Press.
- Gould, S. J. (1988b). Trends as changes in variance: A new slant on progress and directionality in evolution. *Journal of Paleontology*, 62(3), 319–329.
- Gould, S. J. (2002). *The structure of evolutionary theory*. Harvard University Press.
- Gregory, T. R. (2008). Evolutionary trends. *Evolution: Education and Outreach*, 1(3), 259–273.
- Gunz, P., Mitteroecker, P., Neubauer, S., Weber, G. W., & Bookstein, F. L. (2009). Principles for the virtual reconstruction of hominin crania. *Journal of Human Evolution*, 57(1), 48–62.
- Hanski, I. (1999). *Metapopulation ecology*. OUP Oxford.
- Ho, W.-C., & Zhang, J. (2018). Evolutionary adaptations to new environments generally reverse plastic phenotypic changes. *Nature Communications*, 9(1), 1–11.

- Hoffmann, A. A., & Sgrò, C. M. (2011). Climate change and evolutionary adaptation. *Nature*, 470(7335), 479–485.
- Hunt, G., & Carrano, M. T. (2010). Models and methods for analyzing phenotypic evolution in lineages and clades. *Paleontological Society Papers*, 16, 245–269.
- Hunt, G., Hopkins, M. J., & Lidgard, S. (2015). Simple versus complex models of trait evolution and stasis as a response to environmental change. *Proceedings of the National Academy of Sciences*, 112(16), 4885–4890.
- Jones, K. E., Dickson, B. V., Angielczyk, K. D., & Pierce, S. E. (2021). Adaptive landscapes challenge the “lateral-to-sagittal” paradigm for mammalian vertebral evolution. *Current Biology*. <https://doi.org/10.1016/j.cub.2021.02.009>
- Kirschner, M., & Gerhart, J. (1998). Evolvability. *Proceedings of the National Academy of Sciences*, 95(15), 8420–8427.
- Kowalewsky, V. O. (1874). Monographie der gattung Anthracotherium Cuv., und versucheiner natürlichen classification der fossilen huf-tiere. *Palaeontographica*, 22, 210–285.
- Laidlaw, J., Gelfand, Y., Ng, K.-W., Garner, H. R., Ranganathan, R., Benson, G., & Fondon, J. W. (2007). Elevated basal slippage mutation rates among the Canidae. *Journal of Heredity*, 98(5), 452–460.
- Laughlin, D. C., & Messier, J. (2015). Fitness of multidimensional phenotypes in dynamic adaptive landscapes. *Trends in Ecology and Evolution*, 30(8), 487–496.
- Levis, N. A., Isdamer, A. J., & Pfennig, D. W. (2018). Morphological novelty emerges from pre-existing phenotypic plasticity. *Nature Ecology and Evolution*, 2(8), 1289–1297.
- Levis, N. A., & Pfennig, D. W. (2016). Evaluating ‘plasticity-first’ evolution in nature: Key criteria and empirical approaches. *Trends in Ecology and Evolution*, 31(7), 563–574. <https://doi.org/10.1016/j.tree.2016.03.012>
- Lyons, S. K., & Smith, F. A. (2013). Macroecological patterns of body size in mammals across time and space. In F. A. Smith & S. K. Lyons (Eds.), *Animal body size: Linking pattern and process across space, time, and taxonomic group* (pp. 116–144). University of Chicago Press.
- Machado, F. A., Zahn, T. M. G., & Marroig, G. (2018). Evolution of morphological integration in the skull of Carnivora (Mammalia): Changes in Canidae lead to increased evolutionary potential of facial traits. *Evolution*, 72(7), 1399–1419.
- MacLean, H. J., Nielsen, M. E., Kingsolver, J. G., & Buckley, L. B. (2018). Using museum specimens to track morphological shifts through climate change. *Philosophical Transactions of the Royal Society B: Biological Sciences*, 374(1763), 20170404.
- Maestri, R., Monteiro, L. R., Fornel, R., de Freitas, T. R. O., & Patterson, B. D. (2018). Geometric morphometrics meets metacommunity ecology: Environment and lineage distribution affects spatial variation in shape. *Ecography*, 41(1), 90–100.
- Manceau, M., Domingues, V. S., Linnen, C. R., Rosenblum, E. B., & Hoekstra, H. E. (2010). Convergence in pigmentation at multiple levels: Mutations, genes and function. *Philosophical Transactions of the Royal Society B: Biological Sciences*, 365(1552), 2439–2450.
- Mayr, E. (1956). Geographical character gradients and climatic adaptation. *Evolution*, 10(1), 105–108.
- McKinney, M. L. (1990). Classifying and analysing evolutionary trends. In K. J. McNamara (Ed.), *Evolutionary trends* (pp. 28–58). University of Arizona Press.
- McNamara, K. J. (2006). *Evolutionary trends*. American Cancer Society.
- McShea, D. W. (1994). Mechanisms of large-scale evolutionary trends. *Evolution*, 48(6), 1747–1763.
- McShea, D. W. (1998). Possible largest-scale trends in organismal evolution: Eight “live hypotheses.” *Annual Review of Ecology and Systematics*, 29(1), 293–318.
- McShea, D. W. (2005). The evolution of complexity without natural selection, a possible large-scale trend of the fourth kind. *Paleobiology*, 31(sp5), 146–156.
- McShea, D. W., & Brandon, R. N. (2010). *Biology’s first law: The tendency for diversity and complexity to increase in evolutionary systems*. University of Chicago Press.
- McShea, D. W., Wang, S. C., & Brandon, R. N. (2019). A quantitative formulation of biology’s first law. *Evolution*, 73(6), 1101–1115.
- Meiri, S. (2011). Bergmann’s rule – what’s in a name? *Global Ecology and Biogeography*, 20(1), 203–207.
- Meloro, C., & Slater, G. J. (2012). Covariation in the skull modules of cats: The challenge of growing saber-like canines. *Journal of Vertebrate Paleontology*, 32(3), 677–685.
- Menge, B. A. (1992). Community regulation: Under what conditions are bottom-up factors important on rocky shores? *Ecology*, 73(3), 755–765.
- Michaud, M., Veron, G., Peigné, S., Blin, A., & Fabre, A.-C. (2018). Are phenotypic disparity and rate of morphological evolution correlated with ecological diversity in Carnivora? *Biological Journal of the Linnean Society*, 124(3), 294–307.
- Mitchell, J. S., Etienne, R. S., & Rabosky, D. L. (2019). Inferring diversification rate variation from phylogenies with fossils. *Systematic Biology*, 68(1), 1–18.
- Mittelbach, G. G., & Schemske, D. W. (2015). Ecological and evolutionary perspectives on community assembly. *Trends in Ecology and Evolution*, 30(5), 241–247.
- Müller, G. B. (2007). Evo-devo: Extending the evolutionary synthesis. *Nature Reviews Genetics*, 8(12), 943–949.
- O’Higgins, P., Cobb, S. N., Fitton, L. C., Gröning, F., Phillips, R., Liu, J., & Fagan, M. J. (2011). Combining geometric morphometrics and functional simulation: An emerging toolkit for virtual functional analyses. *Journal of Anatomy*, 218(1), 3–15.
- Panagiotopoulou, O., Rankin, J. W., Gatesy, S. M., & Hutchinson, J. R. (2016). A preliminary case study of the effect of shoe-wearing on the biomechanics of a horse’s foot. *PeerJ*, 4, e2164.
- Pang, D., & Thompson, D. N. P. (2011). Embryology and bony malformations of the craniovertebral junction. *Child’s Nervous System*, 27(4), 523–564.
- Pigot, A. L., Sheard, C., Miller, E. T., Bregman, T. P., Freeman, B. G., Roll, U., Seddon, N., Trisos, C. H., Weeks, B. C., & Tobias, J. A. (2020). Macroevolutionary convergence connects morphological form to ecological function in birds. *Nature Ecology and Evolution*, 4(2), 230–239.
- Polly, P. D. (2020). Functional tradeoffs carry phenotypes across the valley of the shadow of death. *Integrative and Comparative Biology*, 60(5), 1268–1282.
- Polly, P. D. (2018). Spatial processes and evolutionary models: A critical review. *Palaeontology*, 62(2), 175–195.
- Polly, P. D., Stayton, C. T., Dumont, E. R., Pierce, S. E., Rayfield, E. J., & Angielczyk, K. D. (2016). Combining geometric morphometrics and finite element analysis with evolutionary modeling: Towards a synthesis. *Journal of Vertebrate Paleontology*, 36(4), e1111225.
- Raia, P., Carotenuto, F., Mondanaro, A., Castiglione, S., Passaro, F., Saggese, F., Melchionna, M., Serio, C., Alessio, L., Silvestro, D., & Fortelius, M. (2016). Progress to extinction: Increased specialisation causes the demise of animal clades. *Scientific Reports*, 6(1), 30965.
- Raia, P., & Fortelius, M. (2013). Cope’s law of the unspecialized, Cope’s rule, and weak directionality in evolution. *Evolutionary Ecology Research*, 15(7), 747–756.
- Rego-Costa, A., Débarre, F., & Chevin, L.-M. (2018). Chaos and the (un)predictability of evolution in a changing environment. *Evolution*, 72(2), 375–385.

- Rosenblum, E. B., Parent, C. E., & Brandt, E. E. (2014). The molecular basis of phenotypic convergence. *Annual Review of Ecology, Evolution, and Systematics*, 45(1), 203–226.
- Rosenzweig, C., Karoly, D., Vicarelli, M., Neofotis, P., Wu, Q., Casassa, G., Menzel, A., Root, T. L., Estrella, N., Seguin, B., Tryjanowski, P., Liu, C., Rawlins, S., & Imeson, A. (2008). Attributing physical and biological impacts to anthropogenic climate change. *Nature*, 453(7193), 353–357.
- Rosenzweig, M. L., & McCord, R. D. (1991). Incumbent replacement: Evidence for long-term evolutionary progress. *Paleobiology*, 17(3), 202–213.
- Rosindell, J., Harmon, L. J., & Etienne, R. S. (2015). Unifying ecology and macroevolution with individual-based theory. *Ecology Letters*, 18(5), 472–482.
- Sæther, B.-E., & Engen, S. (2015). The concept of fitness in fluctuating environments. *Trends in Ecology and Evolution*, 30(5), 273–281.
- Schlager, S., Profico, A., Vincenzo, F. D., & Manzi, G. (2018). Retrodeformation of fossil specimens based on 3D bilateral semilandmarks: Implementation in the R package “Morpho.” *PLoS One*, 13(3), e0194073.
- Schnitzler, J., Theis, C., Polly, P. D., & Eronen, J. T. (2017). Fossils matter – Understanding modes and rates of trait evolution in Musteloidea (Carnivora). *Evolutionary Ecology Research*, 18(2), 187–200.
- Scotland, R. W. (2011). What is parallelism? *Evolution and Development*, 13(2), 214–227.
- Seilacher, A., & Gishlick, A. D. (2015). *Morphodynamics*. CRC Press.
- Seilacher, A. (1970). Arbeitskonzept zur konstruktions-morphologie. *Lethaia*, 3(4), 393–396.
- Seilacher, A. (1991). Self-organizing mechanisms in morphogenesis and evolution. In N. Schmidt-Kittler & K. Vogel (Eds.), *Constructive morphology and evolution* (pp. 251–271). Springer.
- Sherratt, E., Alejandrino, A., Kraemer, A. C., Serb, J. M., & Adams, D. C. (2016). Trends in the sand: Directional evolution in the shell shape of recessing scallops (Bivalvia: Pectinidae). *Evolution*, 70(9), 2061–2073.
- Shoval, O., Sheftel, H., Shinar, G., Hart, Y., Ramote, O., Mayo, A., Dekel, E., & KavanaghAlon, K. U. (2012). Evolutionary trade-offs, Pareto optimality, and the geometry of phenotype space. *Science*, 336(6085), 1157–1160.
- Simpson, G. G. (1944). *Tempo and mode in evolution*. Columbia University Press.
- Stanley, S. M. (1973). An explanation for Cope’s rule. *Evolution*, 27(1), 1–26.
- Stayton, C. T. (2015a). The definition, recognition, and interpretation of convergent evolution, and two new measures for quantifying and assessing the significance of convergence. *Evolution*, 69(8), 2140–2153.
- Stayton, C. T. (2015b). What does convergent evolution mean? The interpretation of convergence and its implications in the search for limits to evolution. *Interface Focus*, 5(6), 20150039.
- Stroud, J. T., Bush, M. R., Ladd, M. C., Nowicki, R. J., Shantz, A. A., & Sweatman, J. (2015). Is a community still a community? Reviewing definitions of key terms in community ecology. *Ecology and Evolution*, 5(21), 4757–4765.
- Tamagnini, D., Meloro, C., & Cardini, A. (2017). Anyone with a long-face? Craniofacial evolutionary allometry (CREA) in a family of short-faced mammals, the Felidae. *Evolutionary Biology*, 44(4), 476–495.
- Tseng, Z. J. (2013). Testing adaptive hypotheses of convergence with functional landscapes: A case study of bone-cracking hypercarnivores. *PLoS One*, 8(5), e65305.
- Venditti, C., Meade, A., & Pagel, M. (2011). Multiple routes to mammalian diversity. *Nature*, 479(7373), 393–396.
- Voje, K. L. (2020). Testing eco-evolutionary predictions using fossil data: Phyletic evolution following ecological opportunity. *Evolution*, 74(1), 188–200.
- Wagner, G. P., & Zhang, J. (2011). The pleiotropic structure of the genotype–phenotype map: The evolvability of complex organisms. *Nature Reviews Genetics*, 12(3), 204–213.
- Whittaker, R. J., Fernández-Palacios, J. M., Matthews, T. J., Borregaard, M. K., & Triantis, K. A. (2017). Island biogeography: Taking the long view of nature’s laboratories. *Science*. <https://doi.org/10.1126/science.aam8326>
- Wright, S. (1932). The roles of mutation, inbreeding, crossbreeding, and selection in evolution. *Proceedings of the Sixth International Congress on Genetics*, 1, 356–366.
- Wright, N. A., Steadman, D. W., & Witt, C. C. (2016). Predictable evolution toward flightlessness in volant island birds. *Proceedings of the National Academy of Sciences*, 113(17), 4765–4770.

Section 2

The methodological Chapters included in this Section are the result of a collaboration with Prof. Pasquale Raia's lab (University of Naples "Federico II"), which main aim is to develop new analytical techniques for macroevolutionary frameworks that stem from a recently formulated phylogenetic comparative method based on phylogenetic ridge regression (Kratsch and McHardy 2014; Castiglione et al. 2018), and represent valuable additions to the R package *RRphylo*. All these Chapters constitute breakthroughs in key aspects of the study of evolutionary trends in macroevolution, that are the statistical assessment of the presence and strength of convergent evolution (Chapter 2), the visualisation of morphological convergence in digital 3D models (Chapter 3), and the estimation of ancestral states in phenotypic data (Chapter 4). Furthermore, each of these Chapters also include a worked example concerning the validation of a morphological evolutionary trend in the craniomandibular complex of a group of carnivorans. In particular, the new convergence function proposed in Chapter 2 is also employed to validate the presence of convergence in the mandibular shape of felids and barbourofelids; the innovative tool for the 3D graphical visualisation of convergent evolution is applied to show cranial similarities in sabertoothed clades of carnivorans and metatherian mammals in Chapter 3; and the new technique for the reconstruction of ancestral states proposed in Chapter 4 is also used to validate the occurrence of Cope's rule in caniforms (Appendix 2).

Chapter 2 - A new, fast method to search for morphological convergence with shape data

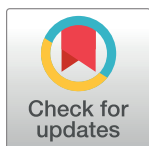
RESEARCH ARTICLE

A new, fast method to search for morphological convergence with shape data

Silvia Castiglione¹, Carmela Serio¹, Davide Tamagnini², Marina Melchionna¹, Alessandro Mondanaro^{1,3}, Mirko Di Febbraro⁴, Antonio Profico², Paolo Piras^{5,6}, Filippo Barattolo¹, Pasquale Raia^{1*}

1 Dipartimento di Scienze della Terra, dell'Ambiente e delle Risorse, University of Naples Federico II, Napoli, Italy, **2** Dipartimento di Biologia Ambientale, Sapienza Università di Roma, Rome, Italy, **3** Dipartimento di Scienze della Terra, University of Florence, Firenze, Italy, **4** Dipartimento di Bioscienze e Territorio, University of Molise, Pesche, Isernia, Italy, **5** Dipartimento di Ingegneria Strutturale e Geotecnica, Sapienza Università di Roma, Rome, Italy, **6** Dipartimento di Scienze Cardiovascolari, Respiratorie, Nefrologiche, Anestesiologiche e Geriatriche, Sapienza Università di Roma, Rome, Italy

* pasquale.raia@unina.it



Abstract

Morphological convergence is an intensely studied macroevolutionary phenomenon. It refers to the morphological resemblance between phylogenetically distant taxa. Currently available methods to explore evolutionary convergence either: rely on the analysis of the phenotypic resemblance between sister clades as compared to their ancestor, fit different evolutionary regimes to different parts of the tree to see whether the same regime explains phenotypic evolution in phylogenetically distant clades, or assess deviations from the congruence between phylogenetic and phenotypic distances. We introduce a new test for morphological convergence working directly with non-ultrametric (i.e. paleontological) as well as ultrametric phylogenies and multivariate data. The method (developed as the function *search.conv* within the R package RRphylo) tests whether unrelated clades are morphologically more similar to each other than expected by their phylogenetic distance. It additionally permits using known phenotypes as the most recent common ancestors of clades, taking full advantage of fossil information. We assessed the power of *search.conv* and the incidence of false positives by means of simulations, and then applied it to three well-known and long-discussed cases of (purported) morphological convergence: the evolution of grazing adaptation in the mandible of ungulates with high-crowned molars, the evolution of mandibular shape in sabertooth cats, and the evolution of discrete ecomorphs among anoles of Caribbean islands. The *search.conv* method was found to be powerful, correctly identifying simulated cases of convergent morphological evolution in 95% of the cases. Type I error rate is as low as 4–6%. We found *search.conv* is some three orders of magnitude faster than a competing method for testing convergence.

OPEN ACCESS

Citation: Castiglione S, Serio C, Tamagnini D, Melchionna M, Mondanaro A, Di Febbraro M, et al. (2019) A new, fast method to search for morphological convergence with shape data. PLoS ONE 14(12): e0226949. <https://doi.org/10.1371/journal.pone.0226949>

Editor: Alistair Robert Evans, Monash University, AUSTRALIA

Received: February 28, 2019

Accepted: December 9, 2019

Published: December 27, 2019

Copyright: © 2019 Castiglione et al. This is an open access article distributed under the terms of the [Creative Commons Attribution License](https://creativecommons.org/licenses/by/4.0/), which permits unrestricted use, distribution, and reproduction in any medium, provided the original author and source are credited.

Data Availability Statement: All files for this study are available within the paper and its Supporting Information files and at <https://github.com/pasraia/RRphylo>.

Funding: The authors received no specific funding for this work.

Competing interests: The authors have declared that no competing interests exist.

Introduction

A species' phenotype depends on its ancestral state and the responses to selection or drift it experiences since that state. Selection towards similar optima in different parts of a tree (which could be described by the Ornstein–Uhlenbeck (OU) mode of evolution [1,2]) generates a pattern of evolutionary convergence [3–6]. Convergence is an intensely studied macroevolutionary pattern [7–11]. Evolutionary convergence is often invoked to explain instances of morphological resemblance between phylogenetically distant clades. Well-known examples include the evolution of wings in bats and birds [12,13], neck elongation in sauropods and giraffes [14], bone cracking ability in percrocotids, borophagine canids and hyaenids [15], hypsodont molars in grazing 'ungulates' [16,17], or the repeated occupation of specific ecomorphs by unrelated *Anolis* species in different Caribbean islands [18,19]. Examples of repeated convergence within a clade, known as iterative evolution, include the evolution of trenchant-heeled lower molar talonids in several canid lineages [12] and elongated and laterally-compressed upper canines within the cat family, Felidae [20]. This by no means exhaustive list just represents a brief account of a diffuse, widely occurring evolutionary pattern [21].

Current methods to address patterns of morphological convergence [22] rely on either: i) the phenotypic analysis of groups of species falling in some pre-selected state (i.e. qualitative categorization) as compared to their ancestors [23]; ii) fitting several OU models to different clades in the phylogenetic tree to see if they evolve towards the same peak (i.e. whether distant clades can be statistically collapsed under a common evolutionary regime [24]); iii) assessing the congruence between phylogenetic and phenotypic distances [18,25] or iv) studying the trajectory of phenotypic change across multiple evolutionary levels [26]. All these methods have advantages and shortcomings. For instance, the comparison of phenotypic to phylogenetic distance matrices may reveal departures from the expected association between the two for reasons other than convergence [6]. Methods based on selective regimes are strongly affected by trait dimensionality and independence [27] and are unsuited to investigate the evolutionary 'history' of convergence [10]. Metrics that necessarily require pre-selected states are strongly influenced by cases of uncertain categorization and by the choice of states. A few methods address convergence by assuming that a certain biological mechanism underpins the pattern [3]. Such methods cannot explain convergence that is not produced by directional processes, and are therefore inadvisable [22].

Here, we present a new method (available as the function *search.conv* in the R package RRphylo) which assesses convergence by testing whether phenotypes in distant clades in a phylogenetic tree are more similar to each other than expected by chance. The method works by computing the angle between the phenotypic vectors of the species as a measure of their similarity and allows identification of the clades (rather than just the species) that converge. We show through simulations that *search.conv* is remarkably powerful and fast. It does not require the convergent clades to be phenotypically unusual as compared to the rest of the tree. In addition, it has low (ca. 5%) Type I error rates (false positives).

We apply *search.conv* to three well-supported cases of morphological convergence, namely the independent adaptation to grazing in perissodactyl and artiodactyl mandibles, the evolution of the sabertooth morphology in machairodont cats and barbouriofelids, and the evolution of distinct ecomorphs by Caribbean *Anolis*. The *search.conv* function together with example files is available at <https://github.com/pasraia/RRphylo>.

Materials and methods

The method is based on phylogenetic ridge regression, *RRphylo* [28]. With *RRphylo*, the phenotypic change between a node and a daughter tip along a phyletic line is described by the

sum of individual contributions at each consecutive branch according to the equation

$\Delta y = \vec{\beta}_1 l_1 + \vec{\beta}_2 l_2 + \dots + \vec{\beta}_n l_n$ where n equals the number of branches intervening between the node and the tip, $\vec{\beta}_{1\dots n}$ are the vectors of regression coefficients (the evolutionary rates) at each branch, and $l_{1\dots n}$ are the branch lengths. Regression coefficients are computed simultaneously for all the branches in the tree and independently for each variable (in the case of multivariate data), by applying to each of them a normalization factor λ which avoids fitting extreme β values and prevents multicollinearity [29].

Dealing with multivariate data, each species at the tree tips is represented by a phenotypic vector, including one entry value for each variable. Naming **A** and **B** the phenotypic vectors of a given pair of species in the tree, the angle θ between them is computed as the inverse cosine of the ratio between the dot product of **A** and **B**, and the product of vectors sizes:

$$\theta = \arccos \frac{\mathbf{A} \bullet \mathbf{B}}{|\mathbf{A}| |\mathbf{B}|}$$

The cosine of angle θ actually represents the correlation coefficient between the two vectors [30]. As such, it exemplifies a measure of phenotypic resemblance [26]. Possible θ values span from 0 to 180 degrees. Small angles (i.e. close to 0°) imply similar phenotypes. At around 90° the phenotypes are dissimilar, whereas towards 180° the two phenotypic vectors point in opposing directions (i.e. the two phenotypes have contrasting values for each variable). For a phenotype with n variables, the two vectors intersect at a vector of n zeros (the origin of the axes in the 3D plot produced by using the [S1 File](#)). However, it is important to note that with geometric morphometric data (PC scores) the origin coincides with the consensus shape (where all PC scores are 0), so that, for instance, a large θ indicates the two species diverge from the consensus in opposite directions and the phenotypic vectors can be visualized in the PC space ([S1 File](#)).

Under the Brownian Motion (BM) model of evolution, the phenotypic dissimilarity between any two species in the tree (hence the θ angle between them) is expected to be proportional to the age of their most recent common ancestor. Under convergence, this expectation is violated and the angle between species should be shallower than expected by their phylogenetic distance (see [S1 File](#), selecting either ‘convergence’ or ‘convergence from similar ancestors’). We developed a new R function, *search.conv*, specifically meant to calculate θ values and to test whether actual θ s between groups of species are smaller than expected by their phylogenetic distance. The function tests for convergence in either entire clades or species grouped under different evolutionary ‘states’ ([Fig 1](#)).

Given two monophyletic clades (subtrees) **C1** and **C2**, *search.conv* computes the mean angle θ_{real} over all possible combinations of pairs of species taking one species per clade. This θ_{real} is divided by the patristic (i.e. the sum of branch lengths) distance between the most recent common ancestors (mrcas) to **C1** and **C2**, **mrcaC1** and **mrcaC2**, respectively ([Fig 1](#)), to account for the fact that the mean angle (hence the phenotypic distance) is expected to increase, on average, with phylogenetic distance ([Fig 2](#)). To assess significance, *search.conv* randomly takes a pair of tips from the tree ($t1$ and $t2$), computes the angle θ_{random} between their phenotypes and divides θ_{random} by the distance between $t1$ and $t2$ respective immediate ancestors (i.e. the distance between the first node $N1$ above $t1$, and the first node $N2$ above $t2$). This procedure is repeated 1,000 times generating θ_{random} per unit time values, directly from the tree and data. The θ_{random} per unit time distribution is used to test whether θ_{real} divided by the distance between **mrcaC1** and **mrcaC2** is statistically significant, meaning it is smaller than 5% of θ_{random} values the two clades are said to converge.

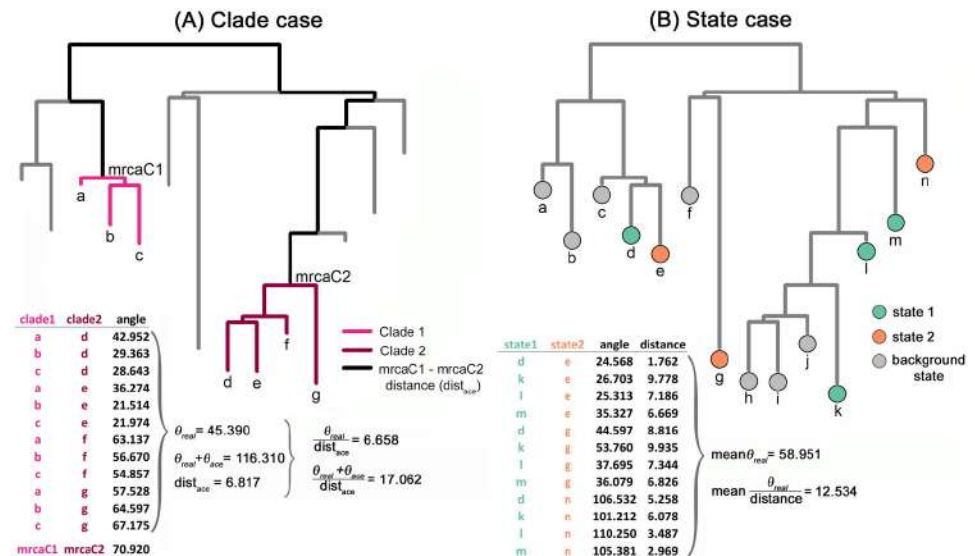


Fig 1. Hypothetical example illustrating how the *search.conv* function algorithm works. In the clade case (A), given any two monophyletic clades in the tree, the mean angle averaged over all possible combinations of two species (one per clade) is computed. This θ_{real} angle is divided by the distance between the most recent common ancestors to the respective clades, mrca1 and mrca2. Significance is assessed by comparing the result of this procedure to 1,000 randomly generated angles θ_{random} computed between species extracted by chance from the tree, divided by their respective distances. Angles are further computed between phenotypes at the mrcas. These θ_{acc} angles are summed to the corresponding θ_{real} to test whether convergence was already present at the beginning of clade history. Ancestral phenotypes are either estimated by *RRphylo* or provided by the user according to the fossil record. In the state case (B), θ_{real} are computed as in the clade case, but taking the mean angle between each combination of pairs of species (taken one per state), divided by their distance.

<https://doi.org/10.1371/journal.pone.0226949.g001>

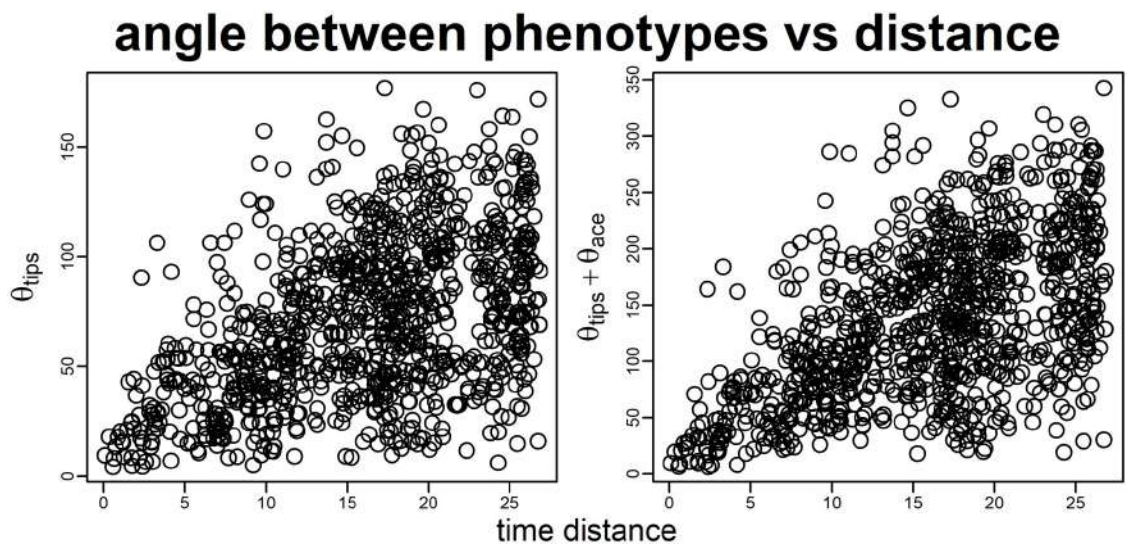


Fig 2. Plot of angles between phenotypic vectors versus time distance. The increase in the mean angle between the phenotypic vectors of all species pairs in the tree θ_{tips} and the distance between the species (left). The sum of θ_{tips} plus the angle between the phenotypes estimated at the first node above each tip θ_{acc} plotted against the distance between these nodes (right). The phenotype was generated according to the Brownian Motion model of evolution with σ^2 (the Brownian rate) = 1. The tree is 100 species wide.

<https://doi.org/10.1371/journal.pone.0226949.g002>

When testing convergence, researchers typically have species phenotypes and, ideally, a phylogenetic tree representing their relationships. This means that while it is usually possible to test convergence among species, it is generally not possible to identify entire clades evolving under convergence. In the real world, these clades actually coincide with **mrcaC1** and **mrcaC2** and their descendants. In *seach.conv*, we devised a strategy to identify **mrcaC1** and **mrcaC2**. In practice, given a pair of candidate nodes tested for the initiation of convergence, the phenotypes at **mrcaC1** and **mrcaC2** are estimated by *RRphylo*, and the angle between the ancestral states (θ_{ace}) is calculated (see the angle between mrcas produced by using the [S1 File](#)). Then, θ_{ace} is added to θ_{real} and the resulting sum divided by the distance between **mrcaC1** and **mrcaC2**. The sum $\theta_{\text{ace}} + \theta_{\text{real}}$ should be small for clades evolving from similar ancestors towards similar daughter phenotypes (see the average angle between tips, ‘mean.dir’, produced by using the [S1 File](#)). Importantly, a small θ_{ace} means similar phenotypes at the mrcas of the two clades, whereas a small θ_{real} implies similar phenotypes between their descendants. It does not mean, though, that the mrcas have to be similar to their own descendants. Two clades might, in principle, start with certain phenotypes and both evolve towards a similar phenotype which is different from the initial shape. This means that the two clades literally evolve along parallel trajectories ([S1 File](#), select the option ‘convergence from similar ancestors’). Under *seach.conv*, simple convergence is distinguished by such instances of convergence with parallel evolution. The former is tested by looking at the significance of θ_{real} . The latter is assessed by testing whether the quantity $\theta_{\text{ace}} + \theta_{\text{real}}$ is small (at $\alpha = 0.05$) compared to the distribution of the same quantity generated by summing the θ_{random} calculated for each randomly selected pair of species *t1* and *t2* plus the angle between the phenotypic estimates at their respective ancestors *N1* and *N2* divided by their distance.

As with many other methods concerned with testing convergence (e.g. [\[10,18,31\]](#)), the *seach.conv* function suffers from the problem that ancestral states estimation entirely depends on the phylogenetic tree and data at hand and the evolutionary model used to fit the states. To help addressing this issue, under *seach.conv* phenotypes at the nodes can be indicated directly by the user, when there is a specific hypothesis (i.e. real fossil specimens) about the phenotype of the most recent common ancestor to the clades. This is useful since the inclusion of fossil information increases power and reliability of comparative analyses of trait evolution [\[32,33\]](#).

Under *seach.conv*, instances of convergence may be either assessed under the ‘automatic mode’ or specifying candidate node pairs. By default, *seach.conv* runs the former, testing all clade pairs which are at least as distant as a one tenth of the tree size, counted as the number of nodes between their most recent common ancestors (i.e. clades 10 nodes apart for a 100 species tree). Alternatively, a time, rather than number of nodes, distance could be specified (we illustrate this procedure in the supplementary information and demonstrate via simulations how robust this alternative is). Although any minimum distance can be specified, it must be reminded that by testing too many node pairs at once potentially introduces Type I error inflation. We empirically found that this just becomes a problem by testing very small clades in very large trees. With the default option (i.e. nodes that are at least as distant as a one tenth of the tree size) Type I error inflation is negligible. As detailed below, we assessed the effect of phylogenetic distance on *seach.conv* Type I and Type II error rates. Our expectation is that the closer the clades are on the tree, the harder it becomes to find convergence, as phenotypic similarity is best explained in this case by phylogenetic proximity.

Several candidate node pairs could map on the same region of the tree, because phenotypic values in close nodes are strongly autocorrelated (for instance, a candidate node pair could be represented by nodes *n1* and *n2*, and another by the pair of nodes immediately bracketing *n1* and *n2*). For each candidate node pair representing a statistically significant signal for convergence, *seach.conv* performs the analysis of multivariate homogeneity of group dispersions by

using the function *betadis* in the R package *vegan* [34], calculates the average distance from group centroids for individual species in the clades, and orders candidate and significant node pairs (if they are > 1 in number) from the least variable to the most. The rationale is that under convergent evolution, species phenotypes are expected to deviate the least from group centroids, at least when the convergent states represent evolutionary attractors [1,2].

The clade-wise approach we have described so far ignores instances of phenotypic convergence that occur at the level of species rather than clades. The *search.conv* function is also designed to deal with this case. To do that, the user must specify distinctive ‘states’ for the species presumed to converge. The function will test convergence between any pair of given states. The species ascribed to a given state may belong anywhere on the tree or be grouped in two separate regions of it, in which case two states are indicated, one for each region. The former design facilitates testing questions such as whether all hypsodont ungulates converge on similar shapes, while latter aids in testing questions such as whether hypsodont artiodactyls converge on hypsodont perissodactyls.

If provided with such ‘states’ *search.conv* will calculate the mean θ_{real} between all possible species pairs evolving under a given state (or between the species in the two states presumed to converge on each other). The θ_{random} angles are calculated by shuffling the states 1,000 times across the tree tips. Both θ_{real} and individual θ_{random} are divided by the distance between the respective tips.

Testing *search.conv* on convergence generated by unknown evolutionary processes

We assessed the power of *search.conv* using both simulation experiments and real cases. The first set of simulations reproduces the existence of phenotypically similar clades or species in distant regions of the tree. This corresponds to the traditional observation of entire clades converging towards similar ecomorphologies (e.g. adaptation to durophagy in the mandible and skull of borophagine canids and modern hyaenids, body shape in ichthyosaurs and dolphins).

We started by generating a paleontological (i.e. non ultrametric) tree with at least 80 species, by using the function *sim.bdtree* in the R package *geiger* (we set birth and death rates at 0.5 and 0.2, respectively [35]). Then, we produced a set of phenotypic data for the tree composed of three uncorrelated variables generated according to the BM model of evolution with variance (the Brownian rate) = 1, using the function *fastBM* in the R package *phytools* [36].

Clade case. To test for convergence between entire clades, our strategy was to select, duplicate, modify, and eventually attach a given clade and its phenotypes to the tree. First, we randomly selected a given subtree *s*. Then, we changed its topology and branch lengths as to produce a new subtree *s'*. The phenotypes in *s'* are similar but not the same as in *s*. Eventually, *s'* and its phenotypes are grafted to a target node on the tree being at least as distant from *s* as one tenth of the tree nodes (Fig 3). Since the two subtrees have similar phenotypes in spite of being phylogenetically distant, they should be found to converge on each other.

To accomplish this procedure, we started by selecting *s* from within the tree among clades having as many as one tenth to one quarter of the tree tips. We deliberately avoided considering subtrees that are too young (i.e. more than 80% of the tree height in terms of distance from the root) given they would represent an unrealistic case of clades which have had very little time to evolve any convergence (Fig 3).

After modifying *s* to produce *s'*, we assigned to their species phenotypes which are similar to each other and different from the rest of the tree, in order to avoid the new tree phenotype representing BM (which predicts no convergence). To produce the new phenotypes for *s* and *s'*, we took the maximum value of each original variable (thereby creating a vector of maxima

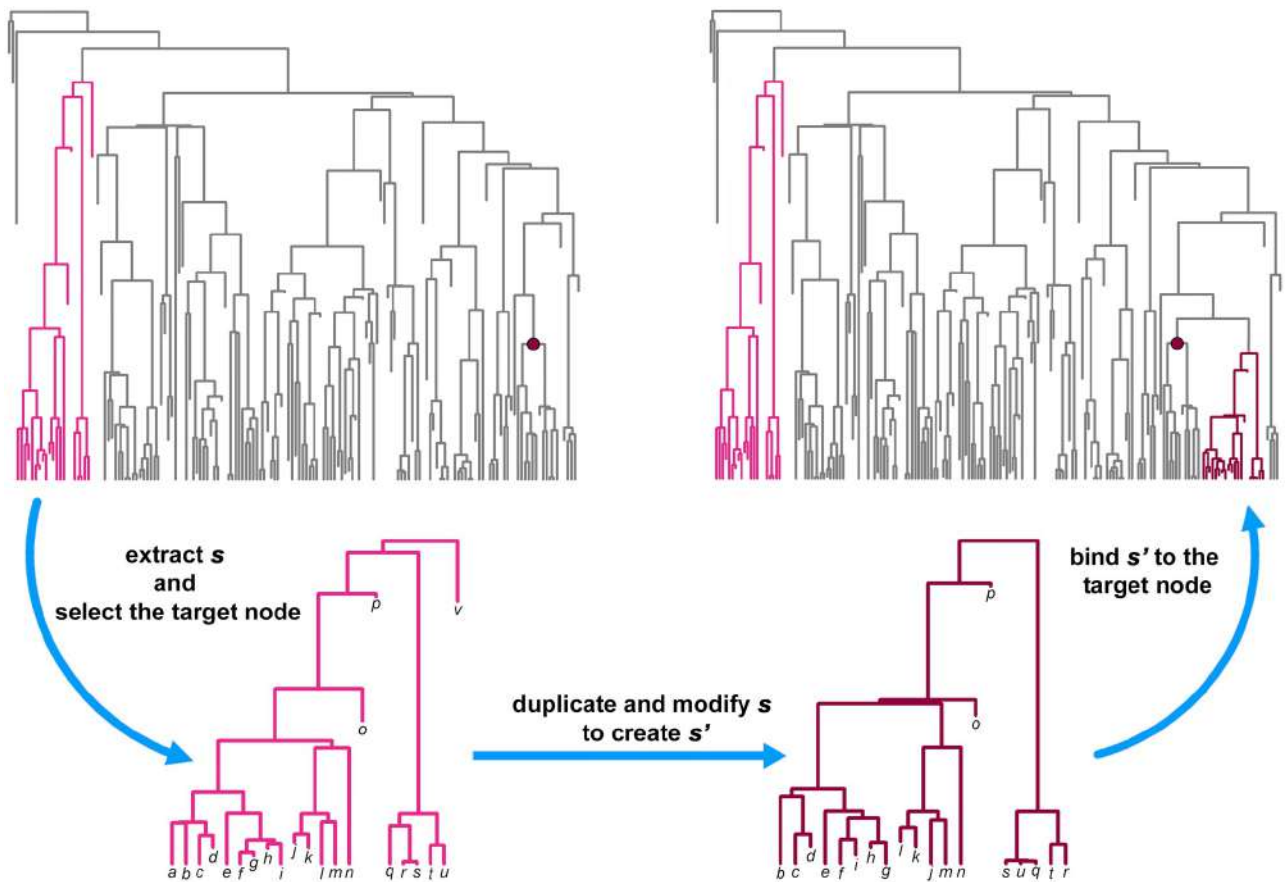


Fig 3. The procedure used to simulate convergence. Clades set to converge are colored. The focal clade (s) is indicated in bright pink, the modified clade (s' dark pink) is grafted at the target node indicated by the dark pink dot.

<https://doi.org/10.1371/journal.pone.0226949.g003>

\vec{m}) and multiplied \vec{m} by a random factor f ranging from 0.5 to 2 to generate a new vector \vec{m}' . Then, for each subclade (s and s') we produced a number n of phenotypes as long as the number of species of each subclade, using the function *jitter* in R. The variables in the new s and s' phenotypes were thus designed to have means equal to \vec{m}' and standard deviations equal to the standard deviations of the original variables.

With $f > 1$ the new phenotypes lay outside the range of the original, BM phenotypes, and the converse with $f < 1$. Thereby, we checked how ‘extreme’ the phenotypic values in s and s' have to be for *search.conv* to detect convergence (see Fig 4). Before attaching s' to the target node, we also dropped two species at random from the subtree and changed its topology and branch lengths by applying the function *swapONE* in RRphylo. By default, this function changes the topology for half of the tree tips and the length of half of the branch lengths (Fig 3). Eventually, the new subtree was rescaled on the height of the clade subtended by the target node (i.e. the maximum distance of its tips from the tree root equals the same distance for tips descending from the new node) so that both s and s' will terminate at the same distance from the root but will have very different heights (Fig 3).

In sum, the two clades set to converge have different topologies, branch lengths, ages and number of tips, only superficial phenotypic resemblance to each other, and may actually be very similar (phenotypically) to other clades in the tree (with $f < 1$, see Figs 3 and 4). While the distribution of phenotypes of the new tree departs from the BM expectation (which would

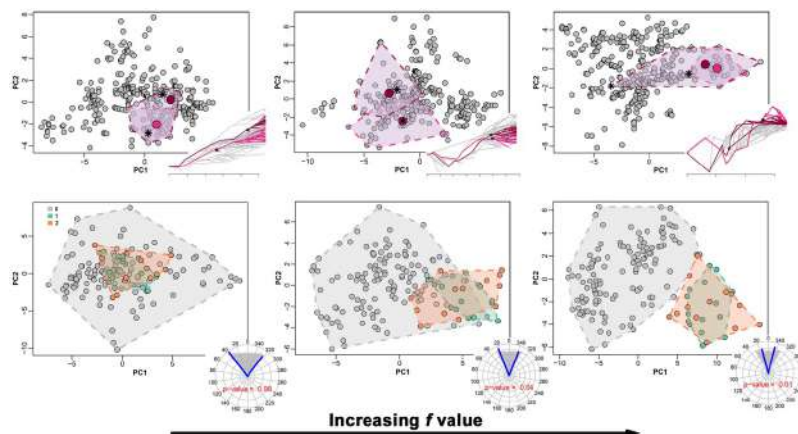


Fig 4. The effect of phenotypic similarity between clades set to converge and the rest of the tree phenotypes on *search.conv* power. In each panel the PC1/PC2 plot of the tree phenotypes are reported. Clades set to converge are indicated by colored convex hulls. Upper row, clade case. Ancestral phenotypes (mrcas) of the clades set to converge are indicated by an asterisk. Large colored dots represent the mean phenotypes (group centroids) of the clades set to converge. A modified traitgram plot is added to the lower right corner in each figure, with branches belonging to the clades set to converge highlighted in color. Lower row, species belonging to states set to converge are indicated by colored convex hulls (0 = background states, 1 and 2 are the states set to converge). To the lower right corner of the quadrants the circular plot reports the mean angle between states (blue lines) and the range of random angles (gray shaded area). The p-value for the convergence test is printed within the circular plots. The *f* values used to simulate the convergent clades are (from the left to the right): 0.2, 0.4 and 0.8.

<https://doi.org/10.1371/journal.pone.0226949.g004>

violate the basic premise for convergent evolution) we deliberately produced phenotypes which are not too different from the rest of the tree phenotypes, to avoid testing *search.conv* with unrealistic or too obvious cases of convergence (see ref. [22] for a similar approach).

We performed *search.conv* on the tree and the attached phenotypic variables both by testing for convergence between all possible combinations of nodes (having proper size and distance) in the tree (the automatic mode) or by indicating target nodes (the specified clades mode). The entire procedure was repeated reducing the distance between convergent clades at three nodes only. In this latter case, the power of *search.conv* is expected to decrease because the phenotypic similarity between clades so close to each other is best explained by phylogenetic proximity rather than by phenotypic convergence. To assess the Type I error rates (i.e. the incidence of false positive instances of convergence found by *search.conv* when in fact there is none) we repeated the same procedure described above to modify the tree topology and branch lengths, and generated on this modified tree a BM phenotype. This way, no convergence is expected to occur between *s* and *s'* or anywhere else in the tree. The complete set of analyses was reiterated 100 times (i.e. for 100 different trees and phenotypes once to assess Type II and then again to assess Type I error rates).

We repeated the analyses to test the performance of *search.conv* with phenotypic variables generated by a non-BM process. To this aim, we rescaled the original tree in accordance with four different evolutionary models (“kappa”, “delta”, “lambda”, and “trend”) by using the function *rescale.phylo* in the package *geiger* [35]. The rescaled trees were used to produce multivariate phenotypes (formed by three variables each) generated according to these evolutionary models and then attached to the original (unscaled) tree. A fifth multivariate trait was generated according to the “drift” model (i.e. having a trend in the phenotypic mean over time) by using the function *setBM* in *RRphylo*. The procedure was repeated 25 times for each model by sampling model parameters (kappa ranging between 0 and 1, delta ranging between 0.1 and 3,

lambda ranging between 0.1 and 1, trend ranging between -0.01 and 0.01, and drift with ds ranging between 0 and 1) at each repetition.

We checked whether the target subtrees are too similar to each other as compared to any other pair of clades in the tree, which would make the test look unreliably powerful and the simulation conditions naive. To this aim, we ran *RRphylo* on the modified tree and phenotype in order to estimate the ancestral phenotypes. Then, we calculated the multivariate Euclidean distance between all the ancestral phenotypes in the tree, to check whether the morphological distance between the two target (i.e. converging) nodes (s and s') fell within the 95% confidence interval of the internode phenotypic distances. The entire procedure was repeated 100 times. At each repetition, we searched for cases of statistically significant convergence between all the nodes in the tree at least as distant from each other as the target nodes.

State case. To test for convergence among groups of species evolving under a single state, we randomly sampled a subgroup including up to one tenth of the number of species in the tree and set it to evolve under a given state. Species in this subgroup were then given new phenotypic values by applying the same procedure as described in the ‘clade’ case.

Similarly, to test for convergence between states, we repeated the procedure for two subgroups, set to converge morphologically on each other (Fig 1). Species in these subgroups were given new phenotypic values as we described in the ‘clade’ case. Yet, one of the two groups’ phenotypes were given twice the standard deviation as the original phenotype. The phenotypes thus fell into three different states: “background state” is the background state produced under BM, “state 1” and “state 2” are the states set to converge (Fig 1). The entire procedure was repeated 100 times.

Testing *search.conv* on convergence generated by known evolutionary processes

The simulation sets described so far assume a pattern-based recognition of convergence, assessing whether phenotypically similar yet phylogenetically distant clades or species do represent convergent evolution regardless of the process generating convergence (see Supplementary S4 File for the R code). Two additional simulation sets address the power of *search.conv* to identify convergence by using an explicit process. We used Stayton’s [22] simulation design to this goal. In keeping with this, we started by using the function *sim.bd.taxa* in TreeSim [37] fixing the number of species at 26 (we set birth and death rates at 0.5 and 0, respectively). Then, we generated ten different phenotypic vectors according to the BM model. The phenotypic variance of the ten variables follows a broken-stick distribution [22]. Two to ten phenotypes were selected at each repetition and attached to the tree. Three species distant no less than three nodes from one another were selected from the tree and tested for convergence. Since all variables were generated under BM, no issue of convergence should be found by *search.conv*. Hence, this simulation set provides an assessment of *search.conv* Type I error rate. A second simulation set was applied to assess Type II error rate, still replicating Stayton’s procedure [22]. At this time, after producing the original, BM phenotypes as described above, three different lineages within the tree were randomly selected to evolve towards a common phenotype according to the OU process, with alpha (the strength of selection) randomly varying between 1 and 50 and theta (the phenotypic attractor) being 1.25 times the maximum values of the original BM phenotype. Both procedures were ran 1,000 times and the number of false positive and false negative instances provided by *search.conv* were recorded. Within the supplementary information, we illustrate these same simulations performed by using a time distance (rather than number of nodes distance) criterion (File S3).

Real cases

We tested three real cases for possible instances of morphological convergence. They represent well-supported instances of morphological convergence during the evolution of the mammalian mandible (cases 1–2) and the colonization of the Caribbean islands by the lizard genus *Anolis* (case 3).

The first case concerns felids. Felids fall in two major ecotypes. Pantherine and feline cats possess robust, conical upper canines. A second ecotype was present in two extinct clades within the cat family, i.e. machairodonts and barbourfelids. The latter is the sister group to true felids. Machairodonts include three tribes [38], one with short and not particularly flattened upper canines, the Metailurini, a second with long, flattened upper canines often possessing crenulated margins, the Homotheriini, and a last tribe with exceptionally long, extremely flat upper canines with smooth margins, the Smilodontini. Smilodontini are the sister clade to Metailurini. Both Homotheriini and Smilodontini are “true” sabertooths [39]. The true sabertooth cats and barbourfelids present highly derived mandibular morphologies, specialized to confer these cats their unique killing behavior, including reduced dentition, low coronoid and condyle processes and protruding incisors [20]. We tested whether mandibular shape in the extinct sabertooth cat clade Machairodontini converges on mandibular shape in Barbourfelidae (the sister clade to all felids which is usually referred to as ‘false’ sabertooth cats). We used geometric morphometric data and the tree published in Piras et al. [38]. The geometric morphometrics data included 83 species and 711 specimens, and we chose 10 landmarks and 23 semi-landmarks to record the mandibular shape (S3 File). We used the first 15 eigenvectors to represent 95% of the cumulative shape variance explained. We ran this experiment with the ‘automatic’ procedure of *search.conv* (i.e. without specifying which clades to be tested).

We further explored the potential effect of specifying ancestral states in finding morphological convergence by applying *search.conv*. To this aim, we repeated the analysis by setting the ancestral mandibular phenotype of barbourfelids and machairodonts to be equal to *Barbourfelis fricki* and *Smilodon fatalis*, respectively.

We compared *search.conv* to an existing method sought to address morphological convergence embedded in the R package *convevol* [40]. To this aim, we performed both *search.conv* (under the ‘state’ condition) and *convratsig* [40] by collapsing barbourfelids and sabertoothed cats under a single state. The function *convratsig* returns four distance-based metrics of convergence and their relative statistical significance obtained by means of randomizations. The C_1 metric is the ratio of phenotypic distance between two (presumably convergent) tips (D_{tip}) to the maximum phenotypic distance (D_{max}) between any pair of taxa in those lineages. When the tips converge, C_1 gets close to 1. The C_2 metric quantifies the magnitude of convergence. It is computed as the difference between D_{max} and D_{tip} . The C_3 and C_4 metrics are computed by dividing C_2 by the total amount of morphological evolution intervening between the tips (i.e. the sum of phenotypic change along the tree branches) and by the total amount of morphological evolution in the entire clade defined by the mrca of convergent tips, respectively. All metrics rely on the estimation of ancestral states at internal nodes (reconstructed according to BM) and none of them include information about the timing for convergent evolution to take place [40].

The second case study was based on hooved mammals (Ungulatomorpha). Hooved mammals fall into two major feeding categories, that is browsing on soft vegetable matter, and grazing on harder vegetable material, typically grasses, whose leaves are rich in silica and therefore result in increased wear rate of the molar tooth crowns. Browsing is typical of most Palaeocene and Eocene ‘ungulates’ and persists today in most deer, tragulids and other small-bodied

forms [41]. With the emergence of grasslands and the spread of grasses, the inclusion of grasses in the diet became widespread in herbivorous mammals [42,43] and is responsible for the rapid diversification of grazing artiodactyls [16]. In morphology, the dietary shift from soft (browsing) to hard and fibrous (grazing) plant material is accompanied by profound changes in the skull and mandible, including the acquisition of high-crowned (hypsodont) molars, longer snout, and deeper mandible [44–46]. This pattern is present in equids, and also appeared several times among Pecora. Nonetheless, true grazing is restricted to a minority of species, most of them being properly defined as mixed-feeders consuming both grasses and soft material [44].

The data were obtained from 353 images in lateral view taken from the scientific literature or directly from specimens (see S2 File for full details), representing 205 species. On each image we recorded nine landmarks to register mandibular shape and analyzed shapes by means of geometric morphometrics (see S3 File for details). We used the five largest eigenvectors, as they represent 95% of the cumulative shape variance explained. The ungulate tree was assembled from literature [16,46,47]. We considered individual species as either grazing artiodactyls, grazing perissodactyls, or “others” (i.e. non convergent) depending on their molar morphology (i.e. degree of hypsodonty) and tested whether grazing ungulates from different parts of the tree converged on similar mandibular morphologies by using the ‘state’ approach.

The third real case pertains to extant lizards of the genus *Anolis*. The genus includes more than 400 species distributed in the Neotropical region and the Caribbean. Insular anoles fall into six distinct ecomorphs which have been intensely studied as a classic example of convergent evolution [19]. The data include a 100 species wide tree for *Anolis* lizards living on the main islands of the Greater Antilles, and 11 phylogenetic principal components extracted analyzing lizards body shapes [48,49] (see Supplementary S4 File for the R code). Six species do not fall into any ecomorph category and are therefore not expected to converge.

Results

Testing convergence generated by unknown evolutionary processes under the automatic mode

The average tree size in the simulation experiments was 192.14 tips (range 156–247). The clades set to converge varied from 17 to 44 species (average 26.74). On average, the heights of the clades set to converge were 64.39% the tree height (range 10.33%–87.76%). The Euclidean distance between s and s' respective *mrca*s phenotypes falls within the 95% confidence intervals of the distribution of inter-node distances in the tree 96% of the times. The distance between the convergent clades was, on average, 98% of the tree height (range 30.14%–166.23%). Despite this great variation in convergent clade size, distance and height, under the automatic mode the Type II error (the rate of false negatives) is as low as 6%. Type I error (false positive) rate is similarly low at 4%. We analyzed the effect of tree size, f , and convergent clades' relative size and distance (that is clade size and the distance between the *mrcaC1* and *mrcaC2* divided to the tree size and height, respectively) on the likelihood to find convergent clades, by regressing these metrics against the p -value calculated for θ_{real} over 100 simulations. The effect of relative clade distance is negative and almost significant ($p = 0.063$) whereas f is positive and significant ($p = 0.037$), meaning that the likelihood of finding convergence increases for clades with distinctive phenotypes and relatively distant from each other on the tree as expected (Fig 4).

As expected, when the simulations were repeated with clades separated by only three nodes, Type I error is 0%, whereas Type II error increases to 54%. These results indicate that *search.conv* does not find convergence between clades that are very close to each other on the tree,

whose phenotypic resemblance is best explained by phylogenetic proximity rather than convergence.

Testing convergence generated by unknown evolutionary processes by specifying candidate clades

The power of *search.conv* to correctly identify the convergent clades when they are specified by the user (i.e. both θ_{real} and $\theta_{\text{real}} + \theta_{\text{ace}}$ are significant) is 71%. However, considering cases when species phenotypes (θ_{real}) are found to be significantly convergent but $\theta_{\text{real}} + \theta_{\text{ace}}$ is not, the identified mrcas for the clades found to converge were correct 88% of the time, within 2 nodes distance from the convergent clades' mrcas. *search.conv* often identifies nodes which are very close to the 'real' mrcas rather than the 'real' mrcas themselves. We found this usually depends on the balancing between the clade set to converge and its sister node, and the strong phenotypic autocorrelation between these clades (because a given clade necessarily includes all of the descendants of its daughter node). When the sister to the real mrca is made up of very few species *search.conv* usually identifies a younger node than the real mrca. Whichever exact mrca pair is identified, 97.5% of the species set to converge are, on average, found to do so.

The Type I and Type II error rates of *search.conv* (automatic mode) are little influenced by how the phenotypes are simulated. The Type I error (the percentage of false positives) remains remarkably low (Table 1). However, some types of phenotypes (most notably 'drift') present high Type II error rate (Table 1).

Testing convergence generated by unknown evolutionary processes using evolutionary states

By using the 'state' specification, the Type I error rate is 5%, either within or between states. Type II error of *search.conv* is 1% when testing for convergence within a group and 6% testing two different states for convergence on each other. We did not find a significant regression between the rank of θ_{real} and f across 100 simulations (within state $p = 0.104$; between states $p = 0.882$). This is not surprising because under the state case species evolving under a single state appear randomly across the tree, hence the effect of f transformation is diffused rather than focusing on a single clade.

Testing convergence generated by known evolutionary processes

We found 47 instances of convergence among groups of three randomly selected species out of 1,000 simulations with phenotypes designed to evolve under the BM model. This means that the Type I error rate of *search.conv*, under this condition, is 4.7%. By using the OU process

Table 1. Type I and Type II error rates.

	Type II error	Type I error
Phenotype type		
browian	6.00%	4.00%
kappa	4.00%	0.00%
delta	12.00%	0.00%
lambda	0.00%	0.00%
trend	12.00%	4.00%
drift	16.00%	4.00%

Type I and Type II error rates with phenotypes simulated according to different evolutionary models.

<https://doi.org/10.1371/journal.pone.0226949.t001>

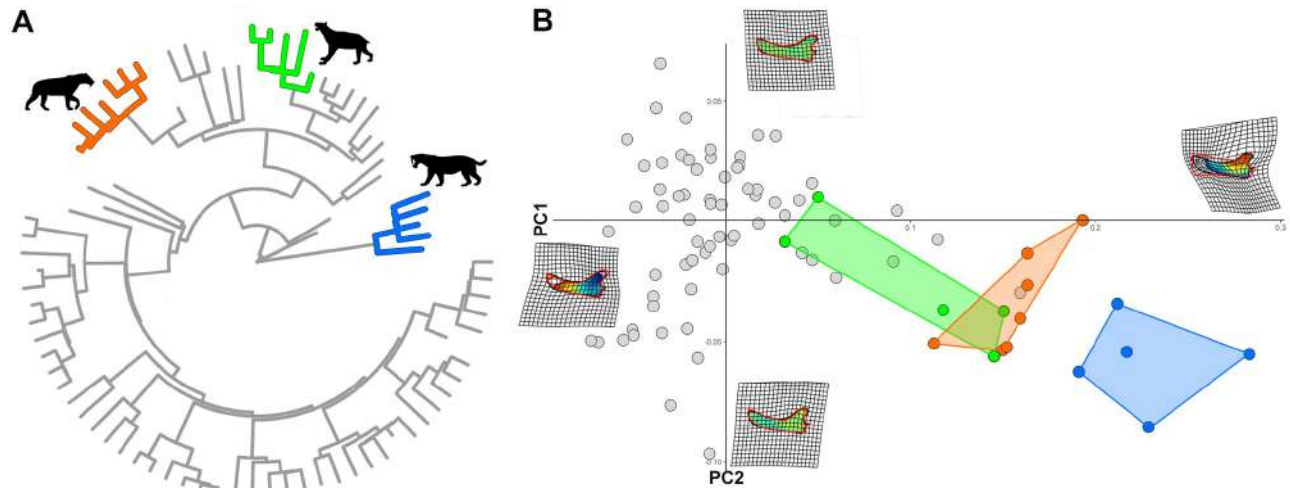


Fig 5. Convergence among mandibular shapes in felids. A) The clades found to converge were Homotheriini (orange) and Barbourfelidae (blue) and Smilodontini (green). B) PC1/PC2 plot showing the position of the convergent clades compared to the rest of the tree. Deformation grids are shown at the extremes of both axes. The silhouette for *Homotherium* was available for reuse under the Creative Commons Attribution 3.0 Unported (<https://creativecommons.org/licenses/by-sa/3.0/>) at <http://phylopic.org/image/c6c2d17b-56b3-4c87-97c4-cd2b7de365fa/> (image by Zimices). The silhouettes for *Smilodon* and *Barbourfelis* are our own work.

<https://doi.org/10.1371/journal.pone.0226949.g005>

to model convergence, we found *search.conv* fails to recognize convergence 45 times out of 1,000 simulation. The corresponding figure for Type II error rate (4.5%) is below the nominal alpha level (5%). By using time distances to select clades for convergence, we found Type I error rate as low as 2% and Type II rate at 4.9% (see supplementary information).

Real case scenarios

Felid mandibles. When testing for convergence between clades, we found two instances of convergent morphological evolution, both pertaining the same clade, Barbourfelidae. The latter includes false saber-toothed cats of the genera *Barbourfelis* and *Albanosmilus*. They were found to be convergent on both Smilodontini and Homotheriini within machairodonts, which represent the true sabertoothed cats (Fig 5). It is noteworthy that *search.conv* effectively failed to find convergence between barbourfelids and Metailurini (Fig 5), which form a clade of machairodont cats sister to Smilodontini but did not possess the full sabertooth morphology. The mean angle between barbourfelids and Smilodontini is 29.93 degrees (Table 2A). The angle between their ancestors is 21.50 degrees. Both θ_{real} and $\theta_{real} + \theta_{ace}$ are statistically smaller than expected by chance ($p = 0.009$ for both). This suggests that the two clades evolved along parallel trajectories. The angle between barbourfelids and Homotheriini is 43.09 degrees, the angle between their reconstructed ancestors is 39.09 degrees, and both θ_{real} and $\theta_{real} + \theta_{ace}$ are statistically significant ($p = 0.019$ and 0.011 , respectively; Table 2A). The computational time was 145 seconds.

By using the mandibular shapes of *Barbourfelis fricki* and *Smilodon fatalis* as the ancestral states to all barbourfelids and machairodonts, respectively, the results are similar to those obtained without specifying phenotypes at the mrca nodes (Table 2B, S3 File), and this may help explaining the good performance of *search.conv* in finding the correct position, hence the true identity, of converging clades.

By performing the analysis collapsing machairodonts and barbourfelids under a single state, *search.conv* produced a small and significant mean angle (19.93 degrees, $p = 0.001$) between convergent species. The computational time was 44 seconds. This latter analysis

Table 2. The results of *search.conv* applied to felid mandibular shape.

A. ACE estimated							
candidate node pairs		θ_{ace}	θ_{real}	distance (# nodes)	distance (years * 10^6)	p (θ_{real})	p ($\theta_{real} + \theta_{ace}$)
Smilodontini	Barbourofelidae	21.50	29.93	9	43.5	0.01	0.01
Homotheriini	Barbourofelidae	39.09	43.09	9	40.8	0.02	0.01
B. ACE indicated							
candidate node pairs		θ_{ace}	θ_{real}	distance (# nodes)	distance (years * 10^6)	p (θ_{real})	p ($\theta_{real} + \theta_{ace}$)
Smilodontini	Barbourofelidae	34.44	29.93	9	43.5	0.01	0.01
Homotheriini	Barbourofelidae	51.67	43.09	9	40.8	0.03	0.03

The results of *search.conv* applied to felid mandibular shape, either by estimating ancestral phenotypes by RRphylo (A), or specifying the ancestral phenotypes to all barbourofelids and all machairodonts to be equal to the phenotype of *Barbourofelis fricki* and *Smilodon fatalis* (B), respectively. ACE = ancestral character state (i.e. the ancestral phenotype), p (θ_{real}) the significance of convergence test restricted to species only, p ($\theta_{real} + \theta_{ace}$) the significance of convergence test for the $\theta_{real} + \theta_{ace}$ sum.

<https://doi.org/10.1371/journal.pone.0226949.t002>

performed by using *convratsig* [40] produced significant results for all the measures (Table 3). The computational time was 21h 48' 7".

Grazing ungulate mandibles. We performed *search.conv* once taking grazers as a single group, then considering grazing artiodactyls and grazing perissodactyls separately.

The mean angle between all grazers collapsed under a single state is 69.62 degrees. This is significant at $p = 0.041$ (see S3 File for figure). The mean angle between grazing artiodactyls and grazing perissodactyls is 77.53 degrees. Although large, we found this angle is less than expected by chance ($p = 0.001$, Fig 6). In fact, the angle θ_{real} increases by 0.51 degrees per million year between grazing artiodactyls and grazing perissodactyls (which are separated by some 152 million years of independent evolution on the 'ungulate' tree, i.e. at least twice as much as the inferred age of the most recent common ancestor to all 'Ungulatomorpha'). This same figure is 0.71 degrees per million year between grazing perissodactyls and "others" and 0.65 between grazing artiodactyls and "others".

Caribbean *Anolis*. By using *search.conv*, we found significant convergence in 5 out of the 6 ecomorphs traditionally recognized for insular anoles (Table 4, see S3 File for figure).

We found convergence in 5 out of 6 different ecomorphs, the only exception being 'trunk' anoles. The *Anolis* species that cannot be ascribed to any ecomorphs are, unsurprisingly, not found to converge. By using the C1 metric, Stayton [22] found 4 of 6 ecomorphs converging. By using the metric C5, convergence is found in 3 ecomorphs. Species not ascribed to an ecomorph were not found to converge for either of the metrics.

Table 3. The results of *convratsig* applied to felid mandibular shape.

	value	p-value
C1	0.259	0
C2	0.058	0
C3	0.110	0
C4	0.013	0

Distance-based measures of convergence and relative significance level as derived by the function *convratsig* in the R package *convevol*.

<https://doi.org/10.1371/journal.pone.0226949.t003>

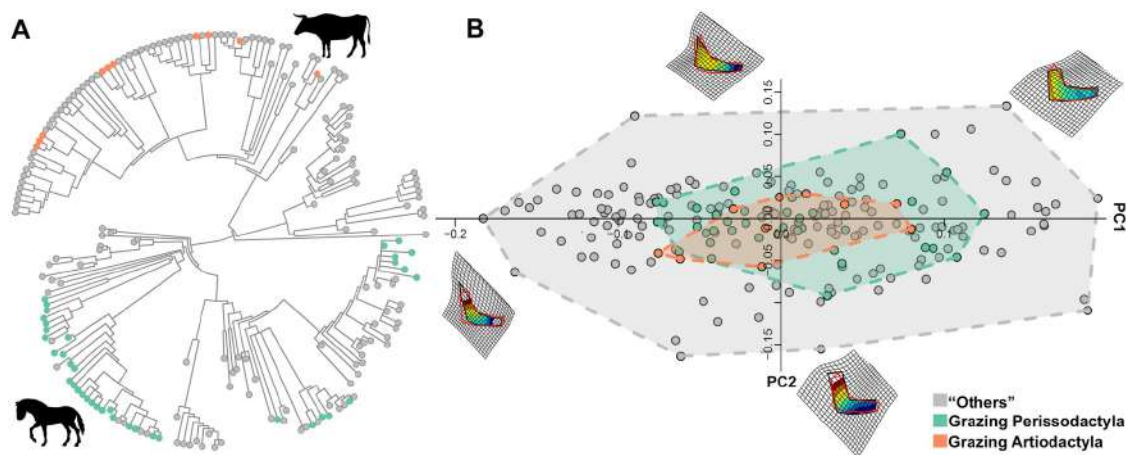


Fig 6. Convergence among mandibular shapes in ungulates. A) The distribution of individual species per state (gray = background state (others), orange = grazing artiodactyls, green = grazing perissodactyls) on the 'ungulate' tree. B) PC1/PC2 plot showing the position of the convergent states (grazers) compared to the rest of the tree. Deformation grids are shown at the extremes of both axes. Animal silhouettes were available under Public Domain license at phylopic (<http://phylopic.org/>). Specifically, *Bos primigenius* (<http://phylopic.org/image/dc5c561e-e030-444d-ba22-3d427b60e58a/>) image by DFoidl (modified by T. Michael Keesey) and *Equus ferus* (<http://phylopic.org/image/85d95128-912c-427a-9542-138e1dbf5651/>) image by Mercedes Yrayzoz (vectorized by T. Michael Keesey) are available for reuse under the Creative Commons Attribution 3.0 Unported (<https://creativecommons.org/licenses/by-sa/3.0/>).

<https://doi.org/10.1371/journal.pone.0226949.g006>

Discussion

Evolutionary convergence has been the focus of many evolutionary studies [6,21]. Morphological convergence arises from adaptation to similar niches by different lineages, which can be separated geographically, phylogenetically and temporally [12], although different processes such as phylogenetic and developmental constraint, and even chance may produce the same pattern [50–53].

There are several methods available in the literature to test the hypothesis of morphological convergence. Most of them rely on the basic assumption that convergence implies stronger phenotypic resemblance than expected by phylogenetic distance. Although the method we propose here, *search.conv*, makes this same assumption, it additionally helps identifying entire clades evolving towards similar shapes and recognizing whether they actually converge from different starting points (which we deem simple convergence) or evolved along parallel

Table 4. Results of convergence within *Anolis* ecomorphs. The left columns represent the results obtained by applying *search.conv*. The last two rightmost columns are the corresponding results pertaining to the metrics C1 and C5, retrieved from [22]. mean angle = the mean angle between species within the ecomorph; mean angle by time = the mean angle between species within the ecomorph divided by time distance; p mean angle = significance level for mean angle; p mean angle by time = significance level for mean angle by time; p-value C1 = significance level for the C1 measure [22]; p-value C5 = significance level for the C5 measure [22].

Ecomorph	<i>search.conv</i>				Stayton 2015	
	mean angle	mean angle by time	p mean angle	p mean angle by time	p-value C ₁	p-value C ₅
Trunk-ground	44.064	32.204	<0.001	<0.001	0.008	0.120
Grass-bush	35.855	24.835	<0.001	<0.001	<0.001	0.386
Crown-giant	20.814	36.305	<0.001	0.003	<0.001	<0.001
Trunk-crown	68.635	45.403	0.002	0.040	0.186	0.011
Twig	30.050	19.695	<0.001	<0.001	<0.001	0.445
Trunk	41.289	43.735	<0.001	0.119	0.252	0.002
None	87.996	53.344	0.317	0.991	0.255	0.763

<https://doi.org/10.1371/journal.pone.0226949.t004>

trajectories (note that under Adams and Collyer's phenotypic trajectory analysis there is no expectation about how large the angle between a pair of phenotypic vectors should be [26]). Our procedure to identify convergence between clades is at least as dependent on ancestral state estimation as many other approaches (e.g. [6,10,23,54]). However, in *search.conv* it is possible to indicate specific phenotypes at nodes, if they are known from the fossil record, which can reduce the impact of ancestral states estimation.

We demonstrate *search.conv*, which is embedded in the R package RRphylo, is robust, has low Type I and Type II error rates, and is very fast even with reasonably large trees. Although the mrcas set to converge are not always found with precision under the automatic mode, the species actually set to converge are correctly identified up to 97.5% of the time, further demonstrating the selection of clade pairs is reasonably precise. When the starting phenotype was modelled to follow an evolutionary model other than BM, the function remains powerful, perhaps with the exception of the 'drift' (a trend in the mean phenotype over time) case. The lower performance of *search.conv* on 'drift-ed' phenotypes might depend on the fact that ancestral state estimation is bounded by the actual phenotypes at the tips, making it evident how highly informative the specification of ancestral phenotypes could be.

We successfully applied *search.conv* to mandibular shape evolution in mammals in two different real cases and to Caribbean islands anole ecomorphs. The first real case study regards the evolution of mandibular shapes in felids. We found "true" sabertooths (Homotheriini and Smilodontini) independently converge on barbourfelids in their mandible morphology. Intriguingly, Metailurini (i.e. "false" sabertooths) which is nested within the machairodont family, were not found to converge on barbourfelids under the automatic mode. This means *search.conv* successfully excluded the false sabertooths from the convergence pattern despite their phylogenetic position close to other "true" sabertoothed machairodont cats [55,56].

We used the felid data to compare *search.conv* to *convevol*'s *convratsig* function. While both functions recognize the same pattern, *search.conv* was found to be three orders of magnitude faster, which could be crucial when it comes to assessing convergence with uncertain state categorization, or to taking the effect of phylogenetic uncertainty into account, as this implies repeating the analyses dozens of times by using different phylogenetic hypotheses.

The second real case application, performed with the 'state' approach, relates to the evolution of hypsodonty due to grass feeding in 'ungulates'. Grazing adaptations in the mandible evolved independently in horses (genus *Equus*) and several bovid lineages, most notably among antelopes. We found evidence for convergent evolution between *Equus* and strictly grazing bovids, such as *Bison*, *Bos*, and *Alcelaphus*. This is especially noteworthy considering that the paleontological tree we used includes a number of non-grazing equids, such as hipparionoid horses and browsing anchitheriine equids, plus several extinct rhinos and tapirs which were all browsers. This demonstrates the method was able to find convergence among grazers despite the effect of phylogeny and body size on mandibular shape variation [46].

The final real case pertains to *Anolis* ecomorphs. We found evidence for convergence in all of them but the 'trunk' ecomorph species. Intriguingly, five of the six 'trunk' groups belong to a single monophyletic clade, indicating that the trunk ecomorph evolved only twice, once for a single clade only present on Hispaniola and then again when Cuban *Anolis loysiana* converged on them.

Compared to other statistical procedures used to test for morphological convergence, *search.conv* offers the possibility to test convergence between entire clades, and allows testing specific 'states' sparsely distributed across the tree. In addition, being much faster than alternative approaches, *search.conv* allows exploring the potential effect of phylogenetic uncertainty and use of fossil phenotypes as ancestral states, that can be crucial in the presence of non-Brownian processes. It must however be noted that not all cases of "convergence" may be

explored best with *search.conv*. There are several instances reported in literature of convergence between closely related clades and even single species with close phylogenetic proximity. We provide a test which is useful to find instances of large-scale morphological resemblance between distant clades that are generally referred to as either ‘convergent’ or just cases of iterative evolution. Caution must be applied to the choice of the ancestral phenotype in the presence of strong phenotypic drift.

Supporting information

S1 File. Angles theta for ancestors and tips of two clades evolving with or without convergence. The R code produces a 3D plot showing the distribution of phenotypes for a > 100 species tree. Two clades are selected to evolve convergent tip phenotypes (simple convergence), convergent tip phenotypes starting from ancestors which are similar to each other (convergence and parallel trajectories) or no convergence. At running the code, the user interactively chooses which kind of simulation to perform and how much the convergent clades have to be different (phenotypically) from the rest of the tree.

(R)

S2 File. Supplementary information for ‘ungulates’. State attribution with references and source for images used in GMM.

(XLSX)

S3 File. Supplementary material. Details of the methods and additional results.

(DOCX)

S4 File. Convergence simulations. R code to perform the simulations.

(R)

Acknowledgments

We are grateful to Lorenzo Rook, Francesco Carotenuto, Gianmarco Tesone, and Martina Piccolo for the comments on earlier version of the manuscript. The authors declare no conflict of interest. Alistair Evans, Roland Sookias and two anonymous reviewers provided insightful comments to an earlier version of this manuscript.

Author Contributions

Conceptualization: Silvia Castiglione, Carmela Serio, Pasquale Raia.

Data curation: Davide Tamagnini.

Formal analysis: Silvia Castiglione, Carmela Serio, Davide Tamagnini, Pasquale Raia.

Investigation: Mirko Di Febbraro, Antonio Profico, Paolo Piras.

Methodology: Pasquale Raia.

Software: Silvia Castiglione, Carmela Serio, Pasquale Raia.

Supervision: Paolo Piras, Pasquale Raia.

Validation: Marina Melchionna, Alessandro Mondanaro, Mirko Di Febbraro, Antonio Profico, Paolo Piras, Filippo Barattolo.

Writing – original draft: Silvia Castiglione, Carmela Serio, Pasquale Raia.

Writing – review & editing: Davide Tamagnini, Marina Melchionna, Alessandro Mondanaro, Mirko Di Febbraro, Antonio Profico, Paolo Piras, Filippo Barattolo.

References

1. Beaulieu JM, Jhwhueng D-C, Boettiger C, O'Meara BC. Modeling stabilizing selection: expanding the Ornstein-Uhlenbeck model of adaptive evolution. *Evolution*. 2012; 66: 2369–2383. <https://doi.org/10.1111/j.1558-5646.2012.01619.x> PMID: 22834738
2. Butler MA, King AA. Phylogenetic Comparative Analysis: A Modeling Approach for Adaptive Evolution. *Am Nat*. 2004; 164: 683–695. <https://doi.org/10.1086/426002> PMID: 29641928
3. Wake DB, Wake MH, Specht CD. Homoplasy: from detecting pattern to determining process and mechanism of evolution. *Science*. 2011; 331: 1032–1035. <https://doi.org/10.1126/science.1188545> PMID: 21350170
4. Bravo GA, Remsen JV Jr., Brumfield RT. Adaptive processes drive ecomorphological convergent evolution in antwrens (Thamnophilidae). *Evolution*. 2014; 68: 2757–2774. <https://doi.org/10.1111/evo.12506> PMID: 25135629
5. Huang S, Roy K, Valentine JW, Jablonski D. Convergence, divergence, and parallelism in marine biodiversity trends: Integrating present-day and fossil data. *Proc Natl Acad Sci*. 2015; 112: 4903–4908. <https://doi.org/10.1073/pnas.1412219112> PMID: 25901312
6. Speed MP, Arbuckle K. Quantification provides a conceptual basis for convergent evolution. *Biol Rev*. 2016; 92: 815–829. <https://doi.org/10.1111/brv.12257> PMID: 26932796
7. Goswami A, Milne N, Wroe S. Biting through constraints: cranial morphology, disparity and convergence across living and fossil carnivorous mammals. *Proc R Soc B Biol Sci*. 2011; 278: 1831–1839. <https://doi.org/10.1098/rspb.2010.2031> PMID: 21106595
8. Ingram T, Kai Y. The Geography of Morphological Convergence in the Radiations of Pacific Sebastes Rockfishes. *Am Nat*. 2014; 184: E115–E131. <https://doi.org/10.1086/678053> PMID: 25325753
9. Serb JM, Sherratt E, Alejandrino A, Adams DC. Phylogenetic convergence and multiple shell shape optima for gliding scallops (Bivalvia: Pectinidae). *J Evol Biol*. 2017; 63: 685–1747. <https://doi.org/10.1111/jeb.13137> PMID: 28667696
10. Moen DS, Morlon H, Wiens JJ. Testing Convergence Versus History: Convergence Dominates Phenotypic Evolution for over 150 Million Years in Frogs. *Syst Biol*. 2015; 65: 146–160. <https://doi.org/10.1093/sysbio/syv073> PMID: 26454873
11. Piras P, Sansalone G, Teresi L, Kotsakis T, Colangelo P, Loy A. Testing convergent and parallel adaptations in talpids humeral mechanical performance by means of geometric morphometrics and finite element analysis. *J Morphol*. 2012; 273: 696–711. <https://doi.org/10.1002/jmor.20015> PMID: 22419178
12. Van Valkenburgh B. Deja vu: the evolution of feeding morphologies in the Carnivora. *Integr Comp Biol*. 2007; 47: 147–163. <https://doi.org/10.1093/icb/icm016> PMID: 21672827
13. Slater GJ. Iterative adaptive radiations of fossil canids show no evidence for diversity-dependent trait evolution. *Proc Natl Acad Sci*. 2015; 112: 4897–4902. <https://doi.org/10.1073/pnas.1403666111> PMID: 25901311
14. Sander PM, Christian A, Clauss M, Fechner R, Gee CT, Griebeler EM, et al. Biology of the sauropod dinosaurs: the evolution of gigantism. *Biol Rev*. 2010; 86: 117–155. <https://doi.org/10.1111/j.1469-185X.2010.00137.x> PMID: 21251189
15. Figueirido B, Tseng ZJ, Martín-Serra A. Skull shape evolution in durophagous carnivorans. *Evolution*. 2013; 67: 1975–1993. <https://doi.org/10.1111/evo.12059> PMID: 23815654
16. Raia P, Carotenuto F, Eronen JT, Fortelius M. Longer in the tooth, shorter in the record? The evolutionary correlates of hypsodonty in Neogene ruminants. *Proc R Soc B Biol Sci*. 2011; 278: 3474–3481. <https://doi.org/10.1098/rspb.2011.0273> PMID: 21471111
17. Janis C. An Evolutionary History of Browsing and Grazing Ungulates. In: Gordon IJ, Prins HHT, editors. *The Ecology of Browsing and Grazing*. Berlin, Heidelberg: Springer; 2008. pp. 21–45.
18. Harmon LJ, Kolbe JJ, Cheverud JM, Losos JB. Convergence and the multidimensional niche. *Evolution*. 2005; 59: 409–421. <https://doi.org/10.1111/j.0014-3820.2005.tb00999.x> PMID: 15807425
19. Losos JB. The Evolution of Convergent Structure in Caribbean Anolis Communities. *Syst. Biol.* 1992; 41:403–420.
20. Christiansen P. Evolutionary convergence of primitive sabertooth craniomandibular morphology: the clouded leopard (*Neofelis nebulosa*) and *Paramachairodus ogygia* compared. *J Mammal Evol*. 2008; 15: 155–179. <https://doi.org/10.1007/s10914-007-9069-z>
21. McGhee GR. *Convergent Evolution: Limited Forms Most Beautiful*. MIT Press; 2011.












22. Stayton CT. The definition, recognition, and interpretation of convergent evolution, and two new measures for quantifying and assessing the significance of convergence. *Evolution*. 2015; 69: 2140–2153. <https://doi.org/10.1111/evo.12729> PMID: 26177938
23. Stayton CT. Testing hypotheses of convergence with multivariate data: morphological and functional convergence among herbivorous lizards. *Evolution*. 2006; 60: 824–841. <https://doi.org/10.1111/j.0014-3820.2006.tb01160.x> PMID: 16739463
24. Ingram T, Mahler DL. SURFACE: detecting convergent evolution from comparative data by fitting Ornstein-Uhlenbeck models with stepwise Akaike Information Criterion. Hansen T, editor. *Met Ecol Evol*. 2013; 4: 416–425. <https://doi.org/10.1111/2041-210X.12034>
25. Muschick M, Indermaur A, Salzburger W. Convergent Evolution within an Adaptive Radiation of Cichlid Fishes. *Curr Biol*. 2012; 22: 2362–2368. <https://doi.org/10.1016/j.cub.2012.10.048> PMID: 23159601
26. Adams DC, Collyer ML. A general framework for the analysis of phenotypic trajectories in evolutionary studies. *Evolution*. 2009; 63: 1143–1154. <https://doi.org/10.1111/j.1558-5646.2009.00649.x> PMID: 19210539
27. Adams DC, Collyer ML. Multivariate Phylogenetic Comparative Methods: Evaluations, Comparisons, and Recommendations. *Syst Biol*. 2017; 67: 14–31. <https://doi.org/10.1093/sysbio/syx055> PMID: 28633306
28. Castiglione S, Tesone G, Piccolo M, Melchionna M, Mondanaro A, Serio C, et al. A new method for testing evolutionary rate variation and shifts in phenotypic evolution. *Met Ecol Evol*. 2018; 62: 181–190. <https://doi.org/10.1111/2041-210X.12954>
29. James G, Witten D, Hastie T, Tibshirani R. An Introduction to Statistical Learning. New York, NY: Springer Science & Business Media; 2013.
30. Zelditch ML, Swiderski DL, Sheets HD. Geometric Morphometrics for Biologists. Academic Press; 2012.
31. Revell LJ, Johnson MA, Schulte JA, Kolbe JJ, Losos JB. A phylogenetic test for adaptive convergence in rock-dwelling lizards. *Evolution*. 2nd edition. 2007; 61: 2898–2912. <https://doi.org/10.1111/j.1558-5646.2007.00225.x> PMID: 17894806
32. Slater GJ, Harmon LJ, Alfaro ME. Integrating fossils with molecular phylogenies improves inference of trait evolution. *Evolution*. 2012; 66: 3931–3944. <https://doi.org/10.1111/j.1558-5646.2012.01723.x> PMID: 23206147
33. Slater GJ, Harmon LJ. Unifying fossils and phylogenies for comparative analyses of diversification and trait evolution. *Met Ecol Evol*. 2013; 4: 699–702. <https://doi.org/10.1111/2041-210X.12091>
34. Oksanen J, Blanchet FG, Friendly M, Kindt R, Legendre P, Mcglinn D, et al. vegan: Community Ecology Package. R package version 2.5–2. 2018. <https://CRAN.R-project.org/package=vegan>
35. Harmon LJ, Weir JT, Brock CD, Glor RE, Challenger W. 2007. GEIGER: investigating evolutionary radiations. *Bioinformatics*. 2007; 24: 129–131. <https://doi.org/10.1093/bioinformatics/btm538> PMID: 18006550
36. Revell LJ. phytools: an R package for phylogenetic comparative biology (and other things). *Met Ecol Evol*. 2012; 3: 217–223. <https://doi.org/10.1111/j.2041-210X.2011.00169.x>
37. Stadler T. TreeSim: Simulating Phylogenetic Trees. R package version 2.3.; 2019; <https://CRAN.R-project.org/package=TreeSim>
38. Piras P, Silvestro D, Carotenuto F, Castiglione S, Kotsakis A, Maiorino L, et al. Evolution of the saber-tooth mandible: A deadly ecomorphological specialization. *Palaeogeogr Palaeoclimatol Palaeoecol*. Elsevier; 2018; 496: 166–174. <https://doi.org/10.1016/j.palaeo.2018.01.034>
39. Christiansen P. Canine morphology in the larger Felidae: implications for feeding ecology. *Biological Journal of the Linnean Society*. Blackwell Publishing Ltd; 2007; 91: 573–592. <https://doi.org/10.1111/j.1095-8312.2007.00819.x>
40. Stayton, CT. conveyol: Analysis of Convergent Evolution. R package version 1.3; 2018; <https://CRAN.R-project.org/package=convevol>
41. Mw Demment, Pj Vansoest. A Nutritional Explanation for Body-Size Patterns of Ruminant and Nonruminant Herbivores. *Am Nat*. 1985; 125: 641–672. <https://doi.org/10.1086/284369>
42. Figueirido B, Janis CM, Pérez-Claros JA, De Renzi M, Palmqvist P. Cenozoic climate change influences mammalian evolutionary dynamics. *Proceedings of the National Academy of Sciences*. National Academy of Sciences; 2012; 109: 722–727. <https://doi.org/10.1073/pnas.1110246108> PMID: 22203974
43. Janis CM. Tertiary mammal evolution in the context of changing climates, vegetation, and tectonic events. *Annu Rev Ecol Syst*. 1993; 24: 467–500. <https://doi.org/10.1146/annurev.es.24.110193.002343>

44. Mendoza M, Janis CM, Palmqvist P. Characterizing complex craniodental patterns related to feeding behaviour in ungulates: a multivariate approach. *J Zool.* 2002; 258: 223–246. <https://doi.org/10.1017/S0952836902001346>
45. Damuth J, Janis CM. On the relationship between hypsodonty and feeding ecology in ungulate mammals, and its utility in palaeoecology. *Biol Rev.* 2011; 86: 733–758. <https://doi.org/10.1111/j.1469-185X.2011.00176.x> PMID: 21418504
46. Raia P, Carotenuto F, Meloro C, Piras P, Pushkina D. The shape of contention: adaptation, history, and contingency in ungulate mandibles. *Evolution.* 2010; 64: 1489–1503. <https://doi.org/10.1111/j.1558-5646.2009.00921.x> PMID: 20015238
47. Raia P, Carotenuto F, Passaro F, Piras P, Fulgione D, Werdelin L, et al. Rapid action in the Palaeogene, the relationship between phenotypic and taxonomic diversification in Coenozoic mammals. *Proc R Soc B Biol Sci.* 2013; 280: 20122244–20122244. <https://doi.org/10.1098/rspb.2012.2244> PMID: 23173207
48. Mahler DL, Ingram T, Revell LJ, Losos JB. Exceptional Convergence on the Macroevolutionary Landscape in Island Lizard Radiations. *Science. American Association for the Advancement of Science;* 2013; 341: 292–295. <https://doi.org/10.1126/science.1232392> PMID: 23869019
49. Mahler DL, Revell LJ, Glor RE, Losos JB. Ecological opportunity and the rate of morphological evolution in the diversification of greater antillean anoles. *Evolution.* Blackwell Publishing Inc; 2010; 64: 2731–2745. <https://doi.org/10.1111/j.1558-5646.2010.01026.x> PMID: 20455931
50. Sanger TJ, Revell LJ, Gibson-Brown JJ, Losos JB. Repeated modification of early limb morphogenesis programmes underlies the convergence of relative limb length in *Anolis* lizards. *Proc R Soc B Biol Sci.* 2012; 279: 739–748. <https://doi.org/10.1098/rspb.2011.0840> PMID: 21849319
51. Losos JB. Convergence, adaptation, and constraint. *Evolution.* 2011; 65: 1827–1840. <https://doi.org/10.1111/j.1558-5646.2011.01289.x> PMID: 21729041
52. Piras P, Maiorino L, Raia P, Marcolini F, Salvi D. Functional and phylogenetic constraints in Rhinocerotinae craniodental morphology. *Evol Ecol Res.* 2010; 128: 897–928.
53. Meloro C, Clauss M, Raia P. Ecomorphology of Carnivora challenges convergent evolution. *Org Divers Evol.* 2015; 15: 711–720. <https://doi.org/10.1007/s13127-015-0227-5>
54. Arbuckle K, Bennett CM, Speed MP. A simple measure of the strength of convergent evolution. Münkemüller T, editor. *Met Ecol Evol.* 2014; 5: 685–693. <https://doi.org/10.1111/2041-210X.12195>
55. Christiansen P. Canine morphology in the larger Felidae: implications for feeding ecology. *Biol J Linn Soc.* 2007; 91: 573–592. <https://doi.org/10.1111/j.1095-8312.2007.00819.x>
56. Meachen-Samuels JA. Morphological convergence of the prey-killing arsenal of sabertooth predators. *Paleobiology.* 2012; 38: 1–14. <https://doi.org/10.1017/S0094837300000373>

Chapter 3 - A method for mapping morphological convergence on three-dimensional digital models: the case of the mammalian sabre-tooth

TECHNICAL REPORT

A METHOD FOR MAPPING MORPHOLOGICAL CONVERGENCE ON THREE-DIMENSIONAL DIGITAL MODELS: THE CASE OF THE MAMMALIAN SABRE-TOOTH

by MARINA MELCHIONNA¹ , ANTONIO PROFICO² ,
SILVIA CASTIGLIONE¹ , CARMELA SERIO³ ,
ALESSANDRO MONDANARO⁴ , MARIA MODAFFERI¹,
DAVIDE TAMAGNINI⁵ , LUIGI MAIORANO⁵ , PASQUALE RAIA^{1,*} ,
LAWRENCE M. WITMER⁶ , STEPHEN WROE⁷  and
GABRIELE SANSALONE⁷ 

¹Dipartimento di Scienze della Terra, dell'Ambiente e delle Risorse, Università di Napoli Federico II, 80126 Napoli, Italy; pasquale.raia@unina.it

²PalaeoHub, Department of Archaeology & Hull York Medical School, University of York, Heslington, UK

³Research Centre in Evolutionary Anthropology & Palaeoecology, School of Biological & Environmental Sciences, Liverpool John Moores University, Liverpool, UK

⁴Dipartimento di Scienze della Terra, Università degli studi di Firenze, 50121 Firenze, Italy

⁵Department of Biology & Biotechnologies 'Charles Darwin', University of Rome 'La Sapienza', viale dell'Università 32, 00185 Rome, Italy

⁶Department of Biomedical Science, Heritage College of Osteopathic Medicine, Ohio University, Athens, OH 45701 USA

⁷Function, Evolution & Anatomy Research Lab, Zoology Division, School of Environmental & Rural Science, University of New England, Armidale, NSW 2351 Australia

*Corresponding author

Typescript received 10 August 2020; accepted in revised form 12 March 2021

Abstract: Morphological convergence can be assessed using a variety of statistical methods. None of the methods proposed to date enable the visualization of convergence. All are based on the assumption that the phenotypes either converge, or do not. However, between species, morphologically similar regions of a larger structure may behave differently. Previous approaches do not identify these regions within the larger structures or quantify the degree to which they may contribute to overall convergence. Here, we introduce a new method to chart patterns of convergence on three-dimensional models using the R function *conv.map*. The convergence between pairs of models is mapped onto them to visualize and quantify the morphological convergence. We applied *conv.map* to a well-known case study, the sabre-tooth morphotype, which has evolved independently among distinct mammalian clades from placentals to metatherians. Although previous authors

have concluded that sabre-tooths kill using a stabbing 'bite' to the neck, others have presented different interpretations for specific taxa, including the iconic *Smilodon* and *Thylacosmilus*. Our objective was to identify any shared morphological features among the sabre-tooths that may underpin similar killing behaviours. From a sample of 49 placental and metatherian carnivores, we found stronger convergence among sabre-tooths than for any other taxa. The morphological convergence is most apparent in the rostral and posterior parts of the cranium. The extent of this convergence suggests similarity in function among these phylogenetically distant species. In our view, this function is most likely to be the killing of relatively large prey using a stabbing bite.

Key words: morphological convergence, *search.conv*, Felidae, Barbourfelidae, Thylacosmilidae, sabre-tooth carnivore.

CONVERGENCE implies the evolution of functionally analogous body parts shared by distantly related species (Losos 2011; Wake *et al.* 2011) and it remains widely studied and reported in the biological and palaeontological literature. Commonly cited cases include neck elongation in sauropods and giraffes (Sander *et al.* 2010),

high-crowned molars in grazing mammals (Janis 2008; Raia *et al.* 2011), the trenchant-heeled condition characterizing the lower molars of hypercarnivorous canids (Van Valkenburgh 2007) and the elongated upper canines (sabres) occurring in a number of carnivorous mammals (Wroe *et al.* 2008). Although an array of different

methods have been proposed to study patterns of convergence (Harmon *et al.* 2005; Stayton 2006; Adams & Collyer 2009; Muschick *et al.* 2012; Ingram & Mahler 2013; Stayton 2015; Castiglione *et al.* 2019) most of these are limited to a simple positive or negative inference. With few exceptions, such as convergence on similar body plans in some fast-swimming marine vertebrates (Lingham-Soliar 2016), studies of morphological convergence have targeted specific body parts (e.g. sabres, long necks, or wings) rather than the larger structures or bodies of which they are part. Excepting a few self-evident cases, currently available methods can determine whether convergence is present, but not identify specific regions within the larger structures and quantify the degree to which they contribute to convergence (McGhee 2011). This may impose limitations when assessing whether convergence is restricted to superficial morphological resemblance, or whether it is a consequence of shared selective pressures (Wainwright 2007; Moen 2019). For instance, by combining finite element analysis and geometric morphometrics to investigate humeral shape in fossorial mammals, Sansalone *et al.* (2020) noted that convergence among digging moles can only be demonstrated when mechanical performance is taken into account with morphology. Almost to the contrary, shared morphologies in sabre-toothed carnivores may obscure a rich functional diversity within the group (Lautenschlager *et al.* 2020). These examples highlight the difference between morphological convergence, which relates to simple phenotypic similarity, and functional convergence, which may take place even without phenotypic resemblance.

We have recently developed a novel and rapid method to address morphological convergence, deployed with the R function *search.conv* (Castiglione *et al.* 2019) embedded in the package *RRphylo* (Castiglione *et al.* 2018). This approach permits the identification of the pattern between entire clades or across unrelated species sparsely occurring across a phylogeny. The *search.conv* function computes the angle between vectors of principal component (PC) scores retrieved from geometric morphometric (GM) data to assess whether two shapes (vectors of PC scores) are morphologically closer (i.e. have a smaller angle between them) than would be predicted by their phylogenetic distance alone. Since principal component analysis (PCA) ordination of GM data represents both affine and non-affine components of shape variation, identifying the PC axes responsible for the pattern of convergence allows us to chart it on the focal biological shapes, then map and quantify the degree to which individual regions contribute to overall convergence on the structures under study. These concepts are central to the new methodology we present here: *conv.map*.

To illustrate how *conv.map* works, we have applied the method to address a classic example of convergence: the independent evolution of sabre-tooth morphology in

mammalian carnivore lineages. All sabre-tooths are defined by the possession of elongated, laterally flattened upper canines (Emerson & Radinsky 1980; Christiansen 2008), which are widely thought to have been applied in the dispatch of relatively large prey (Akersten 1985; McHenry *et al.* 2007).

Variability in skull and postcranial morphology, for example, relative length of the canines and robusticity of the forelimbs, have led researchers to posit differences in killing behaviour between sabre-toothed species (Duckler 1997; Christiansen 2008; Slater & Van Valkenburgh 2008; Christiansen 2011; Figueirido *et al.* 2018). However, most researchers, including those above, have concluded that, notwithstanding these differences, all mammalian sabre-tooths specialized in killing relatively large prey with slashing bites to the neck, as opposed to suffocation through a clamp-and-hold bite that typifies conical toothed cats (Wroe *et al.* 2013; Figueirido *et al.* 2018).

Mechanical modelling has demonstrated that sabre-tooths perform poorly relative to conical toothed predators in lateral shaking of the skull and jaw adductor driven bites, but are better adapted to resist stabbing, dorsoventral ‘bites’ driven by neck muscles. On the basis of finite element-based studies that have included both conical and sabre-toothed species, a continuum has been proposed wherein sabre-tooths with increasingly longer canines are characterized by an increasing capacity to resist stabbing forces, but a diminishing ability to resist laterally directed forces (McHenry *et al.* 2007; Wroe *et al.* 2013; Figueirido *et al.* 2018). However, some authors have proposed widely disparate killing and feeding behaviours, including killing bites to the belly as opposed to the neck, and diets comprised of internal organs, or blood, as opposed to meat. These suggestions have been proposed for both placental (*Smilodon fatalis*) and metatherian (*Thylacosmilus atrox*) taxa (Merriam & Stock 1932; Akersten 1985; Janis *et al.* 2020). Perhaps the most divergent hypothesis forwarded in recent times suggests that the taxon characterized by the most hypertrophied canines of any sabre-tooth, the metatherian *T. atrox*, was not a predator at all, but a highly specialized scavenger (Janis *et al.* 2020).

If killing and feeding behaviour did differ greatly between sabre-tooth taxa, then we might expect to find that similarities in cranial shape were localized and not shared across the functionally relevant regions of the cranium for all taxa. Our objectives here were therefore to determine how many and to what degree different anatomical regions of the cranium were shared across very distantly related clades, and whether these differences were significant.

To address this question, we applied our methodology to a large sample comprising two placental sabre-tooth families, the single known metatherian sabre-tooth, and a wide range of other carnivorous taxa.

MATERIAL AND METHOD

Data preparation

Thirty-two homologous landmarks were sampled manually on 92 specimens. The landmark configuration defines the shape of the dorsal regions of the cranium, including the maxillary bones and the tooth sockets. We excluded the zygomatic arch from the sampling since in fossil specimens it is rarely preserved. We then placed and slid 1000 bilateral semi-landmarks (500 on each side) automatically using the ‘Morpho’ R package (Schlager *et al.* 2020). Taxa included a barbourioid, a dirk-toothed and a scimitar-toothed felid among placentals. We also sampled a range of extant conical toothed cats including *Neofelis* which displays the most morphological features common to extinct sabre-tooths among extant felids (Christiansen 2008). Among metatherians we included the sparassodont *Thylacosmilus atrox*, as well as dasyuromorphians, and the diprotodontian *Thylacoleo carnifex* to provide species phylogenetically close to *Thylacosmilus*. Altogether our data set comprised 49 extant and extinct species (see Melchionna *et al.* 2020, appendix S1 for details).

Taphonomic distortion was present in two fossil specimens (*Barbourioides fricki*, *Homotherium serum*). We symmetrized these (see Melchionna *et al.* 2020, appendix S1 for details) using the function *retroDeformMesh* (Schlager *et al.* 2018). Procrustes superimposition was applied using generalized Procrustes analysis (GPA), implemented with the *procSym* function of the R package ‘Morpho’. GPA rotates, translates and scales landmark configurations to the unit centroid size, that is, the square root of squared differences between landmark coordinates and Centroid coordinates. After GPA, we applied ordination to the aligned coordinates by means of PCA. The resulting PC scores were taken to represent the shape variables.

Searching for convergence

To perform convergence analysis, we implemented the felid tree embedded in the RRphylo package to add the metatherians included in the analysis (see Melchionna *et al.* 2020, appendix S1 for details). We used the tree and shape data to feed the RRphylo package function *search.conv* (Castiglione *et al.* 2019). This function assesses convergence by testing whether phenotypes in distant clades in a phylogenetic tree are more similar to each other than expected from their phylogenetic distance. Phenotypes are represented by vectors of PC scores derived from geometric morphometric data analysis. Since PC axes have a score equal to zero at their intersection, the phenotypic vectors are calculated in relation to the origin of PC axes (the consensus shape in geometric

morphometrics) and the angle they form represents a correlation coefficient. The angle actually spans from 0° to 180°. An angle close to 0° means convergence in shapes, whereas angles around 90° means dissimilarity, and angles close to 180° indicate phenotypes evolving in an opposite direction to the consensus. As the function is also able to test for convergence within one state (or more), we applied *search.conv* to the sabre-tooth group to verify the convergence in the skull shape within the category.

Relative warp analysis

The use of *search.conv* enables us to identify species which show convergent phenotypes. For that purpose, using PCA is ideal as it decomposes the variability of the sample into orthogonal axes describing shape variation around the sample mean shape. However, convergence implies large scale, non-affine shape variation which is best inspected by means of PCA of partial warp scores (relative warp analysis, RWA) weighted by a factor $\alpha > 0$ (α spans from $-\infty$ to $+\infty$; at $\alpha = 0$ RWA corresponds to PCA so that the affine and non-affine components of shape variation are not separated, Rohlf 1993; Rohlf & Bookstein 2003). In the case study reported here, we performed RWA using the Morpho function *relWarp* (Schlager *et al.* 2020) setting the α parameter to 1. Then, we extracted the relative warp scores (RW scores) and the relative warps vectors (RWs).

Mapping convergence

We developed the *conv.map* function to visualize the relative intensity of convergence on 3D surfaces. Although we recommend using RWA with α parameter set to 1, we note that RW scores or PC scores could be used. Given two phenotypic vectors p_1 and p_2 (i.e. vectors of RW scores or PC scores for any two species or group of species found to converge) of length n , the angle α between them is geometrically equivalent to the correlation coefficient between the vectors (Zelditch *et al.* 2012; Castiglione *et al.* 2019). Removing a pair i of corresponding RW scores from both vectors produces the angle α_i between the remaining scores $p_{1[-i]}$ and $p_{2[-i]}$ of length $n-1$. If the removed pair of scores is important to phenotypic similarity $\alpha_i < \alpha$, and vice versa. In *conv.map*, pairs of corresponding RW scores are removed one pair at a time, and the angle between the vectors of remaining RWs computed each time. After the entire procedure is accomplished, the resulting angles $\alpha_{[1..n]}$ are collated into a vector, from the largest to the smallest. This vector would be flat if all RWs are equally responsible for the phenotypic distance between the two original shape vectors. However, RWA decomposes shape

variance in orthogonal axes of maximum variation of decreasing importance, so that the vector of ordered $\alpha_{[1..n]}$ typically presents one or two inflection points. The first inflection point sets apart RW axes which contribute the most to the pattern of convergence (so that removing any one of them provides an angle $\alpha_i \ll \alpha$). The second inflection point, if present, identifies the RW axes responsible for the most important shape differences between the two phenotypic vectors. To locate the first inflection point and therefore select the PC axes responsible for convergence, we applied the function *ede* in the R package ‘inflection’ (Christopoulos 2019). *ede* performs an extreme distance estimator (Christopoulos 2012; Christopoulos 2016) to efficiently locate the inflection points along a curve. By finding the first inflection point the $RW_{conv1,2}$ matrix of $k \times 2$ RW set of scores (one set of k corresponding RW axes for each species) is extracted from the ρ_1 and ρ_2 vectors. This procedure is analogous to the scree plot criterion commonly used for the selection of ‘relevant’ axes in PCA. It differs from the scree plot in that rather than selecting the PC axes explaining (cumulatively) most of the variance, it selects the $RW_{conv1,2}$ set of scores in ρ_1 and ρ_2 that maximizes their similarity.

To evaluate the statistical significance of the RW axes selection procedure, *conv.map* computes the angle α_{conv} between the two vectors in $RW_{conv1,2}$. Then, 10 000 angles are computed by randomly selecting from ρ_1 and ρ_2 pairs of corresponding RW scores of length k and testing whether α_{conv} is smaller than 5% of the random angles, which is expected to occur if ρ_1 and ρ_2 represent convergent shapes and $RW_{conv1,2}$ effectively represents the subset of RW axes that best account for convergence.

We used $RW_{conv1,2}$ to retrieve a new landmark configuration using the *showPC* function in ‘Morpho’. The new configurations (one for each compared group or species) are weighted on the variance responsible for convergence. The function automatically reconstructs a 3D mesh by using the ball-pivoting algorithm (Bernardini *et al.* 1999) as embedded in the *vcgBallPivoting* function in the R package *Rvcg* (Schlager & Girinon 2017). Starting from the new surfaces, *conv.map* estimates the area differences between corresponding triangles of each 3D mesh and the consensus shape mesh of the original RWA (including all species). If the selected groups (or species) are convergent, they should present the same pattern of variation in the same regions of the 3D surface, as compared to the consensus shape. Convergent areas will therefore show small variation (plotted in colour shades), whereas non convergent regions of the 3D surface will be plotted in white. The same procedure could be generalized to >2 shape vectors at once. In this case, the user has to supplement *conv.map* with a p shape vector for each species, and indicate which species were found to converge. Given j species, the function will calculate all the $RW_{conv1..j}$

matrices (one for each pairwise comparison), and selects the RW axes that appear more than once in the $RW_{conv1..j}$ matrices. By default, if $j > 2$ shape vectors are provided, comparisons of convergence mapping are plotted against the consensus shape, alongside pairwise comparisons.

To summarize, the *conv.map* function works as follows:

1. The RW scores responsible for the morphological convergence are selected from ρ_1 and ρ_2 shape vectors.
2. The landmark configurations of the selected species (or means of species groups) are reconstructed using only the RW scores and RWs (the $RW_{conv1,2}$ matrix) responsible for convergence.
3. Triangle meshes of both the landmark configurations referring to ρ_1 and ρ_2 ; and consensus shape are interpolated using the ball-pivoting algorithm.
4. Each surface referring to ρ_1 and ρ_2 is compared to the consensus shape, and 3D mesh triangles areas differences are computed.
5. The mesh triangle areas referring to $RW_{conv1,2}$ are calculated and plotted on the 3D surfaces.

The function also provides the opportunity to exclude some RW axes from the analysis. That is because, for example, in most cases RW1 mostly captures high-order morphological differences driven by phylogeny and size variation in the sample.

As input data, *conv.map* needs: the data frame with the RW (or PC) scores of each group or species to be compared (ρ_1 and ρ_2 dataset); the matrix of RW (or PC) vectors; the consensus configuration (*mshape*); the number of the RW (or PC) that will be excluded from the comparison, if needed (*exclude* = NULL as default setting) (Table 1).

The function returns the index of the RW axes selected in $RW_{conv1,2}$, the angle α between ρ_1 and ρ_2 , the angle α_{conv} between the two vectors in $RW_{conv1,2}$, the angle difference $\alpha - \alpha_{conv}$, the p value for α_{conv} , and plots the 3D surfaces coloured according to the convergence pattern represented by $RW_{conv1,2}$ (Table 2).

Applications of conv.map to sabre-teeths

To chart convergence on sabre-tooth mammals, we first computed mean RW scores for all species in the tree. We treated *Barbourofelis*, *Homotherium*, *Smilodon* and *Thylacosmilus* as sabre-teeths and ran *search.conv* using all PCs as the multivariate dataset representing shape. Alternative classifications of sabre-teeths failed to find convergence for *Neofelis* and *Yoshi*, despite the fact that they are frequently cited as either showing traits shared with sabre-teeths (the former) or belong to the machairodontinae family (the latter). Then, we used *conv.map* starting from a RWA with $\alpha = 1$ to perform a pairwise comparison between sabre-teeths and the consensus shape. We further compared *Barbourofelis fricki* against machairodont

TABLE 1. Explanation of *conv.map* arguments.

Argument name	Explanation
dataset	Data frame (or matrix) with the RW (or PC) scores of the group or species to be compared
pcs	RW (or PC) vectors of all the samples
mshape	The consensus configuration
conv	A named character vector indicating convergent species as ('conv' in 'dataset') and not convergent species ('noconv')
exclude	Integer: the index number of the RW (or PC) to be excluded from the comparison
out.rem	Logical: if TRUE triangles with outlying area difference are removed
show.consensus	Logical: if TRUE, the consensus configuration is included in the comparison
plot	Logical: if TRUE, the pairwise comparisons are plotted; for more than 5 pairwise comparisons, the plot is not shown
col	Character: the colour for the plot
names	Logical: if TRUE, the names of the groups or species are displayed in the 3D plot

TABLE 2. Explanation of *conv.map* returned values.

Value	Explanation
angle.compare	Data frame including the real angles α between the given shape vectors, the angles α_{conv} computed between vectors of the selected RWs (or PCs), the angles between vectors of the non-selected RWs (or PCs), the difference $\alpha - \alpha_{\text{conv}}$, and its p -values
selected.pcs	RWs (or PCs) axes selected for convergence
average.dist	Symmetrical matrix of pairwise distances between 3D surfaces
surfaces1	List of coloured surfaces; if two meshes are given, it represents convergence between mesh A and B charted on mesh A
surfaces2	List of coloured surfaces; if two meshes are given, it represents convergence between mesh A and B charted on mesh B
scale	The value used to set the colour gradient, computed as the maximum of all differences between each surface and the mean shape

cats (averaging the shapes of *Smilodon* and *Homotherium*) and against *Thylacosmilus atrox*.

RESULTS

The *search.conv* analysis revealed that among carnivores, only species within the sabre-tooth category displayed

significant convergence (mean angle = 43.88°; $p = 0.017$). The pairwise angle comparison between *Barbourofelis*, *Homotherium*, *Smilodon* and *Thylacosmilus* is reported in Table 3A. The angle differences (angles computed between scores vectors of the selected RWs against angles between vectors of the non-selected RWs) of all the convergent groups comparisons are significant, while the comparison with the consensus shape is marginally or not significant for each of the sabre-tooths (Table 3A). *Barbourofelis fricki* and *Homotherium serum* have the lowest distances among all pairwise comparisons, which is also evident in the convergence plots (Fig. 1). All sabre-toothed carnivores are equally distant from the consensus shape (Table 3B). The 3D surfaces comparison reveals a marked similarity in the premaxillary and carnassial areas, and in the occipital region on and around the nuchal crest. The difference pattern against the consensus is similar for all sabre-tooth taxa (Fig. 1).

When *Barbourofelis*, the average machairodont cat skull, *Thylacosmilus*, and the consensus shapes are compared to each other, the angle differences for the convergent species are the only statistically significant (or marginally significant) example detected (Table 4A). The average area difference between *Barbourofelis fricki* and the machairodont cats is the smallest, with surfaces showing great affinity in overall shape. *Thylacosmilus atrox* is closer to *Barbourofelis fricki* than to the machairodonts, with a marked similarity in the muzzle area. All groups are distant from the consensus shape (Table 4B, Fig. 2).

DISCUSSION

Convergence is an evolutionary pattern whereby species belonging to distant lineages develop similar structures to perform the same function (Wainwright 2007; Wroe & Milne 2007; Losos 2011; McGhee 2011). Although a variety of methods have been proposed to test for this pattern (Stayton 2006; Arbuckle *et al.* 2014; Speed & Arbuckle 2016; Castiglione *et al.* 2019), they have invariably focused on the recognition of its statistical significance, making the assumption that the shapes under scrutiny contribute isotropically as a whole. However, the evolution of convergent functions may trace to different morphological trajectories (i.e. one to many mapping, Alfaro *et al.* 2005; Serb *et al.* 2017; Renaud *et al.* 2018) and convergence may fail to apply when the objects' functional performance is ignored (Sansalone *et al.* 2020) meaning that the structural properties of the study objects must be acknowledged (Janis *et al.* 2020). Revealing such particularities is possible by inspecting how different areas of the study objects contribute to the pattern of convergence. This is the aim of the current study. By rendering a visual representation of the relative contribution to

TABLE 3. Pairwise comparisons between *Barbourofelis*, *Homotherium*, *Smilodon*, *Thylacosmilus* and the consensus shape: A, pairwise angle comparison; B, pairwise average area differences, rescaled from 0 to 1.

A	Real angle	Selected	Others	Angle difference	p-value
<i>Smilodon</i> – <i>Thylacosmilus</i>	53.351	14.929	143.828	–128.899	<0.001
<i>Barbourofelis</i> – <i>Homotherium</i>	28.620	15.326	64.012	–48.686	<0.001
<i>Homotherium</i> – <i>Smilodon</i>	23.460	20.467	33.301	–12.834	0.061
<i>Barbourofelis</i> – <i>Thylacosmilus</i>	48.382	24.667	117.860	–93.192	<0.001
<i>Barbourofelis</i> – <i>Smilodon</i>	36.887	26.532	76.896	–50.364	0.010
<i>Homotherium</i> – <i>Thylacosmilus</i>	59.022	27.838	138.987	–111.149	<0.001
<i>Barbourofelis</i> –consensus	81.170	45.770	84.033	–38.263	0.067
<i>Thylacosmilus</i> –consensus	87.711	54.637	95.968	–41.331	0.090
<i>Homotherium</i> –consensus	83.943	61.016	86.508	–25.492	0.354
<i>Smilodon</i> –consensus	85.859	66.651	89.063	–22.412	0.366

B	<i>Barbourofelis</i>	<i>Homotherium</i>	<i>Smilodon</i>	<i>Thylacosmilus</i>	Consensus
<i>Barbourofelis</i>	–	0.053	0.069	0.080	0.213
<i>Homotherium</i>	0.053	–	0.066	0.112	0.172
<i>Smilodon</i>	0.069	0.066	–	0.075	0.205
<i>Thylacosmilus</i>	0.080	0.112	0.075	–	0.248
consensus	0.213	0.172	0.205	0.248	–

Real angle, the real angle between the given score vectors; Selected, the angles computed between scores vectors of the selected relative warp vectors (RWs); Others, the angles computed between scores vectors of the non-selected RWs; Angle difference, the difference between Selected and Other angle values; p-value, the statistical significance of the difference in angle between the selected and non-selected RWs.

convergence of different areas of the biological objects under consideration, *conv.map* helps to identify the morphological regions which may have important implications for functional convergence.

Because of its complexity and multipurpose functioning, the vertebrate skull represents an ideal study object to identify and quantify convergence. In the present study the only example of significant morphological convergence we detected within our sample was the sabre-tooth ecomorph. These four taxa share more anatomical features than any of other carnivore groups, suggesting that the influence of a strong selective pressure drove the iterated evolution of shared morphological features. The *conv.map* method revealed a range of shared anatomical features of particular importance. These were in the premaxillary area, the carnassial region, and in the occipital region around the nuchal crest, which were common to all sabre-tooth carnivores despite considerable phylogenetic distances, particularly with respect to *Thylacosmilus*. These areas are likely to enable the peculiar sabre-tooth killing behaviour, requiring masticatory muscle reorientation, strong neck musculature, low condyles and large gape to effectively use the infamous sabres. In our view this strongly supports the consensus view that despite some anatomical differences and possible functional diversification within sabre-tooths (Lautenschlager *et al.* 2020), the sabre-tooth morphotype universally confers a broadly comparable capacity to hunt and rapidly kill relatively

large prey by applying a stabbing bite to the throat assisted by powerful neck muscles (Emerson & Radinsky 1980; Wroe *et al.* 2013), although this specialization may have led to their extinction at different times and locations when large prey became less abundant (Piras *et al.* 2018). Similarities in the rostral and dental areas are likely to represent functional adaptation related to relatively high loadings to which the muzzle was exposed when delivering these stabbing bites. In keeping with this, we found that convergence in sabre-tooths involves the facial region of the skull (particularly in the premaxillary and carnassial area). We also found close similarities in the morphology of occipital area, which was involved in extensive neck muscle depression of the cranium and pull in all sabre-tooths relative to other morphotypes (Duckler 1997; Christiansen 2008). The neurocranium, nasals, and maxillary regions show no bearing on convergence among sabre-tooths and set *Thylacosmilus* apart (Table 4, Fig. 2). Intriguingly, the barbourofelid *Barbourofelis* sits closer to the felid *Homotherium* than it does to *Smilodon*, probably because of similarity in their incisor arcades (Biknevicius *et al.* 1996). We detected greater similarity between *Thylacosmilus* and *Barbourofelis*, suggesting that the metatherian sabre-tooth converged more completely on the highly specialized barbourofelid. Previous work has suggested that these taxa converge on the presence of very long canines, a postorbital bar, mandibular flanges and a number of postcranial characters (Prevosti *et al.* 2012).



FIG. 1. Visualization of the pairwise comparisons of *Barbourofelis*, *Homotherium*, *Smilodon*, *Thylacosmilus*, and the consensus configuration. The colour gradient indicates area differences between the two surfaces. Blue indicates no difference (scale bar rescaled into the range 0–1). In each case, differences between the two taxa are displayed on a reconstruction of the taxon named on the left.

Our findings support the hypothesis that the patterns of convergence on the sabre-tooth cranium provided by the *conv.map* method indicate first-order functional significance, although secondary functional diversity may take place among sabre-tooths (Lautenschlager *et al.* 2020). The absence of convergence in the neurocranium and nasal area is consistent with previously identified features that are not indicative of prey choice or killing method (e.g. the smaller brain of the metatherian *Thylacosmilus*).

The most obvious example here is that the most phylogenetically distant of sabre-tooth taxa, *Thylacosmilus*, is strongly convergent on placental sabre-tooths across regions of the cranium widely considered to be functionally significant. However, a recent study addressing the mechanical performance of *Thylacosmilus* (Janis *et al.* 2020) proposes a very different ecology. Their FEA-based analysis suggested a greater capacity to exert pulling forces in *Thylacosmilus* than in *Smilodon*. It was inferred

TABLE 4. Pairwise comparisons between *Barbourofelis*, machairodont cats (average of *Homotherium* plus *Smilodon*), *Thylacosmilus* and the consensus shape: A, pairwise angle comparison; B, pairwise average area differences, rescaled from 0 to 1.

A	Real angle	Selected	Others	Angle difference	p-value
<i>Barbourofelis</i> – <i>Thylacosmilus</i>	48.382	3.941	93.912	–89.971	0.009
<i>Barbourofelis</i> – Machairodont cats	12.455	7.300	18.475	–11.175	0.073
Machairodont cats – <i>Thylacosmilus</i>	51.846	11.241	103.093	–91.852	0.012
<i>Thylacosmilus</i> –consensus	87.711	51.603	94.427	–42.824	0.285
<i>Barbourofelis</i> –consensus	81.170	55.544	81.629	–26.085	0.413
Machairodont cats – consensus	82.141	62.844	81.833	–18.989	0.474

B	<i>Barbourofelis</i>	Machairodont cats	<i>Thylacosmilus</i>	Consensus
<i>Barbourofelis</i>	–	0.039	0.054	0.347
Machairodont cats	0.039	–	0.085	0.308
<i>Thylacosmilus</i>	0.054	0.085	–	0.371
Consensus	0.347	0.308	0.371	–

Real angle, the real angle between the given score vectors; Selected, the angles computed between scores vectors of the selected relative warp vectors (RWs); Others, the angles computed between scores vectors of the non-selected RWs; Angle difference, the difference between Selected and Other angle values; p-value, the statistical significance of the difference among the angles between the selected and non-selected RWs.

on this basis that *Thylacosmilus* did not deploy killing behaviour common to other sabre-tooths that distinguished them from conical-toothed predators and that it may have been a scavenger. We do not contest the possibility that *Thylacosmilus* was better adapted to exert pulling behaviour, because the only other FEA-based study to include these two taxa did not apply a neck-pulling load case (Wroe *et al.* 2013). On the other hand, we do note that the study of Janis *et al.* (2020) did not include any conical-toothed taxa by way of comparison, whereas the earlier study (Wroe *et al.* 2013) included the conical-toothed *Panthera pardus*. Wroe *et al.* (2013) found that *Thylacosmilus* was better adapted to deliver a stabbing bite that was reliant on head depressing neck musculature than was *Smilodon*, but that both were superior in this respect to *Panthera pardus*. We suggest that *Thylacosmilus* was better adapted to deliver both neck-driven head pulling and depressing functions, but without applying a head-pull load case to a conical-toothed cat as well as to other sabre-tooths there is no mechanics-based evidence to indicate whether a capacity to deliver a head pull is a further defining feature of sabre-tooths or not. As well as FEA-based analysis, an intriguing feature of *Thylacosmilus* identified by Janis *et al.* (2020), determined on the basis of dental microwear patterns, was that *Thylacosmilus* did not habitually consume meat or bone. This raises the possibility that the metatherian sabre-tooth's diet was largely restricted to soft internal organs such as the heart, lungs and liver. These characteristics would make *Thylacosmilus* truly unique among mammalian scavengers, which

typically do consume both bone and meat, as well as internal organs. However, large extant mammalian predators commonly consume these internal organs preferentially over meat and bone (Schaller 1972). We consider it more likely that *Thylacosmilus* may have concentrated on the internal organs of prey it had killed, rather than the carcasses of animals killed by other large South American carnivores (e.g. phorusrhacid birds), which were unlikely to have eaten only meat and/or bone and left the internal organs untouched. Sabre-tooths are characterized by relatively weak jaw closing muscles but large head depressors (Wroe *et al.* 2005; Christiansen 2011). *Thylacosmilus* is extreme with regard to both features (Wroe *et al.* 2013), and we contend that together with the evidence for a diet comprised largely of soft internal organs, these characteristics point to an even more extreme example of sabre-tooth killing and feeding behaviour, as opposed to an entirely divergent ecomorph and diet.

CONCLUSION

The use of three-dimensional models has revolutionized the study of fossils in both palaeontology and palaeoanthropology (Cunningham *et al.* 2014). In morphometric analyses, the implementation of geometric morphometric techniques based on 3D configurations has driven the development of new protocols and software suitable for 3D surfaces. These new technologies allow researchers to virtually restore and realign disarticulated elements (Gunz

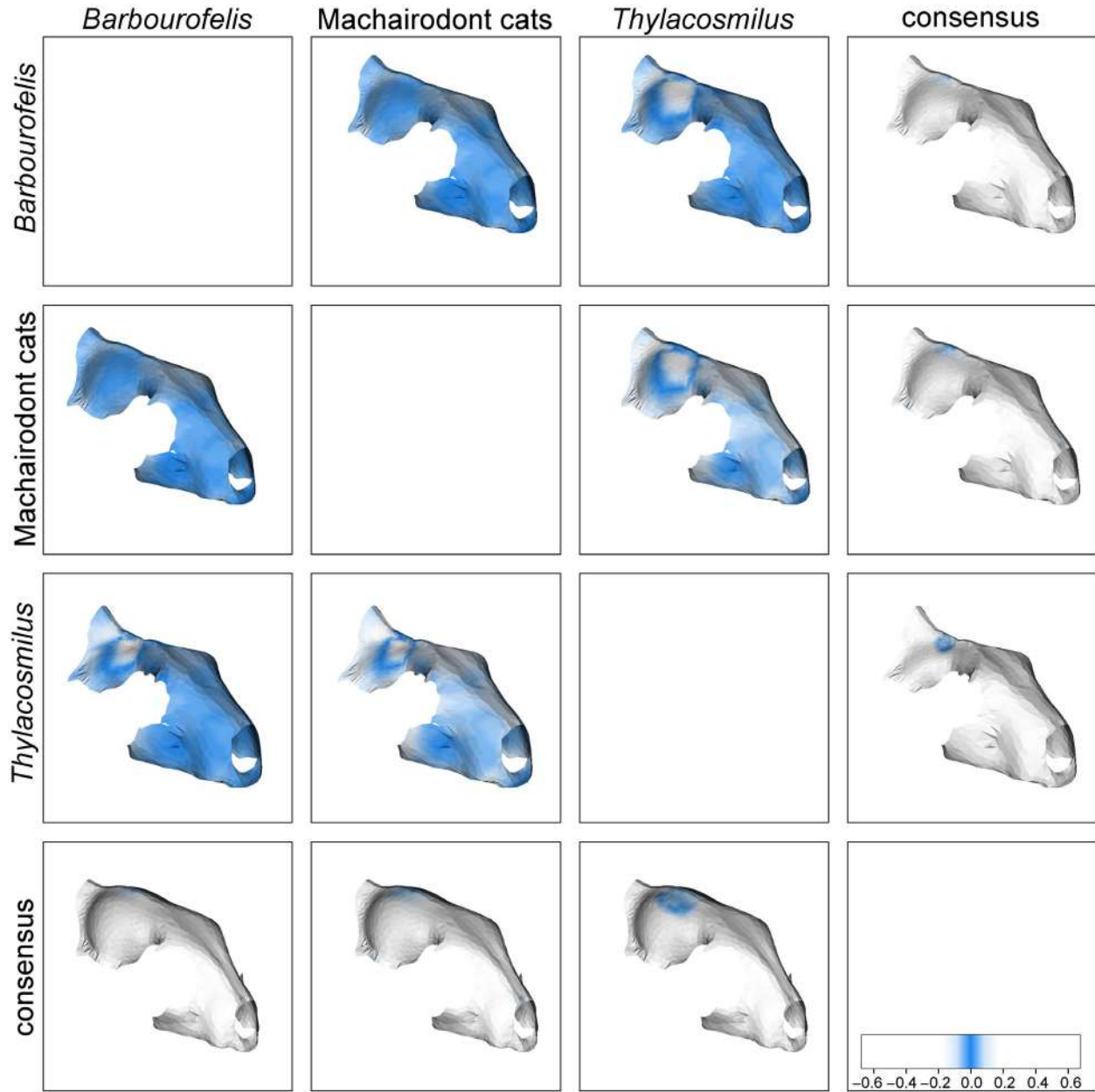


FIG. 2. Visualization of the pairwise comparison between *Barbourofelis*, machairodont cats (*Homotherium* plus *Smilodon*), *Thylacosmilus* and the consensus configuration. The colour gradient indicates area differences between the two surfaces. Blue indicates no difference (scale bar rescaled into the range 0–1). In each case, differences between the two taxa are displayed on a reconstruction of the taxon named on the left.

et al. 2009; Profico *et al.* 2019), and perform the retro-deformation of fossils (i.e. the process of removing distortions in fossils caused by taphonomic forces; Schlager *et al.* 2018) which now permit studying the functional and evolutionary aspects of 3D shape evolution with increased sampling and precision. Here we present a new implementation, named *conv.map*, which allows us to study how patterns of convergence unfold across 3D surfaces. By mapping the regions responsible for the pattern,

conv.map allows us to visualize and ascertain the functional significance of convergence of the biological structures under scrutiny.

Acknowledgements. We are grateful to Stephan Lautenschlager and an anonymous reviewer for providing important advice. 79 specimens included in the present study are from the PhD database of DT, whose PhD project received support from the ‘Avvio alla Ricerca 2019’ funding which is financed by the University of

Rome ‘La Sapienza’. DT also received support from the SYNTHESYS Access programme that is financed by the European Community Research Infrastructure Action under the FP7 (ES-TAF-2750 awarded to DT). LMW acknowledges support from the United States National Science Foundation (IOB-0517257, IOS-1050154, IOS-1456503). We owe a huge debt of thanks to all curators, collection managers and staff, whose help and support was fundamental for the sampling operations. In particular, with anticipated apologies for certainly forgetting to explicitly mention several of the many people to whom thanks are owed, we want to thank: Susana Fraile, Jorge Morales, G  rldine Veron, Aur  lie Verguin, Riccardo Castiglia, Cristiano Dal Sasso, Pierfilippo Cerretti, Adriano De Faveri, Saverio Bartolini Lucenti, Paolo Agnelli, Tony Parker, Itat   Olivares, Agust  n Ruella and Eul  lia Garcia Franquesa. We also want to thank Denis Geraads and Nikolai Spassov for providing DT with a copy of their 3D model of *Y. garevskii*.

Author contributions. MM and DT contributed equally. MM, AP, and PR conceived the study. MM, AP, PR, and SC prepared the code. MM, GS, DT, LW, AM and MMod contributed to collection and preparation of the study sample. MM, SW and PR lead the writing. All the authors contributed to the preparation of the manuscript.

DATA ARCHIVING STATEMENT

Data for this study are available in the Dryad Digital Repository: <https://doi.org/10.5061/dryad.9kd51c5g6>

Editor. Laura Porro

REFERENCES

- ADAMS, D. C. and COLLYER, M. L. 2009. A general framework for the analysis of phenotypic trajectories in evolutionary studies. *Evolution*, **63**, 1143–1154.
- AKERSTEN, W. A. 1985. Canine function in *Smilodon* (Mammalia; Felidae; Machairodontinae). *Natural History Museum of Los Angeles County, Contributions in Science*, **356**, 1–22.
- ALFARO, M. E., BOLNICK, D. I. and WAINWRIGHT, P. C. 2005. Evolutionary consequences of many-to-one mapping of jaw morphology to mechanics in labrid fishes. *The American Naturalist*, **165**, E140–E154.
- ARBUCKLE, K., BENNETT, C. M. and SPEED, M. P. 2014. A simple measure of the strength of convergent evolution. *Methods in Ecology & Evolution*, **5**, 685–693.
- BERNARDINI, F., MITTLEMAN, J., RUSHMEIER, H., SILVA, C. and TAUBIN, G. 1999. The ball-pivoting algorithm for surface reconstruction. *IEEE Transactions on Visualization & Computer Graphics*, **5** (4), 349–359.
- BIKNEVICIUS, A. R., VAN VALKENBURGH, B. and WALKER, J. 1996. Incisor size and shape: implications for feeding behaviors in saber-toothed ‘cats’. *Journal of Vertebrate Paleontology*, **16** (3), 510–521.
- CASTIGLIONE, S., TESONE, G., PICCOLO, M., MELCHIONNA, M., MONDANARO, A., SERIO, C., DI FEBBRARO, M. and RAIA, P. 2018. A new method for testing evolutionary rate variation and shifts in phenotypic evolution. *Methods in Ecology & Evolution*, **9**, 974–983.
- SERIO, C., TAMAGNINI, D., MELCHIONNA, M., MONDANARO, A., DI FEBBRARO, M., PROFICO, A., PIRAS, P., BARATTOLO, F. and RAIA, P. 2019. A new, fast method to search for morphological convergence with shape data. *PLoS One*, **14** (12), e0226949.
- CHRISTIANSEN, P. 2008. Evolutionary convergence of primitive sabertooth craniomandibular morphology: the clouded leopard (*Neofelis nebulosa*) and *Paramachairodus ogygia* compared. *Journal of Mammalian Evolution*, **15**, 155–179.
- 2011. A dynamic model for the evolution of sabrecat predatory bite mechanics. *Zoological Journal of the Linnean Society*, **162**, 220–242.
- CHRISTOPOULOS, D. T. 2012. Developing methods for identifying the inflection point of a convex/concave curve. *arXiv*, 1206.5478.
- 2016. On the efficient identification of an inflection point. *International Journal of Mathematics & Scientific Computing*, **6** (1), 2231–5330.
- 2019. inflection: Finds the inflection point of a curve. R package v.1.3.5. <https://cran.r-project.org/package=inflection>
- CUNNINGHAM, J. A., RAHMAN, I. A., LAUTENSCHLAGER, S., RAYFIELD, E. J. and DONOGHUE, P. C. J. 2014. A virtual world of paleontology. *Trends in Ecology & Evolution*, **29**, 347–357.
- DUCKLER, G. L. 1997. Parietal depressions in skulls of the extinct saber-toothed felid *Smilodon fatalis*: evidence of mechanical strain. *Journal of Vertebrate Paleontology*, **17**, 600–609.
- EMERSON, S. B. and RADINSKY, L. 1980. Functional analysis of sabertooth cranial morphology. *Paleobiology*, **6**, 295–312.
- FIGUEIRIDO, B., LAUTENSCHLAGER, S., P  REZ-RAMOS, A. and VAN VALKENBURGH, B. 2018. Distinct predatory behaviors in scimitar- and dirk- toothed sabertooth cats. *Current Biology*, **28**, 3260–3266.
- GUNZ, P., MITTEROECKER, P., NEUBAUER, S., WEBER, G. W. and BOOKSTEIN, F. L. 2009. Principles for the virtual reconstruction of hominin crania. *Journal of Human Evolution*, **57**, 48–62.
- HARMON, L. J., KOLBE, J. J., CHEVERUD, J. M. and LOSOS, J. B. 2005. Convergence and the multidimensional niche. *Evolution*, **59**, 409–421.
- INGRAM, T. and MAHLER, D. L. 2013. SURFACE: detecting convergent evolution from comparative data by fitting Ornstein-Uhlenbeck models with stepwise Akaike information criterion. *Methods in Ecology & Evolution*, **4**, 416–425.
- JANIS, C. 2008. An evolutionary history of browsing and grazing ungulates. 21–45. In GORDON, I. J. and PRINS, H. H. T. (eds). *The ecology of browsing and grazing*. Springer.
- FIGUEIRIDO, B., DESANTIS, L. and LAUTENSCHLAGER, S. 2020. An eye for a tooth: *Thylacosmilus* was not a marsupial ‘saber-tooth predator’. *PeerJ*, **8**, e9346-36.
- LAUTENSCHLAGER, S., FIGUEIRIDO, B., CASHMORE, D. D., BENDEL, E. M. and STUBBS, T. L. 2020. Morphological convergence obscures functional diversity in

- sabre-toothed carnivores. *Proceedings of the Royal Society B*, **287**, 20201818.
- LINGHAM-SOLIAR, T. 2016. Convergence in thunniform anatomy in lamnid sharks and Jurassic ichthyosaurs. *Integrative & Comparative Biology*, **56**, 1323–1336.
- LOSOS, J. B. 2011. Convergence, adaptation, and constraint. *Evolution*, **65**, 1827–1840.
- McGHEE, G. R. 2011. *Convergent evolution: Limited forms most beautiful*. MIT Press.
- McHENRY, C. R., WROE, S., CLAUSEN, P. D., MORENO, K. and CUNNINGHAM, E. 2007. Supermodeled sabercat, predatory behavior in *Smilodon fatalis* revealed by high-resolution 3D computer simulation. *Proceedings of the National Academy of Sciences*, **104**, 16010–16015.
- MELCHIONNA, M., PROFICO, A., CASTIGLIONE, S., SERIO, C., MONDANARO, A., MODAFFERI, M., TAMAGNINI, D., MAIORANO, L., RAIA, P., WITMER, L. M., WROE, S. and SANSALONE, G. 2020. Data from: A method for mapping morphological convergence on three-dimensional digital models: the case of the mammalian sabre-tooth. *Dryad Digital Repository*. <https://doi.org/10.5061/dryad.9kd51c5g6>
- MERRIAM, J. C. and STOCK, C. 1932. The Felidae of Rancho La Brea. Carnegie Institution of Washington Publication, Publication **422**.
- MOEN, D. S. 2019. What determines the distinct morphology of species with a particular ecology? The roles of many-to-one mapping and trade-offs in the evolution of frog ecomorphology and performance. *The American Naturalist*, **194**, E81–E95.
- MUSCHICK, M., INDERMAUR, A. and SALZBURGER, W. 2012. Convergent evolution within an adaptive radiation of cichlid fishes. *Current Biology*, **22**, 2362–2368.
- PIRAS, P., SILVESTRO, D., CAROTENUTO, F., CASTIGLIONE, S., KOTSAKIS, A., MAIORINO, L., MELCHIONNA, M., MONDANARO, A., SANSALONE, G., SERIO, C., VERO, V. A. and RAIA, P. 2018. Evolution of the sabertooth mandible: a deadly ecomorphological specialization. *Palaeogeography, Palaeoclimatology, Palaeoecology*, **496**, 166–174.
- PREVOSTI, F. J., TURAZZINI, G. F., ERCOLI, M. D. and HINGST-ZAHER, E. 2021. Mandible shape in marsupial and placental carnivorous mammals: a morphological comparative study using geometric morphometrics. *Zoological Journal of the Linnean Society*, **164**, 836–855.
- PROFICO, A., BUZI, C., DAVIS, C., MELCHIONNA, M., VENEZIANO, A., RAIA, P. and MANZI, G. 2019. A new tool for digital alignment in virtual anthropology. *The Anatomical Record*, **302**, 1104–1115.
- RAIA, P., CAROTENUTO, F., ERONEN, J. T. and FORTELIUS, M. 2011. Longer in the tooth, shorter in the record? The evolutionary correlates of hypsodonty in Neogene ruminants. *Proceedings of the Royal Society B*, **278**, 3474–3481.
- RENAUD, S., LEDEVIN, R., PISANU, B., CHAPUIS, J.-L., QUILLFELDT, P. and HARDOUIN, E. A. 2018. Divergent in shape and convergent in function: adaptive evolution of the mandible in Sub-Antarctic mice. *Evolution*, **72**, 878–892.
- ROHLF, F. J. 1993. Relative warp analysis and an example of its application to mosquito. *Contributions to Morphometrics*, **8**, 131.
- and BOOKSTEIN, F. L. 2003. Computing the uniform component of shape variation. *Systematic Biology*, **52**, 66–69.
- SANDER, P. M., CHRISTIAN, A., CLAUSS, M., FECHNER, R., GEE, C. T., GRIEBELER, E. M., GUNGA, H.-C., HUMMEL, J., MALLISON, H., PERRY, S. F., PREUSCHOF, H., RAUHUT, O. W. M., REMES, K., TÜTKEN, T., WINGS, O. and WITZEL, U. 2010. Biology of the sauropod dinosaurs: the evolution of gigantism. *Biological Reviews*, **86**, 117–155.
- SANSALONE, G., CASTIGLIONE, S., RAIA, P., ARCHER, M., DICKSON, B., HAND, S., PIRAS, P., PROFICO, P. and WROE, S. 2020. Decoupling functional and morphological convergence, the study case of fossorial mammalia. *Frontiers in Earth Science*, **8**, 112.
- SCHALLER, G. B. 1972. *The Serengeti lion: A study of predator-prey relations*. University of Chicago Press, 480 pp.
- SCHLAGER, S. and GIRINON, F. 2017. Rvcg: Manipulations of triangular meshes based on the ‘VCGLIB’ API. v.0.1x. <https://cran.r-project.org/web/packages/Rvcg/index.html>
- PROFICO, A., DI VINCENZO, F. and MANZI, G. 2018. Retrodeformation of fossil specimens based on 3D bilateral semi-landmarks: implementation in the R package ‘Morpho’. *PLoS One*, **13**, e0194073.
- JEFFERIS, G., IAN, D. and SCHLAGER, M. S. 2020. Morpho: Calculations and visualisations related to geometric morphometrics. R package v.2.8. <https://cran.r-project.org/web/packages/Morpho/index.html>
- SERB, J. M., SHERRATT, E., ALEJANDRINO, A. and ADAMS, D. C. 2017. Phylogenetic convergence and multiple shell shape optima for gliding scallops (Bivalvia: Pectinidae). *Journal of Evolutionary Biology*, **63**, 685–1747.
- SLATER, G. J. and VAN VALKENBURGH, B. 2008. Long in the tooth: evolution of sabertooth cat cranial shape. *Paleobiology*, **34**, 403–419.
- SPEED, M. P. and ARBUCKLE, K. 2016. Quantification provides a conceptual basis for convergent evolution. *Biological Reviews*, **92**, 815–829.
- STAYTON, C. T. 2006. Testing hypotheses of convergence with multivariate data: morphological and functional convergence among herbivorous lizards. *Evolution*, **60**, 824–841.
- 2015. The definition, recognition, and interpretation of convergent evolution, and two new measures for quantifying and assessing the significance of convergence. *Evolution*, **69**, 2140–2153.
- VAN VALKENBURGH, B. 2007. Deja vu: the evolution of feeding morphologies in the Carnivora. *Integrative & Comparative Biology*, **47**, 147–163.
- WAINWRIGHT, P. C. 2007. Functional versus morphological diversity in macroevolution. *Annual Review of Ecology, Evolution, & Systematics*, **38**, 381–401.
- WAKE, D. B., WAKE, M. H. and SPECHT, C. D. 2011. Homoplasy: from detecting pattern to determining process and mechanism of evolution. *Science*, **331**, 1032–1035.
- WROE, S. and MILNE, N. 2007. Convergence and remarkably consistent constraint in the evolution of carnivore skull shape. *Evolution*, **61**, 1251–1260.
- McHENRY, C. and TOMASON, J. J. 2005. Bite club: comparative biteforce in big biting mammals and the

- prediction of predatory behaviour in fossil taxa. *Proceedings of the Royal Society B*, **272**, 619–625.
- LOWRY, M. B. and ANTÓN, M. 2008. How to build a mammalian super-predator. *Zoology*, **111**, 196–203.
- CHAMOLI, U., PARR, W. C., CLAUSEN, P., RIDGELY, R. and WITMER, L. 2013. Comparative biomechanical modeling of metatherian and placental sabertooths: a different kind of bite for an extreme pouched predator. *PLoS One*, **8**, e66888.
- ZELDITCH, M. L., SWIDERSKI, D. L. and SHEETS, H. D. 2012. *Geometric morphometrics for biologists: a primer*. Academic Press.

Chapter 4 - Ancestral state estimation with phylogenetic ridge regression



Ancestral State Estimation with Phylogenetic Ridge Regression

Silvia Castiglione¹ · Carmela Serio¹ · Alessandro Mondanaro^{1,2} · Marina Melchionna¹ ·
Francesco Carotenuto¹ · Mirko Di Febbraro³ · Antonio Profico⁴ · Davide Tamagnini⁴ · Pasquale Raia¹

Received: 8 October 2019 / Accepted: 9 June 2020
© Springer Science+Business Media, LLC, part of Springer Nature 2020

Abstract

The inclusion of fossil phenotypes as ancestral character values at nodes in phylogenetic trees is known to increase both the power and reliability of phylogenetic comparative methods (PCMs) applications. We implemented the R function *RRphylo* as to integrate fossil phenotypic information as ancestral character values. We tested the new implementation, named *RRphylo-noder* (which is available as part of the *RRphylo* R package) on tree and data generated according to evolutionary processes of differing complexity and under variable sampling conditions. We compared *RRphylo-noder* performance to other available methods for ancestral state estimation, including Bayesian approaches and methods allowing rate variation between the tree branches. We additionally applied *RRphylo-noder* to two real cases studies, the evolution of body size in baleen whales and in caniform carnivores. Variable-rate methods proved to be more accurate than single-rate methods in estimating ancestral states when the pattern of phenotypic evolution changes across the tree. *RRphylo-noder* proved to be slightly more accurate and sensibly faster than Bayesian approaches, and the least sensitive to the kind of phenotypic pattern simulated. The use of fossil phenotypes as ancestral character values noticeably increases the probability to find a phenotypic trend through time when it applies to either the entire tree or just to specific clades within it. We found Cope's rule to apply to both mysticete cetaceans and caniform carnivores. The *RRphylo-noder* implementation is particularly appropriate to study phenotypic evolution in the presence of complex phenotypes generated by different processes acting in different parts the tree, and when suitable information about fossil phenotypes is at hand.

Keywords Ancestral states estimation · Fossil phylogenies · Phenotypic evolution · Phylogenetic comparative methods · Rrphylo

Electronic supplementary material The online version of this article (<https://doi.org/10.1007/s11692-020-09505-x>) contains supplementary material, which is available to authorized users.

✉ Pasquale Raia
pasquale.raia@unina.it

¹ Dipartimento Di Scienze Della Terra, Dell'Ambiente E Delle Risorse, Monte Sant'Angelo, Via Cinthia, 21 - 80126 Napoli, Italy

² Dipartimento Di Scienze Della Terra, Via G. La Pira, 4, 50121 Firenze, Italy

³ Dipartimento Di Bioscienze E Territorio, University of Molise, C. da Fonte Lappone, 86090 Pesche, IS, Italy

⁴ Dipartimento Di Biologia Ambientale, Sapienza Università Di Roma, Rome, Italy

Introduction

Phylogenetic comparative methods (PCMs) are sought to account for species non-independence in analyses of phenotypic evolution, providing robust inference about the process and patterns of evolution (Alfaro et al. 2009; Harmon et al. 2003; Venditti et al. 2011) and the correlation between traits (Felsenstein 1985; Garland and Ives 2000; Revell 2010). The simplest PCMs refer to a constant-rate, non-directional process, namely the Brownian motion model of evolution (BM), and deviations thereof (Freckleton et al. 2002; Harvey and Pagel 1991; O'Meara 2012; Pagel 1997). Several PCMs now allow fitting more complicated evolutionary models, taking stabilizing selection and stasis into account and relaxing the assumption that a single evolutionary rate applies unambiguously across the tree (Castiglione et al. 2018; Elliot and Mooers 2014; O'Meara et al. 2006; Rabosky 2014; Smaers et al. 2016). More importantly, most of these recent PCMs

allow using paleontological trees (Bapst 2013; Pennell and Harmon 2013), which is welcome since there is widespread acknowledgement that the inclusion of fossil information allow better inference about the patterns of taxonomic and phenotypic diversification (Didier et al. 2017; Finarelli and Liow 2016; Heath et al. 2014; Liow et al. 2010; Mitchell et al. 2018; Puttick et al. 2017; Schnitzler et al. 2017; Silvestro et al. 2016; Slater and Harmon 2013).

PCMs allow to estimate ancestral character states (the phenotypic values at the tree nodes) by means of maximum likelihood, treating the phenotypes at the nodes as parameters, in order to find the parameter values that maximize the probability of the tip (observed) data assuming a given evolutionary model (most commonly the BM or Ornstein–Uhlenbeck, OU, Joy et al. 2016). This procedure could be troublesome, since the accuracy of ancestral states estimation is biased if the model does not approximate reality (Chira and Thomas 2016; Cooper et al. 2016; Slater, Harmon, and Alfaro 2012). It has been shown that PCMs may actually provide ancestral estimates that compare very unfavorably to real fossil phenotypes (Webster and Purvis 2002), especially at the root (Gascuel and Steel 2014). To cope with this drawback, several approaches have been developed in order to use fossil species traits as given phenotypic values at the tree nodes to guide the estimation process (Slater and Harmon 2013). Under a Bayesian approach, this is implemented setting fossil phenotypes as node priors (Slater, Harmon, and Alfaro 2012), so that both the priors and the tips are used as observations in the parameter estimation process (Slater, Harmon, and Alfaro 2012).

Models that are not constrained to fit a single evolutionary rate across the tree are better suited to cope with phenotypic vectors whose complexity (herein defined as the result of different phenotypic patterns applying to different parts of the tree) is not captured by simpler evolutionary models (e.g. BM, OU, Early-Burst; Chira and Thomas 2016; Pennell et al. 2015). The downside of such “variable-rates” models is that they could be severely overparametrized, which might reduce their fit to the real data once topological and sampling issues are considered (Castiglione et al. 2018; Chira and Thomas 2016; Eastman et al. 2011; Elliot and Mooers 2014; Rabosky 2014; Venditti et al. 2011).

Here we present an implementation of the R function *RRphylo* (Castiglione et al. 2018) meant to estimate ancestral states taking advantage of explicit fossil information. In contrast to most other methods, under this new implementation, named *RRphylo-noder*, there is no expected distribution of trait changes during evolution (e.g. the normal distribution under BM), so that we expect *RRphylo-noder* could outperform competing methods in the presence of complex phenotypes. We tested this hypothesis by means of extensive simulations and real-case applications. We show that *RRphylo-noder* is faster and increasingly more accurate than

competing methods in reconstructing ancestral states as phenotypic complexity increases.

Materials and Methods

The *RRphylo-noder* implementation is based on phylogenetic ridge regression, *RRphylo* (Castiglione et al. 2018). In *RRphylo* the phenotypic change between any two nodes (or a node and a tip) aligned along a phyletic line is described by the sum of individual contributions at each consecutive branch between the nodes, according to the equation $\Delta y = \vec{\beta}_1 l_1 + \vec{\beta}_2 l_2 + \dots + \vec{\beta}_n l_n$. Here, n equals the number of branches intervening between the nodes, $\vec{\beta}_{1\dots n}$ is the vector of phylogenetic ridge regression coefficients (the evolutionary rates), and $l_{1\dots n}$ are the branch lengths. The vector of regression coefficients $\vec{\beta}$ is computed simultaneously for all the branches in the tree by applying a normalization factor λ which avoids fitting extreme β values and prevents multicollinearity (James et al. 2013).

RRphylo-noder integrates the phenotypic information at internal nodes in the estimation of evolutionary rates and ancestral character states. Given a vector \mathbf{n} of phenotypic values known in advance to be placed at internal nodes (*fossil.states*), a vector of false tips *ftips* of length \mathbf{n} is added to the tree. Each i_{th} element of *ftips* is phenotypically identical to the corresponding *fossil.states* _{i} and is attached to the tree at the position of *fossil.states* _{i} with a branch of length = 0. Then, the vector of regression coefficients ($\vec{\beta}$) is estimated by means of *RRphylo* by using the modified tree and phenotype (which include both *ftips* and the real tips). Since the branch lengths of *ftips* are equal to zero, the phenotypic rate between each *ftips* _{i} and the corresponding node is zero, which means the *fossil.states* and their corresponding *ftips* will have the same phenotypic estimates. After β coefficients are estimated, the vector of phenotypic values at nodes \vec{a} is calculated as usual as:

$$\vec{a} = L' \vec{\beta}$$

where each row of L' represents the path of branch lengths moving from a specific node in the tree. The final step of the algorithm consists in removing *ftips* from the tree, and from the rate and phenotypic vectors.

Simulations

We tested *RRphylo-noder* accuracy and compared it to other available methods for ancestral states estimation. The goals of the simulations were to assess (1) the accuracy of both single-rate and variable-rates methods to ancestral state estimation with complex phenotypes, (2) the effect of sampling on ancestral state estimation and (3) the impact of

using fossil phenotypes as ancestral character states known in advance. We used ape's *ace* (Paradis and Schliep 2018) to represent the simplest, most straightforward method for ancestral character state estimation under BM. The function *fastAnc* in phytools (Revell 2012) is based on BM as *ace*, but additionally allows specifying phenotypic states at nodes. Elliot and Mooers' *StableTraits* (Elliot and Mooers 2014) estimates ancestral states using a generalization of BM to the stable random walk, represented by a symmetrical, zero-centered distribution of phenotypic increments during the evolutionary time defined by the parameters α (the index of stability) and c (the scale). *StableTraits* performs the Bayesian estimation of ancestral states fitting the α and c parameters and allows the comparison with BM. As in *RRphylo-noder*, node priors can be used by grafting zero-branch length false tips to specified nodes. We implemented both *StableTraits* and *StableTraits-Brownian* (that is *StableTraits* referring BM to estimate ancestral states) and wrote a wrapper around *StableTraits* (named *StableTraitsR*) which allows using the function within the R environment and with different operating systems and to specify node priors. We tested both *RRphylo* and *RRphylo-noder* along with all of these other methods. In sum, we used two methods which do not allow to specify phenotypic values known in advance at nodes (*ace* and *RRphylo*), two single-rate methods (*ace* and *fastAnc*), and four methods which allow the evolutionary rate to change across the tree (which we collectively refer to as 'variable-rate' models: *StableTraits-Brownian*, *StableTraits*, *RRphylo* and *RRphylo-noder*). We tested such methods on forty different kinds of phenotypes to assess their performance under phenotypes differing in terms of complexity and under different sampling regimes.

Simulating Trees and Starting (basic) Phenotypes

To produce the phenotypes, we started by creating 100 random phylogenetic trees having 80 species at least (average = 164 species, range = 127–238 species) by using the function *sim.bdtree* in the R package *geiger* (Harmon et al. 2007) setting the birth rate at 0.5 and the death rate at 0.2. For each tree, we first generated a phenotypic vector y under BM, recording both tip (species values) and node (ancestral values) phenotypes, by using the function *fastBM* in the R package *phytools* (Revell 2012). We set the phenotypic mean (i.e. the value at the tree root) at 0 and σ^2 (the Brownian rate) at 1. A second phenotype yt was produced on the same tree by modelling evolution according to Brownian motion with trend (i.e. a trend in the phenotypic mean over time, hereafter referred as 'phenotypic drift') using *fastBM* and specifying the μ parameter (the intensity of the drift) at 0.5. For yt as well, we recorded both the species and ancestral values. The starting phenotypes y and yt were used as they are and

then manipulated to derive more complex phenotypic vectors as explained below.

Simulating Complex Phenotypic Evolution with and Without Ancestral States known in Advance

To test the effect of providing known phenotypes at some nodes, we randomly selected from the starting phenotype a number of nodes N equal to 5% of the nodes in the tree and their ancestral values. The N ancestral values were used as phenotypic values at nodes known in advance (*fossil.states* under the *RRphylo-noder* terminology or node priors under the Bayesian approach terminology). To use ancestral values which were not evolved according to BM (or BM with trend either), we produced a further phenotype shuffling the N ancestral values across the tree nodes. The advantage of shuffling ancestral values is that under BM they are phylogenetically weighted means of the tip phenotypes descending from them, meaning they are constrained within the range of values of the descendant phenotypes, whereas after the shuffling the ancestral values could be outside the phenotypic range of tips descending from them (this is true, for instance, of any clade following Cope's rule). A further manipulation consists in randomly selecting half of the tree nodes to apply a phenotypic trend to the clades descending from them. This way, the tree phenotypic vector is generated by a complex process, whereby a number of clades evolve under phenotypic drift while others do not (by using y as the starting phenotype), or the intensity of drift for individual clades differs from, and could even reverse, the drift imposed to the entire tree (by using yt as the starting phenotype). Such phenotypic drifts specifically applied to selected clades was imposed by multiplying, for each selected clade, the distances of each tip to their corresponding common ancestor by a constant, according to the equation $y' = y + \text{time} * 0.5$, where y' is the 'drifted' phenotype and time is the vector of tip to common ancestor distances. Such complex phenotypes are often reported in literature (Laurin 2004; Hone et al. 2005; Monroe and Bokma 2010; Raia et al. 2012; Benson et al. 2014a; Baker et al. 2015), though their existence is impossible to recognize with abstract evolutionary models (e.g. BM, early-burst) as they applying to the tree as a whole (but see Slater and Pennell 2013).

The whole set of manipulations derives from either y (BM) or yt (BM with trend), a second phenotype with shuffled ancestral values, and a number of complex phenotypes where patterns of phenotypic drift change idiosyncratically across the tree, plus any combination of them (Table 1). All these phenotypic vectors were eventually used to test the effect of sampling on ancestral state estimation as described below.

Table 1 Simulated kinds of phenotypes. The columns indicate how the phenotypes were made more complex departing from the initial (either Brownian motion BM, or BM with trend, DR) applying a number of manipulations and their combinations

Starting phenotype	Shuffling	Drift at individual clades	Random sampling		Biased sampling	
BM	shu	ds5	s1—random	s5—random	s1—bias	s5—bias
		—	s1—random	s5—random	s1—bias	s5—bias
	—	ds5	s1—random	s5—random	s1—bias	s5—bias
		—	s1—random	s5—random	s1—bias	s5—bias
DR	shu	ds5	s1—random	s5—random	s1—bias	s5—bias
		—	s1—random	s5—random	s1—bias	s5—bias
	—	ds5	s1—random	s5—random	s1—bias	s5—bias
		—	s1—random	s5—random	s1—bias	s5—bias

shu the phenotypic values of ancestral values (simulated according to BM or DR either) are shuffled before the analyses, *ds5* half of the ancestral values are selected randomly to be applied a phenotypic drift through time, *s1* 10% of species are removed either at ‘random’ or depending on the value of the phenotype (‘bias’) *s5* the same as *s1* but removing 50% of species. Starting from the left to the right, the initial phenotype is manipulated making it more complex. For instance, starting from the Brownian motion simulation BM, the phenotype is changed shuffling known ancestral states among selected nodes (*shu*), then applying a phenotypic drift to one half of the clades subtended by such selected nodes (*ds5*) and then removing either at random or with biased sampling up to one half of the species from the tree (e.g. *s5* biased)

Simulating the Effect of Sampling

After different kinds of phenotypes have been produced according to the manipulations described so far, a number of tips were removed from the tree as to test the effect of incomplete sampling. Two different kinds of subsampling strategies were applied, either ‘biased or ‘random’. Under the former, the chance of a species to be removed from the tree is inversely proportional to its phenotypic value. This corresponds to real case situations such as, for instance, to the higher chance to fossilize (hence to be sampled in the tree) for large versus small organisms (Behrensmeyer et al. 2000; Meloro et al. 2007). Two sampling schemes were applied. The first consists in removing 10% of the species from the tree, the second consists in removing 50% of the species, under both the ‘random’ and the ‘biased’ designs.

Overall, these procedures originate 20 different kinds of phenotypes deriving from the starting simulation (i.e. *y* or *yt*, either). Each phenotypic combination was repeated 10 times originating a total of $20 \times 2 \times 10 = 400$ simulations. The schematic description of the simulation procedures is presented in Table 1.

Testing Ancestral State Reconstruction Methods Accuracy

The ultimate goal of any ancestral state estimation method is to predict phenotypes at nodes. Under perfect prediction, regressing the simulated phenotypes at nodes against their predictions originates a regression slope = 1 and intercept = 0. For each method, we calculated the slope and the intercept of the regression between simulated and fitted values, and the root mean squared error (*rmse*) of the regression. Under *fastAnc*, ancestral values are not fitted but given

as phenotypic values at nodes known in advance. This means the more ancestral values are provided the lower *fastAnc*’s *rmse* will be. Thus, rather than a measure of the goodness of fit of *fastAnc*, its corresponding *rmse* depends on how many ancestral values are provided. For this reason, beyond *rmse* we calculated the *rmse* over the fitted nodes only (*reduced rmse*) in order to compare *fastAnc* to the other methods. Since *ace* and *RRphylo* make no use of ancestral values, we used only *rmse* to compare the ancestral state estimates of these methods. Mean *rmse* between methods was compared by means of repeated-measures ANOVA using the function *lme* in the R package *nlme* (Pinheiro et al. 2014) taking the kind of phenotype tested as the random effect. The performances of the methods were compared by using the function *glht* in the package *multcomp* (Hothorn et al. 2016).

The effects of changing the pattern of phenotypic drift across the tree, shuffling ancestral values and applying different sampling schemes, combine into phenotypes of increasing complexity, which deviate more and more from the starting *y* and *yt* vectors as different factors are added. To assess how such phenotypic complexity affects methods’ performance, for each method we averaged the 10 *rmse* (and *reduced rmse* as well) per type of phenotype, and collated *rmse*s for the different phenotypes from the smallest to the largest *rmse* as predicted by *ape*’s function *ace*. In this way, the forty *rmse* estimates were effectively ordered from the most similar, to the most dissimilar from BM, which is the evolutionary model *ace* is based upon. Then, we used categorical regression to calculate the slope of methods’ *rmse* (the response variable) against the phenotypic kinds collated from the most similar to Brownian Motion (BM) to the most dissimilar (DR.shu.ds5.s5.bias: a kind of phenotype first produced according to Brownian Motion with trend, and then modified applying shuffling to 5% of the ancestral

states, imposing a phenotypic drift to 50% of the individual clades within the tree, and eventually pruned of 50% of the tips via biased sampling, see Table 1) used as the predictor variable. This way we estimated how *rmse* grows away from BM, for each method. We compared the regression slopes and estimated marginal means per method by using the functions *emrends* and *emmeans*, respectively, in the package *emmeans* (Lenth et al. 2018). Ideally, the shallower the slope of the regression the less sensitive to the phenotype type a method is. Similarly, lower estimated marginal means indicate better prediction accuracy across phenotypes. This same procedure was repeated on *reduced rmse*, using *StableTraits-Brownian* predictions to collate phenotypes from the simplest (i.e. most similar to BM) to the most complex.

Eventually, we used geiger's function *fitContinuous* to compare the penalized AIC (AICc) obtained by fitting the BM and BM with trend (which is named 'drift' in geiger) to the tree and data on the original phenotypes (*y* and *yt*) and after the manipulations. Given the manipulation procedures invert the sign of the phenotypic drift for some clades in the tree (when the original phenotype was BM with trend), or add a drift where there was none (when the original phenotype was BM) we expect *fitContinuous* should fail to recognize the original phenotypic trend (either no such trend under BM or a drift under BM with trend) because of the manipulations. We compared *fitContinuous* results to the corresponding figures obtained by applying *search.trend* to the whole tree.

Testing the Importance of Sampling and Phylogenetic Uncertainty

A perfect prediction of ancestral states values (i.e. corresponding to the slope = 1 and intercept = 0), could indicate that a method is particularly accurate but could also depend on a method being overfit. Overfitting is the major drawback for overparametrized methods such as *RRphylo* and *RRphylo-noder*. An overfit method may appear superior to other methods when assessed for prediction accuracy based on simulated data but could fail to capture the fundamental processes that led to the observed patterns in real data, which represent a subset of the real diversity of the clades, providing much reduced prediction accuracy.

To evaluate the potential for overfit, we applied ANOVA and post-hoc TukeyHSD test to assess whether the slope and intercept of the regression between observed and estimated ancestral states differ among sampling schemes. We similarly assessed whether the phenotypic deviations between known (simulated) and fitted ancestral states estimates change per sampling scheme. Phenotypic deviation was calculated as average percent deviation of the fitted versus simulated ancestral states.

We further measured the ability of *RRphylo-noder* to capture the processes producing the observed patterns in real data. In particular, we analysed the ability of *RRphylo-noder* to reveal the existence of phenotypic drift for the clades that were designed to be so, in spite of sampling. This could be accomplished by using the *RRphylo* package function *search.trend* (Castiglione et al. 2019). The *search.trend* algorithm uses the *RRphylo* phenotypic estimates at nodes and the tip values to test whether there is a phenotypic drift (a change in the mean phenotype over time) departing significantly from the Brownian motion expectation. The algorithm can be applied indifferently to the entire tree or to a selection of internal nodes into the tree (Castiglione et al. 2019). For each clade selected, we calculated the intercept of the regression between the clade phenotypes and time (i.e. the distance of each tip from the tree root) and assumed these intercepts as the ancestral values for each clade, to be passed on to *RRphylo-noder* as known ancestral values. Overfit should result in reduced power to retrieve the imposed phenotypic drift under subsampling. At the same time, this allows to test whether the use of known ancestral values increases the power of *RRphylo-noder* to retrieve the true evolutionary process simulated on the tree. In the *RRphylo* package, we further provide a new function, named *overfitRR*, which tests whether a given phenotypic or rate pattern (either at specific nodes or for the entire tree) is robust to sampling and to phylogenetic uncertainty, that is an important source of concern in phylogenetic comparative methods, especially working with fossil phylogenies (Bapst et al. 2016).

Real Cases

We tested the *RRphylo-noder* method on two real cases. First, we inspected the evolution of body size in mysticete cetaceans. The second real case regards the evolution of body size in caniform carnivores (Online Resource 1).

Baleen whales are among the largest species ever lived. Yet, early Mysticeti include much smaller representatives (Fitzgerald 2012; Serio et al. 2019). The sister group to baleen whales, the Oligocene Aetiocetidae, were toothed whales up to 8 m in body length. We assembled a cetacean phylogenetic tree from the backbone phylogenies in Montgomery et al. (2013) and Marx and Fordyce (2015). The composite phylogeny includes 116 species we had body size estimates for (Online Resource 2). Thirty-six species in the tree are extinct (10 archaeoceti, 23 odontoceti, 3 mysticeti). We tested whether baleen whales body size increased over time, in keeping with Cope's rule (Hone and Benton 2005; Raia et al. 2012) by using *search.trend* (Castiglione et al. 2019). Then, we used *RRphylo-noder* setting *Mystacodon selenensis* (Lambert et al. 2017) body size as the mysticete most recent common ancestor prior. *Mystacodon selenensis* was almost the size of a bottlenose dolphin (McQuate 2017).

It is considered a stem mysticete, perhaps sister to Llanocetidae (Fordyce and Marx 2018). We therefore settled *Mystacodon* body size at 150 kg, which is typical for a bottlenose dolphin. We performed *RRphylo* and *search.trend* on the phylogeny as a whole, either with *Mystacodon* as ancestor of mysticetes, or without it. In addition, we performed, for the sake of comparison, both *RRphylo* and *search.trend* on the same tree and data, but removing extinct mysticeti. Body size estimates for the mysticete most recent common ancestor were further estimated by means of the functions *ace*, *fastAnc*, *StableTraits*, *StableTraits-Brownian* and *RRphylo*, always the full tree (i.e. with fossil species) without using *Mystacodon* body size as the ancestral value to Mysticeti.

To assess the potential for overfit, we developed and applied the newly-implemented *RRphylo* function *overfitRR* to test the effect of sampling on results produced by *search.trend*. This function randomly removes a number of tips corresponding to 25% of the tree size and swaps species phylogenetic position (thereby accounting for phylogenetic uncertainty) by using the *RRphylo* function *swapONE*. Then, it performs *search.trend* on pruned tree and data. The procedure is repeated 100 times and the percentage of significant results returned. In this case, we specified the Mysticeti clade to be tested for temporal trends in phenotypic (body size) mean and rates.

Results

Ancestral State Reconstruction Methods Accuracy: Overall Results

The regression of simulated versus fitted ancestral states gives slope consistently close to 1 and intercept close to 0 for all methods when the starting phenotype was simulated according to BM (Fig. 1, Supplementary Table S1). The same applies when the starting phenotype was simulated according to BM with trend, but intercepts tend to become negative for all methods in this case (Fig. 1, Supplementary Table S2). ANOVA indicated that for 16 out of 40 different kinds of phenotypes there are significant differences among methods in terms of *rmse*. Among them, TukeyHSD indicates *StableTraits-Brownian*, *RRphylo-noder* and *StableTraits* resulted the most accurate methods overall, being selected 16, 15 and 15 times respectively among the best models. The methods *ace* (3) and *RRphylo* (1) still figure among the best candidate models. In terms of *reduced rmse*, only four times we found significant differences between methods. *StableTraits* was selected as the best method 4 times, *StableTraits-Brownian*, *RRphylo-noder* and *fastAnc* 2 times each. Details about the effect of individual factors are available as supplementary information. In general, both *StableTraits* methods and *RRphylo-noder* perform equally well, under a variety of sampling conditions and across different kinds of phenotypes (Online Resource 1). Variable rates methods consistently outperform single-rate methods. Only four times

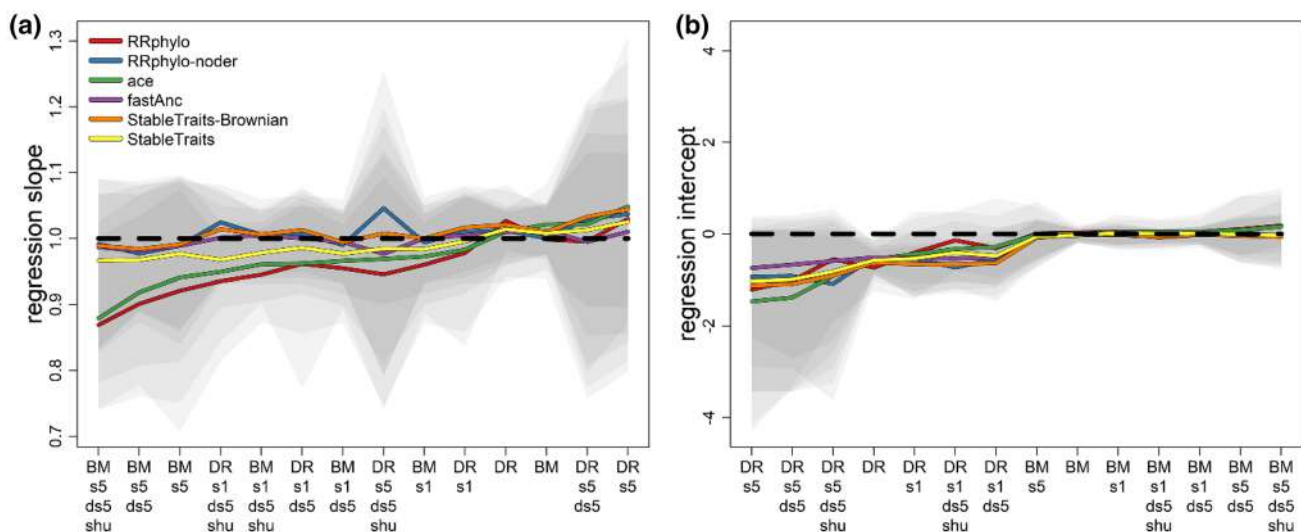


Fig. 1 Patterns of slope and intercept values derived by regressing ancestral states estimated by each method against original values, under different simulation models. A subsample of models is selected as to represent increasing levels of complexity. **a** Along x-axis, mod-

els are sorted in ascending order of slope predicted by using *ace* estimates. **b** Along x-axis, models are sorted in ascending order of intercept predicted by using *ace* estimates. Gray shaded areas represent the 95% confidence intervals for each method

methods without specified ancestral values (*ape*'s *ace* and *RRphylo*) perform as well as methods that allow for their specification.

As the complexity of the evolutionary process generating the simulated phenotypes increases, *RRphylo-noder* and *StableTraits*, in this order, performs best (Fig. 2, Table 2). The estimated marginal means of the regression indicate that all methods with prior phenotypic knowledge about specific nodes in the tree outperform methods with no such information (Table 2) and *RRphylo-noder* is the most accurate method overall. Collating methods' *rmse* differently does not affect this result. *RRphylo-noder* remains the least sensitive to change in the type of phenotype simulated under all possible ordering.

When the original phenotype was simulated according to BM, *fitContinuous* indicated BM describes the data better than the 'drift' model 82% of the times at $\Delta\text{AICc} > 2$ (Burnham and Anderson 2004). With manipulated phenotypes (i.e. phenotypes with values at nodes estimated through a non-BM process) this percentage decreases to 79%. The corresponding figures for *search.trend* are 97.5% on the original BM-generated phenotype *y*, 93% on the phenotype without- and 92% with specifying ancestral values derived from *y* via manipulations. Starting from the phenotype *yt*, generated through the BM with trend process, *fitContinuous* indicated the 'drift' model is more appropriate than BM 100% of the cases with the original phenotype and 98.5% with the manipulated (i.e. phenotypes with values at nodes

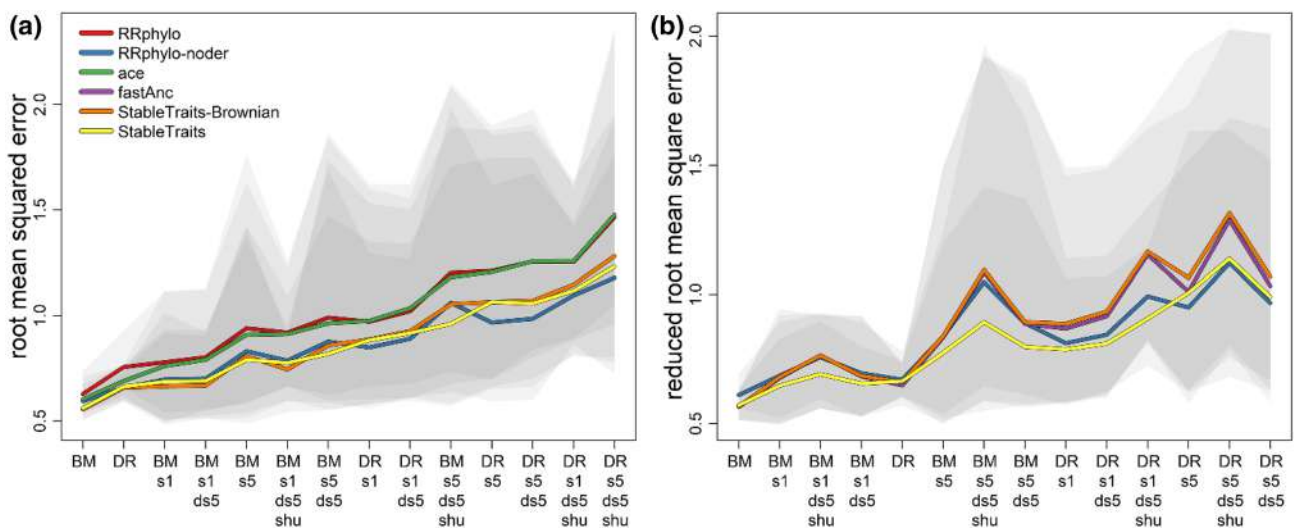


Fig. 2 Patterns of *rmse* and *reduced rmse* across different phenotypes and sampling schemes. A subsample of models is selected as to represent increasing levels of complexity. **a** Along x-axis, models are sorted in ascending order of *rmse* predicted by *ace*. **b** Along x-axis,

models are sorted in ascending order of *reduced rmse* predicted by *StableTraits-Brownian*. Gray shaded areas represent the 95% confidence intervals for each method

Table 2 Methods performance and differences between methods across all types of phenotypes

Method	Slope	95% CI		Emm	95% CI	
<i>rmse</i>						
RRphylo-noder	0.012	0.010	0.013	0.918	0.902	0.934
StableTraits	0.014	0.013	0.015	0.937	0.921	0.953
StableTraits-Brownian	0.015	0.014	0.017	0.945	0.929	0.961
RRphylo	0.016	0.015	0.017	1.062	1.046	1.078
ace	0.017	0.016	0.018	1.070	1.054	1.086
<i>Reduced rmse</i>						
RRphylo-noder	0.011	0.009	0.013	0.918	0.902	0.935
fastAnc	0.014	0.012	0.015	0.910	0.894	0.927
StableTraits	0.015	0.013	0.016	0.937	0.920	0.954
StableTraits-Brownian	0.016	0.014	0.017	0.945	0.928	0.962

'slope' represents the increase in *rmse* or *reduced rmse* either as the phenotype deviates from Brownian motion. 'emm' represents the estimated marginal mean of *rmse* or *reduced rmse* either per method

estimated with a non-BM with trend process) phenotypes derived from *yt*. The corresponding figures for *search.trend* are 79% (original), 84% (manipulated) and 82.5% (manipulated with specified ancestral values).

Assessing the Impact of Sampling

When the tree is subsampled, the slope and intercepts for variable-rates methods remain close to 0 and 1 respectively, when the starting phenotype was *y*, and slightly less than 0 and 1, respectively, when the starting phenotype was *yt* (Fig. 1, Supplementary Tables S7–S8).

We tested whether sampling affects these parameters as well as the percent phenotypic deviation from the simulated parameters by means of ANOVA and post-hoc testing, using the sampling intensity (either 90% of the original tree or 50%) and sampling type (either ‘biased’ or ‘random’) as factors. The results indicate that slopes, intercepts and percent deviations from the original phenotypes are never statistically different with the random sampling, except for *StableTraits* when sampling intensity is 50% (Table 3). With intense sampling (i.e. reducing tree size to 50% of the original tree) and the biased sampling design the slope and intercepts differ significantly from the unsampled tree and data for all methods. Importantly, all single-rate models perform worse, both in terms of slope and intercepts change across sampling levels (Supplementary Table S11).

We used the *search.trend* function in *RRphylo* package to test whether sampling affects the probability to retrieve the correct structure in the data. ANOVA and post-hoc tests indicate there is no significant difference per sampling scheme and intensity. However, the use of ancestral values sensibly increases the possibility to find a phenotypic pattern

at specific clades when it is real. Under different sampling conditions this increase in power is as high as 82.2% on average (Online Resource 1).

Cetacean Body Mass

By applying *search.trend*, we found Cope’s rule to apply to mysticetes, regardless of whether ancestral states are indicated as node priors or ignored. Yet, the regression slope increases adding *Mystacodon* body mass as the ancestor of Mysticeti (Fig. 3, Table 4). The results are robust to the effect of sampling (97% and 74% instances of significant phenotypic trends are found with and without *Mystacodon* body mass as the ancestral value to all Mysticeti, respectively, by removing 25% of the tips randomly with *overfitRR*).

By applying *RRphylo-noder* the cetacean phylogeny produced an estimate of 150.04 kg for the most recent common ancestor of Mysticeti, which is coincident with the *fossil.state* provided (i.e. the size of *Mystacodon selenensis*). The same estimate as calculated by *RRphylo* without *fossil.state* is 385.36 kg. We derived for comparison the corresponding values as estimated by *ape* and *fastAnc* (which is 430.70 kg and 457.85 kg, respectively), and by *StableTraits*. At 150.02 kg.

Discussion

Variable-rates methods, that is *RRphylo-noder* and the two *StableTraits* models, consistently outperform all other methods in terms of ancestral states prediction accuracy (the accuracy of *fastAnc* rapidly decreases with the number of ancestral values used or by shuffling them, Fig. 2).

Table 3 Effect of sampling on prediction performance of variable-rates methods for ancestral states estimation

	Intercept			Slope			Percent phenotypic deviation		
	100%	90%	50%	100%	90%	50%	100%	90%	50%
StableTraits-Brownian									
100%	–	0.957	<0.01	–	0.949	<0.01	–	0.623	0.984
90%	0.996	–	<0.01	1	–	0.001	0.999	–	0.52
50%	0.785	0.736	–	0.096	0.1	–	0.668	0.67	–
StableTraits									
100%	–	0.979	<0.01	–	0.979	<0.01	–	0.616	0.983
90%	0.940	–	<0.01	0.867	–	<0.01	0.999	–	0.511
50%	0.905	0.727	–	0.024	0.087	–	0.701	0.698	–
RRphylo-noder									
100%	–	0.999	<0.01	–	0.988	<0.01	–	0.611	0.988
90%	0.840	–	<0.01	0.955	–	<0.01	0.616	–	0.524
50%	0.979	0.929	–	0.121	0.062	–	0.983	0.511	–

For each sampling level (100, 90 or 50% of the original tree) the results represent p-values of the post hoc Tukey HSD test, either for biased (upper triangle) and random (lower triangle) sampling designs

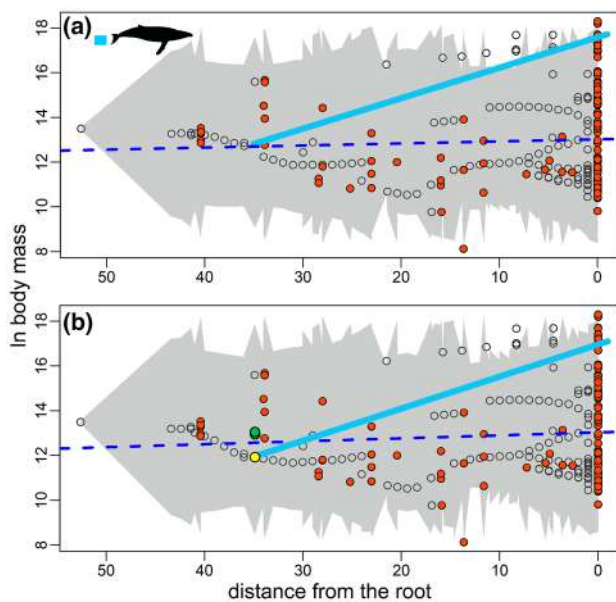


Fig. 3 Cetacean body size versus time plots. White dots represent ancestral estimates at internal nodes, orange dots represent species phenotypes. The regression of phenotypes through time for the entire phylogeny is indicated by a blue dashed line. The phenotypic trend through time for Mysticeti is represented by the solid pale blue line. Upper row: cetaceans body size evolution according to *search.trend* as produced by considering fossil mysticetes, ancestral estimates are derived by the *RRphylo* method. Lower row: cetaceans body size evolution according to *search.trend* as produced by considering fossil mysticetes, ancestral estimates are derived by the *RRphylo-noder* method. The yellow dot represents the ancestral character for *Mystacodon* as estimated by *RRphylo-noder* and *StableTraits* (fitted by using the *StableTraits* software), green dots represent *ace* (fitted by using *ape* function *ace*), and *fastAnc* (fitted by using *phytools* function *fastAnc*). The *ace* estimate is the lowest. The y-axis is in kilograms, time (x-axis) represents the distance from the cetacean tree root

Table 4 Estimates for the body size at the mrca to Mysticeti, as derived by different methods

	Fitted ancestral values (kilograms)	Slope	p-value
RRphylo-noder— <i>Mystacodon</i> as ancestral value	150.04	0.020	<0.01
StableTraits— <i>Mystacodon</i> as ancestral value	150.02	—	—
RRphylo	385.36	0.019	0.01
Ace	430.70	—	—
Fastanc	457.85	—	—

Slopes and p-values for Mysticete body size versus time regression performed by *search.trend*. Significant regression slopes are indicated in bold

However, *RRphylo-noder* is the least sensitive to changes in the complexity of phenotypes and provides the smallest root mean squared error overall (Fig. 2, Table 2). The inclusion of known phenotypic values at internal nodes substantially increases ancestral states estimation accuracy for all methods and regardless of the sampling scheme. With *RRphylo-noder*, this further translates into a nearly twofold increase in the power to detect the phenotypic drift imposed to specific clades within the tree in the simulations. The process generating the phenotypes y and yt is recognized more precisely by *search.trend* with BM and by *fitContinuous* with BM with trend.

We found that all methods provide unbiased estimation of the ancestral states, meaning the estimation error is not correlated with the phenotypic values. However, the intercepts of simulated versus estimated ancestral states tend to be less than zero when the starting phenotype was simulated under a model of phenotypic drift (Fig. 1). Since we designed BM with trend as to exhibit a positive drift, this means that all methods tend to preserve the actual phenotypic pattern at the expense of prediction accuracy. These results comply with our expectations that methods assuming an a priori evolutionary model are more prone to estimation error for all nodes other than the ancestral values known in advance, as compared to *RRphylo-noder*. Still, our results demonstrate that variable rates methods are best suited to cope with tree and data generated under complex phenotypic processes that cannot be captured by abstract evolutionary models (Chira and Thomas 2016; Slater, Harmon, and Alfaro 2012). In *RRphylo* the phenotypic difference between any parent to descendant pair in the tree is fitted as a linear transformation proportional to the time intervening between the two according to a given slope (i.e. the elements of the evolutionary rates vector $\vec{\beta}$) while minimizing rate variation within clades (Castiglione et al. 2018). In contrast, other variable-rate methods refer to a single evolutionary model describing the distribution of phenotypic changes for the whole tree (e.g. the normal distribution in BM, the stable distribution in *StableTraits*). This makes *RRphylo* the least sensible to the actual shape of the distribution of phenotypic change across the tree.

Bayesian estimation of ancestral states, as currently implemented in (at least) *phytools*' *anc.Bayes* and in *geiger*'s *fitContinuousMCMC* (but see Bokma et al. 2015a, b), or *StableTraits* (Elliot and Mooers 2014), accommodates for ancestral state estimation uncertainty and provides credible estimates when node priors are used. Herein, by using both simulations and application to real cases (mysticeti and caniform carnivores, see Online Resource 1 for the latter case study) we demonstrated *RRphylo-noder* performs at least as well as such Bayesian estimation approaches, and bears the advantage of being much faster (nearly twenty times faster according to our simulations)

and less dependent to a specific distribution of phenotypic changes.

One potential problem with method fitting many parameters at once is overfit. Overfit methods tend to perform very well with given data, but they often bear the potential to provide biased and much less precise estimation when data are subsampled. We applied either mild or strong subsampling to our tree and data in the simulations and to one real case (Mysticeti). We found that both *RRphylo-noder* and *StableTraits* are robust to sampling effects but for the most severe sampling design (i.e. removing half of the tree species proportionally to the species phenotypic values). In phylogenetic ridge regression (Kratsch and McHardy 2014) a normalization factor λ is applied to avoid abnormally large phenotypic rate estimates, at the expense of prediction accuracy of tip (species) values. In *RRphylo*, λ maximum likelihood estimation is performed as to minimize the variance of rates within clades, so that phenotypes (and rates) tend to show phylogenetic signal (Castiglione et al. 2018). The structure of rate variation is constrained to maintain patterns of phenotypic evolution within clades and rates are treated as phylogenetically non-independent (Sakamoto and Venditti 2018). A similar approach to reduce overfit, that is the “inheritance” of evolutionary rates over time, is implemented in AUTEUR (Eastman et al. 2011). We guess this is the reason why *RRphylo-noder* is robust to even strong sampling effects. In *StableTraits* the danger of overfit is minimized by penalizing the effective number of parameters in the model by application of a Bayesian Predictive Information Criterion (Elliot and Mooers 2014).

We found Cope’s rule to apply to mysticetes. However, the phenotypic drift becomes much more evident when the bottlenose dolphin-sized *M. selenensis* is placed at the root of the Mysticeti clade (Fig. 3). We similarly found positive evidence for Cope’s rule in canids (Supplementary Fig. S13). Still in this case, this depends on the inclusion of fossil phenotypes known in advance at specific nodes (see Online Resource 1 for full details). The application of *RRphylo-noder* to these case studies demonstrates the importance of using the fossil record to guide the recognition of phenotypic patterns under a PCM context, which has been pointed out several times in other studies (Bokma et al. 2015a, b; Benson et al. 2014; Finarelli and Flynn 2006; Hunt and Slater 2016; Puttick 2016; Puttick and Thomas 2015; Webster and Purvis 2002) and remains evident here also with methods other than *RRphylo-noder* (see Fig. 3).

Although ancestral states estimation is usually difficult (Cooper et al. 2016; Joy et al. 2016) and generally constrained within the limits of actual phenotypes at the tree tips (Gascuel and Steel 2014), new approaches are being developed to provide more sensible estimates. Herein, we demonstrated that *RRphylo-noder* is virtually as powerful in fitting ancestral states as other available methods, and

slightly more accurate in terms of fitting the true ancestral states when the description of phenotypic evolution is not reducible to a simple evolutionary model. This better accuracy probably depends on the fact that *RRphylo-noder* does not need to comply to the predictions of any abstract hypothesis about the tempo and mode of evolutionary change. As such, we believe *RRphylo-noder* is the most appropriate in cases of complex phenotypic distributions. This is especially true by considering that competing methods using Monte Carlo Markov Chain (MCMC) approaches require much longer computational times.

In our simulations we deliberately produced complex phenotypic patterns which change significantly across different branches of the tree. Although simple approaches such as *ace* and *fastAnc* may work well, even better than *RRphylo-noder* when the process behind phenotypic evolution is the BM, we suspect the existence of idiosyncratic evolutionary processes applying to different sections of the tree is common. For instance, body size increase over time, the well-known Cope’s rule, does not apply to all mammalian clades (Monroe and Bokma 2010; Raia et al. 2012), all dinosaurs (Benson et al. 2014; Hone et al. 2005), or all early amniote clades (Laurin 2004), meaning that when these clades are tested for Cope’s rule neither BM or BM with drift may serve as realistic evolutionary models. Benson et al. (2014a) presented an interesting case for change in the intensity of Cope’s rule in pterosaurs because of birds’ diversification starting at the beginning of the Cretaceous. The dinosaur clade including birds (maniraptoran dinosaurs) decreased, rather than increasing in body size throughout the Cretaceous (Lee et al. 2014) while the rest of the dinosaurs were still growing large. Baker et al. (2015) successfully applied a variable-rates model of phenotypic evolution to show that Cope’s rule applies with different intensities to 10 out of 11 mammalian orders. There is evidence that competition and niche incumbency influenced the timing and direction of phenotypic change in turtles (Rosenzweig and McCord 1991), dinosaurs (McNab 2009; Sookias et al. 2012), and insects (Waller and Svensson 2017). We believe that even this short account is enough to suggest that referring to a simple array of evolutionary models could be risky, especially when fossil phenotypes are included. At one time the inclusion of such fossil phenotypes as the ancestral conditions for some clades in the phylogeny does increase the power and reliability of PCMs and makes it less likely that the actual pattern of phenotypic evolution complies to the prediction of any abstract evolutionary model when this is wrong. We believe *RRphylo-noder* constitutes a worthy addition to the PCM toolbox, especially in terms of providing sensible ancestral state estimates with complex phenotypes, and when the recognition of temporal trends in trait evolution is the goal.

Acknowledgements We are grateful to Gianmarco Tesone and Martina Piccolo for sharing the cetacean body size data with us. The authors declare no conflict of interest.

Data Availability The R package RRphylo is available at <https://github.com/pasraia/RRphylo>. Raw data and phylogenetic tree for caniform carnivores are available as example dataset in the R package geiger. Raw data and phylogenetic tree for cetaceans are available as example dataset in the R package RRphylo. The R code to reproduce all the simulations performed in this study, together with raw data for cetaceans are available as Supplementary Information.

Compliance with Ethical Standards

Conflict of interest The authors declare that they have no conflict of interest.

References

- Alfaro, M. E., Santini, F., Brock, C., Alamillo, H., Dornburg, A., Rabosky, D. L., et al. (2009). Nine exceptional radiations plus high turnover explain species diversity in jawed vertebrates. *Proceedings of the National Academy of Sciences of the United States of America*, 106(32), 13410–13414. <https://doi.org/10.1073/pnas.0811087106>.
- Bapst, D. W. (2013). A stochastic rate-calibrated method for time-scaling phylogenies of fossil taxa. *Methods in Ecology and Evolution*, 4(8), 724–733. <https://doi.org/10.1111/2041-210X.12081>.
- Bapst, D. W., Wright, A. M., Matzke, N. J., & Lloyd, G. T. (2016). Topology, divergence dates, and macroevolutionary inferences vary between different tip-dating approaches applied to fossil theropods (Dinosauria). *Biology Letters*, 12, 20160237.
- Baker, J., Meade, A., Pagel, M., & Venditti, C. (2015). Adaptive evolution toward larger size in mammals. *Proceedings of the National Academy of Sciences of the United States of America*, 112, 5093–5098.
- Bokma, F., Godinot, M., Maridet, O., Ladevèze, S., Costeur, L., Solé, F., et al. (2015a). Testing for Depéret's Rule (Body Size Increase) in Mammals using Combined Extinct and Extant Data. *Systematic Biology*, 65, 98–108.
- Behrensmeyer, A. K., Kidwell, S. M., & Gastaldo, R. A. (2000). Taphonomy and paleobiology. *Paleobiology*, 26, 103–147. [https://doi.org/10.1666/0094-8373\(2000\)26\[103:TAPJ2.0.CO;2](https://doi.org/10.1666/0094-8373(2000)26[103:TAPJ2.0.CO;2).
- Benson, R. B. J., Campione, N. E., Carrano, M. T., Mannion, P. D., Sullivan, C., Upchurch, P., et al. (2014). Rates of Dinosaur Body Mass Evolution Indicate 170 Million Years of Sustained Ecological Innovation on the Avian Stem Lineage. *PLoS Biology*, 12, e1001853. <https://doi.org/10.1371/journal.pbio.1001853>.
- Bokma, F., Godinot, M., Maridet, O., Ladevèze, S., Costeur, L., Solé, F., et al. (2015b). Testing for Depéret's Rule (Body Size Increase) in Mammals using Combined Extinct and Extant Data. *Systematic Biology*. <https://doi.org/10.1093/sysbio/syv075>.
- Burnham, K. P., & Anderson, D. R. (2004). Multimodel inference: understanding AIC and BIC in model selection. *Sociological Methods Research*, 33, 261–304.
- Castiglione, S., Serio, C., Mondanaro, A., Di Febbraro, M., Profico, A., Girardi, G., et al. (2019). Simultaneous detection of macroevolutionary patterns in phenotypic means and rate of change with and within phylogenetic trees including extinct species. *PLoS ONE*, 14(1), e0210101–e210113. <https://doi.org/10.1371/journal.pone.0210101>.
- Castiglione, S., Tesone, G., Piccolo, M., Melchionna, M., Mondanaro, A., Serio, C., et al. (2018). A new method for testing evolutionary rate variation and shifts in phenotypic evolution. *Methods in Ecology and Evolution*, 9, 974–983. <https://doi.org/10.1111/2041-210X.12954>.
- Chira, A. M., & Thomas, G. H. (2016). The impact of rate heterogeneity on inference of phylogenetic models of trait evolution. *Journal of Evolutionary Biology*, 29(12), 2502–2518. <https://doi.org/10.1111/jeb.12979>.
- Cooper, N., Thomas, G. H., Venditti, C., Meade, A., & Freckleton, R. P. (2016). A cautionary note on the use of Ornstein Uhlenbeck models in macroevolutionary studies. *Biological Journal of the Linnean Society*, 118(1), 64–77. <https://doi.org/10.1111/bij.12701>.
- Didier, G., Fau, M., & Laurin, M. (2017). Likelihood of Tree Topologies with Fossils and Diversification Rate Estimation. *Systematic Biology*, 66(6), 964–987. <https://doi.org/10.1093/sysbio/syx045>.
- Eastman, J. M., Alfaro, M. E., Joyce, P., Hipp, A. L., & Harmon, L. J. (2011). A Novel Comparative Method For Identifying Shifts In The Rate Of Character Evolution On Trees. *Evolution*, 65(12), 3578–3589. <https://doi.org/10.1111/j.1558-5646.2011.01401.x>.
- Elliot, M. G., & Mooers, A. O. (2014). Inferring ancestral states without assuming neutrality or gradualism using a stable model of continuous character evolution. *BMC evolutionary biology*, 14(1), 226. <https://doi.org/10.1186/s12862-014-0226-8>.
- Felsenstein, J. (1985). Phylogenies and the comparative method. *American Naturalist*, 125, 1–15.
- Finarelli, J. A., & Flynn, J. J. (2006). Ancestral state reconstruction of body size in the Caniformia (Carnivora, mammalia): The effects of incorporating data from the fossil record. *Systematic Biology*, 55(2), 301–313. <https://doi.org/10.1080/10635150500541698>.
- Finarelli, J. A., & Liow, L. H. (2016). Diversification histories for North American and Eurasian carnivores. *Biological Journal of the Linnean Society*, 118(1), 26–38. <https://doi.org/10.1111/bij.12777>.
- Fitzgerald, E. M. G. (2012). Archaeocete-like jaws in a baleen whale. *Biology Letters*, 8(1), 94–96. <https://doi.org/10.1098/rsbl.2011.0690>.
- Fordyce, R. E., & Marx, F. G. (2018). Gigantism Precedes Filter Feeding in Baleen Whale Evolution. *Current biology : CB*, 28(10), 1670–1676.e2. <https://doi.org/10.1016/j.cub.2018.04.027>.
- Freckleton, R. P., Harvey, P. H., & Pagel, M. (2002). Phylogenetic Analysis and Comparative Data: A Test and Review of Evidence. *The American Naturalist*, 160(6), 712–726. <https://doi.org/10.1086/343873>.
- Garland, T., Jr., & Ives, A. R. (2000). Using the Past to Predict the Present: Confidence Intervals for Regression Equations in Phylogenetic Comparative Methods. *The American Naturalist*, 155(3), 346–364. <https://doi.org/10.1086/303327>.
- Gascuel, O., & Steel, M. (2014). Predicting the ancestral character changes in a tree is typically easier than predicting the root state. *Systematic Biology*, 63(3), 421–435. <https://doi.org/10.1093/sysbio/syu010>.
- Harmon, L. J., Schulte, J. A., Larson, A., & Losos, J. B. (2003). Tempo and Mode of Evolutionary Radiation in Iguanoid Lizards. *Science*, 301(5635), 961–964. <https://doi.org/10.1126/science.1084786>.
- Harmon, L. J., Weir, J. T., Brock, C. D., & Glor, R. E. (2007). (2007). GEIGER: investigating evolutionary radiations. *Bioinformatics*, 24, 129–131.
- Harvey, P. H., & Pagel, M. D. (1991). *The comparative method in evolutionary biology*. Oxford: Oxford University Press.
- Heath, T. A., Huelsenbeck, J. P., & Stadler, T. (2014). The fossilized birth-death process for coherent calibration of divergence-time estimates. *Proceedings of the National Academy of Sciences of the United States of America*, 111(29), E2957–E2966. <https://doi.org/10.1073/pnas.1319091111>.
- Hone, D. W. E., Keesey, T. M., Pisani, D., & Purvis, A. (2005). Macroevolutionary trends in the Dinosauria: Cope's rule. *Journal*

- of evolutionary biology, 18(3), 587–595. <https://doi.org/10.1111/j.1420-9101.2004.00870.x>.
- Hone, D., & Benton, M. (2005). The evolution of large size: how does Cope's Rule work? *Trends in ecology & evolution*, 20(1), 4–6. <https://doi.org/10.1016/j.tree.2004.10.012>.
- Hothorn, T., Bretz, F., & Westfall, P. (2008). Simultaneous inference in general parametric models. *Biometrical Journal*, 50(3), 346–363.
- Hunt, G., & Slater, G. (2016). Integrating Paleontological and Phylogenetic Approaches to Macroevolution. *Annual Review of Ecology, Evolution, and Systematics*, 47(1), 189–213. <https://doi.org/10.1146/annurev-ecolsys-112414-054207>.
- James, G., Witten, D., Hastie, T., & Tibshirani, R. (2013). *An Introduction to Statistical Learning* (Vol. 103). New York, NY: Springer Science & Business Media.
- Joy, J. B., Liang, R. H., McCloskey, R. M., Nguyen, T., & Poon, A. F. Y. (2016). Ancestral Reconstruction. *PLoS Computational Biology*, 12(7), e1004763–e1004820. <https://doi.org/10.1371/journal.pcbi.1004763>.
- Kratsch, C., & McHardy, A. C. (2014). RidgeRace: ridge regression for continuous ancestral character estimation on phylogenetic trees. *Bioinformatics*, 30(17), i527–i533. <https://doi.org/10.1093/bioinformatics/btu477>.
- Lambert, O., Martínez-Cáceres, M., Bianucci, G., Di Celma, C., Salas-Gismondi, R., Steurbaut, E., et al. (2017). Earliest Mysticete from the Late Eocene of Peru Sheds New Light on the Origin of Baleen Whales. *Current biology : CB*, 27(10), 1535–1541.e2. <https://doi.org/10.1016/j.cub.2017.04.026>.
- Laurin, M. (2004). The Evolution of Body Size, Cope's Rule and the Origin of Amniotes. *Systematic Biology*, 53(4), 594–622. <https://doi.org/10.1080/10635150490445706>.
- Lee, M. S. Y., Cau, A., Naish, D., & Dyke, G. J. (2014). Dinosaur evolution Sustained miniaturization and anatomical innovation in the dinosaurian ancestors of birds. *Science*, 345(6196), 562–566. <https://doi.org/10.1126/science.1252243>.
- Lenth, R. (2019). emmeans: Estimated Marginal Means, aka Least-Squares Means. R package version 1.4.3.01. <https://CRAN.R-project.org/package=emmeans>.
- Liow, L. H., Quental, T. B., & Marshall, C. R. (2010). When can decreasing diversification rates be detected with molecular phylogenies and the fossil record? *Systematic Biology*, 59(6), 646–659. <https://doi.org/10.1093/sysbio/syq052>.
- Marx, F. G., & Fordyce, R. E. (2015). Baleen boom and bust: a synthesis of mysticete phylogeny, diversity and disparity. *Open Science*, 2(4), 140434–140434. <https://doi.org/10.1098/rsos.140434>.
- McNab, B. K. (2009). Resources and energetics determined dinosaur maximal size. *Proceedings of the National Academy of Sciences of the United States of America*, 106(29), 12184–12188. <https://doi.org/10.1073/pnas.0904000106>.
- McQuate, S. (2017). Fossil of oldest known baleen-whale relative unearthed in Peru. *Nature Publishing Group*. <https://doi.org/10.1038/nature.2017.21966>.
- Meloro, C., Raia, P., & Barbera, C. (2007). Effect of predation on prey abundance and survival in Plio-Pleistocene mammalian communities. *Evolutionary Ecology Research*, 9(3), 505–525.
- Mitchell, J. S., Etienne, R. S., & Rabosky, D. L. (2018). Inferring Diversification Rate Variation From Phylogenies With Fossils. *Systematic Biology*, 68(1), 1–18. <https://doi.org/10.1093/sysbio/syy035>.
- Monroe, M. J., & Bokma, F. (2010). Little evidence for Cope's rule from Bayesian phylogenetic analysis of extant mammals. *Journal of Evolutionary Biology*, 23(9), 2017–2021. <https://doi.org/10.1111/j.1420-9101.2010.02051.x>.
- Montgomery, S. H., Geisler, J. H., McGowen, M. R., Fox, C., Marino, L., & Gatesy, J. (2013). The Evolutionary History Of Cetacean Brain And Body Size. *Evolution*, 67(11), 3339–3353. <https://doi.org/10.1111/evo.12197>.
- O'Meara, B. C. (2012). Evolutionary Inferences from Phylogenies: A Review of Methods. *Annual Review of Ecology, Evolution, and Systematics*, 43(1), 267–285. <https://doi.org/10.1146/annurev-ecolsys-110411-160331>.
- O'Meara, B. C., Anè, C., Sanderson, M. J., & Wainwright, P. C. (2006). Testing for different rates of continuous trait evolution using likelihood. *Evolution*, 60, 922–933.
- Pagel, M. (1997). Inferring evolutionary processes from phylogenies. *Zoologica Scripta*, 26(4), 331–348. <https://doi.org/10.1111/j.1463-6409.1997.tb00423.x>.
- Paradis, E., Schliep, K. (2018). ape 5.0: An environment for modern phylogenetics and evolutionary analyses in R. *Bioinformatics*, 35, 526–528.
- Pennell, M. W., & Harmon, L. J. (2013). An integrative view of phylogenetic comparative methods: connections to population genetics, community ecology, and paleobiology. *Annals of the New York Academy of Sciences*, 1289(1), 90–105. <https://doi.org/10.1111/nyas.12157>.
- Pennell, M. W., FitzJohn, R. G., Cornwell, W. K., & Harmon, L. J. (2015). Model Adequacy and the Macroevolution of Angiosperm Functional Traits. *The American Naturalist*, 186(2), E33–50. <https://doi.org/10.1086/682022>.
- Pinheiro, J., Bates, D., DebRoy, S., Sarkar, D., & R Core Team. (2014). nlme: Linear and nonlinear mixed effects models. R package version 3.1–117.
- Puttick, M. N. (2016). Partially incorrect fossil data augment analyses of discrete trait evolution in living species. *Biology Letters*, 12(8), 20160392. <https://doi.org/10.1098/rsbl.2016.0392>.
- Puttick, M. N., & Thomas, G. H. (2015). Fossils and living taxa agree on patterns of body mass evolution: a case study with Afrotheria. *Proceedings of the Royal Society B: Biological Sciences*, 282(1821), 20152023–20152029. <https://doi.org/10.1098/rspb.2015.2023>.
- Puttick, M. N., O'Reilly, J. E., Tanner, A. R., Fleming, J. F., Clark, J., Holloway, L., et al. (2017). Uncertain-tree: discriminating among competing approaches to the phylogenetic analysis of phenotype data. *Proceedings of the Royal Society B: Biological Sciences*, 284(1846), 20162290. <https://doi.org/10.1098/rspb.2016.2290>.
- Rabosky, D. L. (2014). Automatic Detection of Key Innovations, Rate Shifts, and Diversity-Dependence on Phylogenetic Trees. *PLoS ONE*, 9(2), e89543–e89615. <https://doi.org/10.1371/journal.pone.0089543>.
- Raia, P., Carotenuto, F., Passaro, F., Fulgione, D., & Fortelius, M. (2012). Ecological Specialization in Fossil Mammals Explains Cope's Rule. *The American Naturalist*, 179(3), 328–337. <https://doi.org/10.1086/664081>.
- Revell, L. J. (2010). Phylogenetic signal and linear regression on species data. *Methods in Ecology and Evolution*, 1(4), 319–329. <https://doi.org/10.1111/j.2041-210X.2010.00044.x>.
- Revell, L. J. (2012). phytools: an R package for phylogenetic comparative biology (and other things). *Methods in Ecology and Evolution*, 3(2), 217–223. <https://doi.org/10.1111/j.2041-210X.2011.00169.x>.
- Rosenzweig, M. L., & McCord, R. D. (1991). Incumbent replacement: Evidence for long-term evolutionary progress. *Paleobiology*, 17, 202–213.
- Sakamoto, M., & Venditti, C. (2018). Phylogenetic non-independence in rates of trait evolution. *Biology Letters*, 14(10), 20180502. <https://doi.org/10.1098/rsbl.2018.0502>.
- Schnitzler, J., Theis, C., Polly, P. D., & Eronen, J. T. (2017). Fossils matter—understanding modes and rates of trait evolution in Musteloida (Carnivora). *Evolutionary Ecology Research*, 18, 187–200.
- Serio, C., Castiglione, S., Tesone, G., Piccolo, M., Melchionna, M., Mondanaro, A., et al. (2019). Macroevolution of Toothed Whales Exceptional Relative Brain Size. *Evolutionary Biology*, 46(4), 332–342.


- Silvestro, D., Zizka, A., Bacon, C. D., Cascales-Miñana, B., Salamin, N., & Antonelli, A. (2016). Fossil biogeography: a new model to infer dispersal, extinction and sampling from palaeontological data. *Philosophical Transactions of the Royal Society B: Biological Sciences*, 371(1691), 20150225–20150313. <https://doi.org/10.1098/rstb.2015.0225>.
- Slater, G. J., & Harmon, L. J. (2013). Unifying fossils and phylogenies for comparative analyses of diversification and trait evolution. *Methods in Ecology and Evolution*, 4(8), 699–702. <https://doi.org/10.1111/2041-210X.12091>.
- Slater, G. J., Harmon, L. J., & Alfaro, M. E. (2012). Integrating fossils with molecular phylogenies improves inference of trait evolution. *Evolution*, 66(12), 3931–3944. <https://doi.org/10.1111/j.1558-5646.2012.01723.x>.
- Smaers, J. B., Mongle, C. S., & Kandler, A. (2016). A multiple variance Brownian motion framework for estimating variable rates and inferring ancestral states. *Biological Journal of the Linnean Society*, 118(1), 78–94. <https://doi.org/10.1111/bij.12765>.
- Sookias, R. B., Butler, R. J., & Benson, R. B. J. (2012). Rise of dinosaurs reveals major body-size transitions are driven by passive processes of trait evolution. *Proceedings of the Royal Society B: Biological Sciences*, 279(1736), 2180–2187. <https://doi.org/10.1098/rspb.2011.2441>.
- Venditti, C., Meade, A., & Pagel, M. (2011). Multiple routes to mammalian diversity. *Nature*, 479(7373), 393–396. <https://doi.org/10.1038/nature10516>.
- Waller, J. T., & Svensson, E. I. (2017). Body size evolution in an old insect order: No evidence for Cope's Rule in spite of fitness benefits of large size. *Evolution*, 71(9), 2178–2193. <https://doi.org/10.1111/evo.13302>.
- Webster, A. J., & Purvis, A. (2002). Testing the accuracy of methods for reconstructing ancestral states of continuous characters. *Proceedings of the Royal Society B: Biological Sciences*, 269(1487), 143–149. <https://doi.org/10.1098/rspb.2001.1873>.

Section 3

The Chapters included in this Section apply detailed analytical frameworks to real case studies in order to determine the presence and strength of morphological evolutionary trends in the cranio-mandibular complex of one or multiple carnivoran groups. Almost all these works also assess the impact of ecological variables (e.g., qualitative categories concerning diet or habitat) on the resulting evolutionary patterns. In particular, Chapter 5 aims to test for the occurrence of shape convergence in crania and mandibles of living carnivorans and, to do so, it assess the strength of this evolutionary trend in several dietary categories and textbook examples selected from the literature. Then, the impact of different ecological factors on cranial and mandibular shape of living carnivorans is measured in Chapter 6 in order to detect patterns of covariation and directional responses. Chapter 7 assesses the presence of a recently proposed biological rule (named craniofacial evolutionary allometry) in living and fossil felids, including sabertoothed cats that might constitute an exception to this rule thanks to their unusual rostral morphology and extreme ecomorphological adaptations.

Chapter 5 – Testing the occurrence of convergence in the craniomandibular shape evolution of living carnivorans

Testing the occurrence of convergence in the craniomandibular shape evolution of living carnivorans

Davide Tamagnini,^{1,2,3}  Carlo Meloro,⁴ Pasquale Raia,⁵ and Luigi Maiorano^{1,2}

¹Department of Biology and Biotechnologies "Charles Darwin," University of Rome "La Sapienza," Rome 00185, Italy

²Museum of Zoology, Sapienza Museum Centre, University of Rome "La Sapienza," Rome 00185, Italy

³E-mail: davide.tamagnini@uniroma1.it

⁴Research Centre in Evolutionary Anthropology and Palaeoecology, School of Natural Sciences and Psychology, Liverpool John Moores University, Liverpool L3 3AF, United Kingdom

⁵Dipartimento di Scienze della Terra, dell'Ambiente e delle Risorse, University of Naples Federico II, Napoli 80126, Italy

Received May 30, 2020

Accepted March 28, 2021

Convergence consists in the independent evolution of similar traits in distantly related species. The mammalian craniomandibular complex constitutes an ideal biological structure to investigate ecomorphological dynamics and the carnivorans, due to their phenotypic variability and ecological flexibility, offer an interesting case study to explore the occurrence of convergent evolution. Here, we applied multiple pattern-based metrics to test the occurrence of convergence in the craniomandibular shape of extant carnivorans. To this aim, we tested for convergence in many dietary groups and analyzed several cases of carnivoran convergence concerning either ecologically equivalent species or ecologically similar species of different body sizes described in the literature. Our results validate the occurrence of convergence in ecologically equivalent species in a few cases (as well as in the case of giant and red pandas), but almost never support the occurrence of convergent evolution in dietary categories of living carnivorans. Therefore, convergent evolution in this clade appears to be a rare phenomenon. This is probably the consequence of a complex interplay of one-to-many, many-to-one, and many-to-many relationships taking place between ecology, biomechanics, and morphology.

KEY WORDS: Convergence, diet, ecomorphology, evolutionary trend, geometric morphometrics, skull.

The occurrence of similar traits in distantly related species is commonly known as convergence and implies that those traits are independently pushed to evolve toward a common selective optimum (Wake et al. 2011; Speed and Arbuckle 2017). Convergent evolution can be seen as an example of evolutionary trend (i.e., persistent and directional changes in the state of one or more quantitative traits, resulting in substantial changes through time—McNamara 2006), and specifically one in which multiple groups evolve to reduce their distance in the multivariate trait space (Huang et al. 2015; Stayton 2015a; Bolnick et al. 2018). Convergent evolution may also increase the similarity between distantly related species without completely obliterating the preexisting differences, leading to what is defined as “incom-

plete convergence” (Herrel et al. 2004; Stayton 2006; Losos 2011).

When morphology is investigated, Pigot et al. (2020) suggested that the constraints imposed by the putatively limited number of ecological niches within a clade might contribute to produce recurrent patterns of evolution toward similar morphotypes, thus resulting in iterative evolution of morphological similarities (Simpson 1944, 1953; Coxall et al. 2007; Van Valkenburgh 2007; Slater 2015). This has been observed, for instance, both in flightless birds (Wright et al. 2016; Hume and Martill 2019; Pigot et al. 2020) and in *Anolis* lizards of the Caribbean islands (Losos 1992; Mahler et al. 2013). Although there are many more examples of morphological

convergence in multiple animal and plant groups, Stayton (2008) recently demonstrated using simulations that the detection of this phenomenon depends on the number of species investigated within clades in relation to the number of traits. A further consideration is the growing evidence that convergence is rare in many real case studies. For example, Grossnickle et al. (2020) only found support for incomplete convergence in the skeleton of gliding mammals (presumably constrained by strict biomechanical and physical requirements acting on nonpowered flight). Zelditch et al. (2017) similarly argued that ecomorphological convergence in the jaw shape of squirrels is rare and occurs among ecological categories that are extremely size constrained such as nut-eating and bark-gouging species. The authors suggested that the combination of one-to-many, many-to-one, and many-to-many relationships between ecology and function (which produce a complex structure of the underpinning adaptive landscape) is responsible for the rarity of convergent evolution.

The craniomandibular complex constitutes a suitable biological structure to investigate ecomorphological dynamics in mammals mainly because of the different roles played by its two components: the cranium and the mandible (Moss and Young 1960). The cranium is a functionally complex structure whose morphology is influenced by disparate demands such as protecting the brain, feeding, and agonistic behavior, as well as sensory perception (Cheverud 1981; Hallgrímsson et al. 2007). Besides, the origin of cranial bones is partly heterochronic and developmentally heterogeneous, with some originating endochondrally and others from intramembranous ossification (Sperber 2001). The mandible, in contrast, performs fewer functions mainly related to feeding (i.e., food capturing and processing—Hylander and Johnson 1994), as well as agonistic behaviors, and it is made of a single bone that develops from the simple ossification of an osteogenic membrane (Sperber 2001). Thus, one might expect that these two functionally and anatomically integrated, yet distinct, structures respond differently to evolutionary pressures, with the cranium being potentially subject to a higher number of structural and functional constraints than the mandible.

The study of the craniomandibular complex is particularly interesting in species belonging to clades with substantial phenotypic variability and disparate ecologies, such as the members of the mammalian order Carnivora (henceforth, simply called carnivorans—Ewer 1973; Gittleman 1986). Indeed, this clade represents a common model for ecomorphological investigations, which include the study of morphological convergence in relation to ecological shifts (Radinsky 1981a,b, 1982; Van Valkenburgh 1989, 1991, 2007; Figueirido et al. 2010, 2013; Meloro et al. 2015; Dumont et al. 2016; Michaud et al. 2018).

Convergence has been repeatedly detected in the morphology of both extant and fossil carnivorans (e.g., Van Valkenburgh 2007; Figueirido et al. 2010, 2013; Tseng and Wang 2011;

Meloro et al. 2015). Morphological similarities in species with overlapping diets, such as the giant (*Ailuropoda melanoleuca*) and the red panda (*Ailurus fulgens*), offer some popular textbook examples of ecological convergence in phenotypic adaptations. Although radically different in body size, these two phylogenetically distant species evolved similarities in craniomandibular and appendicular morphology (e.g., wide zygomatic arches, powerful cheek teeth, expanded radial sesamoids), as well as similar physiological adaptations and developmental pathways (e.g., modifications in the amino acid metabolism and mutations in limb development genes—Hu et al. 2017), to specialize on a diet almost exclusively made of bamboo (Salesa et al. 2006; Figueirido et al. 2010). If, for pandas, convergence is found in a pair of species living in the same habitat and the same region, carnivorans provide popular examples of convergent morphological adaptations also in species that evolved in different continents. These pairs of species are commonly seen as “ecologically equivalent,” because they live in different geographical regions but occupy similar ecological niches (Lincoln et al. 1998; Biggins et al. 2011). For instance, the Eurasian raccoon dog (*Nyctereutes procyonoides*) is considered the ecological equivalent of the North American raccoon (*Procyon lotor*—Ward and Wurster-Hill 1990), and the Malayan civet (*Viverra zibetha*) the ecological equivalent of the Holarctic red fox (*Vulpes vulpes*—Larivière and Pasitschniak-Arts 1996; Veron et al. 2014).

The ecological factor most frequently assumed to have produced morphological convergence in carnivorans is diet. This has led many researchers to suggest the existence of broad diet-related ecomorphotypes such as pack hunters (i.e., the spotted hyena and large wild canids—Meloro et al. 2015) or durophagous feeders (common among ursids, mustelids, and hyaenids—Figueirido et al. 2013). However, Meloro et al. (2015) also observed that morphological convergence in the mandible of carnivorans heavier than 7 kg is rare when comparing species belonging to the same dietary category, probably because of a rapid diversification in terms of size and a less evolutionary malleable shape occurring in this clade. If confirmed, this would suggest that overlapping diets may contribute to morphological convergence but do not necessarily lead to it.

Craniomandibular convergence in carnivorans has already been tested by several authors comparing linear measurements or qualitative morphological features (Gaubert et al. 2005) as well as by applying geometric morphometrics (GMM—Figueirido et al. 2010, 2013; Meloro et al. 2015, 2017). However, despite these many studies on the Carnivora, convergence has never been extensively explored in this clade using a large taxonomic sample representative of its vast ecomorphological disparity. In this study, we assessed the presence and strength of convergence in the shape of the craniomandibular complex of living carnivorans, using GMM and three different pattern-based (i.e.,

able to detect patterns regardless of the processes behind them) indices designed for detecting the occurrence of retained and/or evolved similarity: C1 (Stayton 2015b), θ (Castiglione et al. 2019), and Wheatsheaf (Arbuckle et al. 2014) metrics. More precisely, we investigated morphological convergence by grouping species based on the type of prevalent food in their diet. Then, we considered several cases of potential morphological convergence by focusing on ecologically equivalent species of broadly similar body size or sympatric taxa with strong similarity in diet and habitat but large differences in size.

Materials and Methods

DATA COLLECTION, SAMPLES, GMM, AND PHYLOGENY

Cranial and mandibular photographic samples were collected by the same operator (CM) using a digital SLR Nikon D40 equipped with a Nikkor 70–200 mm lens, at a focal length of 100 mm. A horizontal tripod was employed to position the camera above the specimens to hold the camera still and minimize photographic distortions (e.g., Muir et al. 2012). A spirit level was used to verify that the camera and the specimen were approximately parallel.

Samples consist of 529 crania photographed in ventral view and 554 mandibles in lateral view. They represent more than 60% of the existing carnivoran species diversity (188 out of 296). The taxonomy adopted in this study followed the IUCN Red List website (<https://www.iucnredlist.org>). Almost all specimens, except for a few (i.e., three crania and three mandibles of *Mirounga leonina*) made available by the Falkland Islands Elephant Seal Research Group (<http://eleseal.org/>), came from museum collections including National Museums of Scotland (Edinburgh), World Museum (Liverpool), Natural History Museum (London), Kenya National Museums (Nairobi), and Royal Museum for Central Africa (Tervuren). Sample compositions are detailed in Table S1 and a full list with catalogue numbers is available upon request.

All individuals were adults, as assessed by the presence of complete dentition and the fusion of cranial sutures. For each species, a minimum of one cranium and one mandible was collected, including both sexes whenever available. When multiple specimens belonging to the same species were available, morphological data were averaged within species, obtaining pooled-sex data. Using a few individuals to represent a species is never ideal (Cardini 2020), but nonetheless feasible in macroevolutionary analyses with wide phylogenetic scope (e.g., Drake and Klingenberg 2010; Meloro and O'Higgins 2011).

The two-dimensional landmark digitization was performed using the software TPSDig (version 2.21—Rohlf 2015) by a single operator (DT) to avoid interoperator biases (e.g.,

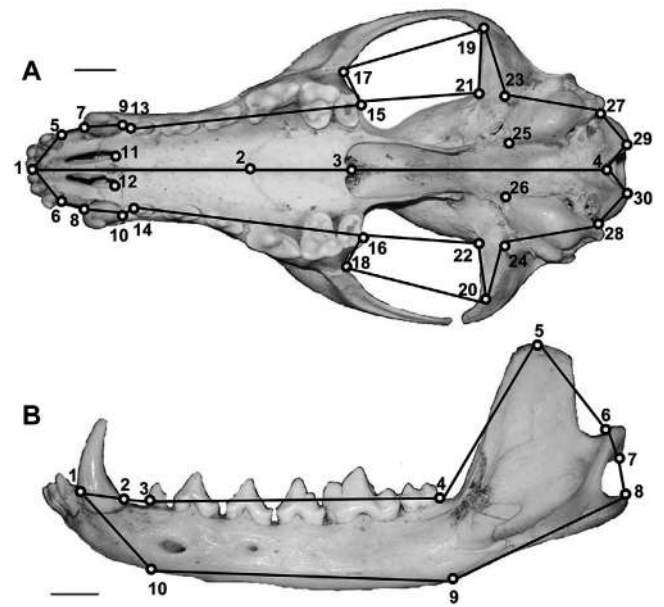


Figure 1. Landmark configuration, together with the wireframe, on cranium (A) and mandible (B) of red fox (*Vulpes vulpes*). Scale bar is 1 cm.

misinterpretation of landmark definitions). Landmark configurations for the cranium and the mandible are shown in Figure 1, and their anatomical definitions are provided in Table 1. The selected configuration of landmarks generally followed Meloro and O'Higgins (2011) and Tamagnini et al. (2017) to describe the main morphofunctional regions of the craniomandibular complex. This configuration ensured the anatomical correspondence of homologous landmarks among all the specimens without particular references to the postcanine dentition, except for the length of the tooth row, because premolars and molars are indistinguishable in the seals and the walrus.

To remove nonshape variation from two dimensional Cartesian coordinates of landmarks, we employed the Procrustes superimposition (Rohlf and Slice 1990; Adams et al. 2004, 2013) using the software MorphoJ (version 1.06d; Klingenberg 2011). This procedure consists of three steps: (1) the standardization of size, (2) the removal of translational variation, and (3) the minimization of rotational differences (Rohlf and Slice 1990). Because we are using two-dimensional measurements of three-dimensional structures, the flattening of the third dimension inevitably introduces an error (Roth 1993). However, previous studies on crania and mandibles of marmots and living equids (Cardini 2014; Cardini and Chiapelli 2020) suggested that results are likely to be robust to the error of two- to three-dimensional approximation, as long as landmarks are approximately coplanar (as in our data) and differences relatively large, as typical of macroevolutionary analyses.

Table 1. Definitions of the anatomical landmarks.

Cranium
Midplane
1 Most anterior point on premaxilla
2 Meeting point of maxilla and palatine
3 Posterior endpoint of palatine
4 Most anterior point on the rim of the foramen magnum
Bilateral
5–6 Posteromedial point on the alveolar margin of the last upper incisor
7–8 Anteromedial point on the alveolar margin of the canine
9–10 Posteromedial point on the alveolar margin of the canine
11–12 Most posterior edge of the palatine foramen
13–14 Anteromedial point on the alveolar margin of the premolar starting the upper premolar row
15–16 Posteromedial point on the alveolar margin of the last tooth of the upper jaw
17–18 Anterior point of maximum curvature on the interior side of the zygomatic arch
19–20 Posterior point of maximum curvature on the interior side of the zygomatic arch
21–22 Interior side margin of the glenoid fossa
23–24 Medial side margin of the glenoid fossa
25–26 Meeting point of basioccipital, basisphenoid, and tympanic bulla
27–28 and 29–30 Edges of the occipital condyle
Mandible
1 Most anterior point on the alveolar margin of the canine
2 Most posterior point on the alveolar margin of the canine
3 Anterior point on the alveolar margin of the first tooth in the premolar row
4 Posterior point on the alveolar margin of the last tooth in the molar row
5 Tip of the coronoid process
6–7 Maximum depth of the condylar process
8 Most lateral extreme point of the angular process
9 Vertical projection of 4 perpendicular to the line defined by (3–4)
10 Vertical projection of 3 perpendicular to the line defined by (3–4)

The background for comparative analyses was provided by a molecular phylogeny from the 10KTrees project (Arnold et al. 2010). This phylogeny is a consensus based on 14 mitochondrial genes, 14 autosomal genes, and one gene from the Y-chromosome. The node ages were inferred using 16 fossil calibration points, extracted from the Paleobiology Database (<http://paleodb.org>).

MORPHOLOGICAL CONVERGENCE

To test for convergence in dietary groups, each species was ascribed to one out of nine mutually exclusive dietary categories following Christiansen and Wroe (2007) for terrestrial carnivores, and Jones et al. (2013) for pinnipeds. The categories are as follows: large prey hunters, medium prey hunters, small prey hunters, herbivores/frugivores, insectivores, piscivores, crustaceans, molluscivores, and omnivores (Fig. 2). These are all the possible ecological groups obtained adopting a dietary categorization based on the main food item consumed by living carnivores. Large, medium, and small prey hunters were distinguished based on the comparison between the size of the predator and the size of its most common prey. Omnivores included species relying almost in similar proportions on two or more food items. Whenever the attribution of a species was not provided in Christiansen and Wroe (2007) or Jones et al. (2013) or it was uncertain, we decided the most likely dietary group relying on the information available in the *Handbook of the Mammals of the World - Volumes 1 and 4* (Wilson and Mittermeier 2009, 2014, and references therein).

As anticipated, besides testing convergence among species within each dietary group, we also explored whether convergence is supported in cases of species considered ecologically equivalent in different biogeographical regions (i.e., red fox—Malayan civet, raccoon dog—raccoon, Iberian lynx—fossa, and spotted hyena—wolverine) or ecologically similar but living in sympatry thanks to large differences in body size (i.e., giant panda—red panda).

C1, θ , AND WHEATSHEAF INDEX

To test for the strength of shape convergence, we computed three different metrics designed for detecting the occurrence of retained and/or evolved similarity: C1, θ , and Wheatshaf index.

C1 is a distance-based measure “representing the proportion of the maximum distance between the putatively convergent species that has been ‘closed’ by subsequent evolution, and thus ranges from 0 to 1 as convergence increases” (Stayton 2015b, p. 2144). For instance, $C1 = 0.5$ indicates that the convergent species closed 50% of the maximum phenotypic distance between them. To assess significance, this approach simulates evolution via Brownian motion (i.e., null hypothesis) using the input tree and parameters derived from the observed data, returning a C1 metric for each simulation and calculating the *P*-value from the number of times the simulated value exceeds the observed value. C1 metric is designed for detecting the occurrence of evolved similarity (i.e., convergence). C1 was computed and tested using the functions *convrat* and *convratsig*, embedded in the package *convevol* (Stayton 2015b).

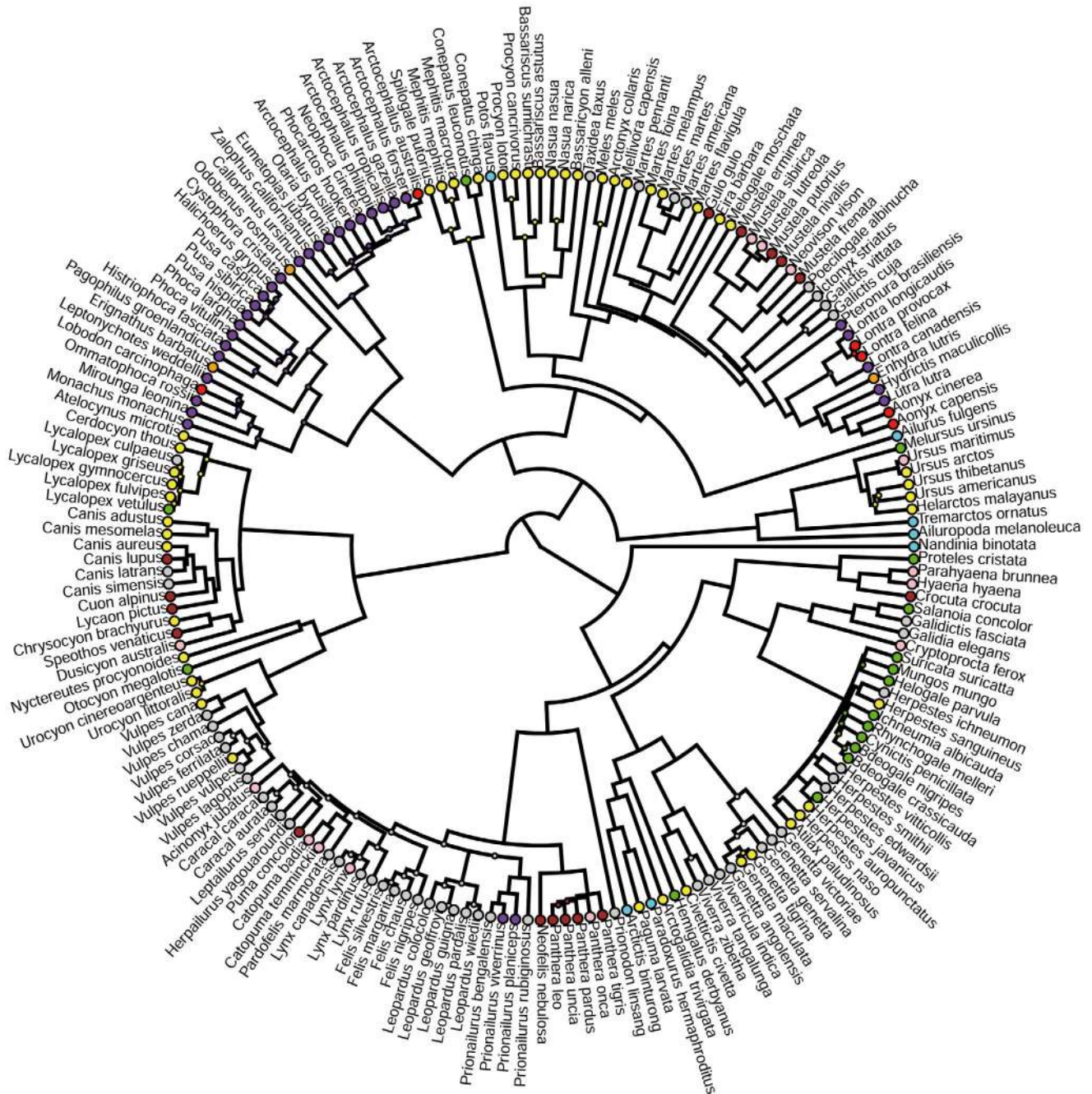


Figure 2. Circular dendrogram representing the 10KTrees phylogeny (Arnold et al. 2010), and showing the distribution of each food item category in living carnivorans. Large prey hunters are represented in brown, medium prey hunters in pink, small prey hunters in grey, herbivores/frugivores in turquoise, insectivores in green, piscivores in purple, crustacevores in red, molluscivores in orange, and omnivores in yellow.

θ is the average angle between the phenotypic vectors of putatively convergent species in the multivariate shape space (Castiglione et al. 2019). The cosine of angle θ represents the correlation coefficient between these vectors (Zelditch et al. 2012). Thus, θ is a measure of the resemblance between the phenotypes (Adams and Collyer 2009), which, under a Brownian Motion (BM) model, is expected to decrease proportionally to the time

since divergence from a common ancestor. The test estimates whether the mean time-distance-standardized θ scores between all pairs of species evolving under a given state (e.g., dietary category) are lower than expected under BM, which would indicate retained and/or evolved similarity. Time-distance-standardized θ was implemented with the function *search.conv*, embedded in the package *RRphylo* (Castiglione et al. 2018, 2019).

The third and last metric we used is the Wheatsheaf index. This index is the ratio between the average phylogenetically corrected phenotypic distance computed for the entire sample to the same distance calculated only for the putatively convergent species (e.g., species in the same dietary category). Similar to C1, this index relies on phenotypic distances, whereas θ relies on angles between phenotypic vectors. To assess significance for the Wheatsheaf index, we followed the bootstrapping approach of Arbuckle et al. (2014, p. 687), which “resamples the tips of the tree along with their trait values and thus obtains a distribution of possible Wheatsheaf indices given the phylogeny and the trait values for each species. The *P*-value is equal to the proportion of bootstrap samples that are greater than or equal to the value of the index calculated from the original data set.” As discussed in previous studies (Stayton 2015b; Arbuckle and Speed 2016), higher values of this index indicate not only a greater degree of clustering among the convergent taxa, but also greater distinctiveness of them, making it appropriate to test for “incomplete convergence,” but potentially conflating convergence with retained similarity. For this reason, although using only the Wheatsheaf index (as well as θ) is inadvisable to assess if a group underwent convergent evolution, combining this metric with others more strictly designed for detecting the occurrence of convergence (e.g., C1) might allow researchers to distinguish between cases of convergence and retained similarity (e.g., phases of reduced or null evolutionary rate). Wheatsheaf index was computed and tested using the functions *windex* and *test.windex*, embedded in the package *windex* (Arbuckle and Minter 2015).

C1, θ , and Wheatsheaf index were applied to each of the nine dietary categories adopted in this study (Fig. 2) to test for the presence of shape convergence in our sample. Then, these metrics were further applied to test convergence on the cases concerning either ecologically equivalent species or ecologically similar species of different body sizes. All analyses employed comparative tests using the 10Ktrees phylogeny as an estimate of evolutionary relationships. The significance of each test was assessed performing 1000 simulations against random expectations following Arbuckle et al. (2014), Stayton (2015b), and Castiglione et al. (2019). Following the example of Maiorano et al. (2008), we also adopted a multiple testing correction metric, the *Q*-value (Storey 2002; Storey and Tibshirani 2003; Storey et al. 2004), to take into account the simultaneous implementation of several tests, which could inflate type I errors. The *Q*-value metric is also suitable for cases where a dependency exists between a portion of the performed tests (Benjamini and Yekutieli 2001). All significance tests were carried out at the $\alpha = 0.05$ level. Morphological data, R code, and phylogeny used in this study are provided as Supporting Information.

Results

TESTS IN DIETARY CATEGORIES

For the mandible, C1 ranged from 0 to 0.123 (Table 2), with none of the tests reaching significance, which suggests a lack of strong evidence for convergence in any of the dietary categories we tested. Mandibular time-distance-standardized θ ranged, depending on the dietary group, from 0.615 to 1.035 (Table 2). Only omnivore carnivorans reached significance in both their mandibular *P*- and *Q*-values regarding this metric (Fig. 3). This indicates that, within omnivores, there is more retained and/or evolved similarity than expected using a BM model of evolution. Finally, Wheatsheaf indices ranged from 0.501 to 1.736 in the mandible for all the ecological categories (Table 2). Small prey hunters and omnivores returned significant *P*-values in the mandible regarding the Wheatsheaf index, whereas only omnivores returned a significant *Q*-value: this outcome indicates the occurrence of retained and/or evolved similarity in omnivore carnivorans and, less convincingly, in small prey hunters.

Cranial C1 scores ranged from 0.006 to 0.130 (Table 3), with only large prey hunters being significant (both for *P*- and *Q*-values). Cranial time-distance-standardized θ ranged from 0.686 to 3.560 for all the dietary categories (Table 3). Only omnivore carnivorans reached significance in their cranial *P*-value regarding this metric (Fig. 3), whereas none of the *Q*-values was significant. Finally, Wheatsheaf index scores ranged, for cranial shape, from 0.631 to 1.822 (Table 3). Insectivores, omnivores, and medium prey hunters reached significance in both their cranial *P*- and *Q*-values regarding this metric, whereas herbivores/frugivores returned only a significant *P*-value.

TESTS IN SELECTED CASES OF ECOLOGICALLY EQUIVALENT SPECIES AND SYMPATRIC SPECIES WITH SIMILAR ECOLOGY BUT LARGE SIZE DIFFERENCES

In the selected cases of species with broadly similar ecological niches living either in separate biogeographical regions or sympatrically thanks to large body size differences, mandibular C1 scores were greater than 0.305 (min score = 0.305, max score = 0.598) for all the considered cases included in Table 4. The cases red fox—Malayan civet, giant panda—red panda, and raccoon dog—raccoon reached significance in both *P*- and *Q*-values in the mandible regarding the C1 metric, whereas the case Iberian lynx—fossa returned only a marginally significant *P*-value. Mandibular shape time-distance-standardized θ ranged from 0.220 to 0.520 (Table 4). The red fox—Malayan civet, raccoon dog—raccoon, and spotted hyena—wolverine, as well as giant panda—red panda, were all (Fig. 4) significant in terms of both *P*- and *Q*-values. Finally, Wheatsheaf indices for the mandible ranged from 1.914 to 10.348 (Table 4), but significance

Table 2. Mandibular C1, time-distance-standardized θ , and Wheatsheaf index scores, *P*-values, and *Q*-values relative to the dietary categories adopted to test the occurrence of shape convergence. Significant *P*-values and *Q*-values at $\alpha = 0.05$ are underlined.

Dietary category	C1			Time-distance-standardized θ			Wheatsheaf index		
	Score	<i>P</i> -value	<i>Q</i> -value	Score	<i>P</i> -value	<i>Q</i> -value	Score	<i>P</i> -value	<i>Q</i> -value
Herbivores/Frugivores	0.046	0.803	0.999	0.660	0.111	0.500	1.736	0.069	0.373
Insectivores	0.106	0.219	0.593	1.035	0.984	0.999	0.824	0.105	0.500
Crustacivores	0.104	0.409	0.919	0.993	0.871	0.999	0.831	0.148	0.510
Molluscivores	0.000	0.999	0.999	1.018	0.866	0.999	0.746	0.872	0.999
Piscivores	0.066	0.891	0.999	0.615	0.287	0.674	0.501	0.998	0.999
Omnivores	0.123	0.230	0.593	0.718	<u>0.001</u>	<u>0.011</u>	1.226	<u>0.001</u>	<u>0.011</u>
Large prey hunters	0.091	0.651	0.999	0.779	0.539	0.999	0.929	0.594	0.999
Medium prey hunters	0.074	0.921	0.999	0.897	0.915	0.999	1.086	0.150	0.510
Small prey hunters	0.091	0.731	0.999	0.740	0.171	0.513	0.928	<u>0.021</u>	0.142

(in both *P*- and *Q*-values) was reached only in the case raccoon dog—raccoon.

For the same cases used in the tests on mandibular shape, cranial C1s ranged from 0.156 to 0.322 (Table 4). With C1, the case giant panda (red panda) was significant for both *P*- and *Q*-values, whereas the spotted hyena (wolverine) test was marginally significant only for the *P*-value. Cranial time-distance-standardized θ ranged from 0.230 to 0.614 (Table 4), with only the red fox (Malayan civet) and giant panda (red panda) significant using both *P*- and *Q*-values (Fig. 4). Cranial Wheatsheaf indices were larger than 1.877 (range = 1.877–5.525; Table 4), but none of them reached significance.

Discussion

IS THERE SHAPE CONVERGENCE IN THE CARNIVORAN CRANIOMANDIBULAR COMPLEX?

Our results support three main conclusions: (1) retained similarity occurs in omnivores (significant θ and Wheatsheaf index, but nonsignificant C1 and thus no clear evidence of convergence), (2) compelling evidence of convergence within dietary classes is very rare (i.e., only cranial shapes of large prey hunters converge as suggested by their significant C1, whereas mandibular shapes do not converge in any dietary class), and (3) two cases of ecologically equivalent species (i.e., red fox—Malayan civet; raccoon dog—raccoon) converge only in mandibular shape and one case of ecologically similar species of different body sizes converges in both cranial and mandibular shape (i.e., giant and red pandas).

Omnivores tend to cluster around a mean shape (Fig. 3), which has an elongated rostrum and relatively long tooth rows in both the upper and lower jaw. This is often associated with a full dental formula (Ewer 1973), a condition common in the small-sized species belonging to the carnivoran stem group, such as those of the genus *Gustafsonia* (Tomiya and Tseng 2016, but

see Werdelin 1996 for different morphologies in the carnivoran stem group). Although our results could lead to suppose the occurrence of convergent evolution in omnivore carnivorans at first, the fact that the volume of shape space occupied by omnivores is considerably large in relation to the overall shape space occupied by all species (Fig. 3), together with the lack of significance for their C1s, suggests the occurrence of evolutionary conservatism as a more likely scenario (i.e., closely related species more similar than would be expected based on their phylogenetic relationships—Losos 2008; Moen et al. 2013). According to this hypothesis, a common ancestor of omnivore carnivorans evolved the omnivore condition (that therefore arose only once in this group) and its descendants represent just a continuation of a successful morphotype. This scenario supports Simpson (1944, 1953) who suggested that evolution largely occurs within relatively narrow adaptive zones, because those wandering too far from the peaks of an adaptive zone are “weeded out by selection, whereas new zones are colonized when rapid bursts of evolution propel a species across the selectively disadvantageous space between zones” (Polly 2008, p. 3). In particular, our results are compatible with the existence of an omnivore adaptive zone in the craniomandibular shape evolution of living carnivorans, with other specialized species emerging from this region of the multivariate shape space. A similar pattern might explain how pinnipeds moved toward a progressively more specialized aquatic lifestyle and evolved a remarkably distinctive ankle shape, hugely dissimilar from those of their closer terrestrial relatives among the caniforms (Polly 2008). In contrast, terrestrial carnivorans, despite specializing for different types of terrestrial locomotion, largely retained a broadly similar foot bone morphology. This, together with other plesiomorphies, contributed to mislead taxonomists into splitting the carnivorans into pinnipeds and fissipeds, a subordinal classification no longer valid because of the paraphyletic state of the fissipeds (Arnason et al. 2007).

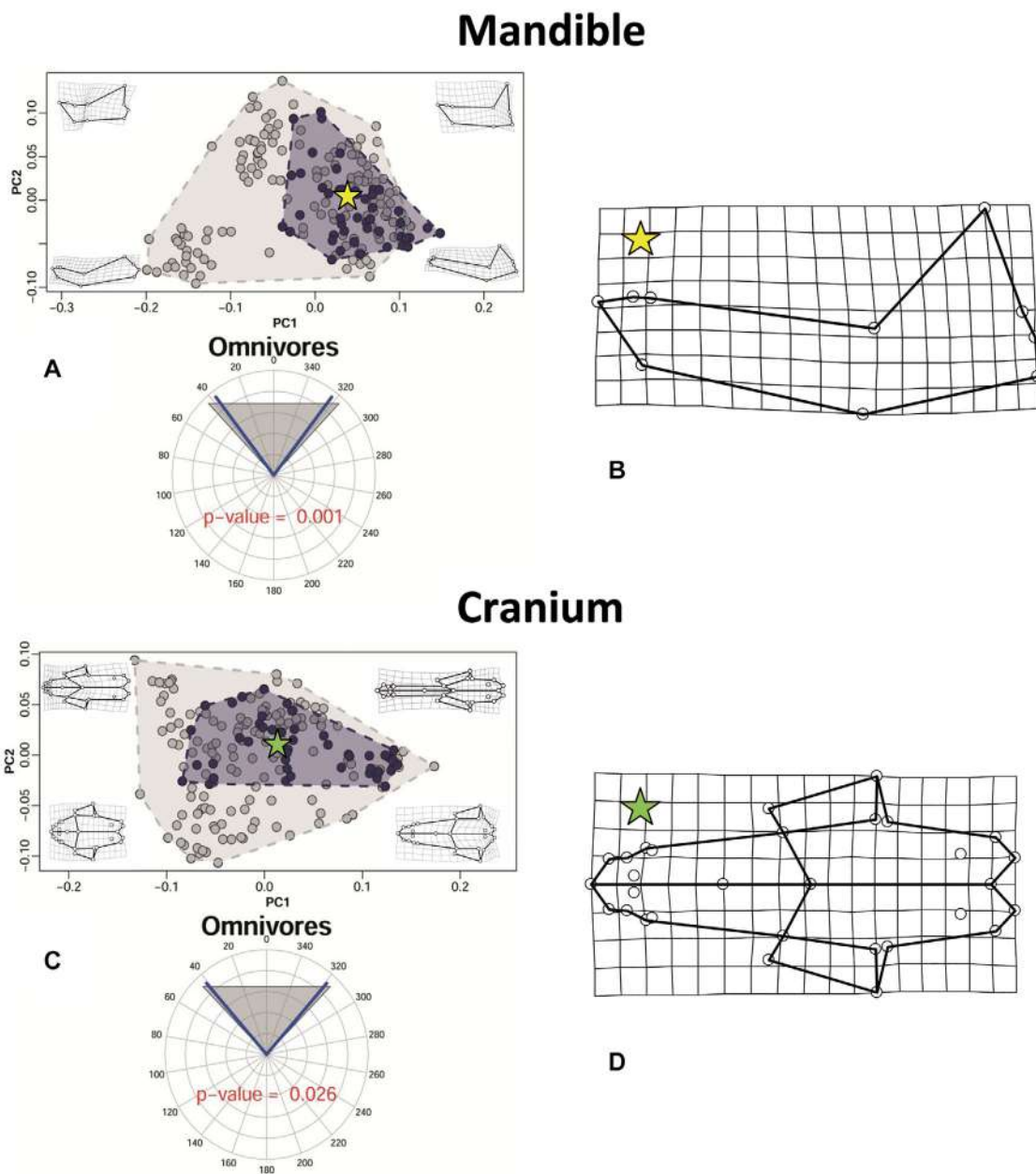


Figure 3. Scatterplots of mandibular (A) and cranial (C) shape variation summarized by PC1 (51.4% of variance explained for the mandible and 47.8% for the cranium) and PC2 (20.7% of variance explained for the mandible and 20.0% for the cranium). Gray convex hulls contain all the sampled species, whereas blue convex hulls contain the omnivore carnivorans. The circular plots report the mean time-distance-standardized θ , between the species set to converge (blue lines) and the range of random angles expected under the Brownian Motion (gray shaded area). The P -value for the time-distance-standardized θ test is printed within the circular plots. Deformation grids and wireframes show the shape deformation corresponding to each quadrant of shape space. Yellow and green stars represent, respectively, the position of mandibular (B) and cranial (D) consensus shapes of omnivores in the shape space.

When it comes to the species that preponderantly consume a single food item, diet-related convergence is supported in large prey hunters, but only for cranial shape. Many other groups (e.g., insectivores, medium prey hunters) showed significant P -values and/or Q -values only according to the Wheatsheaf index. Because this score is also influenced by a permanent condition of

reduced (or null) evolutionary rate, our findings suggest that this outcome is the product of an extended phase of reduced shape change occurring in these categories. The discrepancy between the results of the tested metrics might be produced by the occurrence of multiple morphological optima for species belonging to the same ecological category (i.e., a phenomenon

Table 3. Cranial C1, time-distance-standardized θ , and Wheatsheaf index scores, *P*-values, and *Q*-values relative to the dietary categories adopted to test the occurrence of shape convergence. Significant *P*-values and *Q*-values at $\alpha = 0.05$ are underlined.

Dietary category	C1			Time-distance-standardized θ			Wheatsheaf index		
	Score	<i>P</i> -value	<i>Q</i> -value	Score	<i>P</i> -value	<i>Q</i> -value	Score	<i>P</i> -value	<i>Q</i> -value
Herbivores/Frugivores	0.045	0.653	0.999	0.686	0.169	0.513	1.822	<u>0.014</u>	0.108
Insectivores	0.066	0.723	0.999	0.959	0.874	0.999	0.960	<u>0.001</u>	<u>0.011</u>
Crustacivores	0.035	0.881	0.999	0.973	0.831	0.999	0.721	0.285	0.674
Molluscivores	0.006	0.782	0.999	0.760	0.603	0.999	0.660	0.990	0.999
Piscivores	0.049	0.962	0.999	3.560	0.998	0.999	0.631	0.145	0.510
Omnivores	0.104	0.231	0.593	0.746	<u>0.026</u>	0.156	1.133	<u>0.001</u>	<u>0.011</u>
Large prey hunters	0.130	<u>0.001</u>	<u>0.011</u>	0.864	0.857	0.999	1.032	0.151	0.510
Medium prey hunters	0.062	0.848	0.999	0.839	0.775	0.999	1.265	<u>0.003</u>	<u>0.027</u>
Small prey hunters	0.084	0.692	0.999	0.811	0.691	0.999	0.842	0.465	0.999

Table 4. Mandibular (upper half) and cranial (lower half) C1, time-distance-standardized θ , and Wheatsheaf index scores, *P*-values, and *Q*-values relative to the list of cases concerning either ecologically equivalent species or ecologically similar species of different body sizes selected from the literature to test the occurrence of shape convergence. Significant *P*-values and *Q*-values at $\alpha = 0.05$ are underlined.

Mandible	C1			Time-distance-standardized θ			Wheatsheaf index		
	Score	<i>P</i> -value	<i>Q</i> -value	Score	<i>P</i> -value	<i>Q</i> -value	Score	<i>P</i> -value	<i>Q</i> -value
Red fox—Malayan civet	0.497	<u>0.001</u>	<u>0.005</u>	0.232	<u>0.021</u>	<u>0.033</u>	6.813	0.162	0.129
Raccoon dog—Raccoon	0.598	<u>0.001</u>	<u>0.005</u>	0.245	<u>0.016</u>	<u>0.033</u>	10.348	<u>0.009</u>	<u>0.029</u>
Iberian lynx—Fossa	0.305	<u>0.050</u>	0.061	0.520	0.294	0.173	1.914	0.251	0.154
Spotted hyena—Wolverine	0.386	<u>0.059</u>	0.068	0.241	<u>0.018</u>	<u>0.033</u>	5.849	0.252	0.154
Giant panda—Red panda	0.445	<u>0.001</u>	<u>0.005</u>	0.220	<u>0.012</u>	<u>0.032</u>	3.090	0.155	0.129

Cranium	C1			Time-distance-standardized θ			Wheatsheaf index		
	Score	<i>P</i> -value	<i>Q</i> -value	Score	<i>P</i> -value	<i>Q</i> -value	Score	<i>P</i> -value	<i>Q</i> -value
Red fox—Malayan civet	0.289	0.099	0.093	0.230	<u>0.009</u>	<u>0.029</u>	3.424	0.680	0.361
Raccoon dog—Raccoon	0.156	0.208	0.147	0.497	0.194	0.147	3.736	0.148	0.129
Iberian lynx—Fossa	0.169	0.238	0.154	0.614	0.351	0.200	2.528	0.073	0.078
Spotted hyena—Wolverine	0.314	<u>0.049</u>	0.061	0.404	0.089	0.089	5.525	0.212	0.147
Giant panda—Red panda	0.322	<u>0.020</u>	<u>0.033</u>	0.322	<u>0.034</u>	<u>0.049</u>	1.877	0.444	0.244

known as many-to-one mapping of form to function—Alfaro et al. 2005; Wainwright et al. 2005; Collar et al. 2014; Sansalone et al. 2020). It might be a consequence of different developmental constraints taking place in phylogenetically distant clades. Recent studies demonstrated that shifts from hypo- to hypercarnivory and vice versa are mainly due to variations in both the snout length and the dentition in canids, contrary to most other carnivorous groups in which these transitions are due to changes occurring in the dentition (Van Valkenburgh 1991; Holliday and Stepan 2004; Slater et al. 2009; Damasceno et al. 2013; Machado et al. 2018; Machado 2020). Otherwise, this pattern can be a product of ecological variation that was not accounted for in our categorization such as the impact of selective factors

other than diet on craniomandibular shape evolution of these categories.

All the metrics relative to the remaining dietary categories (e.g., piscivores, molluscivores) were not significant, therefore indicating that neither convergence nor conservatism is likely to have impacted the shape variation of these groups through time. This outcome can be produced by the occurrence of neutral or divergent evolution because these patterns represent the null hypothesis of the employed metrics (Arbuckle et al. 2014; Stayton 2015b; Castiglione et al. 2019). For example, molluscivore carnivores include species that rely on alternative strategies to feed on invertebrates protected by a hard shell. These strategies range from suction-feeding (e.g., walrus) and, even more

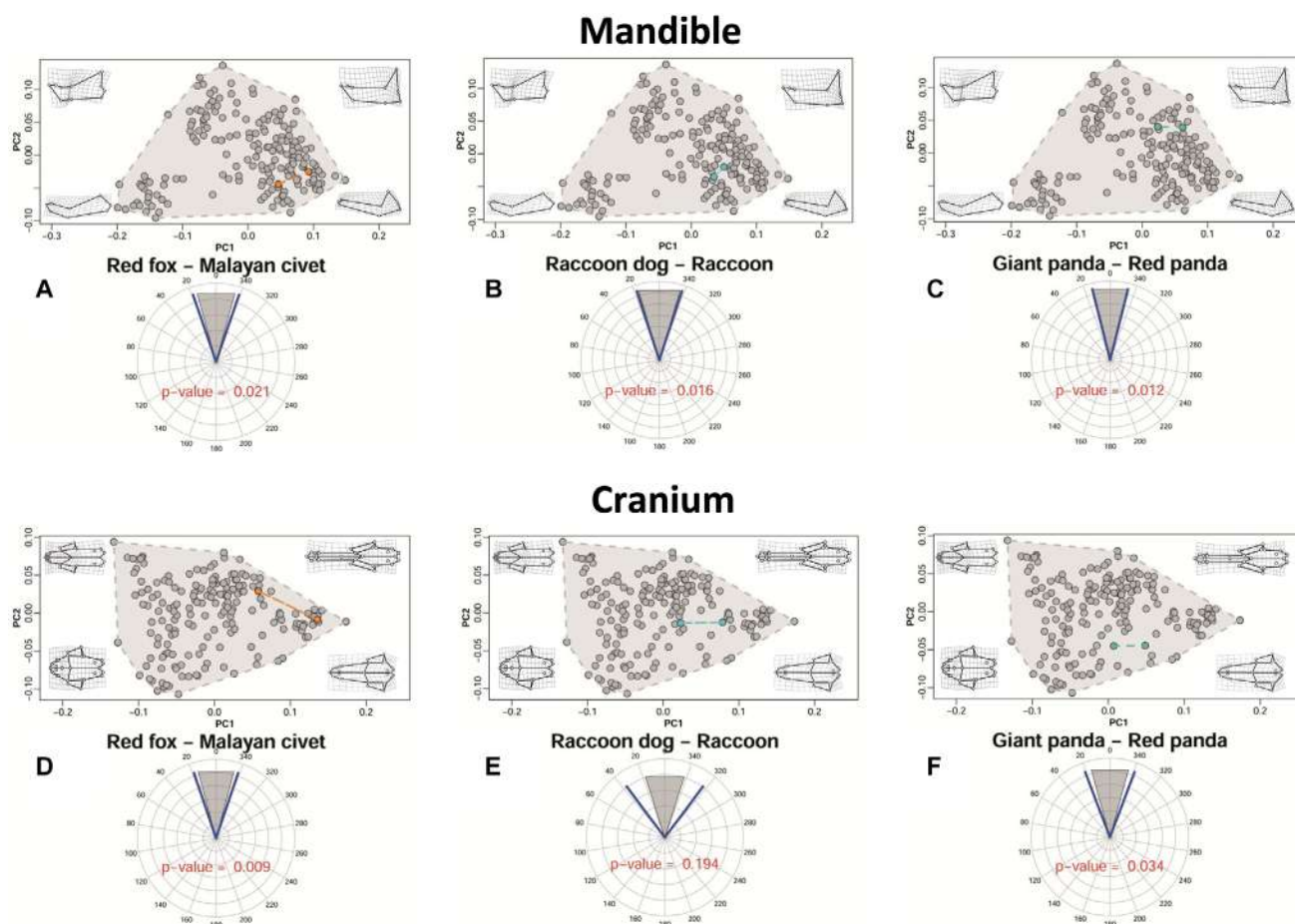


Figure 4. Scatterplots of mandibular (A–C) and cranial (D–F) shape variation summarized by PC1 and PC2. Gray convex hulls contain all the sampled species, whereas orange, light blue, and green convex hulls, respectively, contain the red fox—Malayan civet, the raccoon dog—raccoon, and the giant panda—red panda cases. The circular plots report the time-distance-standardized θ , between the species set to converge (blue lines) and the range of random angles expected under the Brownian Motion (gray shaded area). The P -value for the time-distance-standardized θ test is printed within the circular plots. Deformation grids and wireframes show the shape deformation corresponding to each quadrant of shape space.

commonly, shell-crushing (e.g., sea otter), to using the mandible as an anchor to dislodge hard-shelled organisms from hard substrates, as it likely happened in the extinct marine arctoid *Kolponomos* (Tseng et al. 2016). Thus, independent evolution of similar diets can either produce convergence but can also, and probably more commonly among carnivorans, push species toward different directions in the craniomandibular multivariate trait space (Boessenecker 2012, 2017; Timm-Davis et al. 2015; Radinsky 1981b).

If tests within broad dietary groups were mostly and consistently nonsignificant, evidence for evolutionary convergence was stronger when we compared ecologically equivalent species or cases with large size differences but very similar diets (i.e., the giant panda and red panda). This is especially evident for the mandible (with three instances of significance using both

time-distance-standardized θ and C1) and is not incompatible with the mainly negative findings from the tests on dietary groups. As briefly mentioned, the set of tests on diet investigates the average degree of clustering within a group. Because of this averaging, even when results are negative (no support for conservatism/convergence on average) in a group, one cannot exclude that specific pairs of species within that same group could, nevertheless, be convergent. This is clearly the case of the giant and the red pandas (strongly convergent) within the herbivores/frugivores, which are for the rest hardly showing any clustering. Simply, the specific case is “lost” when results are averaged across all members of that group, a fairly obvious point but still one to bear in mind when assessing convergence: the level of the analysis is crucial and large-scale studies might miss important details. Our analyses indicate that convergence

occurred three times in ecologically equivalent species or in cases with large size differences but very similar diets, involving in the first case two small prey hunters (red fox and Malayan civet), in the second case two omnivore species (North American raccoon and raccoon dog) and in the last case two herbivore/frugivore species (giant and red pandas). Therefore, ecological equivalence might produce convergence within the same dietary category in many different carnivoran ecomorphotypes. This is coherent with previous micro- and macroevolutionary studies in mammals (e.g., convergence between ecologically equivalent bank voles in Southern Eurasia—Ledevin et al. 2018; convergence between Afrotheria and Laurasiatheria—Gheerbrant et al. 2016). Our results also suggest that convergence might happen, to a certain degree, even in ecologically similar species of hugely different size, as confirmed by the case of giant and red pandas.

COMPARISON WITH PREVIOUS CONVERGENCE STUDIES ON CARNIVORANS AND DIFFERENT CASE STUDIES: AGREEMENT OR DISAGREEMENT?

Taken as a whole, our results indicate that convergent evolution in the craniomandibular complex of living carnivorans is a rare phenomenon, which infrequently occurs within dietary groups. This conclusion is in good agreement with Meloro et al. (2015), who argued that, in this clade, mandibular shape is highly conserved within many dietary categories, whereas convergent evolution appears to be uncommon. Slater and Friscia (2019) also suggested that an early burst adaptive radiation characterizes the evolution of some functional ecomorphological traits (mainly related to the dentition) of extant and recently extinct terrestrial carnivorans. Early bursts imply that the evolutionary rate in a clade decreases exponentially through time, as niches are filled and ecological opportunity is exhausted (Harmon et al. 2010; Slater and Pennell 2014). Thus, pronounced divergence and rapid evolution may occur early in the adaptive radiation, whereas slower rates and conservatism would be typical of later stages. The relative rarity of convergence we found here fits well with the pioneering research of Radinsky (1981a,b), who used linear cranial measurements to explore the specializations in carnivoran hunters and concluded that they tend to involve highly idiosyncratic features. Consistently with Radinsky (1981a,b), we found the occurrence of an omnivore adaptive zone in carnivoran cranial evolution. Especially if the ancestor of this order was an omnivore, one might speculate that species with more specialized diets branched off from this generalist root and evolved in different directions and, even when they colonized similar trophic niches, only rarely converged toward similar craniomandibular shapes. In contrast, omnivores broadly retained the ancestral shape, which was already well adapted to their generalist niche.

Convergence in cases concerning either ecologically equivalent species or ecologically similar species of different body

sizes (that always compared only two putatively convergent species in our analyses) was found to be a more frequent pattern as compared to convergence within dietary categories. This evidence is in line with the results obtained by Stayton (2008) analyzing a large number of datasets (simulated in the absence of functional or developmental constraints). Stayton demonstrated that, comparing multiple datasets with an equal number of species and variables, the most recurrent case of convergence is the one concerning only two observations undergoing convergent evolution across the entire tree. The simulations also pointed out that an increase in the number of species is expected to produce higher levels of convergence, whereas a greater number of variables simultaneously taken into account is likely to lower the frequency of the episodes of convergent evolution. In this sense, our study is in an intermediate position because it relies on 16 dimensions for the mandible and 28 for the cranium (i.e., numbers comparable to those employed in studies that questioned a recurrent occurrence of convergence in carnivorans or squirrels—Meloro et al. 2015; Zelditch et al. 2017), but also includes an unprecedented number of species for a research about shape convergence.

Zelditch et al. (2017) suggested that shape convergence is more likely to occur in size-constrained niches in squirrels. The box-whisker plots representing the size variation among our adopted dietary categories (Fig. S1) suggest a different scenario for living carnivorans: none of the ecological groups exhibits an extremely reduced size disparity and convergence could possibly have occurred only in a group (i.e., large prey hunters) that possesses an average size disparity. Nevertheless, convergence is rare in the craniomandibular shape evolution of carnivorans (as well as of squirrels), if compared with case studies such as desert lizards (Melville et al. 2006), Australian and North American snakes (Grundler and Rabosky 2014), or mainland *Anolis* (Moreno-Arias and Calderón-Espinosa 2016). Zelditch et al. (2017) suggested that this outcome might be produced by a complex interplay of one-to-many, many-to-one, and many-to-many relationships taking place between ecology, biomechanics, and morphology.

CONCLUSIONS AND FUTURE DIRECTIONS

Convergence of craniomandibular shape rarely accompanies convergence in diet; taken together convergence and conservatism seem to have limited the disparity of Carnivora. Stayton (2008) showed that increasing taxonomic coverage is crucial for a powerful investigation of evolutionary convergence in morphology. The inclusion of a large number of small- and medium-sized carnivoran species that are generally poorly sampled in ecomorphological research (e.g., viverrids that are often excluded in this field of study—Gaubert and Veron 2003; Gaubert et al. 2005) might indeed be one of the reasons that allowed us to rule out

the occurrence of convergence in many dietary categories and also to validate the presence of conservatism in the omnivore group.

Nonetheless, the general lack of conclusive evidence for convergence in broad dietary groups of carnivorans does not exclude the possibility that specific cases of ecologically equivalent species might have partially converged toward similar morphologies, as confirmed by our results concerning the mandible. Results of studies of ecomorphological convergence are, however, influenced by a variety of factors, which suggest caution in interpreting them. Certainly, before trying any hypotheses on the processes behind the patterns, there is an increasingly important need to carefully test the robustness and generalizability of descriptive studies, like our and the vast majority of ecomorphological analyses.

We used multiple pattern-based metrics designed for detecting the occurrence of retained and/or evolved similarity, each with a slightly different biological meaning. This allowed us not only to test for the presence of convergence, but also to distinguish between episodes of convergent evolution and conservatism, that are the most common processes leading to trait similarity (Moen et al. 2013). Our results support the existence of a complex relationship taking place between ecology, biomechanics, and morphology that makes convergent evolution a rare phenomenon. Ecological equivalence was the only condition that produced convergence in more than one occasion for carnivorans. Further studies about the interaction between ecological equivalence and convergence could be extremely interesting for further clarifying the mechanisms leading to a condition of evolved trait similarity. Increasing the number of studies that disprove the occurrence of convergent evolution in a specific clade, like ours, is a pivotal need in evolutionary biology and might ease the quest for previously unknown episodes of convergence.

AUTHOR CONTRIBUTIONS

DT, CM, PR, and LM conceptualized the study. CM collected the data. DT, CM, and LM analyzed and interpreted the data. DT provided the computed code. All the authors wrote the manuscript and gave final approval of the version to be published.

ACKNOWLEDGMENTS

The authors would like to thank A. Cardini for many helpful suggestions regarding both analyses and text. The authors are also grateful to several museum institutions and curators for kindly providing access to museum collections: P. Jenkins and A. Salvador (NHM, London); A. Kitchener (Royal Museum of Scotland, Edinburgh); T. Parker (Liverpool World Museum); and E. Gilissen and W. Wendelen (Royal Museum for Central Africa, Tervuren, Belgium). F. Galimberti and S. Sanvito (Elephant Seal Research Group) provided us helpful insights on the ecology of the marine carnivorans, the pinnipeds. This research received support from the SYNTHESYS programme (ES-TAF-2750 awarded to DT) and

the “Avvio alla Ricerca” funds provided by the University of Rome “La Sapienza” (AR11916B48429BEB awarded to DT).

CONFLICT OF INTEREST

The authors declare no conflict of interest.

DATA ARCHIVING

Morphological datasets, phylogeny, and R script supporting the results of this article are archived in Dryad (<https://doi.org/10.5061/dryad.bg79cnpb1>) and/or provided as Supporting Information.

SSE MEMBERSHIP

DT is a member of the Society for the Study of Evolution.

LITERATURE CITED

- Adams, D. C., and M. L. Collyer. 2009. A general framework for the analysis of phenotypic trajectories in evolutionary studies. *Evolution* 63:1143–1154.
- Adams, D. C., F. J. Rohlf, and D. E. Slice. 2004. Geometric morphometrics: ten years of progress following the ‘revolution.’ *Ital. J. Zool.* 71:5–16.
- . 2013. A field comes of age: geometric morphometrics in the 21st century. *Hystrix It. J. Mamm.* 24:7–14.
- Alfaro, M. E., D. I. Bolnick, and P. C. Wainwright. 2005. Evolutionary consequences of many-to-one mapping of jaw morphology to mechanics in labrid fishes. *Am. Nat.* 165:E140–E154.
- Arbuckle, K., and A. Minter. 2015. windex: analyzing convergent evolution using the Wheat sheaf index in R. *Evol. Bioinform.* 11:11–14.
- Arbuckle, K., and M. P. Speed. 2016. Analysing convergent evolution: a practical guide to methods. Pp. 23–36 in P. Pontarotti, ed. *Evolutionary biology: convergent evolution, evolution of complex traits, concepts and methods*. Springer International Publishing, Cambridge, U.K.
- Arbuckle, K., C. M. Bennett, and M. P. Speed. 2014. A simple measure of the strength of convergent evolution. *Methods Ecol. Evol.* 5:685–693.
- Arnason, U., A. Gullberg, A. Janke, and M. Kullberg. 2007. Mitogenomic analyses of caniform relationships. *Mol. Phylogenetics Evol.* 45:863–874.
- Arnold, C., L. J. Matthews, and C. L. Nunn. 2010. The 10kTrees website: a new online resource for primate phylogeny. *Evol. Anthropol.* 19:114–118.
- Benjamini, Y., and D. Yekutieli. 2001. The control of the false discovery rate in multiple testing under dependency. *Ann. Stat.* 29:1165–1188.
- Biggins, D. E., L. R. Hanebury, B. J. Miller, and R. A. Powell. 2011. Black-footed ferrets and Siberian polecats as ecological surrogates and ecological equivalents. *J. Mammal.* 92:710–720.
- Boessenecker, R. W. 2012. A new marine vertebrate assemblage from the Late Neogene Purisima Formation in Central California, part II: pinnipeds and cetaceans. *Geodiversitas* 35:815–940.
- . 2017. A new Early Pliocene record of the toothless walrus *Valenictus* (Carnivora, Odobenidae) from the Purisima Formation of Northern California. *PaleoBios* 34:1–6.
- Bolnick, D. I., R. D. H. Barrett, K. B. Oke, D. J. Rennison, and Y. E. Stuart. 2018. (Non)Parallel evolution. *Annu. Rev. Ecol. Evol. Syst.* 49:303–330.
- Cardini, A. 2014. Missing the third dimension in geometric morphometrics: how to assess if 2D images really are a good proxy for 3D structures? *Hystrix It. J. Mamm.* 25:73–81.

- . 2020. Modern morphometrics and the study of population differences: good data behind clever analyses and cool pictures? *Anat. Rec.* 303:2747–2765.
- Cardini, A., and M. Chiapelli. 2020. How flat can a horse be? Exploring 2D approximations of 3D crania in equids. *Zoology* 139:125746.
- Castiglione, S., G. Tesone, M. Piccolo, M. Melchionna, A. Mondanaro, C. Serio, M. D. Febbraro, and P. Raia. 2018. A new method for testing evolutionary rate variation and shifts in phenotypic evolution. *Methods Ecol. Evol.* 9:974–983.
- Castiglione, S., C. Serio, D. Tamagnini, M. Melchionna, A. Mondanaro, M. D. Febbraro, A. Profico, P. Piras, F. Barattolo, and P. Raia. 2019. A new, fast method to search for morphological convergence with shape data. *PLoS One* 14:e0226949.
- Cheverud, J. M. 1981. Relationships among ontogenetic, static, and evolutionary allometry. *Am. J. Phys. Anthropol.* 59:139–149.
- Christiansen, P., and S. Wroe. 2007. Bite forces and evolutionary adaptations to feeding ecology in carnivores. *Ecology* 88:347–358.
- Collar, D. C., J. S. Reece, M. E. Alfaro, P. C. Wainwright, and R. S. Mehta. 2014. Imperfect morphological convergence: variable changes in cranial structures underlie transitions to durophagy in moray eels. *Am. Nat.* 183:E168–E184.
- Coxall, H. K., P. N. Pearson, P. A. Wilson, and P. F. Sexton. 2007. Iterative evolution of digitate planktonic foraminifera. *Paleobiology* 33:495–516.
- Damasceno, E. M., E. Hingst-Zaher, and D. Astúa. 2013. Bite force and encephalization in the Canidae (Mammalia: Carnivora). *J. Zool.* 290:246–254.
- Drake, A. G., and C. P. Klingenberg. 2010. Large-scale diversification of skull shape in domestic dogs: disparity and modularity. *Am. Nat.* 175:289–301.
- Dumont, M., C. E. Wall, L. Botton-Divet, A. Goswami, S. Peigné, and A.-C. Fabre. 2016. Do functional demands associated with locomotor habitat, diet, and activity pattern drive skull shape evolution in musteloid carnivorans? *Biol. J. Linn. Soc.* 117:858–878.
- Ewer, R. F. 1973. *The carnivores*. Cornell Univ. Press, Ithaca, NY.
- Figueirido, B., F. J. Serrano-Alarcón, G. J. Slater, and P. Palmqvist. 2010. Shape at the cross-roads: homoplasy and history in the evolution of the carnivoran skull towards herbivory. *J. Evol. Biol.* 23:2579–2594.
- Figueirido, B., Z. J. Tseng, and A. Martín-Serra. 2013. Skull shape evolution in durophagous carnivorans. *Evolution* 67:1975–1993.
- Gaubert, P., and G. Veron. 2003. Exhaustive sample set among Viverridae reveals the sister-group of felids: the linsangs as a case of extreme morphological convergence within Feliformia. *Proc. R. Soc. B* 270:2523–2530.
- Gaubert, P., W. C. Wozencraft, P. Cordeiro-Estrela, and G. Veron. 2005. Mosais of convergences and noise in morphological phylogenies: what's in a viverrid-like carnivoran? *Syst. Biol.* 54:865–894.
- Gheerbrant, E., A. Filippo, and A. Schmitt. 2016. Convergence of afrotherian and laurasiatherian ungulate-like mammals: first morphological evidence from the Paleocene of Morocco. *PLoS ONE* 11:e0157556.
- Gittleman, J. L. 1986. Carnivore life history patterns: allometric, phylogenetic, and ecological associations. *Am. Nat.* 127:744–771.
- Grossnickle, D. M., M. Chen, J. G. A. Wauer, S. K. Pevsner, L. N. Weaver, Q.-J. Meng, D. Liu, Y.-G. Zhang, and Z.-X. Luo. 2020. Incomplete convergence of gliding mammal skeletons. *Evolution* 74:2662–2680.
- Grundler, M. C., and D. L. Rabosky. 2014. Trophic divergence despite morphological convergence in a continental radiation of snakes. *Proc. R. Soc. B* 281:20140413.
- Hallgrímsson, B., D. E. Lieberman, W. Liu, A. F. Ford-Hutchinson, and F. R. Jirik. 2007. Epigenetic interactions and the structure of phenotypic variation in the cranium. *Evol. Dev.* 9:76–91.
- Harmon, L. J., J. B. Losos, T. J. Davies, R. G. Gillespie, J. L. Gittleman, W. B. Jennings, K. H. Kozak, M. A. McPeck, F. Moreno-Roark, T. J. Near, et al. 2010. Early bursts of body size and shape evolution are rare in comparative data. *Evolution* 64:2385–2396.
- Herrel, A., B. Vanhooydonck, and R. V. Damme. 2004. Omnivory in lacertid lizards: adaptive evolution or constraint? *J. Evol. Biol.* 17:974–984.
- Holliday, J. A., and S. J. Stepan. 2004. Evolution of hypercarnivory: the effect of specialization on morphological and taxonomic diversity. *Paleobiology* 30:108–128.
- Hu, Y., Q. Wu, S. Ma, T. Ma, L. Shan, X. Wang, Y. Nie, Z. Ning, L. Yan, Y. Xiu, et al. 2017. Comparative genomics reveals convergent evolution between the bamboo-eating giant and red pandas. *Proc. Natl. Acad. Sci. USA* 114:1081–1086.
- Huang, S., K. Roy, J. W. Valentine, and D. Jablonski. 2015. Convergence, divergence, and parallelism in marine biodiversity trends: integrating present-day and fossil data. *Proc. Natl. Acad. Sci. USA* 112:4903–4908.
- Hume, J. P., and D. Martill. 2019. Repeated evolution of flightlessness in Dryolimnas rails (Aves: Rallidae) after extinction and recolonization on Aldabra. *Zool. J. Linn. Soc.* 186:666–672.
- Hylander, W. L., and K. R. Johnson. 1994. Jaw muscle function and wishboning of the mandible during mastication in macaques and baboons. *Am. J. Phys. Anthropol.* 94:523–547.
- Jones, K. E., C. B. Ruff, and A. Goswami. 2013. Morphology and biomechanics of the pinniped jaw: mandibular evolution without mastication. *Anat. Rec.* 296:1049–1063.
- Klingenberg, C. P. 2011. MorphoJ: an integrated software package for geometric morphometrics. *Mol. Ecol. Resour.* 11:353–357.
- Larivière, S., and M. Pasitschniak-Arts. 1996. *Vulpes vulpes*. *Mamm. Species* 537:1–11.
- Ledevin, R., P. Chevret, Z. Helvacı, J. R. Michaux, and S. Renaud. 2018. Bank voles in Southern Eurasia: vicariance and adaptation. *J. Mammal. Evol.* 25:119–129.
- Lincoln, R. J., G. A. Boxshall, and P. F. Clark. 1998. *A dictionary of ecology, evolution and systematics*. 2nd ed. Cambridge Univ. Press, Cambridge, NY.
- Losos, J. B. 1992. The evolution of convergent structure in Caribbean Anolis communities. *Syst. Biol.* 41:403–420.
- . 2008. Phylogenetic niche conservatism, phylogenetic signal and the relationship between phylogenetic relatedness and ecological similarity among species. *Ecol. Lett.* 11:995–1003.
- . 2011. Convergence, adaptation, and constraint. *Evolution* 65 (7): 1827–1840.
- Machado, F. A. 2020. Selection and constraints in the ecomorphological adaptive evolution of the skull of living Canidae (Carnivora, Mammalia). *Am. Nat.* 196:197–215.
- Machado, F. A., T. M. G. Zahn, and G. Marroig. 2018. Evolution of morphological integration in the skull of Carnivora (Mammalia): changes in Canidae lead to increased evolutionary potential of facial traits. *Evolution* 72:1399–1419.
- Mahler, D. L., T. Ingram, L. J. Revell, and J. B. Losos. 2013. Exceptional convergence on the macroevolutionary landscape in island lizard radiations. *Science* 341:292–295.
- Maiorano, L., A. Falcucci, and L. Boitani. 2008. Size-dependent resistance of protected areas to land-use change. *Proc. R. Soc. B* 275:1297–1304.
- McNamara, K. J. 2006. Evolutionary trends. Pp. 1–7 in *Encyclopedia of life sciences*. Wiley-Blackwell, Hoboken, NJ.
- Meloro, C., and P. O'Higgins. 2011. Ecological adaptations of mandibular form in fissiped Carnivora. *J. Mammal. Evol.* 18:185–200.
- Meloro, C., M. Clauss, and P. Raia. 2015. Ecomorphology of Carnivora challenges convergent evolution. *Org. Divers. Evol.* 15:711–720.

- Meloro, C., J. Hunter, L. Tomsett, R. P. Miguez, F. J. Prevosti, and R. P. Brown. 2017. Evolutionary ecomorphology of the Falkland Islands wolf *Dusicyon australis*. *Mammal Rev.* 47:159–163.
- Melville, J., L. J. Harmon, and J. B. Losos. 2006. Intercontinental community convergence of ecology and morphology in desert lizards. *Proc. R. Soc. B* 273:557–563.
- Michaud, M., G. Veron, S. Peigné, A. Blin, and A.-C. Fabre. 2018. Are phenotypic disparity and rate of morphological evolution correlated with ecological diversity in Carnivora? *Biol. J. Linn. Soc.* 124:294–307.
- Moen, D. S., D. J. Irschick, and J. J. Wiens. 2013. Evolutionary conservatism and convergence both lead to striking similarity in ecology, morphology and performance across continents in frogs. *Proc. R. Soc. B* 280:20132156.
- Moreno-Arias, R. A., and M. L. Calderón-Espinosa. 2016. Patterns of morphological diversification of mainland Anolis lizards from northwestern South America. *Zool. J. Linn. Soc.* 176:632–647.
- Moss, M. L., and R. W. Young. 1960. A functional approach to craniology. *Am. J. Phys. Anthropol.* 18:281–292.
- Muir, A. M., P. Vecsei, and C. C. Krueger. 2012. A perspective on perspectives: methods to reduce variation in shape analysis of digital images. *Trans. Am. Fish. Soc.* 141:1161–1170.
- Pigot, A. L., C. Sheard, E. T. Miller, T. P. Bregman, B. G. Freeman, U. Roll, N. Seddon, C. H. Trisos, B. C. Weeks, and J. A. Tobias. 2020. Macroevolutionary convergence connects morphological form to ecological function in birds. *Nat. Ecol. Evol.* 4:230–239.
- Polly, P. D. 2008. Adaptive zones and the pinniped ankle: a three-dimensional quantitative analysis of carnivoran tarsal evolution. Pp. 167–196 in E. J. Sargis and M. Dagosto, eds. *Mammalian evolutionary morphology: a tribute to Frederick S. Szalay*. Springer, Dordrecht, The Netherlands.
- Radinsky, L. B. 1981a. Evolution of skull shape in carnivores: 1. Representative modern carnivores. *Biol. J. Linn. Soc.* 15:369–388.
- . 1981b. Evolution of skull shape in carnivores: 2. Additional modern carnivores. *Biol. J. Linn. Soc.* 16:337–355.
- . 1982. Evolution of skull shape in carnivores: 3. The origin and early radiation of the modern carnivore families. *Paleobiology* 8:177–195.
- Rohlf, F. 2015. The Tps series of software. *Hystrix It. J. Mamm.* 26:1–4.
- Rohlf, F. J., and D. Slice. 1990. Extensions of the Procrustes method for the optimal superimposition of landmarks. *Syst. Zool.* 39:40–59.
- Roth, V., 1993. On three-dimensional morphometrics, and on the identification of landmark points. Pp. 41–61 in L. F. Marcus, E. Belle, and A. G. Valdecausas, eds. *Contributions to morphometrics*. Monografias series, Museo Nacional de Ciencias Naturales. Madrid, Spain.
- Salesa, M. J., M. Antón, S. Peigné, and J. Morales. 2006. Evidence of a false thumb in a fossil carnivore clarifies the evolution of pandas. *Proc. Natl. Acad. Sci. USA* 103:379–382.
- Sansalone, G., S. Castiglione, P. Raia, M. Archer, B. Dickson, S. Hand, P. Piras, A. Profico, and S. Wroe. 2020. Decoupling functional and morphological convergence, the study case of fossorial mammalia. *Front. Earth Sci.* 8:112.
- Simpson, G. G. 1944. *Tempo and mode in evolution*. Columbia Univ. Press, New York.
- . 1953. *The major features of evolution*. Univ. Presses of California, Columbia & Princeton, Bognor Regis, U.K.
- Slater, G. J. 2015. Iterative adaptive radiations of fossil canids show no evidence for diversity-dependent trait evolution. *Proc. Natl. Acad. Sci. USA* 112:4897–4902.
- Slater, G. J., and A. R. Friscia. 2019. Hierarchy in adaptive radiation: a case study using the Carnivora (Mammalia). *Evolution* 73:524–539.
- Slater, G. J., and M. W. Pennell. 2014. Robust regression and posterior predictive simulation increase power to detect early bursts of trait evolution. *Syst. Biol.* 63:293–308.
- Slater, G. J., E. R. Dumont, and B. V. Valkenburgh. 2009. Implications of predatory specialization for cranial form and function in canids. *J. Zool.* 278:181–188.
- Speed, M. P., and K. Arbuckle. 2017. Quantification provides a conceptual basis for convergent evolution. *Biol. Rev.* 92:815–829.
- Sperber, G. H. 2001. *Craniofacial development*. Pap/Cdr edition. BC Decker, Hamilton, Canada.
- Stayton, C. T. 2006. Testing hypotheses of convergence with multivariate data: morphological and functional convergence among herbivorous lizards. *Evolution* 60:824–841.
- . 2008. Is convergence surprising? An examination of the frequency of convergence in simulated datasets. *J. Theor. Biol.* 252:1–14.
- . 2015a. What does convergent evolution mean? The interpretation of convergence and its implications in the search for limits to evolution. *Interface Focus* 5:20150039.
- . 2015b. The definition, recognition, and interpretation of convergent evolution, and two new measures for quantifying and assessing the significance of convergence. *Evolution* 69:2140–2153.
- Storey, J. D. 2002. A direct approach to false discovery rates. *J. R. Stat. Soc. B* 64:479–498.
- Storey, J. D., and R. Tibshirani. 2003. Statistical significance for genomewide studies. *Proc. Natl. Acad. Sci. USA* 100:9440–9445.
- Storey, J. D., J. E. Taylor, and D. Siegmund. 2004. Strong control, conservative point estimation and simultaneous conservative consistency of false discovery rates: a unified approach. *J. R. Stat. Soc. B* 66:187–205.
- Tamagnini, D., C. Meloro, and A. Cardini. 2017. Anyone with a long-face? Craniofacial evolutionary allometry (CREA) in a family of short-faced mammals, the Felidae. *Evol. Biol.* 44:476–495.
- Timm-Davis, L. L., T. J. DeWitt, and C. D. Marshall. 2015. Divergent skull morphology supports two trophic specializations in otters (Lutrinae). *PLoS ONE* 10:e0143236.
- Tomiya, S., and Z. J. Tseng. 2016. Whence the beardedogs? Reappraisal of the Middle to Late Eocene ‘Miacis’ from Texas, USA, and the origin of Amphicyonidae (Mammalia, Carnivora). *R. Soc. Open Sci.* 3:160518.
- Tseng, Z. J., and X. Wang. 2011. Do convergent ecomorphs evolve through convergent morphological pathways? Cranial shape evolution in fossil hyaenids and borophagine canids (Carnivora, Mammalia). *Paleobiology* 37:470–489.
- Tseng, Z. J., C. Grohé, and J. J. Flynn. 2016. A unique feeding strategy of the extinct marine mammal Kolponomos: convergence on sabretooths and sea otters. *Proc. R. Soc. B* 283:20160044.
- Van Valkenburgh, B. 1989. Carnivore dental adaptations and diet: a study of trophic diversity within guilds. Pp. 410–436 in J. L. Gittleman, ed. *Carnivore behavior, ecology, and evolution*. Springer US, Boston, MA.
- . 1991. Iterative evolution of hypercarnivory in canids (Mammalia: Carnivora): evolutionary interactions among sympatric predators. *Paleobiology* 17:340–362.
- . 2007. Déjà vu: the evolution of feeding morphologies in the Carnivora. *Integr. Comp. Biol.* 47:147–163.
- Veron, G., M. Willsch, V. Dacosta, M.-L. Patou, A. Seymour, C. Bonillo, A. Couloux, S. T. Wong, A. P. Jennings, J. Fickel, et al. 2014. The distribution of the Malay civet *Viverra zibetha* (Carnivora: Viverridae) across Southeast Asia: natural or human-mediated dispersal? *Zool. J. Linn. Soc.* 170:917–932.
- Wainwright, P. C., M. E. Alfaro, D. I. Bolnick, and C. D. Hulsey. 2005. Many-to-one mapping of form to function: a general principle in organismal design? *Integr. Comp. Biol.* 45:256–262.
- Wake, D. B., M. H. Wake, and C. D. Specht. 2011. Homoplasy: from detecting pattern to determining process and mechanism of evolution. *Science* 331:1032–1035.

- Ward, O. G., and D. H. Wurster-Hill. 1990. *Nyctereutes procyonoides*. *Mamm. Species* 358:1–5.
- Werdelin, L. 1996. Carnivoran ecomorphology: a phylogenetic perspective. Pp. 582–624 in J. L. Gittleman, ed. *Carnivore behavior, ecology and evolution*. Cornell Univ. Press, Ithaca, NY.
- Wilson, D. E., and R. A. Mittermeier. 2009. *Handbook of mammals of the world: carnivores: 1*. Lynx Edicions, Barcelona, Spain.
- . 2014. *Handbook of the mammals of the world: sea mammals: 4*. Lynx Edicions, Barcelona, Spain.
- Wright, N. A., D. W. Steadman, and C. C. Witt. 2016. Predictable evolution toward flightlessness in volant island birds. *Proc. Natl. Acad. Sci. USA* 113:4765–4770.
- Zelditch, M. L., D. L. Swiderski, and H. D. Sheets. 2012. *Geometric morphometrics for biologists: a primer*. 2nd ed. Academic Press, Amsterdam, The Netherlands.
- Zelditch, M. L., J. Ye, J. S. Mitchell, and D. L. Swiderski. 2017. Rare ecomorphological convergence on a complex adaptive landscape: body size and diet mediate evolution of jaw shape in squirrels (Sciuridae). *Evolution* 71:633–649.

Associate Editor: M. Zelditch
Handling Editor: T. Chapman.

Supporting Information

Additional supporting information may be found online in the Supporting Information section at the end of the article.

Table S1. Species and sample sizes.

Figure S1. Box-whisker plots of natural logarithm of centroid size (lnCS) across the adopted ecological categorizations are based on differences in the main food item. Limits on boxes (light cranium, dark mandible) correspond to the first and third quartiles, whereas the internal black line represents the median.

Supporting Material

**Chapter 6 – Macroevolutionary ecomorphology of the Carnivora skull:
adaptations and constraints in the extant species**

Macroevolutionary ecomorphology of the Carnivora skull: adaptations and constraints in the extant species

CARLO MELORO^{1,*} and DAVIDE TAMAGNINI²

¹Research Centre in Evolutionary Anthropology and Palaeoecology, School of Biological and Environmental Sciences, Liverpool John Moores University, Liverpool, UK

²Department of Biology and Biotechnologies 'Charles Darwin', University of Rome La Sapienza, Rome, Italy

Received 28 April 2021; revised 1 July 2021; accepted for publication 30 July 2021

The mammalian order Carnivora is characterized by a broad taxonomic and ecological diversity. By using a large sample of extant species, we tested the impact of ecological factors on carnivoran skull (cranium and mandible) morphology, taking advantage of a combined geometric morphometrics and comparative method approach. We implemented several evolutionary models to account for different tempo and mode of evolution in size and shape data. These models validated the association between skull morphology and diet at the interspecific scale. The functional distinction between pinniped (aquatic) and fissiped (mostly terrestrial) taxa was found valid only in mandible shape and cranial size. High levels of morphological disparity and evolutionary rates were identified in specialized dietary groups, and positive association between rates and disparity was found for skull size. Cranium and mandible showed consistent patterns of covariation that reflect constrained functional processes, which stabilize the ecomorphological evolution of Carnivora. Aquatic adaptations allowed carnivorans to invade and persist within novel regions of the mandibular morphospace. This ecological shift did not increase morphological disparity but occurred at a faster rate than in terrestrial species. Those species exhibit a stronger level of cranio-mandibular covariation due to constraints imposed by more demanding masticatory adaptations.

ADDITIONAL KEYWORDS: comparative methods – cranium – diet – fissipeds – geometric morphometrics – mandible – phylogenetic generalized least squares – pinnipeds – shape.

INTRODUCTION

Macroevolutionary theory seeks to identify patterns and processes of biological variation above the species level that occur over a large temporal scale (Jablonski, 2017). When variation is linked to ecological adaptations, it provides support for the theory of ecomorphology (Wainwright, 1991). The ultimate aim of ecomorphology is to infer ecology from the organismal phenotype, but this relationship is not always linear and can be difficult to detect (Barr, 2018).

Association between morphology and ecological adaptations has been identified at different taxonomic scales, with patterns at the family level being the commonest tested (i.e. Kappelman, 1988; Elton *et al.*, 2016; Barr, 2018). A major caveat in ecomorphology relies on the implementation of phylogenetic comparative methods (PCMs) to test its intuitive assumption (Barr

& Scott, 2014; Scott & Barr, 2014). This is because morphological traits generally do not vary randomly between species (i.e. star-like phylogeny fits the data), but follow a hierarchical structure that allows detection of what is defined as the phylogenetic signal (= tendency for closely related species to resemble each other in phenotypic traits; Blomberg *et al.*, 2003). The emergence of multivariate PCMs increasingly allowed the detection of phylogenetic signal (Adams, 2014a) and the implementation of ecomorphological comparative tests in a broad range of anatomical structures and clades (Harmon *et al.*, 2005; Stuart-Fox & Moussalli, 2007; Barr, 2014; Sherratt *et al.*, 2016; Serb *et al.*, 2017).

The vertebrate skull has received particular attention for testing the relationship between species variation and ecological adaptations (Westneat, 2005). Without doubt, vertebrate skulls (traditionally thought to be composed by two modules: the cranium and the mandible; Moss & Young, 1960; Cheverud, 1982) are designed for multiple functions. These include

*Corresponding author. E-mail: c.meloro@ljmu.ac.uk

protection of vital soft-tissue organs, such as the brain and the eyes, but also as an anchor for muscles and ligaments that allow motion for searching, ingesting and processing food (Kardong, 2012). For this reason, the morphological variation of the vertebrate skull is considered the result of a complex interplay of factors, which generate trade-offs between form and function. Mammals, in particular, provide compelling evidence for such trade-offs. On the one side, biomechanical and developmental processes constrain mammalian skull variation at the interspecific scale, so that similar patterns are observed between clades (e.g. cranial evolutionary allometry; Cardini & Polly, 2013). On the other side, broad dietary adaptations at the level of entire mammalian clades (Price *et al.*, 2012) evidently resulted in a wide diversification of forms (Janis, 1990; Pineda-Munoz *et al.*, 2016).

Since the earliest biometric studies, Carnivora have been the focus of macroevolutionary investigations due to the broad ecological adaptations exhibited by living members of this clade and to its rich taxonomic diversity (Crusafont-Pairó & Truyols-Santonja, 1956, 1957; Ewer, 1973; Gittleman, 1985). In spite of a large number of studies, we lack a fully comprehensive, comparative framework to interpret phenotypic variation in the entire clade. Studies by Radinsky (1981), Figueirido *et al.* (2011), Meloro & O'Higgins (2011), Prevosti *et al.* (2012), Michaud *et al.* (2018, 2020) and Slater & Friscia (2019) have covered skull ecomorphological adaptation in terrestrial forms (named fissipeds), while Bininda-Emonds *et al.* (2000), Echarrri & Prevosti (2015), Jones *et al.* (2015) and Machado *et al.* (2018, 2019) attempted to explore living Carnivora, including also the aquatic subclade of pinnipeds. As a monophyletic group, pinnipeds are part of the arctoid clade and their diversification coincides with the acquisition of extreme phenotypic adaptations towards a semi-aquatic lifestyle (i.e. the pinniped ankle; Polly, 2008). Since the aquatic environment provides novel challenges to locomotory and feeding adaptations (Estes, 1989; Adam & Berta, 2002; Botton-Divet *et al.*, 2017, 2018), we expect morphological diversification in the carnivoran skull to expand rapidly when clades invaded the aquatic niche. Jones *et al.* (2015) explicitly tested this expectation on a sample of representative Carnivora crania, but did not find evidence for a burst in the shape diversification of pinnipeds. Whether or not this theory might apply to the morphological evolution of the mandible is still not known.

Using a large sample of carnivoran species (64% of the extant diversity), we tested the impact of dietary and aquatic adaptations on skull size and shape. By looking at crania and mandibles separately, we expected to identify patterns of macroevolutionary covariation to differ in relation to ecological adaptations (Figueirido

et al., 2013; Segura *et al.*, 2020). Because carnivoran skull and dental morphology do not consistently evolve under a Brownian motion mode of evolution (Meloro & Raia, 2010; Slater & Friscia, 2019), we implemented within a geometric morphometrics (GMM) framework a way to allow comparisons of size and shape data, as well as disparity and evolutionary rates under a selection of different evolutionary models. Dietary adaptations should strongly impact skull size and shape, while level of morphological disparity and evolutionary rates are expected to vary among the diet categories, depending on how functionally demanding they are (Meloro *et al.*, 2015a; Felice *et al.*, 2019; Sansalone *et al.*, 2019). Specializations towards aquatic lifestyle should equally influence interspecific variation in the skull of Carnivora and level of covariation between the cranium and the mandible [see, for example, Michaud *et al.* (2020) on feliform carnivorans].

MATERIAL AND METHODS

SPECIMENS AND LANDMARK DATA

Two-dimensional landmark coordinates were collected on a sample of 529 crania (in ventral view) and 554 mandibles (lateral view), representative of 188 out of 295 Carnivora species. Specimens were housed at several institutions, including: Royal Museum for Central Africa (Tervuren), Kenya National Museums (Nairobi), Natural History Museum (London), World Museum (Liverpool), Elephant Seal Research Group (Falkland Islands) and National Museums of Scotland (Edinburgh) (for a full list see Data Availability and Supporting Information, Table S1). Each photographed specimen was adult, as indicated by complete dentition and/or high degree of cranial suture closure. For each species, at least one mandible and one cranium were sampled, but an individual of each sex was included whenever possible.

Pictures were taken of the cranium (ventral view) and the mandible (lateral view) using a Manfrotto tripod and a Nikon D40 (Nikkor lens 55–200 mm, focus set at 100 mm) positioned at least one meter above the specimen to minimize distortion due to the camera lens.

Hemi-mandibles in lateral view and crania in ventral view were chosen as best approximation of 3D skull size and shape variation, as empirically demonstrated by Cardini (2014); we restricted our biological interpretation to these views only. Landmarks (cranium = 30, mandible = 10) were digitized using tpsDig 2 (Rohlf 2015) to cover general aspects of skull geometry and to ensure homology without particular references to the postcanine dentition, since in pinnipeds premolars and molars are indistinguishable (Fig. 1; Supporting Information, Table S2).

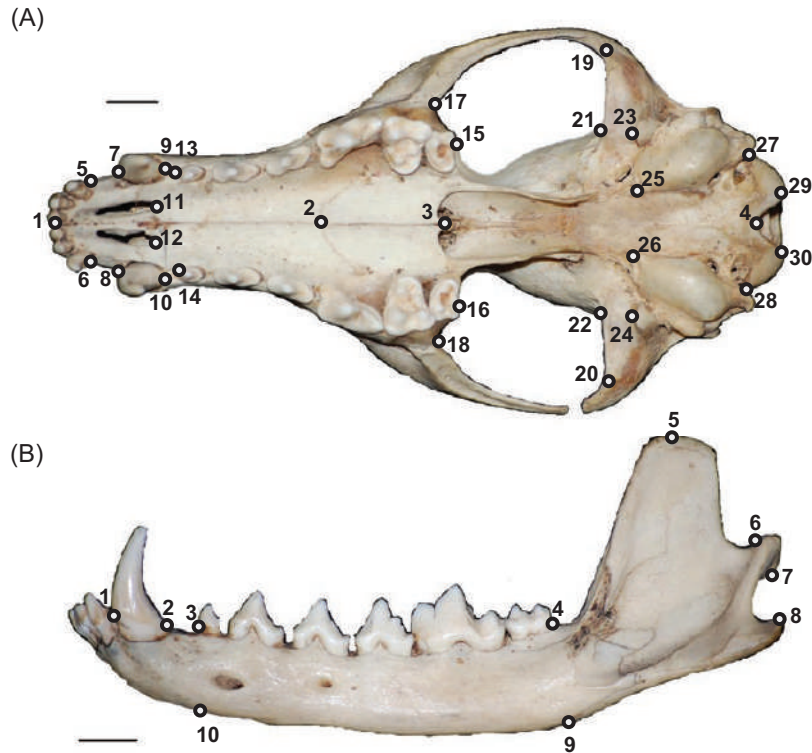


Figure 1. Landmark configuration on cranium (A) and mandible (B) of red fox (*Vulpes vulpes*). Scale bar is 1 cm.

Size and shape data were obtained from Cartesian coordinates (x, y) of landmarks using the Generalized Procrustes Analysis (GPA; Rohlf & Slice, 1990) following three steps: (1) the standardization of size (division of the landmark coordinates of each specimen by its centroid size CS, the square root of the sum of squared distances of landmarks from their barycentre), (2) the removal of translational variation (barycentres from all specimens are superimposed) and (3) the minimization of rotational differences (least-square minimization of the sum of squared distances of corresponding landmarks in a sample). GPA was separately applied to the cranium and the mandible. Data obtained for each specimen were averaged by species for all the subsequent analyses. Sensitivity analyses on a subsample of 50 species with sufficient sexed individuals ensured negligible impact of landmark digitization error, asymmetry and sexual dimorphism on interspecific size and shape variation.

ECOLOGICAL CATEGORIZATIONS

Different dietary classifications have been applied to Carnivora in relation to food type and mode of consumption (Van Valkenburgh, 1989). We followed Christiansen & Wroe (2007) who account for food type and relative prey size. These categories were implemented for the pinnipeds, following Jones *et al.*

(2013), to discriminate piscivores from molluscivores and crustacevives. Whenever the attribution of a species included in our sample was not provided in the studies that originally proposed the categorizations or was uncertain, we assessed it relying on the information available in the *Handbook of the mammals of the world – Volumes 1 and 4* (Wilson & Mittermeier, 2009, 2014 and references therein). Additionally, to test the strength of selective pressure imposed by the aquatic environment, we generated a second categorization: fissiped/pinniped. Although phylogenetic, this categorization is also functional because pinnipeds show a distinct locomotory pattern from the other terrestrial carnivorans (Polly, 2008; Supporting Information, Table S1).

COMPARATIVE ANALYSES: THE BROWNIAN MOTION MODEL

A molecular phylogeny inclusive of the 188 sampled species was generated using the 10K tree project (Arnold *et al.*, 2010). This phylogeny is based on 14 mitochondrial genes, 14 autosomal genes and one gene from the Y-chromosome, all available on GenBank. For the tree inference, the authors used MrBayes (v.3.2; Ronquist & Huelsenbeck, 2003) and node ages were inferred using 16 fossil calibration points, extracted from the Paleobiology Database (<http://paleodb.org>).

Although more updated molecular phylogenies have recently been proposed for Carnivora (i.e. [Hassanin et al., 2021](#)), they do not include several taxa for which we were able to obtain morphological data. The Carnivora supertree ([Nyakatura & Bininda-Emonds, 2012](#)) was equally avoided in order to rigorously test evolutionary hypotheses on the morphological evolution of the skull ([Gaubert et al., 2005](#)).

The molecular phylogeny ([Supporting Information, Fig. S1](#)) was employed to apply comparative methods ([Harvey & Purvis, 1991](#)) on size and shape data in order to: (1) assess the degree of phylogenetic signal in the Carnivora skull measured by the K statistics and its multivariate extension K_{multiv} (to quantify how much the phylogeny fits the data; [Adams, 2014a](#)); (2) test for the impact of ecological categorizations on skull size and shape (using the distance based method Procrustes ANOVA and its phylogenetic equivalent D -PGLS, whose statistical significance is assessed via permutations; [Adams & Collyer, 2015](#)); (3) assess differences in morphological disparity (= MD, quantified as the Procrustes variance obtained from residuals of a linear model fit; this was phylogenetically corrected using residuals of PGLS models; [Michaud et al., 2018](#)); (4) assess differences in evolutionary rates (estimated using the σ^2 statistic that quantifies the rate of variance accumulation in traits over time, while accounting for phylogenetic relationships; [Adams, 2014b](#)) between ecological categories; and (5) test the degree of covariation between cranium and mandible shape at macroevolutionary scale using partial least squares (PLS; [Rohlf & Corti, 2000](#)) and its phylogenetic equivalent ([Adams & Felice, 2014](#)). This test was also repeated within the broader categories of fissiped and pinniped using the ‘effect size’ metric ([Adams & Collyer, 2016](#)) to quantify the strength of morphological integration. Since masticatory constraints are assumed to differ in ecological groups, we expected different patterns of macroevolutionary covariation in these components of the skull ([Linde-Medina et al., 2016](#)).

All these analyses were performed in the R v.4.2.0 computing language (R Development Core Team, 2020), package ‘geomorph’ v.4.0.0 by applying the functions *procd.lm*, *procd.pgls*, *morphol.disparity* and *compare.evol.rates* ([Adams & Otárola-Castillo, 2013](#)). The functions *procd.pgls* and *compare.evol.rates* assume morphological data to follow Brownian motion mode of evolution, i.e. the amount of evolutionary change in a given phenotypic trait is proportional to branch lengths (i.e. time if the phylogeny is a chronogram; [Garland et al., 1992](#)).

COMPARATIVE ANALYSES: BEYOND BROWNIAN MOTION

Alternative models of trait evolution have been tested on Carnivora skull and dentition, including delta, kappa,

lambda, Ornstein–Uhlenbeck (OU) and early burst (EB) ([Meloro & Raia, 2010](#); [Slater & Friscia, 2019](#)). OU accounts for evolutionary phenomena like stabilizing/divergent selection and stasis so that traits can evolve towards a single or multiple optima ([Hansen, 1997](#); [Butler & King, 2004](#); [Beaulieu et al., 2012](#)). Delta, kappa and lambda models are branch-length transformations that stretch basal or terminal nodes approximating, respectively, gradual accelerations/slowdowns in the rate of trait evolution through time, gradualism or punctuated equilibrium conditions, or different levels of phylogenetic signal ([Pagel, 1997, 1999a, 1999b](#)). Finally, EB assumes exponentially reducing diversification rates through time, typical of adaptive radiations ([Harmon et al., 2010](#); [Ingram et al., 2012](#)). These models were tested on both skull size and shape data using the function *transformPhylo.ML* in the package ‘motmot’ v.2.1.3 ([Thomas & Freckleton, 2012](#)). To identify the ability of maximum likelihood in detecting the best mode of evolution for shape data, we simulated multivariate Brownian motion datasets with the dimensionality introduced by our shape data (20 Procrustes coordinates for the mandible and 60 for the cranium). We ran the simulations 100 times to detect how often Brownian was misidentified by the other models of evolution using log-likelihood, following the same recommendation of [Adams & Collyer \(2018\)](#) with the packages ‘geiger’ v.2.0.7 ([Harmon et al., 2008](#)) and ‘motmot’ v.2.1.3 ([Thomas & Freckleton, 2012](#)). For the OU model, we tested only how BM compared with OU1 (often mentioned as ‘single stationary peak’) following [Cooper et al. \(2016\)](#) who have already identified high rates of model misspecification with single traits for phylogenies smaller than 200 taxa.

Additionally, we ran the same simulations on Brownian datasets that were first subjected to a principal component analysis to ensure that the function *transformPhylo.ML* was not affected by data rotation ([Adams & Collyer, 2018](#)).

To implement the best mode of evolution into PGLS models, disparity and evolutionary rates, residuals of each PGLS that assumed BM were tested against the evolutionary models that exhibited the lowest misspecification rates using the function *transformPhylo.ML*. The branch lengths of the original phylogeny were subsequently transformed according to the model parameter with the highest maximum likelihood. The PGLS was run again with the new transformed phylogeny and residuals re-checked for BM (see: [Zelditch et al., 2017](#)). For PLS, both matrices of shape data (= Procrustes coordinates of cranium and mandible) were combined using the function *cbind* ([Meloro et al., 2017](#)) and tested for mode of evolution with *transformPhylo.ML*. Branch lengths of the phylogeny were transformed accordingly and the new resulting tree was implemented into the function *phylo.integration*.

RESULTS

SIZE AND SHAPE VARIATION

Phylomorphospace shows in both cranial and mandibular shape variation a strong influence of phylogeny, with species clustering in the morphospace according to their family (Fig. 2). For the cranium, PC1 (47.09% var.) describes the elongation of the rostrum relative to the braincase, with canids homogeneously occupying positive scores, while felids and mustelids

occupy negative ones (Fig. 2A). PC2 (20.1% var.) relates to changes in the braincase and zygomatic region, with species at the most negative extreme (e.g. *Mustela nivalis* and *Hesperestes* spp.) showing a relative elongation of the braincase and a shortening of the zygomatic arches, while on the positive extreme, felids are characterized by wider zygoma and rostrum but short braincase (Fig. 2A). PC3 (9.7% var.) best separates fissipeds from pinnipeds (negative scores),

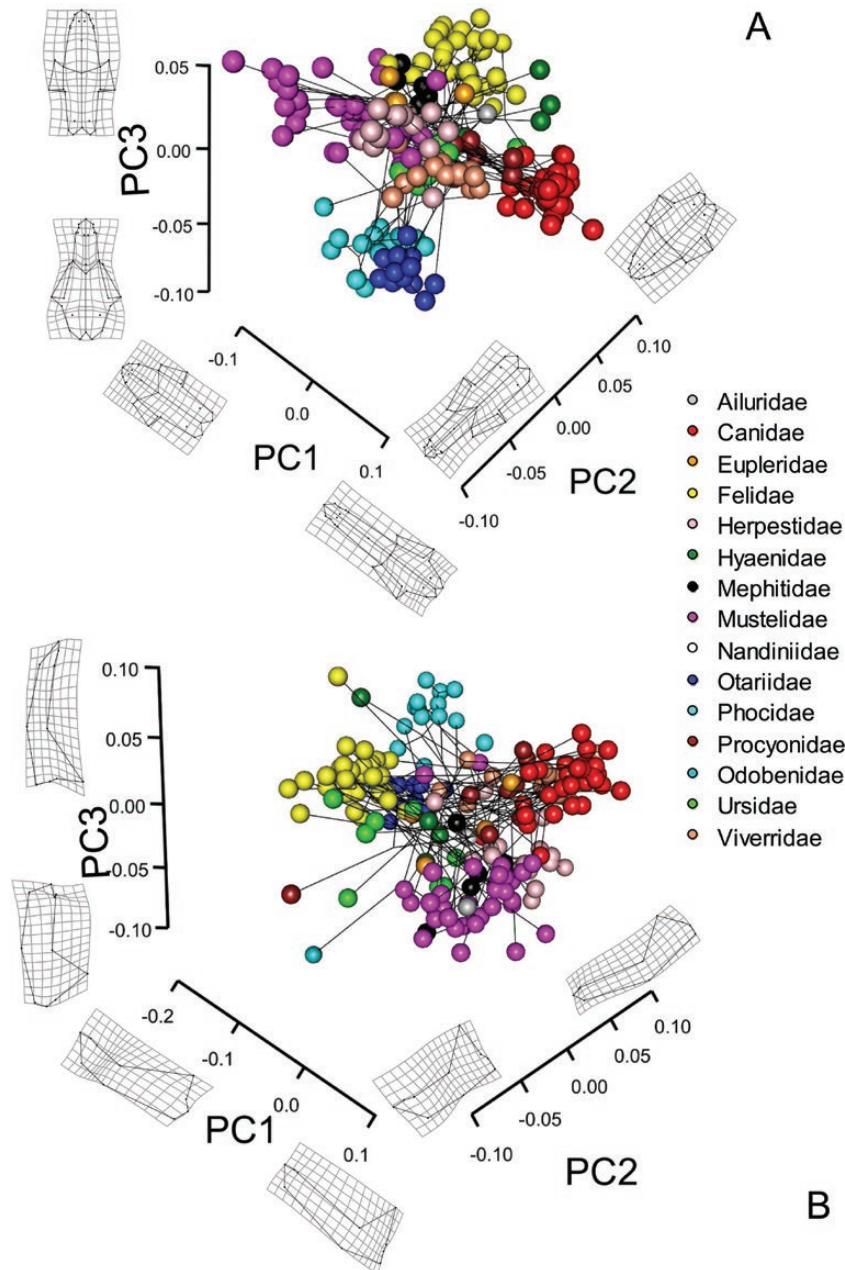


Figure 2. Phylomorphospaces for the cranium (A) and the mandible (B) with respective thin plate spline deformations. Families are colour-coded.

since it relates to the palatal relative width (wider in fissipeds than in pinnipeds), as well as the relative elongation of the zygoma (Fig. 2A).

For the mandible, PC1 (51.5% var.) separates Otariidae, Phocidae and Odobenidae (negative scores) from the other Carnivora, due to their shorter ramus relative to the corpus (Fig. 2B). On PC2 shape changes occur mostly for the corpus region that is thicker in procyonids and ursids (negative scores) rather than pinnipeds and herpestids/canids (positive scores). PC3 (10.9% var.) encompasses changes in the diastema between lower canine and premolar/molar raw shape data and separates felids, phocids and Malagasy carnivorans from the other groups (Fig. 2B). A strong and significant phylogenetic signal ($P < 0.001$) is confirmed for cranium and mandible shape ($K_{multi} = 0.57$ in both cases), as well as size (cranium $K = 0.70$, mandible $K = 0.72$).

Procrustes ANOVA models (Table 1) identify in cranial and mandibular shape a significant impact of diet, which explains the highest percentage of variation followed by the fissiped/pinniped category. Models for size mirror shape data, although when phylogeny is accounted for assuming Brownian, the fissiped/pinniped distinction is non-significant for crano-mandibular size and cranium shape (Table 1). Evolutionary allometry significantly impacts cranial (c. 9% after phylogenetic correction), more than mandibular, shape variation; however, it does not affect the significance of the ecological models (Supporting Information, Table S3).

ECOMORPHOLOGICAL MODELS BEYOND BROWNIAN MOTION

The BM simulated datasets are consistently detected by lambda (min $\lambda = 0.999857$ and all upper CI = 1), EB (> 95% of cases the ACDC (accelerating-decelerating) parameters approach 0.00 = BM) and, to lesser extent, kappa ($\kappa > 0.88$ in every simulation and $\kappa > 0.94$ in 95% cases). OU1 rarely approaches alpha parameters equal to 0.0, which is expected by BM, and the same applies for delta that is expected to be 1.00. The distribution of likelihood differences between each model and BM confirms high rates of misspecification for OU1 and delta (Supporting Information, Figs S2–S4). Results of these simulations are insensitive to data rotation (Supporting Information, Fig. S5).

For the Carnivora skull shape data, lambda is detected as the best mode of evolution, showing similar parameters for the cranium ($\lambda = 0.85$) and the mandible ($\lambda = 0.84$). Size data instead are fitted by kappa, a result congruent with the function *fit.continuous* (Revell, 2012). Cranium and mandible again exhibit similar kappa (0.57 and 0.59, respectively; Supporting Information, Table S4).

The implementation of different evolutionary models does not alter much the ecomorphological

Table 1. Summary statistics for Procrustes ANOVA models computed to test the influence of diet and pinniped vs. fissiped categorization (=Pinn/Fiss) on cranial and mandibular size and shape. Non-significant P values are highlighted in bold

		OLS			PGLS (BM)			PGLS (model fit)			Z	P				
		df1	df2	R ²	F	Z	P	R ²	F	Z			Param	R ²	F	
Cranium Shape	Diet	8	179	0.179	4.875	5.502	0.001	0.062	1.487	2.013	0.018	λ:0.867	0.070	1.690	2.692	0.004
	Fiss/Pinn	1	186	0.091	18.608	4.526	0.001	0.004	0.686	-0.573	0.717	λ:0.523	0.010	1.916	1.463	0.076
Mandible Shape	Diet	8	179	0.310	10.069	7.655	0.001	0.088	2.150	3.765	0.001	λ:0.855	0.094	2.311	4.347	0.001
	Fiss/Pinn	1	186	0.336	93.917	6.709	0.001	0.013	2.480	1.969	0.024	λ:0.568	0.042	8.160	3.994	0.001
Cranium Size	Diet	8	179	0.284	8.878	6.096	0.001	0.120	3.054	2.500	0.007	K:0.558	0.123	3.126	2.655	0.005
	Fiss/Pinn	1	186	0.323	88.607	5.538	0.001	0.016	3.020	1.378	0.081	K:0.839	0.029	5.535	1.346	0.027
Mandible Size	Diet	8	179	0.220	6.301	4.884	0.001	0.085	2.073	1.739	0.041	K:0.544	0.100	2.481	2.607	0.018
	Fiss/Pinn	1	186	0.257	64.276	5.034	0.001	0.011	2.103	1.069	0.148	K:0.814	0.018	3.343	1.113	0.061
Cranium Allometry	Allometry	1	186	0.093	19.168	4.877	0.001	0.093	19.086	6.203	0.001	λ:0.856	0.097	19.991	5.601	0.001
		1	186	0.113	23.630	5.095	0.001	0.014	2.713	2.385	0.006	λ:0.848	0.019	3.593	2.839	0.003

patterns observed. In all cases, the lambda model provides a better fit than Brownian for shape data (with parameters varying around 0.52–0.87), while kappa transformation (values between 0.54–0.84) is preferred for size (Table 1; Supporting Information, Fig. S6). The fissiped/pinniped categorization is still a non-significant factor for cranial, but not mandibular, shape. For size, the opposite pattern occurred (significant for the cranium, non-significant for the mandible; Table 1). Skull size and shape variation were significantly impacted by diet. Interspecific allometry in shape still holds after implementing lambda, although it is much weaker in the mandible (1.9% var.) than in the cranium (9.7% var.) (Table 1).

DISPARITY AND EVOLUTIONARY RATES

Morphological disparity is consistently higher in fissipeds than in pinnipeds. This applies for both shape and size traits no matter if Brownian, lambda or kappa models are implemented (Table 2). Evolutionary rates are significantly higher in pinnipeds on cranium and mandible shape (if lambda model is accounted for, Table 2), while no distinction is found for size.

The interpretation of disparities and evolutionary rates between diet categories is better simplified by a scatterplot (Felice *et al.*, 2018) showing the values corrected following lambda and kappa models for shape and size data, respectively (for values based on BM, see Supporting Information, Fig. S7). When shape is concerned, specialized forms of diet, such as molluscivory, exhibit a considerably high disparity

and evolutionary rate (Fig. 3). The lowest shape disparity is found in the herbivores/frugivore group for the cranium and insectivores for the mandible, while high disparities are equally detectable for piscivores and crustaceivores. In size, a significant and positive association is detected between morphological disparity and evolutionary rates following a ‘carnivory’ gradient, with piscivores and herbivores/frugivores showing the lowest disparities and rates that are gradually increasing in small-, medium- and large-prey specialists (Fig. 3). Molluscivores are outliers due to their relatively lower disparity values for high evolutionary rates in cranial size.

MACROEVOLUTIONARY COVARIATION

The PLS models identify in all cases significant levels of covariation between cranium and mandible shape (Table 3). In Carnivora as whole, the covariation is partially driven by changes in relative rostrum elongation coinciding with changes in relative corpus length (Fig. 4). Pinnipeds homogeneously occupy negative PLS scores being characterized by a short rostrum, wider zygoma, short mandibular corpus and wider ramus region. Covariation in pinnipeds is strongly influenced by the unusual morphology of the walrus, *Odobenus* Brisson, 1762, with a broad rostral region (due to the presence of highly developed tusks) and wider and short mandibular corpus (Fig. 4). Phocids that occupy negative scores are characterized by a narrower rostrum, broader braincase, wider ramus and relatively slender corpus. The implementation of Brownian or

Table 2. Morphological disparity (MD) and evolutionary rates (EvolRates) parameters and *P*-values (in bold if not significant) computed for fissipeds and pinnipeds in cranium (Cra) and mandible (Mand) shape and size. Additional abbreviations: shape = SH, lnCS = natural logarithm of centroid size

				MD	<i>P</i> -value	EvolRates	<i>P</i> -value
Brownian	SH	Cra	Pinniped	0.007	0.021	6.69E-06	0.001
			Fissiped	0.010		4.12E-06	
		Mand	Pinniped	0.006	0.001	1.77E-05	0.76
			Fissiped	0.010		1.72E-05	
	lnCS	Cra	Pinniped	0.061	0.013	0.004	0.185
			Fissiped	0.190		0.005	
		Mand	Pinniped	0.063	0.010	0.004	0.124
			Fissiped	0.247		0.006	
Model fit	SH	Cra	Pinniped	0.007	0.014	5.66E-06	0.001
			Fissiped	0.010		3.42E-06	
		Mand	Pinniped	0.006	0.001	1.02E-05	0.002
			Fissiped	0.010		7.71E-06	
	lnCS	Cra	Pinniped	0.064	0.014	0.008	0.341
			Fissiped	0.191		0.011	
		Mand	Pinniped	0.062	0.010	0.008	0.198
			Fissiped	0.252		0.012	

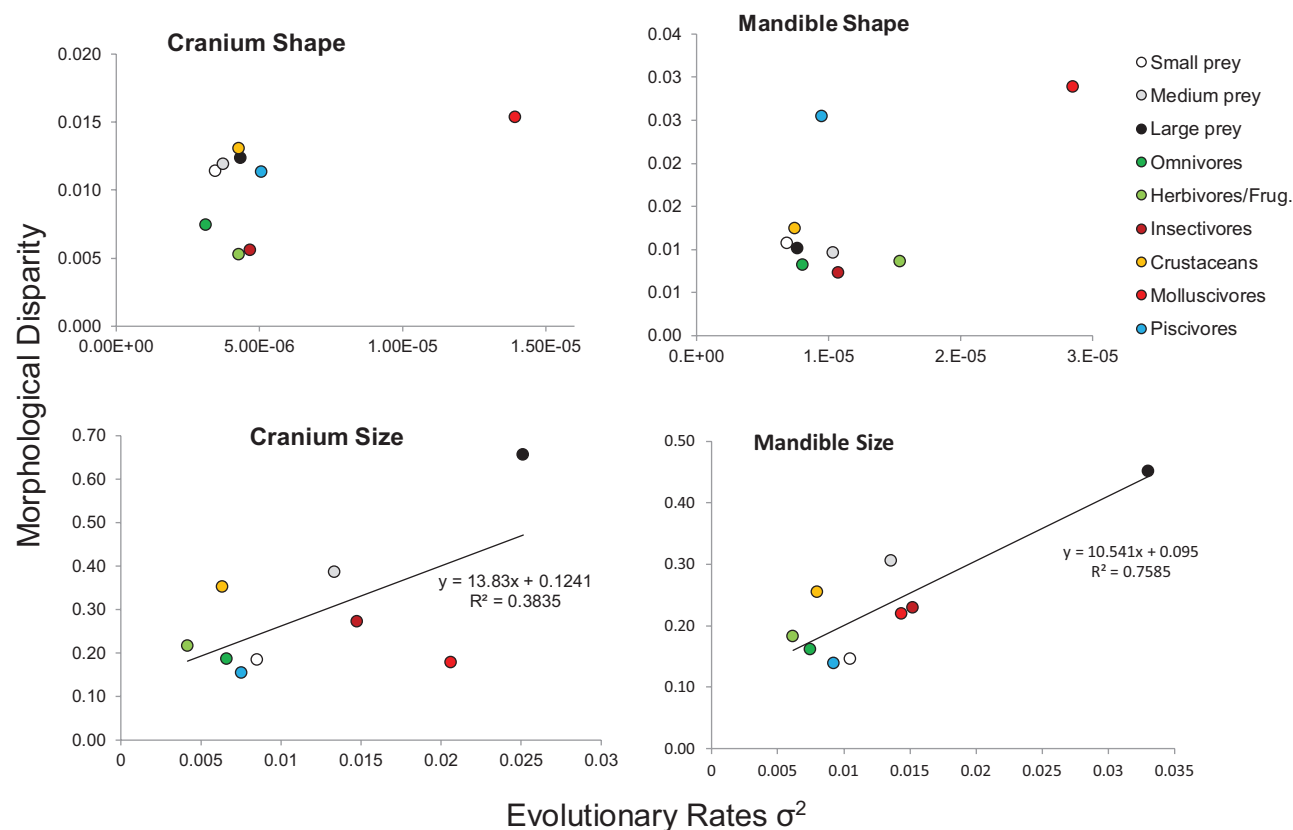


Figure 3. Scatterplot of evolutionary rates vs. morphological disparity after phylogenetic correction following lambda (for shape) or kappa (for size) mode of evolution. Line of best fit is shown when association between the two variables was tested as statistically significant ($P < 0.05$).

Table 3. Correlation coefficient (r) and ‘effect size’ (ES) showed for partial least squares models performed without phylogenetic correction, after assuming Brownian or lambda transformation. Symbols denote significantly different ‘effect size’ between Fissiped and Pinniped (* for standard PLS and ^ for PLS-Lambda)

		Carnivora	Fissiped	Pinniped
PLS	r	0.724	0.81	0.86
	ES	13.292	12.725*	4.61*
PLS-BM	r	0.679	0.629	0.835
	ES	11.015	8.269	3.429
PLS -Lambda	r	0.719	0.7	0.836
	ES	12.13	10.669^	3.487^
	λ	0.812	0.765	0.935

lambda models (those are fitted on lower dimensional matrix of 44 PC scores whose simulations proved to be identical to the Procrustes raw shape data; [Supporting Information, Fig. S5](#)) significantly decrease the ‘effect size’ in the whole sample and confirm fissipeds, to

have greater ‘effect size’ than pinnipeds, although their correlation coefficient in PLS1 vector is lower ([Table 3](#)).

DISCUSSION

Cranial and mandibular morphologies within Carnivora are clearly partitioned at family level. Since early morphometric studies, this pattern was apparent in both size and shape components of the skull, while the detection of ecological adaptations is subtler ([Crusafont-Pairó & Truyols-Santonja, 1956, 1957; Radinsky, 1981; Meloro *et al.*, 2008, 2011; Figueirido *et al.*, 2011; Prevosti *et al.*, 2012](#)). We were able to identify a contained impact of ecological functional groups that persist to some extent after Brownian motion or other alternative modes of evolution are accounted for ([Table 1](#)). More specifically, diet is consistently linked with all aspects of cranial and mandibular morphology, explaining the higher level of variation in size rather than shape. Diet generally accounted for *c.* 10% in shape variance, which was similarly found in some other mammalian and vertebrate groups (e.g. 10% in primates, [Meloro *et al.*,](#)

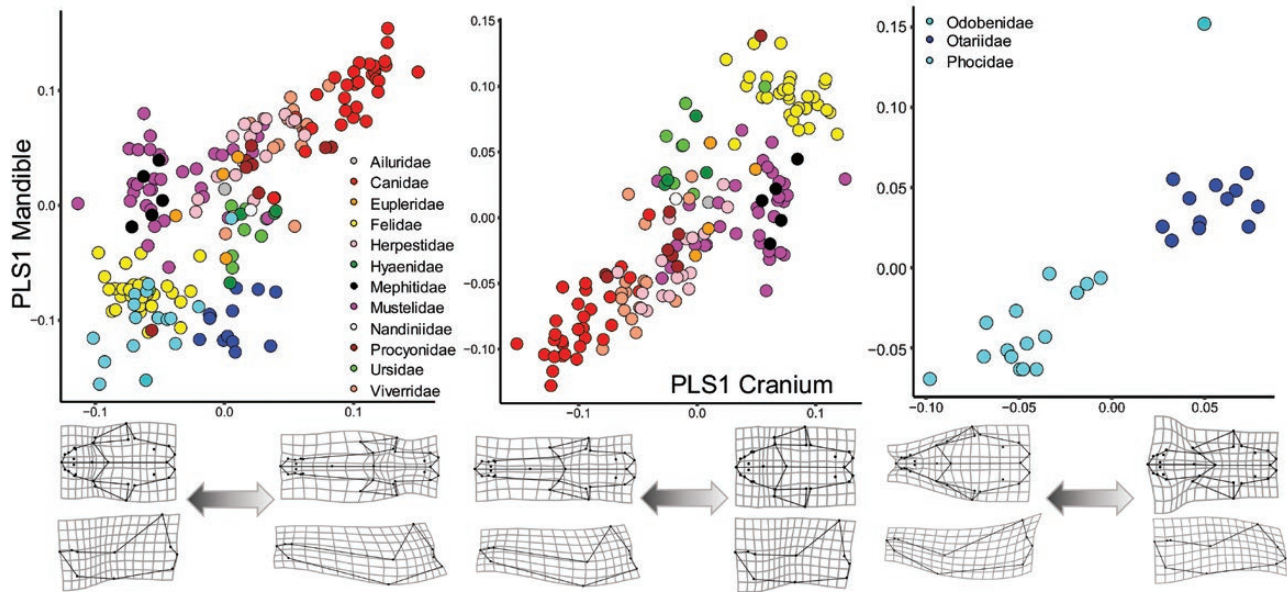


Figure 4. Partial least squares of cranium vs. mandible shape without phylogenetic correction to show taxonomic distribution and the respective thin plate spline PLS vector deformations on the total sample (left), subsample of fissipeds (middle) and subsample of pinnipeds (right).

2015b; 13% in bats, [Giacomini et al., 2021](#); 10% in birds, [Felice et al., 2019](#)). The broader categorization related to aquatic adaptation is even less relevant but identified significantly distinct patterns in the cranium and the mandible. For the cranium, the invasion of aquatic niches did not impact shape, but affected size, with pinnipeds being consistently larger than terrestrial carnivores due to thermoregulation, basal metabolic costs and food intake functions imposed by the aquatic environment ([Gearty et al., 2018](#)). In the mandible we found the opposite, with shape differences becoming apparent on the PC3 axis, which describes a coronoid process close to the condyle indicative of a short temporalis attachment area. Taken to the extreme, such variation might lead to the reductions in the ramus observed in cetaceans ([Berta et al., 2015](#)). [Ito & Endo \(2016\)](#) reported for the spotted seal (*Phoca largha* Pallas, 1811) muscle masses comparatively much smaller (almost 50% in the temporalis) than those of a similar sized fissiped [cougar, *Puma concolor* (Linnaeus, 1771)] and [Laakkonen & Jernvall \(2020\)](#) have recently reported the same pattern for two species of ringed seals (*Pusa* Scopoli, 1771 spp.). Food acquisition and prey preference play key roles to explain such a difference in masticatory muscles between fissipeds and pinnipeds. Terrestrial carnivores, whose mandibular size is comparatively similar to that of pinnipeds (taxa generally heavier than 20 kg), prey upon species much larger than themselves ([Carbone et al., 1999](#)). For this reason, they need to cope with comparatively higher masticatory stresses during prey acquisition and mastication ([Biknevicius & Van](#)

[Valkenburgh, 1996](#)) when compared to pinnipeds that specialize on fish or marine invertebrates. This pattern is also consistent with the hypothesis of [Jones et al. \(2013\)](#) that masticatory muscles in pinnipeds might be comparatively weaker than in fissipeds due to the necessity to produce a high bite force in combat rather than chewing. These ecological factors altogether are modulated by evolutionary allometry that impacts more the cranium (involved in multiple functions and with more complex developmental modularity; [Cardini & Polly, 2013](#); [Evans et al., 2017](#)) than the mandible whose primary function is mastication ([Meloro et al., 2015a](#); [Linde-Medina et al., 2016](#)).

The implementation of different evolutionary models corroborates these hypotheses with generally consistent results occurring, assuming Brownian motion or alternative modes of evolution. For cranial and mandibular size, we detected kappa parameters remarkably similar to those found by [Meloro & Raia \(2010\)](#) on the first lower molar (= carnassial) length of living and fossil fissipeds, ranging between 0.53 and 0.57. Similarly for skull shape, lambda was identified as the best transformation following the findings of [Meloro & Raia \(2010\)](#) on lower carnassial angular height (a proxy for degree of hypo- vs. hypercarnivory). Lambda is a way to incorporate different levels of phylogenetic signal (similarity between the phenotypic traits due to common ancestry) and is effective in phylogenetic regression of univariate traits ([Revell, 2010](#)). The recent work of [Slater & Friscia \(2019\)](#) suggests that the lower slicing vs.

grinding area of Carnivora possibly evolved following the early burst model. However, their dataset did not include pinnipeds, but incorporated fossils. This suggests that the ecological arguments to support carnivoran diversification applies at different hierarchical taxonomic scales. Pinnipeds represent an important 'taxonomic' component of Carnivora that 'escaped' functional constraints dictated by carnassial morphology, evolving different feeding strategies, including suction, grip and tear (Hocking *et al.*, 2017).

Our models led to further macroevolutionary interpretations related to morphological disparities and evolutionary rates. We found consistent differences in disparity values between fissipeds and pinniped taxa. This result is expected considering the higher taxonomic diversity of fissipeds covering 12 families, vs. only three of pinnipeds. Applying rarefaction or other disparity metrics (Navarro, 2003) did not alter this trend (see Supporting Information, Table S5). Within Carnivora, Wesley-Hunt (2005) has already shown concordant increase of morphological disparity through time vs. taxonomic diversity, and although pinnipeds exhibit a relatively higher evolutionary rate in cranium and mandibular shape (if lambda model is implemented; Table 2), their disparity remains comparably lower than fissipeds. Considering that the earliest pinniped differentiation occurred in the Late Oligocene (27–25 Mya; Berta *et al.*, 2015), while fissipeds emerged 65 Mya, we can still note a relatively rapid shape diversification in the skull.

Apparently, aquatic adaptations provided Carnivora of limited ecomorphological opportunities of diversification in a consistently different region of the morphospace (particularly for the mandible; see also: Polly, 2008). These ecological opportunities are bounded within the constraints associated with feeding in the water that includes, for aquatic carnivores: biting that implies crushing or pierce feeding, grip and tear of the prey and suction [framework originally proposed by Hocking *et al.* (2017), redefined by Kienle *et al.* (2017)]. Size evolution is equally bounded in pinnipeds due to the functional constraints imposed by the marine environment. Similar patterns of reduced disparity associated with an extreme lifestyle were also found in subterranean moles (Sansalone *et al.*, 2019). It is likely that this macroevolutionary trend could be persistent across different mammalian groups.

When dietary categories were concerned, we noted that highly demanding feeding imposed by the consumption of molluscs resulted in exceptionally high disparity and evolutionary rate for both cranial and mandibular shape. This category was identified for the sea otter, *Enhydra lutris* (Linnaeus, 1758), as well as the two pinnipeds: the bearded seal *Erignathus barbatus* (Erxleben, 1777) and the walrus *Odobenus rosmarus* (Linnaeus, 1758). The consumption of molluscs by these

species is achieved with different behaviours affected by the morphology: *Enhydra* use bunodont molars to crush molluscs, while *Odobenus* tusks greatly affect its cranial and mandibular morphology. The other aquatic diets equally showed higher levels of disparities, but relatively slower rates. This pattern can be justified by the presence of disparate fissipeds [i.e. otters, as well as the small, flat-headed cat *Prionailurus planiceps* (Vigors & Horsfield, 1827)] and pinniped taxa with a cranio-mandibular shape that is distinct due to differences in dental morphologies and mastication. On the other hand, size disparities and rates follow a positive association. A strict linear association is expected under neutral evolution (Felsenstein, 1985) and the trend we found in our data evidently relates to the nature of our ecological diet categorization that account for a size gradient into feeding function. Groups showing lower size disparity are characterized by a diet that is not energetically demanding (e.g. herbivores and frugivores), while increasing level of specializations towards large prey provides more opportunity for size variation. Carbone *et al.* (1999) identified the size constraint beyond large-prey specialization that fits into the pattern we observed here. Lack of positive association between disparities and rates in shape is common in vertebrate skulls and was equally not detected by Michaud *et al.* (2018) in fissiped Carnivora. Within this context, the framework proposed by Felice *et al.* (2018) suggests that the level of integration among structures perhaps provides constraints that do not favour neutral evolutionary processes. To some extent, we explored this issue by looking at the level of functional covariation between the cranium and the mandible. This was consistently detected in the whole sample and subsample as expected by biomechanical efficiency.

Fissipeds exhibit higher effect size than pinnipeds, corroborating the hypothesis that aquatic specializations provided novel ecomorphological opportunities by relaxing dental (i.e. pinnipeds have lost the carnassials functionality) and muscular constraints associated with food mastication. Indeed, pinnipeds occupy negative PLS scores due to their relatively short rostrum, short corpus and less-developed ramus (Fig. 4). In fissipeds, the relative rostrum elongation and expansion of temporal fossa impose mandibles to evolve a longer corpus and taller ramus (e.g. canids).

CONCLUSION

The cranio-mandibular complex of living Carnivora showed weak but consistent association between size, shape and dietary specializations. The adaptation towards a more aquatic lifestyle experienced by pinnipeds identified for the mandible shape novel opportunities of

morphospace invasion related to the relaxation of chewing constraints and masticatory muscles (as proposed in Jones *et al.*, 2015). Molluscivory has been identified as the diet category with the highest level of disparity and evolutionary rate in shape due to its specific functional demand. The subtle impact of diet perhaps relates to the inadequacy of categorizing ecological specializations that in Carnivora are rarely devoted to one food type only (see also: Tamagnini *et al.*, 2021). Selective processes are channelled at broad taxonomic scale, as supported by Michaud *et al.* (2018) who identified a strong association between morphological disparities and ecological specializations at the family level. Covariation patterns in the skull shape of Carnivora reflect morphological stability necessary for the correct biomechanical function related to mastication.

ACKNOWLEDGEMENTS

The authors are grateful to several museum institutions and curators for kindly providing access to museum collections: P. Jenkins, A. Salvador (NHM, London); A. Kitchener (Royal Museum of Scotland, Edinburgh); T. Parker (Liverpool World Museum); E. Gilissen and W. Wendelen (Royal Museum for Central Africa, Tervuren, Belgium). Andrea Cardini, Dean Adams and Michael Collyer kindly stimulated this project during its initial stage, while Filippo Galimberti and Simona Sanvito (Elephant Seal Research Group) provided us with helpful insights on pinniped ecology.

Meloro C. was supported by the Leverhulme Trust project 'Taxon-free palaeontological methods for reconstructing environmental change' during data collection at the NHM of London, and by the European Community's programme 'Structuring the European Research Area' Synthesys at the Royal Museum for Central Africa project 'Ecomorphology of extant African carnivores' (BE-TAF 4901). The European mobility programme ERASMUS plus supported Tamagnini D. to conduct this research while visiting Liverpool John Moores University.

DATA AVAILABILITY

The data underlying this article are available in the Dryad Digital Repository, at <https://datadryad.org/stash/share/6s2IZtvxBkoCSe9pISRwoD4eklFUsuTzm580RgCTT1s>.

REFERENCES

Adam PJ, Berta A. 2002. Evolution of prey capture strategies and diet in the Pinnipedimorpha (Mammalia, Carnivora). *Oryctos* **4**: 83–107.

- Adams DC. 2014a.** A generalized K statistic for estimating phylogenetic signal from shape and other high-dimensional multivariate data. *Systematic Biology* **63**: 685–697.
- Adams DC. 2014b.** Quantifying and comparing phylogenetic evolutionary rates for shape and other high-dimensional phenotypic data. *Systematic Biology* **63**: 166–177.
- Adams DC, Collyer ML. 2015.** Permutation tests for phylogenetic comparative analyses of high-dimensional shape data: what you shuffle matters. *Evolution* **69**: 823–829.
- Adams DC, Collyer ML. 2016.** On the comparison of the strength of morphological integration across morphometric datasets. *Evolution* **70**: 2623–2631.
- Adams DC, Collyer ML. 2018.** Multivariate phylogenetic comparative methods: evaluations, comparisons, and recommendations. *Systematic Biology* **67**: 14–31.
- Adams DC, Felice RN. 2014.** Assessing trait covariation and morphological integration on phylogenies using evolutionary covariance matrices. *PLoS One* **9**: e94335.
- Adams DC, Otárola-Castillo E. 2013.** Geomorph: an R package for the collection and analysis of geometric morphometric shape data. *Methods in Ecology and Evolution* **4**: 393–399.
- Arnold C, Matthews LJ, Nunn CL. 2010.** The 10kTrees Website: a new online resource for primate phylogeny. *Evolutionary Anthropology* **19**: 114–118.
- Barr WA. 2014.** Functional morphology of the bovid astragalus in relation to habitat: controlling phylogenetic signal in ecomorphology. *Journal of Morphology* **275**: 1201–1216.
- Barr WA. 2018.** Ecomorphology. In: Croft DA, Su DF, Simpson SW, eds. *Methods in paleoecology*. Cham: Springer, 339–349.
- Barr WA, Scott RS. 2014.** Phylogenetic comparative methods complement discriminant function analysis in ecomorphology. *American Journal of Physical Anthropology* **153**: 663–674.
- Braulieu JM, Jhvueng D-C, Boettiger C, O'Meara BC. 2012.** Modelling stabilizing selection: expanding the Ornstein–Uhlenbeck model of adaptive evolution. *Evolution* **66**: 2369–2383.
- Berta A, Sumich JL, Kovacs KM. 2015.** *Marine mammals (third edition)*. London: Elsevier, Inc.
- Biknevicius AR, Van Valkenburgh B. 1996.** Design for killing: craniodental adaptations of predators. In: Gittleman JL, ed. *Carnivore behavior, ecology, and evolution*, Vol. 2. Ithaca: Cornell University Press, 393–428.
- Bininda-Emonds OR, Gittleman JL. 2000.** Are pinnipeds functionally different from fissiped carnivores? The importance of phylogenetic comparative analyses. *Evolution* **54**: 1011–1023.
- Blomberg SP, Garland T Jr, Ives AR. 2003.** Testing for phylogenetic signal in comparative data: behavioral traits are more labile. *Evolution* **57**: 717–745.
- Botton-Divet L, Cornette R, Houssaye A, Fabre AC, Herrel A. 2017.** Swimming and running: a study of the convergence in long bone morphology among semi-aquatic mustelids (Carnivora: Mustelidae). *Biological Journal of the Linnean Society* **121**: 38–49.

- Botton-Divet L, Houssaye A, Herrel A, Fabre AC, Cornette R. 2018.** Swimmers, diggers, climbers and more, a study of integration across the mustelids' locomotor apparatus (Carnivora: Mustelidae). *Evolutionary Biology* **45**: 182–195.
- Butler MA, King AA. 2004.** Phylogenetic comparative analysis: a modeling approach for adaptive evolution. *The American Naturalist* **164**: 683–695.
- Carbone C, Mace GM, Roberts SC, Macdonald DW. 1999.** Energetic constraints on the diet of terrestrial carnivores. *Nature* **402**: 286–288.
- Cardini A. 2014.** Missing the third dimension in geometric morphometrics: how to assess if 2D images really are a good proxy for 3D structures? *Hystrix, the Italian Journal of Mammalogy* **25**: 73–81.
- Cardini A, Polly PD. 2013.** Larger mammals have longer faces because of size-related constraints on skull form. *Nature Communication* **4**: 2458.
- Cheverud JM. 1982.** Phenotypic, genetic, and environmental morphological integration in the cranium. *Evolution* **36**: 499–516.
- Christiansen P, Wroe S. 2007.** Bite forces and evolutionary adaptations to feeding ecology in carnivores. *Ecology* **88**: 347–358.
- Cooper N, Thomas GH, Venditti C, Meade A, Freckleton RP. 2016.** A cautionary note on the use of Ornstein Uhlenbeck models in macroevolutionary studies. *Biological Journal of the Linnean Society* **118**: 64–77.
- Crusafont-Pairó M, Truyols-Santonja J. 1956.** A biometric study of the evolution of fissiped carnivores. *Evolution* **10**: 314–332.
- Crusafont-Pairó M, Truyols-Santonja J. 1957.** Estudios masterométricos en la evolución Fisípedos. I. Los módulos angulares ay b. II. Los parámetros lineales P, C, y T. *Boletino Instituto Geológico y Minero España* **68**: 1–140.
- Echarri S, Prevosti FJ. 2015.** Differences in mandibular disparity between extant and extinct species of metatherian and placental carnivore clades. *Lethaia* **48**: 196–204.
- Elton S, Jansson A-U, Meloro C, Louys J, Plummer T, Bishop LC. 2016.** Exploring morphological generality in the Old World monkey postcranium using an ecomorphological framework. *Journal of Anatomy* **228**: 534–560.
- Estes JA. 1989.** Adaptations for aquatic living by carnivores. In: Gittleman JL, ed. *Carnivore behavior, ecology, and evolution*. Boston: Springer, 242–282.
- Evans KM, Waltz BT, Tagliacollo VA, Sidlauskas BL, Albert JS. 2017.** Fluctuations in evolutionary integration allow for big brains and disparate faces. *Scientific Reports* **7**: 40431.
- Ewer RF. 1973.** *The carnivores*. Ithaca: Cornell University Press.
- Felice RN, Randau M, Goswami A. 2018.** A fly in a tube: macroevolutionary expectations for integrated phenotypes. *Evolution* **72**: 2580–2594.
- Felice RN, Tobias JA, Pigot AL, Goswami A. 2019.** Dietary niche and the evolution of cranial morphology in birds. *Proceedings of the Royal Society B: Biological Sciences* **286**: 20182677.
- Felsenstein J. 1985.** Phylogenies and the comparative method. *The American Naturalist* **125**: 1–15.
- Figueirido B, MacLeod N, Krieger J, De Renzi M, Pérez-Claros JA, Palmqvist P. 2011.** Constraint and adaptation in the evolution of carnivorous skull shape. *Paleobiology* **37**: 490–518.
- Figueirido B, Tseng ZJ, Martín-Serra A. 2013.** Skull shape evolution in durophagous carnivores. *Evolution* **67**: 1975–1993.
- Garland T, Harvey PH, Ives AR. 1992.** Procedures for the analysis of comparative data using phylogenetically independent contrasts. *Systematic Biology* **41**: 18–32.
- Gaubert P, Wozencraft WC, Cordeiro-Estrela P, Veron G. 2005.** Mosaics of convergences and noise in morphological phylogenies: what's in a viverrid-like carnivore? *Systematic Biology* **54**: 865–894.
- Gearty W, McClain CR, Payne JL. 2018.** Energetic tradeoffs control the size distribution of aquatic mammals. *Proceedings of the National Academy of Sciences of the USA* **115**: 4194–4199.
- Giacomini G, Herrel A, Chaverri G, Brown RP, Russo D, Scaravelli D, Meloro C. 2021.** Functional correlates of skull shape in Chiroptera: feeding and echolocation adaptations. *Integrative Zoology* doi:10.1111/1749-4877.12564.
- Gittleman JL. 1985.** Carnivore body size: ecological and taxonomic correlates. *Oecologia* **67**: 540–554.
- Hansen TF. 1997.** Stabilizing selection and the comparative analysis of adaptation. *Evolution* **51**: 1341–1351.
- Harmon LJ, Kolbe JJ, Cheverud JM, Losos JB. 2005.** Convergence and the multidimensional niche. *Evolution* **59**: 409–421.
- Harmon LJ, Weir JT, Brock CD, Glor RE, Challenger W. 2008.** GEIGER: investigating evolutionary radiations. *Bioinformatics* **24**: 129–131.
- Harmon LJ, Losos JB, Jonathan Davies T, Gillespie RG, Gittleman JL, Bryan Jennings W, Kozak KH, McPeck MA, Moreno-Roark F, Near TJ, Purvis A. 2010.** Early bursts of body size and shape evolution are rare in comparative data. *Evolution* **64**: 2385–2396.
- Harvey PH, Purvis A. 1991.** Comparative methods for explaining adaptations. *Nature* **351**: 619–624.
- Hassanin A, Veron G, Ropiquet A, Jansen van Vuuren B, Lécuyer A, Goodman SM, Haider J, Nguyen TT. 2021.** Evolutionary history of Carnivora (Mammalia, Laurasiatheria) inferred from mitochondrial genomes. *PLoS One* **16**: e0240770.
- Hocking DP, Marx FG, Park T, Fitzgerald EM, Evans AR. 2017.** A behavioural framework for the evolution of feeding in predatory aquatic mammals. *Proceedings of the Royal Society B: Biological Sciences* **284**: 20162750.
- Ingram T, Harmon LJ, Shurin JB. 2012.** When should we expect early bursts of trait evolution in comparative data? Predictions from an evolutionary food web model. *Journal of Evolutionary Biology* **25**: 1902–1910.
- Ito K, Endo H. 2016.** Comparative study of physiological cross-sectional area of masticatory muscles among species of Carnivora. *Mammal Study* **41**: 181–190.

- Jablonski D.** 2017. Approaches to macroevolution: 1. General concepts and origin of variation. *Evolutionary Biology* **44**: 427–450.
- Janis C.** 1990. Correlation of cranial and dental variables with dietary preferences in mammals: a comparison of macropodoids and ungulates. *Memoirs of the Queensland Museum* **28**: 349–366.
- Jones KE, Ruff CB, Goswami A.** 2013. Morphology and biomechanics of the pinniped jaw: mandibular evolution without mastication. *Anatomical Records* **296**: 1049–1063.
- Jones KE, Smaers JB, Goswami A.** 2015. Impact of the terrestrial-aquatic transition on disparity and rates of evolution in the carnivoran skull. *BMC Evolutionary Biology* **15**: 8.
- Kappelman J.** 1988. Morphology and locomotor adaptations of the bovid femur in relation to habitat. *Journal of Morphology* **198**: 119–130.
- Kardong KV.** 2012. *Vertebrates: comparative anatomy, function, evolution*. New York: McGraw-Hill.
- Kienle SS, Law CJ, Costa DP, Berta A, Mehta RS.** 2017. Revisiting the behavioural framework of feeding in predatory aquatic mammals. *Proceedings of the Royal Society B: Biological Sciences* **284**: 20171035.
- Laakkonen J, Jernvall J.** 2020. Muscles of mastication and the temporo-mandibular joint of the Saimaa (*Pusa hispida saimensis*) and Baltic (*Pusa hispida botnica*) ringed seals. *Annales Zoologici Fennici* **57**: 21–29.
- Linde-Medina M, Boughner JC, Santana SE, Diogo R.** 2016. Are more diverse parts of the mammalian skull more labile? *Ecology and Evolution* **6**: 2318–2324.
- Machado FA, Zahn TMG, Marroig G.** 2018. Evolution of morphological integration in the skull of Carnivora (Mammalia): changes in Canidae lead to increased evolutionary potential of facial traits. *Evolution* **72**: 1399–1419.
- Machado FA, Hubbe A, Melo D, Porto A, Marroig G.** 2019. Measuring the magnitude of morphological integration: the effect of differences in morphometric representations and the inclusion of size. *Evolution* **73**: 2518–2528.
- Meloro C, O'Higgins P.** 2011. Ecological adaptations of mandibular form in fissiped Carnivora. *Journal of Mammalian Evolution* **18**: 185–200.
- Meloro C, Raia P.** 2010. Cats and dogs down the tree: the tempo and mode of evolution in the lower carnassial of fossil and living Carnivora. *Evolutionary Biology* **37**: 177–186.
- Meloro C, Raia P, Piras P, Barbera C, O'Higgins P.** 2008. The shape of the mandibular corpus in large fissiped carnivores: allometry, function and phylogeny. *Zoological Journal of the Linnean Society* **154**: 832–845.
- Meloro C, Raia P, Carotenuto F, Cobb SN.** 2011. Phylogenetic signal, function and integration in the subunits of the carnivoran mandible. *Evolutionary Biology* **38**: 465–475.
- Meloro C, Clauss M, Raia P.** 2015a. Ecomorphology of Carnivora challenges convergent evolution. *Organismal Diversity and Evolution* **15**: 711–720.
- Meloro C, Cáceres NC, Carotenuto F, Sponchiado J, Melo GL, Passaro F, Raia P.** 2015b. Chewing on the trees: constraints and adaptation in the evolution of the primate mandible. *Evolution* **69**: 1690–1700.
- Meloro C, Hunter J, Tomsett L, Portela Miguez R, Prevosti FJ, Brown RP.** 2017. Evolutionary ecomorphology of the Falkland Islands wolf *Dusicyon australis*. *Mammal Review* **47**: 159–163.
- Michaud M, Veron G, Peigné S, Blin A, Fabre A-C.** 2018. Are phenotypic disparity and rate of morphological evolution correlated with ecological diversity in Carnivora? *Biological Journal of the Linnean Society* **124**: 294–307.
- Michaud M, Veron G, Fabre A-C.** 2020. Phenotypic integration in feliform carnivores: Covariation patterns and disparity in hypercarnivores versus generalists. *Evolution* **74**: 2681–2702.
- Moss ML, Young RW.** 1960. A functional approach to craniology. *American Journal of Physical Anthropology* **18**: 281–292.
- Navarro N.** 2003. MDA: a MATLAB-based program for morphospace-disparity analysis. *Computers & Geosciences* **29**: 655–664.
- Nyakatura K, Bininda-Emonds OR.** 2012. Updating the evolutionary history of Carnivora (Mammalia): a new species-level supertree complete with divergence time estimates. *BMC Biology* **10**: 1–31.
- Pagel M.** 1997. Inferring evolutionary processes from phylogenies. *Zoologica Scripta* **26**: 331–348.
- Pagel M.** 1999a. The maximum likelihood approach to reconstructing ancestral character states of discrete characters on phylogenies. *Systematic Biology* **48**: 612–622.
- Pagel M.** 1999b. Inferring the historical patterns of biological evolution. *Nature* **401**: 877–884.
- Pineda-Munoz S, Lazagabaster IA, Alroy J, Evans AR.** 2016. Inferring diet from dental morphology in terrestrial mammals. *Methods in Ecology and Evolution* **8**: 481–491.
- Polly D.** 2008. Adaptive zones and the pinniped ankle: a three-dimensional quantitative analysis of carnivoran tarsal evolution. In: Dagosto M, ed. *Mammalian evolutionary morphology: a tribute to Frederick S. Szalay*. Dordrecht: Springer, 167–196.
- Prevosti FJ, Turazzini GF, Ercoli MD, Hingst-Zaher E.** 2012. Mandible shape in marsupial and placental carnivorous mammals: a morphological comparative study using geometric morphometrics. *Zoological Journal of the Linnean Society* **164**: 836–855.
- Price SA, Hopkins SS, Smith KK, Roth VL.** 2012. Tempo of trophic evolution and its impact on mammalian diversification. *Proceedings of the National Academy of Sciences of the USA* **109**: 7008–7012.
- R Development Core Team.** 2020. *R: a language and environment for statistical computing*. Version 4.0.2. Vienna: R Foundation for Statistical Computing. Available at: <http://cran.R-project.org>
- Radinsky LB.** 1981. Evolution of skull shape in carnivores: 1. Representative modern carnivores. *Biological Journal of the Linnean Society* **15**: 369–388.
- Revell LJ.** 2010. Phylogenetic signal and linear regression on species data. *Methods in Ecology and Evolution* **1**: 319–329.

- Revell LJ. 2012.** Phytools: an R package for phylogenetic comparative biology (and other things). *Methods in Ecology and Evolution* **3**: 217–223.
- Rohlf FJ. 2015.** The tps series of software. *Hystrix, the Italian Journal of Mammalogy* **26**: 9–12.
- Rohlf FJ, Corti M. 2000.** Use of two-block partial least-squares to study covariation in shape. *Systematic Biology* **49**: 740–753.
- Rohlf FJ, Slice D. 1990.** Extensions of the Procrustes method for the optimal superimposition of landmarks. *Systematic Zoology* **39**: 40–59.
- Ronquist F, Huelsenbeck JP. 2003.** MrBayes 3: Bayesian phylogenetic inference under mixed models. *Bioinformatics* **19**: 1572–1574.
- Sansalone G, Colangelo P, Loy A, Raia P, Wroe S, Piras P. 2019.** Impact of transition to a subterranean lifestyle on morphological disparity and integration in talpid moles (Mammalia, Talpidae). *BMC Evolutionary Biology* **19**: 1–15.
- Scott RS, Barr WA. 2014.** Ecomorphology and phylogenetic risk: implications for habitat reconstruction using fossil bovids. *Journal of Human Evolution* **73**: 47–57.
- Segura V, Cassini GH, Prevosti FJ, Machado FA. 2020.** Integration or modularity in the mandible of canids (Carnivora: Canidae): a geometric morphometric approach. *Journal of Mammalian Evolution* **28**: 145–157.
- Serb JM, Sherratt E, Alejandrino A, Adams DC. 2017.** Phylogenetic convergence and multiple shell shape optima for gliding scallops (Bivalvia: Pectinidae). *Journal of Evolutionary Biology* **30**: 1736–1747.
- Sherratt E, Alejandrino A, Kraemer AC, Serb JM, Adams DC. 2016.** Trends in the sand: Directional evolution in the shell shape of recessing scallops (Bivalvia: Pectinidae). *Evolution* **70**: 2061–2073.
- Slater GJ, Friscia AR. 2019.** Hierarchy in adaptive radiation: a case study using the Carnivora (Mammalia). *Evolution* **73**: 524–539.
- Stuart-Fox D, Moussalli A. 2007.** Sex-specific ecomorphological variation and the evolution of sexual dimorphism in dwarf chameleons (*Bradypodion* spp.). *Journal of Evolutionary Biology* **20**: 1073–1081.
- Tamagnini D, Meloro C, Raia P, Maiorano L. 2021.** Testing the occurrence of convergence in the craniomandibular shape evolution of living carnivorans. *Evolution* **75–7**: 1738–1752.
- Thomas GH, Freckleton RP. 2012.** MOTMOT: models of trait macroevolution on trees. *Methods in Ecology and Evolution* **3**: 145–151.
- Van Valkenburgh B. 1989.** Carnivore dental adaptations and diet: a study of trophic diversity within guilds. In: Gittleman JL, ed. *Carnivore behavior, ecology, and evolution*. Boston: Springer, 410–436.
- Wainwright PC. 1991.** Ecomorphology: experimental functional anatomy for ecological problems. *American Zoologist* **31**: 680–693.
- Wesley-Hunt GD. 2005.** The morphological diversification of carnivores in North America. *Paleobiology* **3**: 35–55.
- Westneat MW. 2005.** Skull biomechanics and suction feeding in fishes. In: Shadwick R, Lauder G, eds. *Fish physiology, fish biomechanics*, Vol. 23. Cambridge: Academic Press, 29–75.
- Wilson DE, Mittermeier RA. 2009.** *Handbook of mammals of the world: carnivores: 1*. Barcelona: Lynx Edicions.
- Wilson DE, Mittermeier RA. 2014.** *Handbook of the mammals of the world: sea mammals: 4*. Barcelona: Lynx Edicions.
- Zelditch ML, Ye J, Mitchell JS, Swiderski DL. 2017.** Rare ecomorphological convergence on a complex adaptive landscape: body size and diet mediate evolution of jaw shape in squirrels (Sciuridae). *Evolution* **71**: 633–649.

SUPPORTING INFORMATION

Additional Supporting Information may be found in the online version of this article at the publisher's web-site.

Table S1: List of species analysed and their diet categorizations.

Table S2: Anatomical definition for landmarks of the cranium and the mandible.

Table S3: Summary statistics for Procrustes ANOVA models computed to test the influence of diet, pinniped vs. fissiped (= Pinn/Fiss), and predation on cranial (= Cran.) and mandibular (= Mand.) shape after accounting for allometry. Non-significant *P* values are highlighted in bold.

Table S4: Parameter estimates and their maximum likelihood performed for both cranial and mandibular size and shape data. The EB parameter and maximum likelihood values are not reported because they were always identical to BM.

Table S5. Morphological disparity parameters expressed as 'sum of ranges' and 'mean distance to centroid' computed on cranium and mandible shape morphospace. The disparity values obtained for fissipeds (*n* = 160) were rarefied to the smallest sample size of pinnipeds (*n* = 28). 95% confidence interval were obtained after 100 bootstrap resampling. Disparity parameters are presented for raw shape data, or phylogenetically corrected using residuals of the pgl's model: shape~fissiped/pinniped assuming Brownian, or after fitting best mode of evolution (λ = 0.523 for the cranium shape; λ = 0.568 for the mandible shape).

Figure S1: Phylogenetic tree of 188 extant Carnivora. Branch lengths are proportional to time of divergence, tip labels are colour-coded according to family.

Figure S2: Likelihood differences based on comparisons of several evolutionary models (delta, kappa, lambda, OU1 and EB) simulated 100 times under a single-rate BM model. The dataset simulated a sample of 188 cases \times 20 variables, the dimensionality of mandible shape data.

Figure S3: Likelihood differences based on comparisons of several evolutionary models (delta, kappa, lambda, OU1 and EB) simulated 100 times under a single-rate BM model. The dataset simulated a sample of 188 cases \times 60 variables, the dimensionality of cranial shape data.

Figure S4: Likelihood differences based on comparisons of several evolutionary models (delta, kappa, lambda, OU1 and EB) simulated 100 times under a single-rate BM model. The dataset simulated a sample of 188 cases \times 80 variables, the dimensionality of cranial + mandibular shape data combined.

Figure S5: Likelihood differences based on comparisons of Lambda evolutionary model simulated 100 times under a single-rate BM model. The dataset simulated a sample of 188 cases \times 44 PC variables (obtained from 100 simulated Procrustes coordinates datasets), which correspond to the PCA dimensionality of cranial + mandibular shape data combined. Likelihood differences are shown also for the original variables, and their distribution is identical. At the bottom, simulation for $N = N = 80$ (the fissipeds).

Figure S6: Distribution of $-2 \times \log$ -likelihood for each model shown in Table 1. OLS = ordinary least squares, PGLS = phylogenetic generalized least squares (assuming Brownian), PGLS-mf = phylogenetic generalized least squares model fit (following best mode of evolution for the residual). Mand. = Mandible.

Figure S7: Scatterplots of evolutionary rates vs. morphological disparity (phylogenetically corrected assuming BM) in cranial and mandibular size and shape for diet categories.

Chapter 7 – Purrs, roars, and claws: Do conical and sabertoothed cats represent an exception to craniofacial evolutionary allometry?

The American Naturalist

Purrs, roars, and claws: Do conical and sabertoothed cats represent an exception to craniofacial evolutionary allometry? --Manuscript Draft--

Manuscript Number:	
Full Title:	Purrs, roars, and claws: Do conical and sabertoothed cats represent an exception to craniofacial evolutionary allometry?
Short Title:	CREA in conical and sabertoothed cats
Article Type:	Major Article
Manuscript Classifications:	Allometry; carnivores; Carnivory; Macroevolution; Morphometrics
Additional Information:	
Question	Response
Data Accessibility during Peer Review. Data and code should be accessible during peer review. If there are no data or code for your submission, please indicate so here. If you are uploading data using the integrated Dryad upload system, or uploading them directly (e.g. as a zip file), please type, " Uploaded. " If data are available from elsewhere on the web, please type the link where editors and reviewers can find your data. The information in this field will be provided to reviewers.	Uploaded.

Purrs, roars, and claws: Do conical and sabertoothed cats represent an exception to craniofacial evolutionary allometry?

Article type

Major article

Main title

Purrs, roars, and claws: Do conical and sabertoothed cats represent an exception to craniofacial evolutionary allometry?

Running title

CREA in conical and sabertoothed cats

Keywords

Evolutionary allometry; Macroevolution; Carnivora; CREA hypothesis; Sabertoothed cats

Abstract Word Count

209

Total Word Count

4700

Data Accessibility Statement

Morphological datasets, phylogeny and R script supporting the result of the present paper will be archived in Dryad upon acceptance and are also provided as Supporting Information.

Conflict of Interest Statement

The authors declare no conflict of interest.

List of elements included in the manuscript

The present manuscript includes two figures and one table in the main text. The supplementary material includes two figures, five tables, and one SI appendix.

Abstract

CREA is an evolutionary trend proposing that, among closely related species, the smaller-sized of the group would appear paedomorphic with proportionally smaller rostra and larger braincases. Here, we use a phylogenetically broad cranial dataset, 3D geometric morphometrics, and phylogenetic comparative methods to assess the validity and strength of CREA in the most species-rich groups of extinct and living felids. In particular, we aim to explore whether sabertoothed cats, thanks to their unusual rostral morphology, constitute an exception to CREA, even testing the impact of taxonomic rank, phylogeny, and mode of evolution on this evolutionary trend. Our results unambiguously provided support to the validity of CREA within Felidae as a whole and within the small and medium-sized felines. By contrast, big cats, like Pantherinae and Machairodontinae, failed to support CREA. The adoption of different landmark configurations, phylogenetic hypotheses, and corrections for phylogenetic effect had a limited impact on CREA pattern recognition within felids. Our findings suggest that Pantherinae and Machairodontinae constitute one of the first well-supported exceptions to this biological rule currently known. We hypothesize the acquisition of specific cranial features resulting from extreme ecological specialisation - such as sabertoothed upper canines - to represent a preferential way to escape from common evolutionary patterns of morphological variation such as CREA.

49

50 **Introduction**

51 A central goal in present-day research in macroevolution is to unravel patterns and processes
52 that determine phenotypic evolutionary trajectories over long-time scales (Gould 1980;
53 Hautmann 2020; Tamagnini et al. 2021a). Some phenotypes evolve as persistent and
54 directional changes in the state of one or more quantitative traits resulting in a substantial
55 evolutionary trend (Alroy 2000; McNamara 2006). Among such trends, there are the so-called
56 biological rules, which are the results of directional responses to ecological, climatic or
57 biological gradients and occur in a large number of different clades (Raerinne 2011;
58 Tamagnini et al. 2021a). Typical examples of biological rules are Bergmann's, Allen's or
59 Cope's rules which represent directional variations in species traits (e.g., body size or surface-
60 area-to-volume ratio) over latitudinal, elevation or temporal gradients (Bergmann 1847; Allen
61 1877; Rensch 1948).

62 When it comes to research on evolutionary trends, the formulation of a new biological
63 rule, known as CRaniofacial Evolutionary Allometry (CREA – Cardini and Polly 2013;
64 Cardini 2019), recently reached the centre of the stage. CREA alleges that, among closely
65 related species, the smaller-sized of the group would appear paedomorphic with
66 proportionally smaller rostra and larger braincases (Cardini and Polly 2013; Tamagnini et al.
67 2017; Cardini 2019). CREA roots its concept in evolutionary allometry, which is traditionally
68 defined in morphometrics as the presence of patterns of size-related variations in
69 morphological traits (in the case of CREA, rostral and braincase shape) at the
70 macroevolutionary scale (Klingenberg 2016). These variations are measured by comparing
71 adults belonging to different closely related species among each other (Klingenberg and
72 Zimmermann 1992). Although the processes underpinning CREA are not yet fully

understood, growing evidence suggests that adult allometric patterns reflect either strong evolutionary constraints or lines of least evolutionary resistance in morphological evolution (Marroig and Cheverud 2005; Voje et al. 2013; Raia et al. 2015; Cardini 2019). Following the example of Radinsky (1985), who first tested for the occurrence of evolutionary allometry in the cranium of several mammalian clades, a discrete number of studies already addressed the occurrence and strength of CREA within mammalian lineages. These investigations confirmed the validity of CREA within groups ranging from metatherians (e.g., wallabies and kangaroos belonging to the genus *Macropus* – Cardini et al. 2015) to placentals (e.g., Australian rodents, pangolins, and many other clades belonging to all superorders of placental mammals – Cardini 2019; Ferreira-Cardoso et al. 2020; Marcy et al. 2020). Further confirmation was even found in other vertebrate clades, such as birds of prey (Bright et al. 2016) and temnospondyl amphibians (Angielczyk and Ruta 2012). By contrast, CREA was supported only in a limited number of fossil nonmammalian synapsids (Krone et al. 2019).

Within mammals, species belonging to the order Carnivora (henceforth referred to as carnivorans) represent a classical case study for morphological macroevolution thanks to their substantial ecological flexibility, high taxonomic diversity, and remarkable morphological variability (Ewer 1973; Gittleman 1986). Carnivorans were also frequently investigated in studies that constituted the bedrock of modern ecomorphology and aimed to determine the interactions between morphological evolution and ecology (e.g., Van Valkenburgh 1989; Figueirido and Soibelzon 2010; Figueirido et al. 2011; Meloro and O'Higgins 2011; Law et al. 2018; Michaud et al. 2018, 2020; Meloro and Tamagnini 2021). Research on evolutionary trends makes no exception, as evidenced by numerous studies concerning directional patterns of evolution (and their ecological correlates) in carnivorans (e.g., biological rules – Meiri et al. 2004, 2008; Diniz-Filho et al. 2009; convergence – Figueirido et al. 2013; Meloro et al.

2015; Castiglione et al. 2019; Melchionna et al. 2021; Tamagnini et al. 2021b; divergent evolution – Slater and Friscia 2019). Previous investigations performed within terrestrial carnivorans applying both traditional and geometric morphometric techniques fully supported the presence of CREA in living musteline mustelids (i.e., weasels, ferrets, and minks - Radinski 1985), canids (i.e., wolves, wild dogs, and foxes – Cardini 2019) and herpestids (i.e., mongooses – Cardini and Polly 2013; Cardini 2019). Analogous approaches suggested the pattern may be present in living felids, although big cats were hypothesised to be a partial exception to CREA (Tamagnini et al. 2017).

Thanks to the peculiar adaptations to their hypercarnivorous lifestyle (Therrien 2005a, b), the morphological evolution of felids has always caught the interest of evolutionary biologists (Meachen-Samuels and Van Valkenburgh 2009a, b). This also applies to paleontological research, in which sabertoothed cats (i.e., extinct subfamily Machairodontinae) represent one of the most fascinating and renowned groups for ecomorphological studies due to their extreme dentary adaptations (e.g., Simpson 1941; Emerson and Radinsky 1980; Van Valkenburgh 2007). Ranging from medium-sized species with an approximative weight of around 30kg (e.g., *Yoshi garevskii* – Spassov and Geraads 2015) to predators weighing more than 430kg (e.g., *Smilodon populator* – Manzuetti et al. 2020), sabertoothed cats combine short lower premolar rows and reduced posterior cusps in lower carnassials (m1), which are typical of all felids (Piras et al. 2013), to extremely elongated, laterally-compressed, and curved upper canines that protrude from the mouth when closed (i.e., saber-like teeth - Turner and Antón 1997). Relying on upper canine morphology, Machairodontinae are subdivided into different ecomorphotypes that range from dirk-toothed and scimitar-toothed cats (i.e., tribes Homotherini, Machairodontini, and Smilodontini, commonly known as true sabertooths – Figure 1) to species showing only incipient

development of the saber-like teeth (i.e., tribe Metailurini, often defined as false sabertooths – Antón 2013). This latter condition might reflect the tendency to prey on relatively smaller herbivores compared to the true sabretooths (Slater and Van Valkenburgh 2008; Lautenschlager et al. 2020).

Conical-toothed felids, including fossil and living Felinae and Pantherinae (Fig. 1), display higher ecomorphological flexibility compared to sabertooths, that have been generally interpreted as hyperspecialised predators of large ungulates and juvenile proboscideans (Anyonge 1996; Meachen-Samuels 2012; Van Valkenburgh et al. 2016). The extreme phenotype and hyperspecialisation of sabertoothed cats were demonstrated to have significantly increased their extinction risk (Van Valkenburgh 2007; Piras et al. 2018). Among conical-toothed cats, the central relevance of the distinction between small (i.e., Felinae) and big cats (i.e., Pantherinae) has been confirmed by molecular phylogenetics (Johnson et al. 2006; Agnarsson et al. 2010). Similarly, big cats appear inhomogeneous in terms of size, geographic distribution, and diversity when comparing their main lineages, which include the smaller and sabertoothed-like clouded leopards (i.e., Indomalayan endemic genus *Neofelis*) and the large-sized and globally widespread genus *Panthera* (Christiansen 2006, 2008; Sicuro 2011; Sicuro and Oliveira 2011).

To date, studies assessing CREA that include paleontological data are extremely rare (but see Radinski 1985; Krone et al. 2019), and none of them relies on modern techniques of 3D morphological quantification (e.g., 3D geometric morphometrics). This knowledge gap persists despite that the inclusion of fossil data has already been suggested to be a key feature for improving the accuracy of allometric analyses, increasing taxonomic sampling, and detecting potential exceptions to CREA (Tamagnini et al. 2017; Krone et al. 2019). Given their distinctiveness in behaviour, ecological niche, and cranial anatomy, extinct and living

felids represent a fascinating case-study to test for the presence and strength of CREA (Tamagnini et al. 2017), with sabertoothed cats potentially constituting an exception to this biological rule because of their unusual rostral morphology (Meloro and Slater 2012).

Here, we use 3D geometric morphometrics on a phylogenetically broad cranial dataset (n = 51 inclusive of fossil and extant species) in combination with phylogenetic comparative methods to assess CREA in the most species-rich groups of felids, including: the entire family Felidae, its three subfamilies (i.e., Felinae, Pantherinae, and Machairodontinae), the genus *Panthera* and the true sabertooths. To do so, we explore whether phylogenetic uncertainty and different evolutionary models of phenotypic changes through time may have an impact on CREA outcomes. The combination of these tests aims to answer two meaningful questions in mammalian macroevolution: what is the impact of taxonomic rank, phylogeny, and mode of evolution on CREA within the hypercarnivorous clade of Felidae? Do sabertoothed cats, with their extreme cranial adaptations, constitute an exception to this biological rule?

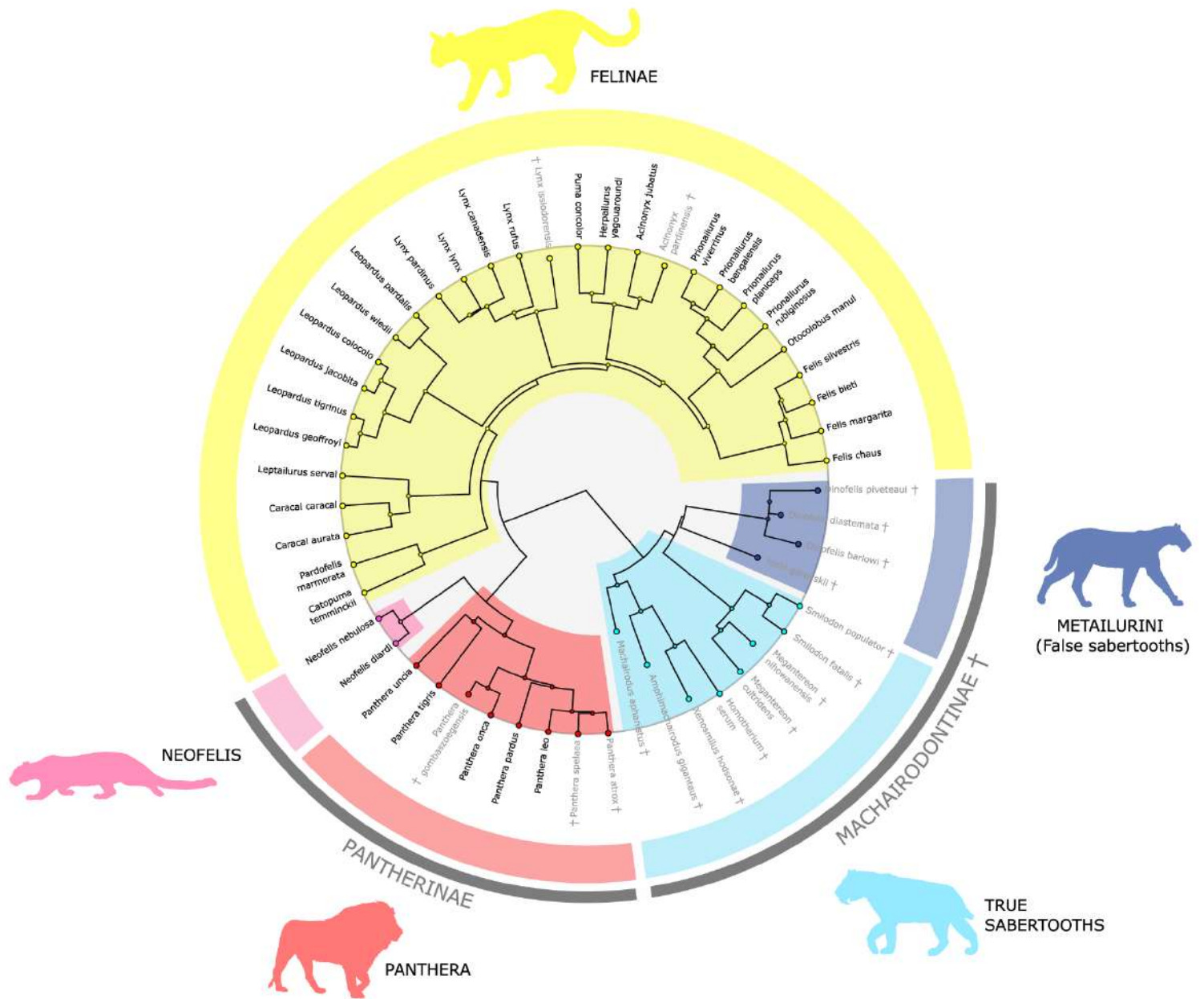


Figure 1: Circular dendrogram representing the phylogeny from Piras et al. (2018) showing the distribution of each taxon in our allometric analyses on living and extinct felids. The subfamily Felinae is represented in yellow, the subfamily Pantherinae includes the genus *Panthera* (in red) and the genus *Neofelis* (in pink) and the subfamily Machairodontinae includes true sabertooths (i.e., tribes Homotherini, Machairodontini, and Smilodontini - in light blue) and false sabertooths (i.e., tribe Metailurini - in blue).

Material and Methods

Sample and data collection

The morphological sample consisted of 98 felid crania, including almost 90% of the extant species diversity (34 out of 38) and 17 fossil species (12 sabertoothed and five conical-toothed cats). All individuals were adults, as assessed by the complete dentition and fusion of their cranial sutures. Sample composition is detailed in *SI Appendix*, Table S1. For each species, both sexes were included in the data whenever possible. Using a single (or a few) individual(s) to represent a species is considered adequate in a macroevolutionary analysis involving large interspecific and intergeneric differences (e.g., Drake and Klingenberg 2010; Meloro and O'Higgins 2011). When multiple specimens belonging to the same species were available, morphological data were averaged within species, obtaining pooled-sex data (see *SI Appendix* for sensitivity analyses regarding sexual dimorphism). The vast majority of digital 3D models used in this study was collected by the same operator (D.T.) employing a digital SLR Nikon D7000 camera attached to a Nikkor 40 mm macro lens to perform photogrammetric reconstructions. Photogrammetry was applied following guidelines from Falkingham (2012) and Mallison and Wings (2014). Additionally, a small proportion (i.e., c. 25%) of the specimens was either taken from online repositories (i.e., DigiMorph, MorphoSource, Phenome10K, Sketchfab, and digital collections of Primate Research Institute (Kyoto) and Museu de Ciències Naturals (Barcelona)) and/or deriving from materials included in previous studies (e.g., Adams et al. 2015; Spassov and Geraads 2015; Geraads and Spassov 2020; Tseng et al. 2016). These 3D models were obtained using photogrammetry, computed tomography or surface laser scanning techniques. Multi-technique datasets including models deriving from the use of all these methods were recently demonstrated to be suitable for assessing the presence and the strength of allometry in macroevolutionary

analyses with wide phylogenetic scope (Giacomini et al. 2019). The taxonomy adopted in this study followed the IUCN Red List website (<https://www.iucnredlist.org>) for living species and previous ecomorphological studies for fossil ones (e.g., Piras et al. 2018).

Landmark configurations, digitisation, and geometric morphometrics

The landmark configuration is shown in Figure S1, and the definition of each landmark is provided in Table S2. Allometric analyses were performed using a set of 30 landmarks (30L configuration - *SI Appendix*, Tab. S2) at first and then redone including only a subset of 10 landmarks (10L configuration - *SI Appendix*, Tab. S2, rows with grey background). The former configuration was used since it describes general functional aspects of cranial morphology, whereas the latter was selected to capture more specifically the relative proportions of the face and the braincase.

3D landmark digitisation was performed using the software Stratovan Checkpoint (Wiley et al. 2005) by a single operator (DT) to avoid inter-operator biases. The repeatability and precision of landmark configurations were tested (*SI Appendix*). Details about the retrodeformation of distorted fossil specimens and the estimation of missing landmarks are provided in *SI Appendix*. In order to remove non-shape variation from three-dimensional Cartesian coordinates of landmarks, we employed the Procrustes superimposition method (Rohlf and Slice 1990; Adams et al. 2004). This procedure consists of three steps: the standardization of size, the removal of translational variation, and the minimization of rotational differences (Rohlf and Slice 1990). Procrustes superimposition was performed using the software MorphoJ (version 1.06d, Klingenberg 2011). As this study does not focus on the analysis of asymmetries and given the low amount of variance explained by the asymmetric component of shape on the cranial sample (< 5% of the total shape variance), all

allometric analyses focused only on the symmetric component of shape variation
(Klingenberg et al. 2002).

Allometric regressions

Cranial evolutionary allometry was tested on a sample of pooled-sex species means by regressing shape coordinates against the natural logarithm of centroid size, since using the logarithm of size is considered good practice in allometric analyses when the range of size is as large as in our case (Klingenberg 2016). As anticipated, all multivariate regressions were performed using the 30L configuration and then repeated using the 10L configuration. The regressions were performed within the family Felidae (51 species) and then replicated within its three subfamilies (i.e., conical-toothed Felinae and Pantherinae - 29 and 10 species respectively; sabertoothed Machairodontinae - 12 species). Finally, the regressions were repeated within the genus *Panthera* (8 species) to assess if the exclusion of the genus *Neofelis* (that was previously suggested to be a morphological outlier – Christiansen 2006, 2008) may impact the allometric results found within the subfamily Pantherinae, and redone within true sabertooths (i.e., tribes Homotherini, Machairodontini, and Smilodontini - 8 species) to evaluate if the exclusion of false sabertooths (i.e., tribe Metailurini) may substantially alter the results obtained considering all the sabertooths at the same time.

Multivariate regressions were performed without applying any phylogenetic correction (i.e., ordinary least squares regressions - OLS) and then redone applying phylogenetic comparative methods by means of the implementation of two different models of evolution (i.e., Brownian Motion conditions – BM; the most likely model of evolution according to a phylogenetic ridge regression – RR) into phylogenetic generalized least squares (PGLS) regressions. Brownian motion evolution is a constant and non-directional random diffusion-

like process as resulting from neutral evolution (Garland et al. 1992). By contrast, phylogenetic ridge regression estimates branch-specific evolutionary rates and ancestral states under a wide range of models of trait evolution (Castiglione et al. 2018; Clavel et al. 2019) and multiplies branch lengths by branch-specific evolutionary rates to accommodate rate variation across the tree. All comparative analyses were performed twice, relying on two different phylogenies inclusive of fossil and living felids (taken from Piras et al. (2018) and Faurby et al. (2019)) as estimates of evolutionary relationships.

The allometric regressions were performed using the R packages *geomorph* (Adams and Otárola-Castillo 2013) and *RRphylo* (Castiglione et al. 2018). The significance of each test was assessed by performing 1000 simulations against random expectations. We also used a Bonferroni correction in order to take into account the simultaneous implementation of several tests, which could inflate type I errors (Bonferroni 1936). The morphological data, R code, and phylogenies used in this study are provided in *SI Appendix*. The visualization of opposite extremes of the allometric trajectories was done warping, by means of thin-plate spline, a single specimen from our sample selected on a case-by-case basis.

Results

Patterns of allometric shape changes

The variance explained by evolutionary allometry ranged from 10.5% to 40.2% in all OLS and PGLS allometric regressions performed within Felidae (Table 1). All these tests reached statistical significance after applying a Bonferroni correction (P-values = 0.001). Larger felids showed relatively enlarged rostra combined with reduced and arrow-shaped braincases (Figure 2A for 30L configuration; *SI Appendix*, Figure S2A for 10L configuration). These species also experienced a dorso-ventral compression of the cranium.

Results of allometric regressions performed within the subfamily Felinae largely overlapped those obtained for Felidae as a whole: the percentage of shape variance explained by the allometric component ranged from 14.1% to 23.3% within Felinae, and all the tests maintained their statistical significance after a Bonferroni correction (P-values = 0.001 - Tab. 1). Larger feline species were characterized by an evident increase in prognathism, as well as a pronounced reduction of braincase volume (Fig. 2B; *SI Appendix*, Fig. S2B).

Within the subfamily Pantherinae, R^2 ranged from 0.107 to 0.391 in all allometric regressions (Tab. 1). Statistical significance was reached by five out of 10 regressions within this group, but only OLS regressions on both the 30L and 10L configurations were significant after a Bonferroni correction (P-values = 0.001 and 0.002, respectively). Allometric shape changes within Pantherinae described a dorso-ventral flattening and a reduction of the braincase in larger species, paired with an enlargement of both the rostrum and the nasal cavity (Fig. 2C; *SI Appendix*, Fig. S2C). However, allometric shape variations within this subfamily appeared to be weaker than those found within felids and the subfamily Felinae.

Within Machairodontinae, R^2 ranged from 0.083 to 0.226 in all OLS and PGLS allometric regressions (Tab. 1). None of these tests was statistically significant, except for RR PGLS regressions performed on both 30L and 10L configurations using the Faurby et al. (2019) phylogeny (P-values = 0.011 and 0.015, respectively), and none of them reached statistical significance after applying a Bonferroni correction. Larger sabertoothed cats mainly differed from their smaller relatives for a marked widening of the sagittal crest and a lateral compression of the cranium (Fig. 2D; *SI Appendix*, Fig. S2D). Larger Machairodontinae showed a slight enlargement of the rostrum, but it was decoupled from a reduction of the braincase.

Results and patterns of allometric shape changes obtained within the genus *Panthera* largely overlap with those obtained within the subfamily Pantherinae (i.e., only OLS regression on the 30L configuration reached significance after a Bonferroni correction - Tab. 1; Fig. 2E; *SI Appendix*, Fig. S2E). Similarly, regressions performed on true sabertooths produced outcomes comparable to those obtained within Machairodontinae since none of the allometric regressions reached significance ($R^2_{\min} = 0.059$; $R^2_{\max} = 0.274$; P-values ≥ 0.093 - Tab. 1; Fig. 2F; *SI Appendix*, Fig. S2F).

Impact of landmark configuration, phylogenetic correction, and phylogeny on CREA

Both landmark configurations used in this study returned comparable results in terms of allometric shape variation. Changes in R^2 produced by using a different landmark configuration were smaller than 0.098 for all the considered cases, regardless of the taxonomic group, comparative method or phylogeny (Tab. 1). 30L and 10L configurations returned comparable results in terms of statistical significance, except for seven cases. However, even if these cases were significant only according to one landmark configuration, all these tests did not reach statistical significance after applying a Bonferroni correction, except for the OLS regression within genus *Panthera* performed on 30L configuration, which still resulted marginally significant (P-value = 0.002 - Tab. 1).

Regressions performed without any comparative method (i.e., OLS regressions) returned results largely overlapping to those from their phylogenetically-informed counterparts (i.e., BM and RR PGLS regressions). An exception to this pattern was represented by the subfamily Pantherinae, in which only OLS regressions relative to both landmark configurations, as opposed to PGLS regressions, resulted significant after a Bonferroni correction (Tab. 1). The genus *Panthera* showed such a discrepancy as well, but

303 only with regard to the 30L configuration. The comparison between BM and RR PGLS
304 regressions produced homogenous results within felids and any other tested subclade.
305 Although four cases, which relied on the Faurby et al. (2019) phylogeny, reached statistical
306 significance according to only one model of evolution at first, none of these tests was still
307 significant after a Bonferroni correction.

308 Changing the phylogenetic tree used as a background for the phylogenetic
309 comparative methods had a negligible impact on CREA in felids and every other considered
310 subclade. Variations in R^2 produced by using different phylogenetic trees were smaller than
311 0.133 for all the considered cases. All PGLS regressions returned a similar statistical
312 significance when comparing results obtained using the two phylogenies, except for three
313 cases relative to the 30L configuration and one case relative to the 10L one (Tab. 1).
314 However, although these cases were significant only according to one phylogenetic tree, none
315 of the tests reached statistical significance after applying a Bonferroni correction.

316

30L configuration

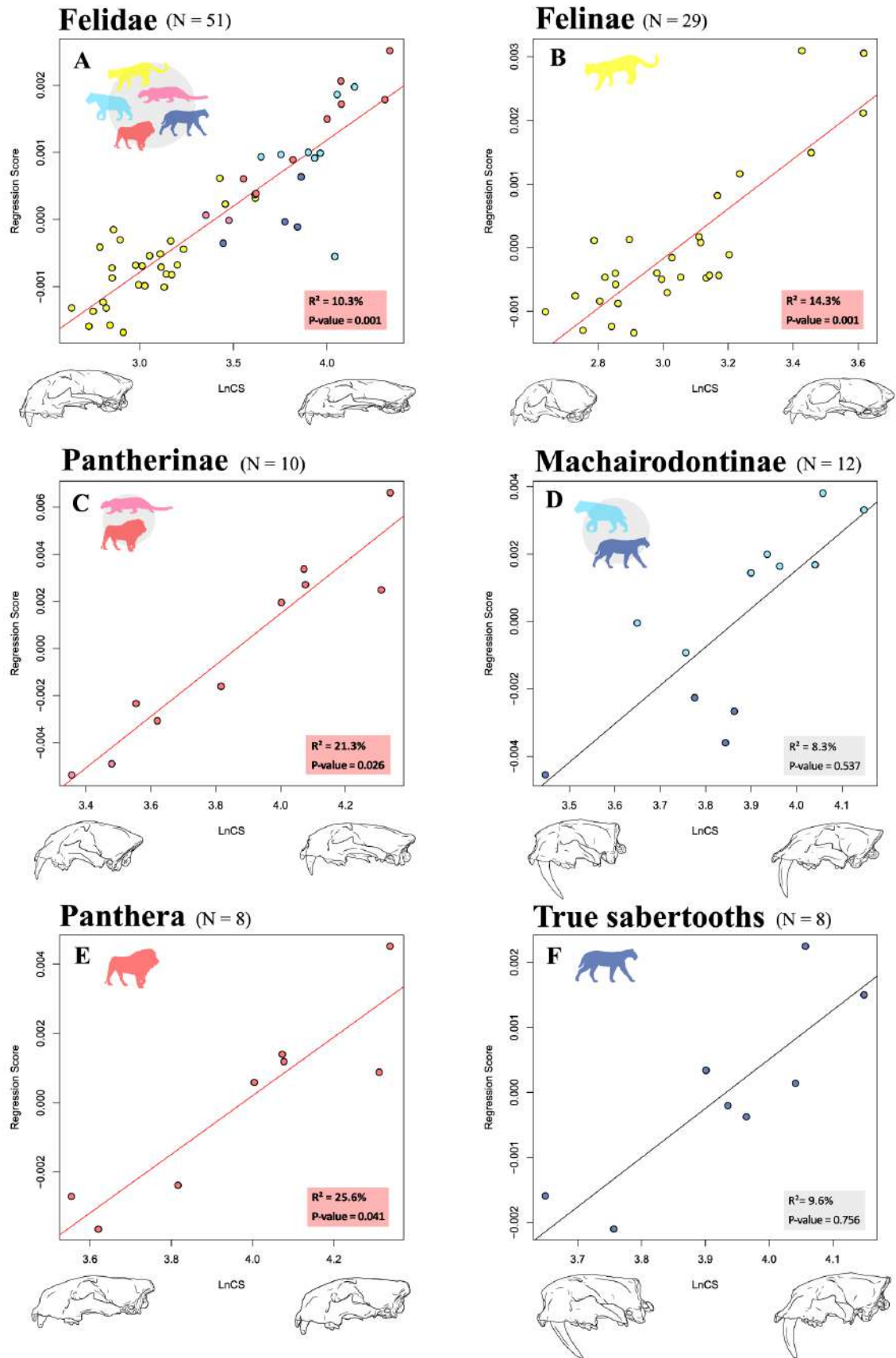


Figure 2: Scatterplots of shape regression scores versus natural logarithm of centroid size obtained using the 30L configuration, Piras et al. (2018) phylogeny, and BM PGLS concerning Felidae (A), Felinae (B), Pantherinae (C), Machairodontinae (D), genus *Panthera* (E), and true sabertooths (F). Patterns of allometric shape variation are shown by means of 3D surfaces warped using thin-plate spline.

Sample	Phylogeny	Phylogenetic Comparative Method (PCM)	30L configuration				10L configuration			
			R ²	F	Z	P-value	R ²	F	Z	P-value
Felidae	No phylo	No PCM (OLS)	0.412	34.333	6.023	<u>0.001</u>	0.420	35.458	5.610	<u>0.001</u>
	Piras et al. 2018	BM PGLS	0.103	5.599	4.464	<u>0.001</u>	0.110	6.082	3.917	<u>0.001</u>
		RR PGLS	0.134	7.556	5.285	<u>0.001</u>	0.139	7.901	4.498	<u>0.001</u>
	Faurby et al. 2019	BM PGLS	0.110	6.069	4.621	<u>0.001</u>	0.105	5.745	3.617	<u>0.001</u>
		RR PGLS	0.139	7.917	5.412	<u>0.001</u>	0.151	8.739	4.633	<u>0.001</u>
	Felinae	No phylo	No PCM (OLS)	0.233	8.194	4.481	<u>0.001</u>	0.220	7.599	3.991
Piras et al. 2018		BM PGLS	0.143	4.523	3.687	<u>0.001</u>	0.176	5.757	3.531	<u>0.001</u>
		RR PGLS	0.149	4.724	3.952	<u>0.001</u>	0.155	4.942	3.406	<u>0.001</u>
Faurby et al. 2019		BM PGLS	0.141	4.430	3.608	<u>0.001</u>	0.151	4.816	3.374	<u>0.001</u>
		RR PGLS	0.155	4.942	4.154	<u>0.001</u>	0.161	5.177	3.597	<u>0.001</u>
Pantherinae		No phylo	No PCM (OLS)	0.391	5.131	3.097	<u>0.001</u>	0.383	4.963	2.696
	Piras et al. 2018	BM PGLS	0.213	2.169	1.770	<u>0.026</u>	0.205	2.063	1.335	0.084
		RR PGLS	0.221	2.266	1.936	<u>0.019</u>	0.207	2.089	1.413	0.082
	Faurby et al. 2019	BM PGLS	0.154	1.452	0.863	0.216	0.107	0.959	0.233	0.430
		RR PGLS	0.214	2.180	1.837	<u>0.015</u>	0.211	2.135	1.434	0.071
	Machairodontinae	No phylo	No PCM (OLS)	0.143	1.662	1.156	0.133	0.162	1.927	1.328
Piras et al. 2018		BM PGLS	0.083	0.903	-0.087	0.537	0.101	1.129	0.421	0.365
		RR PGLS	0.093	1.020	0.180	0.428	0.112	1.263	0.661	0.265
Faurby et al. 2019		BM PGLS	0.113	1.272	0.680	0.258	0.109	1.223	0.600	0.275
		RR PGLS	0.226	2.919	2.276	<u>0.011</u>	0.200	2.502	2.016	<u>0.015</u>
<i>Panthera</i>		No phylo	No PCM (OLS)	0.307	2.659	2.160	<u>0.002</u>	0.310	2.695	1.825
	Piras et al. 2018	BM PGLS	0.256	2.062	1.600	<u>0.041</u>	0.244	1.934	1.158	0.115
		RR PGLS	0.249	1.995	1.609	<u>0.037</u>	0.253	2.030	1.318	0.095
	Faurby et al. 2019	BM PGLS	0.170	1.227	0.560	0.314	0.120	0.820	0.078	0.504
		RR PGLS	0.243	1.931	1.554	<u>0.036</u>	0.248	1.976	1.299	0.095
	True sabertooths	No phylo	No PCM (OLS)	0.085	0.560	-0.820	0.789	0.132	0.910	0.091
Piras et al. 2018		BM PGLS	0.096	0.638	-0.754	0.756	0.173	1.253	0.530	0.326
		RR PGLS	0.073	0.474	-1.261	0.886	0.123	0.845	-0.066	0.564
Faurby et al. 2019		BM PGLS	0.176	1.281	0.575	0.275	0.274	2.260	1.449	0.093
		RR PGLS	0.059	0.376	-1.740	0.960	0.136	0.945	0.107	0.482

Table 1: Results of the allometric regressions performed on 30L and 10L configurations using OLS and Brownian Motion (BM) or phylogenetic ridge regression (RR) PGLS. Significant P-values at $\alpha = 0.05$ are underlined and in bold when still significant after a Bonferroni correction.

Discussion

Implications for the cranial evolution of felids

Assessing the strength and pervasiveness of evolutionary trends, such as CREA, is essential to shed light on the macroevolutionary dynamics. Felids epitomize a meaningful case-study for research on evolutionary allometry in mammalian biology thanks to their specialised cranial morphology, paired with the hypercarnivorous lifestyle shared by the entire clade. Our results unambiguously provided support to the validity of CREA within the entire family Felidae and within the small and medium-sized felines. By contrast, our analyses confuted the occurrence of CREA within any other group (e.g., subfamilies Pantherinae and Machairodontinae). Overall, the adoption of different landmark configurations, phylogenetic hypotheses, and corrections for phylogenetic effect had a limited impact on CREA pattern recognition within felids.

Conical-toothed cats returned opposite results in terms of presence and strength of CREA when comparing Felinae to Pantherinae. CREA was always significant within fossil and extant felines, basically reconfirming the results obtained in previous 2D GMM research performed on living cats (Tamagnini et al. 2017). Coherently with our findings, Slater and Van Valkenburgh (2008, Pp. 415) stated that shape evolution in the cranium of felines is mainly driven “by allometry, rather than functional or phylogenetic factors”. Even in the case of pantherines, we assessed the presence of CREA following the suggestions of Tamagnini et al. (2017) by analysing the fossil record of the group and relying on phylogenetic corrections adequate for handling extinct species. Our results partially differed from the findings of Tamagnini et al. (2017), who hypothesised the presence of CREA in modern pantherines, except for the genus *Neofelis*. Unexpectedly, our findings did not validate the occurrence of this evolutionary trend neither in the entire subfamily Pantherinae nor in the genus *Panthera*,

therefore excluding a differential impact of evolutionary allometry between large-sized pantherines and clouded leopards. This evidence also helps refuting the idea that clouded leopards constitute morphological outliers within the subfamily Pantherinae. This is in line with recent studies, relying on cranial biomechanics and feeding performance in living felids (Slater and Van Valkenburgh 2009) and cranial similarities between conical and sabertoothed cats in the multivariate shape space (Slater and Van Valkenburgh 2009), that disproved phenotypic convergent evolution of the clouded leopard towards the sabertoothed morphotype.

In keeping with our findings, previous GMM studies performed on 2D datasets led the authors to hypothesise a reduced impact of evolutionary allometry in determining cranial shape variations in many sabertoothed lineages (i.e., Machairodontinae, Barbourofelidae, and Nimravidae – Slater and Van Valkenburgh 2008; Meloro and Slater 2012). Although relying on phylogenetic comparative methods that accounted only for BM mode of evolution and potentially problematic morphological data (see Cardini 2014; Buser et al. 2018 for potential issues resulting from the adoption of cranial lateral views in GMM), the markedly modular framework adopted by Meloro and Slater (2012) clearly demonstrated that the rostral shape of sabertooths is highly influenced by the relative canine length, probably as a result of the need for a wide gape angle and to accommodate the enormous canine roots within the facial skeleton. These authors also pointed out that the shape evolution of the braincase in sabertooths is driven by the interaction between relative canine length and cranial size and follows a similar trajectory to the one observed in conical-toothed cats. Even if our analyses support a slightly different (but still statistically non-significant) allometric pattern in both Machairodontinae and true sabertooths, our results are consistent with Meloro and Slater (2012, Pp. 682) that the adaptation to elongate upper canines “result in a decoupling of the

allometry-driven feline pattern of integration between the rostrum and braincase”. This evidence also disproves the hypothesis that the cranial shape evolution of sabertoothed cats results from a mere case of cooptation and extension of the allometric trend observed in conical-toothed cats (e.g., Slater and Van Valkenburgh 2008), whose cranial morphology is strongly impacted by trade-offs between the need to increase gape and the ability to resist unpredictable loadings deriving from prey handling (Slater and Van Valkenburgh 2009). The absence of evolutionary allometry is also in line with recent biomechanical simulations performed on several functional parameters (i.e., mandibular gape angle, bending strength, and bite force) that highlighted a remarkably high functional variability among different sabertoothed lineages (e.g., smilodontines, metailurines, homotherines, and barbourfelids – Lautenschlager et al. 2020). Despite the occurrence of convergent evolution in the cranial morphology of sabertooths, this pattern disproved the existence of a single consistent trend towards functional optimization for this morphotype, indicating that it was probably produced by slight differences in hunting/killing strategies resulting in several episodes of ecological niche partitioning within sabertoothed lineages (Figueirido et al. 2018; Janis et al. 2020; Lautenschlager et al. 2020; Melchionna et al. 2021).

General considerations about the dynamics behind evolutionary allometry and CREA

Morphological allometry is a ubiquitous phenotypic evolutionary pattern that can be viewed as a form of integration (i.e., the tendency of multiple traits to covary throughout a biological structure as defined by Hallgrímsson et al. 2019), whose tempo and mode of evolution are often preserved by conditions of evolutionary conservatism (Houle et al. 2019). In particular, morphological allometric relationships are often maintained by natural selection acting on the genetic and pleiotropic architecture that underlies this evolutionary pattern (Bolstad et al.

2015; Houle et al. 2019). Craniofacial allometry makes no exception and is suspected to be highly polygenic and heavily impacted by epigenetic influences, with a possible role of environmental and genetic perturbations in disrupting the existing allometric relationships (Hallgrímsson et al. 2019). Therefore, it is hardly surprising that CREA is a pervasive biological rule that was already confirmed in several groups of mammals. Previous studies demonstrated that allometric trajectories are reasonably parallel within this clade (although in the presence of discrete fluctuations in the strength of the trend - Cardini and Polly 2013; Cardini 2019). The main evolutionary stimuli and dynamics involved in the occurrence of CREA still need to be fully understood (Cardini 2019). Potential (and non-mutually exclusive) explanations range from the need to face dietary, biomechanical, and metabolic trade-offs (Cardini and Polly 2013), through the existence of genetic correlations between craniofacial morphology and body mass (Joganic et al. 2018), to the presence of constraints imposed by evo-devo dynamics (which would limit morphological evolution in many directions of the multivariate trait space and would enhance changes along specific lines of least evolutionary resistance - Marroig and Cheverud 2005; Renaud and Auffray 2013). Understanding these dynamics is even more important given the analogy between the CREA pattern and other fascinating evolutionary trends, such as the domestication syndrome (Sánchez-Villagra et al. 2017; Wilson 2018; Lord et al. 2020; Wilson et al. 2021), which closely follow a pattern similar to those typical of intraspecific post-natal ontogenetic changes (Cardini 2019).

Within this extremely complex scenario, our findings unambiguously pointed out that pantherines and sabertoothed cats constitute well-supported exceptions to CREA. The members of both these clades can be considered snouted/massive headed cats (Sicuro 2011), characterised by elongated rostra that accommodate massive dentitions (Holliday and Stepan

2004; Segura et al. 2017). The fundamental role of teeth in shaping CREA was already suggested by previous studies that highlighted how the need to house large hypsodont teeth in specific ungulate lineages or possess relatively long palate and tooth rows in clouded leopards might have the potential to break this evolutionary trend (Tamagnini et al. 2017; Cardini 2019). The decoupling between relative face length and body size was also pointed out in the evolution of hominins and is supposed to be linked with a reduced need for powerful masticatory muscles (paired with an expansion of brain dimensions) deriving from a gradual increase of preprocessed food consumption throughout the history of the clade (Marcucio et al. 2011; Cardini and Polly 2013). These considerations lead us to hypothesise that biomechanics is a key factor in determining the presence and strength of CREA. This is unsurprising considering that recent research on phenotypic evolutionary trends pointed out how this type of evolutionary patterns is heavily influenced by a complex interplay between evolutionary factors such as environment, evo-devo constraints, phylogeny, and biological function (i.e., theory of morphodynamics – Seilacher and Gishlick 2015; Briggs 2017; Tamagnini et al. 2021a). The acquisition of extreme features concerning any of these evolutionary factors (e.g., adapting biomechanically demanding structures such as sabertoothed upper canines; occupying extremely narrow and specialised ecological niches) is likely to represent a preferential way to escape from common evolutionary patterns of morphological variation such as CREA, but this is likely to be frequently achieved at the cost of higher extinction rates as suggested by the absence of CREA in many extinct lineages of nonmammalian synapsids (Krone et al. 2019; see also Piras et al. 2018 for analogues considerations in sabertoothed cats). For these reasons, further research on CREA should be more focused on lineages (and their fossil records) that are peculiar for some of their ecological, biomechanical or evo-devo adaptations in order to clarify the mechanisms

involved in this biological rule. Elucidating the dynamics underpinning CREA seems a possible goal only passing through the detection of exceptions to the rule now more than ever, and recent new methods to quantify morphological variation and test for different and complex evolutionary models certainly paved the way toward some major breakthroughs in this field in the near future.

Literature Cited

- Adams, D. C., and E. Otárola-Castillo. 2013. geomorph: an r package for the collection and analysis of geometric morphometric shape data. *Methods Ecol. Evol.* 4:393–399.
- Adams, D. C., F. J. Rohlf, and D. E. Slice. 2004. Geometric morphometrics: ten years of progress following the ‘revolution.’ *Ital. J. Zool.* 71:5–16.
- Adams, J. W., A. Olah, M. R. McCurry, and S. Potze. 2015. Surface model and tomographic archive of fossil primate and other mammal holotype and paratype specimens of the Ditsong National Museum of Natural History, Pretoria, South Africa. *PLOS ONE* 10:e0139800.
- Agnarsson, I., M. Kuntner, and L. J. May-Collado. 2010. Dogs, cats, and kin: a molecular species-level phylogeny of Carnivora. *Mol. Phylogenet. Evol.* 54:726–745.
- Allen, J. A. 1877. The influence of physical conditions in the genesis of species.
- Alroy, J. 2000. Understanding the dynamics of trends within evolving lineages. *Paleobiology* 26:319–329.
- Angielczyk, K. D., and M. Ruta. 2012. The roots of amphibian morphospace: a geometric morphometric analysis of Paleozoic temnospondyls. *Fieldiana Life Earth Sci.* 2012:40–58.
- Anton, M. 2013. Sabertooth. Indiana Univ. Press, Bloomington.

463 Anyonge, W. 1996. Microwear on canines and killing behavior in large carnivores: saber
 464 function in *Smilodon fatalis*. J. Mammal. 77:1059–1067.

465 Bergmann, C. 1847. Über die verhältnisse der wärmeökonomie der thiere zu ihrer größe.

466 Bolstad, G. H., J. A. Cassara, E. Márquez, T. F. Hansen, K. van der Linde, D. Houle, and C.
 467 Pélabon. 2015. Complex constraints on allometry revealed by artificial selection on
 468 the wing of *Drosophila melanogaster*. Proc. Natl. Acad. Sci. USA 112:13284–13289.

469 Bonferroni, C. E. 1936. Teoria statistica delle classi e calcolo delle probabilità.

470 Briggs, D. E. G. 2017. Seilacher, konstruktions-morphologie, morphodynamics, and the
 471 evolution of form. J. Exp. Zool. B Mol. Dev. Evol. 328:197–206.

472 Bright, J. A., J. Marugán-Lobón, S. N. Cobb, and E. J. Rayfield. 2016. The shapes of bird
 473 beaks are highly controlled by nondietary factors. Proc. Natl. Acad. Sci. USA
 474 113:5352–5357.

475 Buser, T. J., B. L. Sidlauskas, and A. P. Summers. 2018. 2D or not 2D? Testing the utility of
 476 2D vs. 3D landmark data in geometric morphometrics of the sculpin subfamily
 477 Oligocottinae (Pisces; Cottoidea). Anat. Rec. 301:806–818.

478 Cardini, A. 2019. Craniofacial allometry is a rule in evolutionary radiations of placentals.
 479 Evol. Biol. 46:239–248.

480 Cardini, A. 2014. Missing the third dimension in geometric morphometrics: how to assess if
 481 2D images really are a good proxy for 3D structures? Hystrix It. J. Mamm. 25:73–81.
 482 Associazione Teriologica Italiana.

483 Cardini, A., D. Polly, R. Dawson, and N. Milne. 2015. Why the long face? Kangaroos and
 484 wallabies follow the same ‘rule’ of cranial evolutionary allometry (CREA) as
 485 placentals. Evol. Biol. 42:169–176.

486 Cardini, A., and P. D. Polly. 2013. Larger mammals have longer faces because of size-related

487 constraints on skull form. Nat. Commun. 4:1–7.

488 Castiglione, S., C. Serio, D. Tamagnini, M. Melchionna, A. Mondanaro, M. D. Febbraro, A.
489 Profico, P. Piras, F. Barattolo, and P. Raia. 2019. A new, fast method to search for
490 morphological convergence with shape data. PLOS ONE 14:e0226949.

491 Castiglione, S., G. Tesone, M. Piccolo, M. Melchionna, A. Mondanaro, C. Serio, M. D.
492 Febbraro, and P. Raia. 2018. A new method for testing evolutionary rate variation and
493 shifts in phenotypic evolution. Methods Ecol. Evol. 9:974–983.

494 Christiansen, P. 2008. Evolutionary convergence of primitive sabertooth craniomandibular
495 morphology: the clouded leopard (*Neofelis nebulosa*) and *Paramachairodus ogygia*
496 compared. J. Mammal. Evol. 15:155–179.

497 Christiansen, P. 2006. Sabertooth characters in the clouded leopard (*Neofelis nebulosa*
498 Griffiths 1821). J. Morphol. 267:1186–1198.

499 Clavel, J., L. Aristide, and H. Morlon. 2019. A penalized likelihood framework for high-
500 dimensional phylogenetic comparative methods and an application to New-World
501 monkeys brain evolution. Syst. Biol. 68:93–116.

502 Diniz- Filho, J. A. F., M. Á. Rodríguez, L. M. Bini, M. Á. Olalla- Tarraga, M. Cardillo, J. C.
503 Nabout, J. Hortal, and B. A. Hawkins. 2009. Climate history, human impacts and
504 global body size of Carnivora (Mammalia: Eutheria) at multiple evolutionary scales. J.
505 Biogeogr. 36:2222–2236.

506 Drake, A. G., and C. P. Klingenberg. 2010. Large-scale diversification of skull shape in
507 domestic dogs: disparity and modularity. Am. Nat. 175:289–301.

508 Emerson, S. B., and L. Radinsky. 1980. Functional analysis of sabertooth cranial morphology.
509 Paleobiology 6:295–312.

510 Ewer, R. F. 1973. The carnivores. Cornell Univ. Press, Ithaca, N.Y.

511 Falkingham, P. L. 2012. Acquisition of high resolution three-dimensional models using free,
512 open-source, photogrammetric software. *Palaeontol. Electron.* 15:1–15.

513 Faurby, S., L. Werdelin, and A. Antonelli. 2019. Dispersal ability predicts evolutionary
514 success among mammalian carnivores. *bioRxiv* 755207.

515 Ferreira-Cardoso, S., G. Billet, P. Gaubert, F. Delsuc, and L. Hautier. 2020. Skull shape
516 variation in extant pangolins (Pholidota: Manidae): allometric patterns and systematic
517 implications. *Zool. J. Linn. Soc.* 188:255–275.

518 Figueirido, B., S. Lautenschlager, A. Pérez-Ramos, and B. Van Valkenburgh. 2018. Distinct
519 predatory behaviors in scimitar- and dirk-toothed sabertooth cats. *Curr. Biol.* 28:3260-
520 3266.e3.

521 Figueirido, B., N. MacLeod, J. Krieger, M. D. Renzi, J. A. Pérez-Claros, and P. Palmqvist.
522 2011. Constraint and adaptation in the evolution of carnivoran skull shape.
523 *Paleobiology* 37:490–518.

524 Figueirido, B., and L. H. Soibelzon. 2010. Inferring palaeoecology in extinct tremarctine
525 bears (Carnivora, Ursidae) using geometric morphometrics. *Lethaia* 43:209–222.

526 Figueirido, B., Z. J. Tseng, and A. Martín- Serra. 2013. Skull shape evolution in durophagous
527 carnivorans. *Evolution* 67:1975–1993.

528 Garland, T., P. H. Harvey, and A. R. Ives. 1992. Procedures for the analysis of comparative
529 data using phylogenetically independent contrasts. *Syst. Biol.* 41:18–32.

530 Geraads, D., and N. Spassov. 2020. A skull of *Machairodus* Kaup, 1833 (Felidae, Mammalia)
531 from the late Miocene of Hadjidimovo (Bulgaria), and its place in the evolution of the
532 genus. *Geodiversitas* 42:123–137.

533 Giacomini, G., D. Scaravelli, A. Herrel, A. Veneziano, D. Russo, R. P. Brown, and C.
534 Meloro. 2019. 3D Photogrammetry of bat skulls: perspectives for macro-evolutionary

analyses. *Evol. Biol.* 46:249–259.

Gittleman, J. L. 1986. Carnivore life history patterns: allometric, phylogenetic, and ecological associations. *Am. Nat.* 127:744–771.

Gould, S. J. 1980. Is a new and general theory of evolution emerging? *Paleobiology* 6:119–130.

Gunz, P., P. Mitteroecker, S. Neubauer, G. W. Weber, and F. L. Bookstein. 2009. Principles for the virtual reconstruction of hominin crania. *Journal of Human Evolution* 57:48–62.

Hallgrímsson, B., D. C. Katz, J. D. Aponte, J. R. Larson, J. Devine, P. N. Gonzalez, N. M. Young, C. C. Roseman, and R. S. Marcucio. 2019. Integration and the developmental genetics of allometry. *Integr. Comp. Biol.* 59:1369–1381.

Hautmann, M. 2020. What is macroevolution? *Palaeontology* 63:1–11.

Holliday, J. A., and S. J. Steppan. 2004. Evolution of hypercarnivory: the effect of specialization on morphological and taxonomic diversity. *Paleobiology* 30:108–128.

Houle, D., L. T. Jones, R. Fortune, and J. L. Sztepanacz. 2019. Why does allometry evolve so slowly? *Integr. Comp. Biol.* 59:1429–1440.

Janis, C. M., B. Figueirido, L. DeSantis, and S. Lautenschlager. 2020. An eye for a tooth: *Thylacosmilus* was not a marsupial “saber-tooth predator.” *PeerJ* 8:e9346.

Joganic, J. L., K. E. Willmore, J. T. Richtsmeier, K. M. Weiss, M. C. Mahaney, J. Rogers, and J. M. Cheverud. 2018. Additive genetic variation in the craniofacial skeleton of baboons (genus *Papio*) and its relationship to body and cranial size. *Am. J. Phys. Anthropol.* 165:269–285.

Johnson, W. E., E. Eizirik, J. Pecon-Slattery, W. J. Murphy, A. Antunes, E. Teeling, and S. J. O’Brien. 2006. The late Miocene radiation of modern Felidae: a genetic assessment.

559 Science 311:73–77.

560 Klingenberg, C. P. 2011. MorphoJ: an integrated software package for geometric
561 morphometrics. *Mol. Ecol. Resour.* 11:353–357.

562 Klingenberg, C. P. 2016. Size, shape, and form: concepts of allometry in geometric
563 morphometrics. *Dev. Genes Evol.* 226:113–137.

564 Klingenberg, C. P., M. Barluenga, and A. Meyer. 2002. Shape analysis of symmetric
565 structures: quantifying variation among individuals and asymmetry. *Evolution*
566 56:1909–1920.

567 Klingenberg, C. P., and M. Zimmermann. 1992. Static, ontogenetic, and evolutionary
568 allometry: a multivariate comparison in nine species of water striders. *Am. Nat.*
569 140:601–620.

570 Krone, I. W., C. F. Kammerer, and K. D. Angielczyk. 2019. The many faces of synapsid
571 cranial allometry. *Paleobiology* 45:531–545.

572 Lautenschlager, S., B. Figueirido, D. D. Cashmore, E.-M. Bendel, and T. L. Stubbs. 2020.
573 Morphological convergence obscures functional diversity in sabre-toothed carnivores.
574 *Proc. R. Soc. B* 287:20201818.

575 Law, C. J., E. Duran, N. Hung, E. Richards, I. Santillan, and R. S. Mehta. 2018. Effects of
576 diet on cranial morphology and biting ability in musteloid mammals. *J. Evol. Biol.*
577 31:1918–1931.

578 Lord, K. A., G. Larson, R. P. Coppinger, and E. K. Karlsson. 2020. The history of farm foxes
579 undermines the animal domestication syndrome. *Trends Ecol. Evol.* 35:125–136.

580 Mallison, H., and O. Wings. 2014. Photogrammetry in paleontology – A practical guide. *J.*
581 *Paleontol. Tech.* 12:1–31.

582 Manzuetti, A., D. Perea, W. Jones, M. Ubilla, and A. Rinderknecht. 2020. An extremely large

583 saber-tooth cat skull from Uruguay (late Pleistocene–early Holocene, Dolores
584 Formation): body size and paleobiological implications. *Alcheringa* 44:332–339.

585 Marcucio, R. S., N. M. Young, D. Hu, and B. Hallgrímsson. 2011. Mechanisms that underlie
586 co-variation of the brain and face. *Genesis* 49:177–189.

587 Marcy, A. E., T. Guillaume, E. Sherratt, K. C. Rowe, M. J. Phillips, and V. Weisbecker. 2020.
588 Australian rodents reveal conserved cranial evolutionary allometry across 10 million
589 years of murid evolution. *Am. Nat.* 196:755–768

590 Marroig, G., and J. M. Cheverud. 2005. Size as a line of least evolutionary resistance: diet and
591 adaptive morphological radiation in New World monkeys. *Evolution* 59:1128–1142.

592 McNamara, K. J. 2006. Evolutionary trends. P. in *eLS*. American Cancer Society.

593 Meachen-Samuels, J. A. 2012. Morphological convergence of the prey-killing arsenal of
594 sabertooth predators. *Paleobiology* 38:1–14.

595 Meachen-Samuels, J., and B. V. Valkenburgh. 2009a. Craniodental indicators of prey size
596 preference in the Felidae. *Biol. J. Linn. Soc.* 96:784–799.

597 Meachen-Samuels, J., and B. V. Valkenburgh. 2009b. Forelimb indicators of prey-size
598 preference in the Felidae. *J. Morphol.* 270:729–744.

599 Meiri, S., N. Cooper, and A. Purvis. 2008. The island rule: made to be broken? *Proc. R. Soc.*
600 B 275:141–148.

601 Meiri, S., T. Dayan, and D. Simberloff. 2004. Carnivores, biases and Bergmann’s rule. *Biol.*
602 J. Linn. Soc. 81:579–588.

603 Melchionna, M., A. Profico, S. Castiglione, C. Serio, A. Mondanaro, M. Modafferi, D.
604 Tamagnini, L. Maiorano, P. Raia, L. M. Witmer, S. Wroe, and G. Sansalone. 2021. A
605 method for mapping morphological convergence on three-dimensional digital models:
606 the case of the mammalian sabre-tooth. *Palaeontology* 64:573–584.

607 Meloro, C., M. Clauss, and P. Raia. 2015. Ecomorphology of Carnivora challenges
608 convergent evolution. *Org. Divers. Evol.* 15:711–720.

609 Meloro, C., and P. O’Higgins. 2011. Ecological adaptations of mandibular form in fissiped
610 Carnivora. *J. Mammal. Evol.* 18:185–200.

611 Meloro, C., and G. J. Slater. 2012. Covariation in the skull modules of cats: the challenge of
612 growing saber-like canines. *J. Vertebr. Paleontol.* 32:677–685.

613 Meloro, C., and D. Tamagnini. 2021. Macroevolutionary ecomorphology of the Carnivora
614 skull: adaptations and constraints in the extant species. *Zool. J. Linn. Soc.*

615 Michaud, M., G. Veron, and A.-C. Fabre. 2020. Phenotypic integration in feliform carnivores:
616 covariation patterns and disparity in hypercarnivores versus generalists. *Evolution*
617 74:2681–2702.

618 Michaud, M., G. Veron, S. Peigné, A. Blin, and A.-C. Fabre. 2018. Are phenotypic disparity
619 and rate of morphological evolution correlated with ecological diversity in Carnivora?
620 *Biol. J. Linn. Soc.* 124:294–307.

621 Piras, P., L. Maiorino, L. Teresi, C. Meloro, F. Lucci, T. Kotsakis, and P. Raia. 2013. Bite of
622 the cats: relationships between functional integration and mechanical performance as
623 revealed by mandible geometry. *Syst. Biol.* 62:878–900.

624 Piras, P., D. Silvestro, F. Carotenuto, S. Castiglione, A. Kotsakis, L. Maiorino, M.
625 Melchionna, A. Mondanaro, G. Sansalone, C. Serio, V. A. Vero, and P. Raia. 2018.
626 Evolution of the sabertooth mandible: a deadly ecomorphological specialization.
627 *Palaeogeogr. Palaeoclimatol. Palaeoecol.* 496:166–174.

628 Radinsky, L. B. 1985. Approaches in evolutionary morphology: a search for patterns. *Annu.*
629 *Rev. Ecol. Syst.* 16:1–14.

630 Raerinne, J. 2011. Allometries and scaling laws interpreted as laws: a reply to Elgin. *Biol.*

Philos. 26:99–111.

Raia, P., F. Passaro, F. Carotenuto, L. Maiorino, P. Piras, L. Teresi, S. Meiri, Y. Itescu, M. Novosolov, M. A. Baiano, R. Martínez, and M. Fortelius. 2015. Cope’s Rule and the universal scaling law of ornament complexity. *Am. Nat.* 186:165–175.

Renaud, S., and J.-C. Auffray. 2013. The direction of main phenotypic variance as a channel to evolution: cases in murine rodents. *Hystrix It. J. Mamm.* 24:85–93.

Rohlf, F. J., and D. Slice. 1990. Extensions of the Procrustes method for the optimal superimposition of landmarks. *Syst. Zool.* 39:40–59.

Rensch, B. 1948. Histological changes correlated with evolutionary changes in body size. *Evolution* 2:218–230.

Sánchez-Villagra, M. R., V. Segura, M. Geiger, L. Heck, K. Veitschegger, and D. Flores. 2017. On the lack of a universal pattern associated with mammalian domestication: differences in skull growth trajectories across phylogeny. *R. Soc. Open Sci.* 4:170876.

Schlager, S. 2017. Morpho and Rvcg – Shape analysis in R: R-packages for geometric morphometrics, shape analysis and surface manipulations. Pp. 217–256 in G. Zheng, S. Li, and G. Székely, eds. *Statistical shape and deformation analysis*. Academic Press.

Schlager, S., A. Profico, F. D. Vincenzo, and G. Manzi. 2018. Retrodeformation of fossil specimens based on 3D bilateral semi-landmarks: Implementation in the R package “Morpho.” *PLOS ONE* 13:e0194073.

Segura, V., G. H. Cassini, and F. J. Prevosti. 2017. Three-dimensional cranial ontogeny in pantherines (*Panthera leo*, *P. onca*, *P. pardus*, *P. tigris*; Carnivora:, Felidae). *Biol. J. Linn. Soc.* 120:210–227.

Seilacher, A., and A. D. Gishlick. 2015. *Morphodynamics*. CRC Press.

655 Sicuro, F. L. 2011. Evolutionary trends on extant cat skull morphology (Carnivora: Felidae): a
 656 three-dimensional geometrical approach. *Biol. J. Linn. Soc.* 103:176–190.

657 Sicuro, F. L., and L. F. B. Oliveira. 2011. Skull morphology and functionality of extant
 658 Felidae (Mammalia: Carnivora): a phylogenetic and evolutionary perspective. *Zool. J.*
 659 *Linn. Soc.* 161:414–462.

660 Simpson, G. G. 1941. The function of saber-like canines in carnivorous mammals. *Am. Mus.*
 661 *Novit.* 1130:1-12. Saber-like canines.

662 Slater, G. J., and A. R. Friscia. 2019. Hierarchy in adaptive radiation: a case study using the
 663 Carnivora (Mammalia). *Evolution* 73:524–539.

664 Slater, G. J., and B. Van Valkenburgh. 2009. Allometry and performance: the evolution of
 665 skull form and function in felids. *J. Evol. Biol.* 22:2278–2287.

666 Slater, G. J., and B. Van Valkenburgh. 2008. Long in the tooth: evolution of sabertooth cat
 667 cranial shape. *Paleobiology* 34:403–419.

668 Spassov, N., and D. Geraads. 2015. A New Felid from the Late Miocene of the Balkans and
 669 the Contents of the Genus *Metailurus* Zdansky, 1924 (Carnivora, Felidae). *J.*
 670 *Mammal. Evol.* 22:45–56.

671 Tamagnini, D., D. Canestrelli, C. Meloro, P. Raia, and L. Maiorano. 2021a. New avenues for
 672 old travellers: phenotypic evolutionary trends meet morphodynamics, and both enter
 673 the global change biology era. *Evol. Biol.* 48:379-393.

674 Tamagnini, D., C. Meloro, and A. Cardini. 2017. Anyone with a long-face? Craniofacial
 675 evolutionary allometry (CREA) in a family of short-faced mammals, the Felidae.
 676 *Evol. Biol.* 44:476–495.

677 Tamagnini, D., C. Meloro, P. Raia, and L. Maiorano. 2021b. Testing the occurrence of
 678 convergence in the craniomandibular shape evolution of living carnivorans*.

679 Evolution 75:1738–1752.

680 Therrien, F. 2005a. Feeding behaviour and bite force of sabretoothed predators. Zool. J. Linn.
681 Soc. 145:393–426.

682 Therrien, F. 2005b. Mandibular force profiles of extant carnivorans and implications for the
683 feeding behaviour of extinct predators. J. Zool. 267:249–270.

684 Tseng, Z. J., C. Grohé, and J. J. Flynn. 2016. A unique feeding strategy of the extinct marine
685 mammal *Kolponomos*: convergence on sabretooths and sea otters. Proc. R. Soc. B
686 283:20160044.

687 Turner, A., and M. Antón. 1997. The big cats and their fossil relatives. Columbia Univ. Press,
688 New York.

689 Valkenburgh, B. V., M. W. Hayward, W. J. Ripple, C. Meloro, and V. L. Roth. 2016. The
690 impact of large terrestrial carnivores on Pleistocene ecosystems. Proc. Natl. Acad. Sci.
691 USA 113:862–867.

692 Van Valkenburgh, B. 1989. Carnivore dental adaptations and diet: a study of trophic diversity
693 within guilds. Pp. 410–436 in J. L. Gittleman, ed. Carnivore behavior, ecology, and
694 evolution. Springer US, Boston, MA.

695 Van Valkenburgh, B. 2007. Déjà vu: the evolution of feeding morphologies in the Carnivora.
696 Integr. Comp. Biol. 47:147–163.

697 Viscosi, V., and A. Cardini. 2011. Leaf morphology, taxonomy and geometric
698 morphometrics: A simplified protocol for beginners. PLOS ONE 6:e25630.

699 Voje, K. L., T. F. Hansen, C. K. Egset, G. H. Bolstad, and C. Pélabon. 2014. Allometric
700 constraints and the evolution of allometry. Evolution 68:866–885.

701 Wiley, D. F., N. Amenta, D. A. Alcantara, D. Ghosh, Y. J. Kil, E. Delson, W. Harcourt-
702 Smith, F. J. Rohlf, K. St. John, and B. Hamann. 2005. Evolutionary morphing.

Wilson, L. A. B. 2018. The evolution of ontogenetic allometric trajectories in mammalian domestication. *Evolution* 72:867–877.

Wilson, L. A. B., A. Balcarcel, M. Geiger, L. Heck, and M. R. Sánchez-Villagra. 2021. Modularity patterns in mammalian domestication: assessing developmental hypotheses for diversification. *Evol. Lett.* 5:385–396.

Data archiving

Morphological datasets, phylogeny and R script supporting the results of the present paper are archived in Dryad and/or provided as Supporting Information.

Figure and Table captions

Main text

Table 1: Results of the allometric regressions performed on 30L and 10L configurations using OLS and Brownian Motion (BM) or phylogenetic ridge regression (RR) PGLS. Significant P-values at $\alpha = 0.05$ are underlined and in bold when still significant after a Bonferroni correction.

Figure 1: Circular dendrogram representing the phylogeny from Piras et al. (2018) showing the distribution of each taxon in our allometric analyses on living and extinct felids. The subfamily Felinae is represented in yellow, the subfamily Pantherinae includes the genus *Panthera* (in red) and the genus *Neofelis* (in pink) and the subfamily Machairodontinae includes true sabertooths (i.e., tribes Homotherini, Machairodontini, and Smilodontini - in light blue) and false sabertooths (i.e., tribe Metailurini - in blue).

Figure 2: Scatterplots of shape regression scores versus natural logarithm of centroid size obtained using the 30L configuration, Piras et al. (2018) phylogeny, and BM PGLS

concerning Felidae (A), Felinae (B), Pantherinae (C), Machairodontinae (D), genus *Panthera* (E), and true sabertooths (F). Patterns of allometric shape variation are shown by means of 3D surfaces warped using thin-plate spline.

Supplementary Information

Table S1: List of sampled specimens with ID code, species name, subfamily, sex, and museum location.

Table S2: Definitions of the anatomical landmarks used in the 30L configuration. The 10L configuration includes only the rows with grey background.

Table S3: Allometric regressions comparing pooled-sex, male and female datasets performed on the 30L configuration using OLS and Brownian Motion (BM) or phylogenetic ridge regression (RR) PGLS. Significant P-values at $\alpha = 0.05$ are underlined and in bold when still significant after a Bonferroni correction.

Table S4: Allometric regressions comparing pooled-sex, male and female datasets performed on the 10L configuration using OLS and Brownian Motion (BM) or phylogenetic ridge regression (RR) PGLS. Significant P-values at $\alpha = 0.05$ are underlined and in bold when still significant after a Bonferroni correction.

Table S5: List of missing landmarks. Landmarks requiring a symmetrization to be estimated are in red, whereas landmarks requiring a thin-plate spline-based interpolation to be estimated are in black.

Figure S1: Landmarks used to quantify allometric shape variation in the cranium of felids. (A) dorsal view; (B) anterior view; (C) caudal view; (D) lateral view; (E) ventral view. Landmarks are represented by yellow dots.

750 **Figure S2:** Scatterplots of shape regression scores versus natural logarithm of centroid size
751 obtained using the 10L configuration, Piras et al. (2018) phylogeny, and BM PGLS
752 concerning Felidae (A), Felinae (B), Pantherinae (C), Machairodontinae (D), genus *Panthera*
753 (E), and true sabertooths (F). Patterns of allometric shape variation are shown by means of 3D
754 surfaces warped using thin-plate spline.

1 ***SI Appendix***

2 **Repeatability and precision of landmarks**

3 The repeatability and precision of landmark configurations (i.e., digitizing error) were
4 evaluated considering each specimen included in the total sample. To do so, landmarks were
5 digitized twice by the same operator (DT) with a ten-day interval in order to assess the
6 digitising error (Viscosi and Cardini 2011). For both landmark configurations (i.e., 30L and
7 10L) adopted in this study, a cluster analysis relying on the unweighted pair group method
8 with arithmetic mean (UPGMA) was performed on the Procrustes coordinates resulting from
9 first and second replicas. In both the configurations, the two replicas of the same individual
10 clustered together for almost every specimen (i.e., 97 out of 98 correct pairs in the 30L
11 configuration and 94 out of 98 correct pairs in the 10L configuration representing 99% and
12 96% of total cases, respectively), showing that the shape components resulting from both
13 these landmark configurations were highly repeatable. For size, a correlation between the
14 centroid sizes of the replicas was computed for each configuration and both these tests
15 returned a correlation coefficient (r) higher than 0.999 (P -value = 0.0001 in both cases),
16 indicating that also the size component was highly repeatable.

18 **Sexual dimorphism**

19 The impact of sexual dimorphism in shape was assessed performing UPGMA cluster analyses
20 on a subsample including the 21 living species of felids (55% of the existing species
21 diversity) for which at least one male and one female per species were included in the total
22 sample. In particular, a UPGMA cluster analysis was performed, for both landmark
23 configurations, on the Procrustes coordinates (averaged within species) corresponding to the
24 female-only, the male-only and the pooled-sex means. In both configurations, the three means

of the same species clustered together in a large number of cases (i.e., 17 out of 21 correct triads in the 30L configuration and 15 out of 21 correct triads in the 10L configuration representing 81% and 71% of total cases, respectively), indicating a reduced impact of sexual dimorphism on shape.

For size, all the possible correlations between the centroid sizes of the three means were computed for each configuration. All the performed tests returned a correlation coefficient (r) higher than 0.966 (P -value = 0.0001 in all the cases), indicating that also the impact of sexual dimorphism on size was negligible.

To further investigate the impact of sexual dimorphism on CREA, we performed a battery of regressions similar to the one used in the main analyses (i.e., OLS, BM PGLS, and RR PGLS regressions relying on two different phylogenies - see subsection 'Allometric regressions' in the Methods section), comparing the results obtained using the female-only, male-only and pooled-sex subsamples that were already used for UPGMA cluster analyses on shape and centroid size correlations. All the regressions were significant, regardless of the chosen landmark configuration (i.e., 30L – Table S3; 10L – Table S4), even after applying a Bonferroni correction (i.e., all P -values < 0.003). The amount of shape variance explained by evolutionary allometry varied little throughout the entire battery of regressions. In particular, the R^2 obtained from OLS regressions ranged from 0.383 to 0.488, regardless of the adopted subsample and landmark configuration. The R^2 obtained from BM PGLS regressions ranged from 0.230 to 0.332, regardless of the considered subsample, landmark configuration and phylogenetic tree. Finally, the R^2 obtained from RR PGLS regressions ranged from 0.162 to 0.372, regardless of the adopted subsample, landmark configuration and phylogeny. Overall, these results indicated a negligible impact of sexual dimorphism on CREA in felids.

Dataset	Sample	Phylogeny	Phylogenetic Comparative Method (PCM)	R ²	F	Z	P-value
Pooled-sex	Felidae	No phylo	No PCM (OLS)	0.488	18.121	4.461	<u>0.001</u>
		Piras et al. 2018	BM PGLS	0.321	9.002	3.854	<u>0.001</u>
			RR PGLS	0.259	6.641	3.978	<u>0.001</u>
		Faurby et al. 2019	BM PGLS	0.311	8.595	3.971	<u>0.001</u>
			RR PGLS	0.353	10.383	4.334	<u>0.001</u>
		Female	Felidae	No phylo	No PCM (OLS)	0.398	12.575
Piras et al. 2018	BM PGLS			0.230	5.680	3.697	<u>0.001</u>
	RR PGLS			0.185	4.326	3.788	<u>0.001</u>
Faurby et al. 2019	BM PGLS			0.230	5.675	3.846	<u>0.001</u>
	RR PGLS			0.261	6.711	4.300	<u>0.001</u>
Male	Felidae			No phylo	No PCM (OLS)	0.418	13.641
		Piras et al. 2018	BM PGLS	0.275	7.203	3.934	<u>0.001</u>
			RR PGLS	0.202	4.820	3.680	<u>0.001</u>
		Faurby et al. 2019	BM PGLS	0.261	6.704	4.134	<u>0.001</u>
			RR PGLS	0.271	7.060	4.197	<u>0.001</u>

Table S3: Allometric regressions comparing pooled-sex, male and female datasets performed on the 30L configuration using OLS and Brownian Motion (BM) or phylogenetic ridge regression (RR) PGLS. Significant P-values at $\alpha = 0.05$ are underlined and in bold when still significant after a Bonferroni correction.

Dataset	Sample	Phylogeny	Phylogenetic Comparative Method (PCM)	R ²	F	Z	P-value
Pooled-sex	Felidae	No phylo	No PCM (OLS)	0.480	17.563	4.296	<u>0.001</u>
		Piras et al. 2018	BM PGLS	0.332	9.455	3.823	<u>0.001</u>
			RR PGLS	0.275	7.213	3.756	<u>0.001</u>
		Faurby et al. 2019	BM PGLS	0.331	9.398	4.023	<u>0.001</u>
			RR PGLS	0.372	11.238	4.304	<u>0.001</u>
		Female	Felidae	No phylo	No PCM (OLS)	0.383	11.789
Piras et al. 2018	BM PGLS			0.239	5.954	3.540	<u>0.001</u>
	RR PGLS			0.195	4.614	3.457	<u>0.001</u>
Faurby et al. 2019	BM PGLS			0.240	6.015	3.630	<u>0.001</u>
	RR PGLS			0.270	7.041	4.059	<u>0.001</u>
Male	Felidae			No phylo	No PCM (OLS)	0.399	12.597
		Piras et al. 2018	BM PGLS	0.243	6.100	3.446	<u>0.001</u>
			RR PGLS	0.162	3.686	2.757	<u>0.002</u>
		Faurby et al. 2019	BM PGLS	0.239	5.978	3.655	<u>0.001</u>
			RR PGLS	0.256	6.554	3.778	<u>0.001</u>

Table S4: Allometric regressions comparing pooled-sex, male and female datasets performed on the 10L configuration using OLS and Brownian Motion (BM) or phylogenetic ridge regression (RR) PGLS. Significant P-values at $\alpha = 0.05$ are underlined and in bold when still significant after a Bonferroni correction.

Missing landmarks and retrodeformation

An extremely reduced number of missing landmarks occurred, due to the presence of partially damaged specimens, both in 30L (70 missing landmarks out of 2940 expected landmarks – 2.4% of the total) and in 10L (28 out of 980 – 2.9% of the total) configurations. The estimation of missing landmarks was performed in two mutually exclusive methods as detailed in Table S5. For bilateral landmarks (Tab. S5, in red), we performed a symmetrization relying on their bilateral counterparts whenever available (Gunz et al. 2009). Symmetrizations were performed using the function *fixLMmirror* embedded in the package *Morpho* (Schlager 2017). For landmarks placed on the midline and bilateral landmarks for which a bilateral counterpart was not available (Tab. S5, in black), we used the thin-plate spline to interpolate missing landmarks on a reference specimen, that was obtained from a set of specimens for which all landmarks were present (Gunz et al. 2009). This set of specimens was selected in a hierarchical way case by case, meaning that the interpolation was performed at the lowest taxonomic level in which enough specimens were available to complete the procedure (Tab. S5). Thin-plate spline-based estimations were performed using the function *estimate.missing* embedded in the package *Morpho*. Whenever both the methods of missing landmark estimation were required in the same specimen, we first performed the symmetrisation step and then the thin-plate spline-based interpolation.

The fossil specimens included in the present study were generally well preserved, particularly in terms of deformation caused by taphonomic processes. However, in the very few individuals (i.e., two specimens belonging to *Machairodus aphanistus* and *Panthera gombaszoegensis*, respectively) in which minor damages occurred, we virtually restored them using the retrodeformation procedure described in Schlager et al. (2018). In particular, these specimens were retrodeformed using up to ten pairs of symmetrical landmarks and up to five

73 bilateral sets of semi-landmarks homogeneously distributed along curves. This procedure was
74 performed using the package *Morpho*.

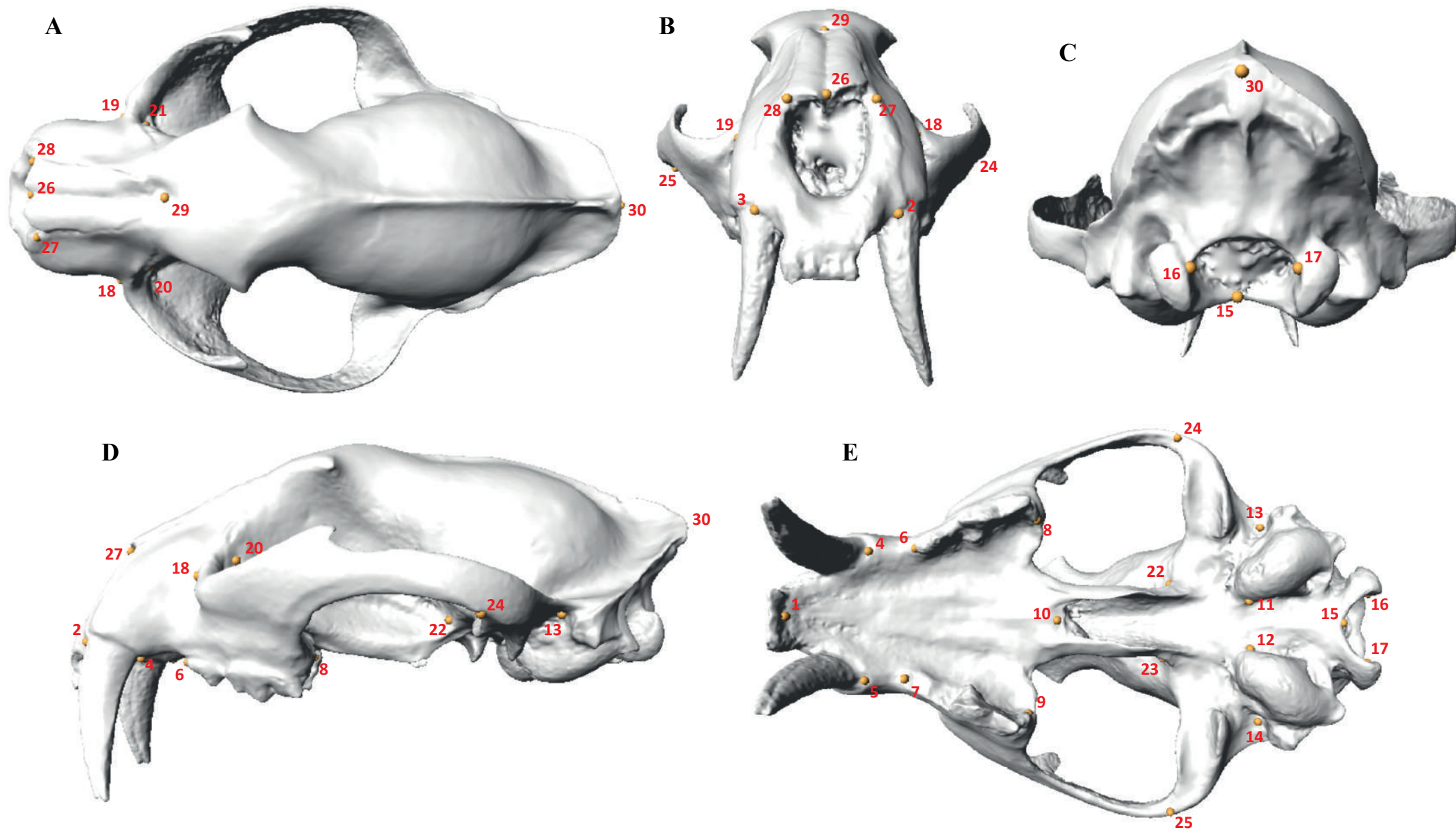


Figure S1: Landmarks used to quantify allometric shape variation in the cranium of felids. (A) dorsal view; (B) anterior view; (C) caudal view; (D) lateral view; (E) ventral view. Landmarks are represented by yellow dots.

10L configuration

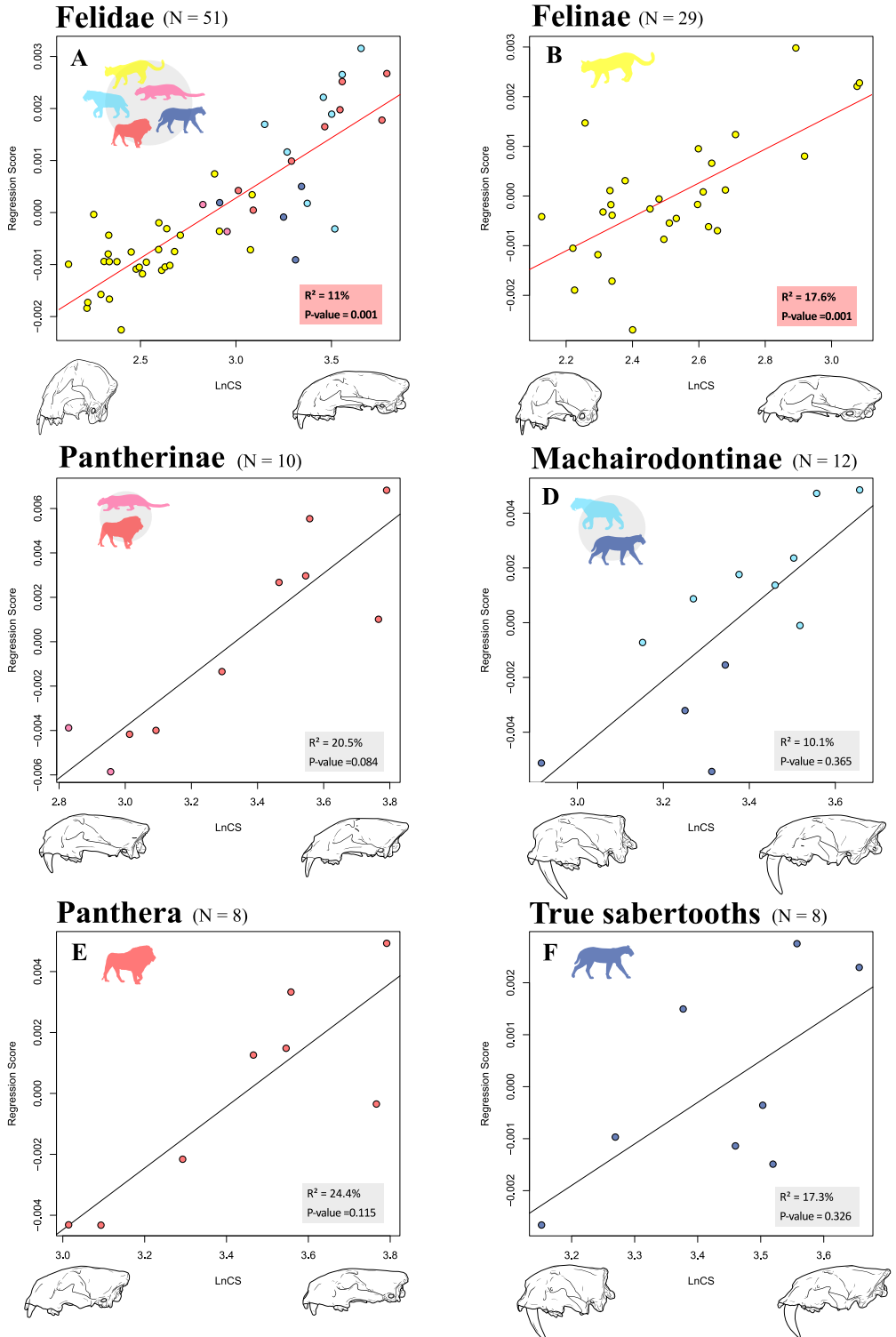


Figure S2: Scatterplots of shape regression scores versus natural logarithm of centroid size obtained using the 10L configuration, Piras et al. (2018) phylogeny, and BM PGLS concerning Felidae (A), Felinae (B), Pantherinae (C), Machairodontinae (D), genus Panthera (E), and true sabertooths (F). Patterns of allometric shape variation are shown by means of 3D surfaces warped using thin-plate spline.

ID	Species name	Subfamily	Sex
Acinonyx_jubatus_F_MZUF-1831	<i>Acinonyx jubatus</i>	Felinae	Female
Acinonyx_jubatus_M_MZUF-2135	<i>Acinonyx jubatus</i>	Felinae	Male
Acinonyx_pardinensis_U_NMBS.St.V.975	<i>Acinonyx pardinensis</i>	Felinae	Unknown
Caracal_aurata_F_MNHN.CG1939.687	<i>Caracal aurata</i>	Felinae	Female
Caracal_aurata_M_MNHN.CG1940-1213	<i>Caracal aurata</i>	Felinae	Male
Caracal_caracal_F_MNHN.CG2015-2093	<i>Caracal caracal</i>	Felinae	Female
Caracal_caracal_M_MZUF-1752	<i>Caracal caracal</i>	Felinae	Male
Catopuma_temminckii_F_MNHN.CG1939.2152	<i>Catopuma temminckii</i>	Felinae	Female
Catopuma_temminckii_M_MNHN.CG1962-2927	<i>Catopuma temminckii</i>	Felinae	Male
Dinofelis_barlowi_U_DNMMNH.BF55-22	<i>Dinofelis barlowi</i>	Machairodontinae	Unknown
Dinofelis_piveteaui_U_DNMMNH.KA61	<i>Dinofelis piveteaui</i>	Machairodontinae	Unknown
Felis_bieti_U_MNHN.CG1893-151	<i>Felis bieti</i>	Felinae	Unknown
Felis_chaus_F_MNHN.CG2015-1302	<i>Felis chaus</i>	Felinae	Female
Felis_chaus_U_MZUF-12308	<i>Felis chaus</i>	Felinae	Unknown
Felis_concolor_U_PRIZ891	<i>Puma concolor</i>	Felinae	Unknown
Felis_margarita_U_IMNH.R-938	<i>Felis margarita</i>	Felinae	Unknown
Felis_serval_U_ac0141	<i>Leptailurus serval</i>	Felinae	Unknown
Felis_silverstris_F_MNHN.CG1995-448	<i>Felis silvestris</i>	Felinae	Female
Felis_silvestris_M_SAP.ZOO.84	<i>Felis silvestris</i>	Felinae	Male
Felis_silvestris_U_ha0066	<i>Felis silvestris</i>	Felinae	Unknown
Herpailurus_jaguarundi_F_MNHN.CG2001-1292	<i>Herpailurus yagouaroundi</i>	Felinae	Female
Herpailurus_jaguarundi_M_MNHN.CG1966-7	<i>Herpailurus yagouaroundi</i>	Felinae	Male
Homotherium_serum_U_TMM.933-3444	<i>Homotherium serum</i>	Machairodontinae	Unknown
Leopardus_colocolo_F_MNHN.CG1897-1261	<i>Leopardus colocolo</i>	Felinae	Female
Leopardus_geoffroyi_F_MNHN.CG1912-748	<i>Leopardus geoffroyi</i>	Felinae	Female
Leopardus_jacobita_U_MNHN.CG2006-546	<i>Leopardus jacobita</i>	Felinae	Unknown
Leopardus_pajeros_F_MLP.1913	<i>Leopardus colocolo</i>	Felinae	Female
Leopardus_pardalis_F_MNHN.CG1998-1866	<i>Leopardus pardalis</i>	Felinae	Female
Leopardus_pardalis_M_MNHN.CH1902-50	<i>Leopardus pardalis</i>	Felinae	Male
Leopardus_pardalis_U_SAP.ZOO.Aula_A	<i>Leopardus pardalis</i>	Felinae	Unknown
Leopardus_tigrina_F_MNHN.CG2006-542	<i>Leopardus tigrinus</i>	Felinae	Female
Leopardus_tigrinus_M_MZUF-4054	<i>Leopardus tigrinus</i>	Felinae	Male

Table S1: List of sampled specimens with ID code, species name, subfamily, sex, and museum location.

Leopardus_wiedii_F_IMNH.R-601	<i>Leopardus wiedii</i>	Felinae	Female
Leptailurus_serval_F_MNHN.CG1995-452	<i>Leptailurus serval</i>	Felinae	Female
Leptailurus_serval_M_MNHN.CG1958-164	<i>Leptailurus serval</i>	Felinae	Male
Lynx_canadensis_F_IMNH.R-213	<i>Lynx canadensis</i>	Felinae	Female
Lynx_canadensis_M_UWBM80612	<i>Lynx canadensis</i>	Felinae	Male
Lynx_issiodorensis_U_MNCN63887	<i>Lynx issiodorensis</i>	Felinae	Unknown
Lynx_issiodorensis_U_NMBS.Prr.200	<i>Lynx issiodorensis</i>	Felinae	Unknown
Lynx_lynx_F_MG-2-2013_852	<i>Lynx lynx</i>	Felinae	Female
Lynx_lynx_M_MG-2-2013_839	<i>Lynx lynx</i>	Felinae	Male
Lynx_pardina_U_MNCN16784	<i>Lynx pardinus</i>	Felinae	Unknown
Lynx_rufus_F_MNHN.CG2012-1024	<i>Lynx rufus</i>	Felinae	Female
Lynx_rufus_M_UV.155	<i>Lynx rufus</i>	Felinae	Male
Lynx_rufus_M_UWBM32046	<i>Lynx rufus</i>	Felinae	Male
Lynx_rufus_U_IMNH.R-115	<i>Lynx rufus</i>	Felinae	Unknown
Machairodus_aphanistus_U_BAT-105-E6-92	<i>Machairodus aphanistus</i>	Machairodontinae	Unknown
Machairodus_giganteus_U_HD-9196	<i>Amphimachairodus giganteus</i>	Machairodontinae	Unknown
Mayailurus_iriomotensis_M_PRIZ774	<i>Prionailurus bengalensis</i>	Felinae	Male
Megantereon_cultridens_U_NMBS.L.P.18	<i>Megantereon cultridens</i>	Machairodontinae	Unknown
Megantereon_cultridens_U_NMBS.Se.311	<i>Megantereon cultridens</i>	Machairodontinae	Unknown
Megantereon_nihowanensis_U_CB-20	<i>Megantereon nihowanensis</i>	Machairodontinae	Unknown
Neofelis_diardi_M_MNHN.CG1879-2133	<i>Neofelis diardi</i>	Pantherinae	Male
Neofelis_nebulosa_F_MNHN.CG1971-86	<i>Neofelis nebulosa</i>	Pantherinae	Female
Neofelis_nebulosa_M_MZUF-1024	<i>Neofelis nebulosa</i>	Pantherinae	Male
Otocolobus_manul_F_MNHN.CG2009.251	<i>Otocolobus manul</i>	Felinae	Female
Otocolobus_manul_M_MNHN.CG2010-646	<i>Otocolobus manul</i>	Felinae	Male
Panthera_atrox_U_CB2900-3	<i>Panthera atrox</i>	Pantherinae	Unknown
Panthera_gombaszoegensis_U_NMBS.V.A.1953	<i>Panthera gombaszoegensis</i>	Pantherinae	Unknown
Panthera_leo_F_MNHN.A12259	<i>Panthera leo</i>	Pantherinae	Female
Panthera_leo_M_MNHN.CG1938-632	<i>Panthera leo</i>	Pantherinae	Male
Panthera_leo_U_ab0030	<i>Panthera leo</i>	Pantherinae	Unknown
Panthera_leo_U_ab0031	<i>Panthera leo</i>	Pantherinae	Unknown
Panthera_leo_U_DUNUC2021	<i>Panthera leo</i>	Pantherinae	Unknown
Panthera_leo_U_MVZ.117849	<i>Panthera leo</i>	Pantherinae	Unknown

Panthera_leo_U_SAP.ZOO.Sala_lettura	<i>Panthera leo</i>	Pantherinae	Unknown
Panthera_onca_F_MNHN.CG1962-2880	<i>Panthera onca</i>	Pantherinae	Female
Panthera_onca_M_MZUF-501	<i>Panthera onca</i>	Pantherinae	Male
Panthera_onca_U_MZB2003-1528	<i>Panthera onca</i>	Pantherinae	Unknown
Panthera_onca_U_PRIZ890	<i>Panthera onca</i>	Pantherinae	Unknown
Panthera_onca_U_WML.D.2-1.11.1853	<i>Panthera onca</i>	Pantherinae	Unknown
Panthera_pardus_F_MZUF-1221	<i>Panthera pardus</i>	Pantherinae	Female
Panthera_pardus_M_MNHN.CG1998-1249	<i>Panthera pardus</i>	Pantherinae	Male
Panthera_pardus_U_AMNH.113745	<i>Panthera pardus</i>	Pantherinae	Unknown
Panthera_pardus_U_IMNH.R-2372	<i>Panthera pardus</i>	Pantherinae	Unknown
Panthera_pardus_U_WML.18.5.97.4	<i>Panthera pardus</i>	Pantherinae	Unknown
Panthera_spelaea_U_IMNH.###	<i>Panthera spelaea</i>	Pantherinae	Unknown
Panthera_tigris_F_MNHN.CG1895-355	<i>Panthera tigris</i>	Pantherinae	Female
Panthera_tigris_M_MNHN.CG1985-1860	<i>Panthera tigris</i>	Pantherinae	Male
Panthera_tigris_U_SAP.ANTRO.2954	<i>Panthera tigris</i>	Pantherinae	Unknown
Panthera_uncia_F_MNHN.CG2016-1664	<i>Panthera uncia</i>	Pantherinae	Female
Panthera_uncia_M_MNHN.CG1998-1248	<i>Panthera uncia</i>	Pantherinae	Male
Pardofelis_marmorata_U_MNHN.CG1886-25	<i>Pardofelis marmorata</i>	Felinae	Unknown
Prionailurus_bengalensis_F_MNHN.CG1954-293	<i>Prionailurus bengalensis</i>	Felinae	Female
Prionailurus_planiceps_U_MNHN.CG1873-228	<i>Prionailurus planiceps</i>	Felinae	Unknown
Prionailurus_rubiginosus_U_MNHN.CG1872-70	<i>Prionailurus rubiginosus</i>	Felinae	Unknown
Prionailurus_viverrinus_F_MNHN.CG2015-1300	<i>Prionailurus viverrinus</i>	Felinae	Female
Puma_concolor_F_UV.4117	<i>Puma concolor</i>	Felinae	Female
Puma_concolor_M_MNHN.CG1926-250	<i>Puma concolor</i>	Felinae	Male
Puma_concolor_U_IMNH.R-27	<i>Puma concolor</i>	Felinae	Unknown
Puma_concolor_U_ISM.ZOO.693928	<i>Puma concolor</i>	Felinae	Unknown
Puma_concolor_U_MZB2003-1534	<i>Puma concolor</i>	Felinae	Unknown
Smilodon_fatalis_U_F.AM.14349	<i>Smilodon fatalis</i>	Machairodontinae	Unknown
Smilodon_neogaeus_U_MSMN.V371	<i>Smilodon populator</i>	Machairodontinae	Unknown
Smilodon_populator_U_MNHN-P-957	<i>Smilodon populator</i>	Machairodontinae	Unknown
Therailurus_diastemata_U_NMBS.Rss83	<i>Dinofelis diastemata</i>	Machairodontinae	Unknown
Xenosmilus_hodsonae_U_BC-113	<i>Xenosmilus hodsonae</i>	Machairodontinae	Unknown
Yoshi_garevskii_U_MMNH-Sk-69	<i>Yoshi garevskii</i>	Machairodontinae	Unknown

Landmark	Description
1	Prosthion: antero-inferior point on projection of pre-maxilla between central incisors
2, 3	Antero-medial point on the alveolar margin of the canine
4, 5	Postero-medial point on the alveolar margin of the canine
6, 7	Maxilla: anterior extreme of tooth row (before first premolar)
8, 9	Maxilla: posterior midpoint onto alveolar margin of last molar
10	Palatine: posterior edge on the midline
11, 12	Basioccipital, basisphenoid and tympanic bulla: meeting point
13, 14	Dorsal tip of acoustic meatus
15	Basion: anterior-most point of foramen magnum
16, 17	Posterior extremity of occipital condyle along margin of foramen magnum
18, 19	Infraorbital foramen (dorsal tip on side external to the orbit)
20, 21	Lacrimal foramen
22, 23	Foramen rotundum
24, 25	Zygo-temp inferior: infero-lateral point of zygomatico (jugal) - temporal (squamosal) suture on lateral face of zygomatic arch
26	Rhinion: most anterior midline point on nasals
27, 28	Nasal And pre-maxilla: meeting point on margin of piriform aperture
29	Nasion: midline point on fronto-nasal suture
30	Inion: most posterior point of the cranium

Table S2: Definitions of the anatomical landmarks used in the 30L configuration. The 10L configuration includes only the rows with grey background.

Conclusions

The present Thesis confirms that carnivorans represent an ideal case study for analyses concerning morphological directional evolution and phenotypic evolutionary trends in general. The inclusion of fossil morphologies constitutes one of the most valuable addition to many of the analytical frameworks adopted in the previous Chapters and it is a quite uncommon practice in ecomorphological research. This feature deeply influenced the results concerning the presence of Cope's rule in caniforms (Chapter 4, Appendix 2) and the occurrence of craniofacial evolutionary allometry in felids (i.e., extinct sabertoothed cats were found to be an exception to the rule and, similarly, living and extinct pantherines did not supported his evolutionary trend, contrary to previous investigations conducted only on extant pantherines - Chapter 7; cf. Tamagnini et al. 2017). Similarly, the high taxonomic coverage that characterise many of the morphological samples used in the present Thesis is likely to have greatly improved the ability to validate/confute the occurrence of evolutionary trends within the considered samples. For example, the inclusion of a large number of carnivoran species, and especially of many species of small and medium size generally poorly sampled in ecomorphological research (e.g., viverrids), might be one of the reasons why analyses in Chapter 5 detected broad similarities among omnivores (although in this case likely due to conservatism) contrary to many previous studies available in the literature.

The present Thesis provides several examples of how to apply pattern-based methods on the study of many different evolutionary trends (e.g., convergence – Chapter 2, 3, and 5; Cope's rule – Chapter 4, Appendix 2; craniofacial evolutionary allometry – Chapter 7). As discussed in Chapter 1, these methods bind the validation of an evolutionary pattern to the mere fulfilment of mathematical or geometrical criteria, are suitable for making inferences about different systems in broad comparative data, and often allow users to steer *post hoc* studies on the mechanisms responsible for the observed patterns. In particular, the adoption of multiple pattern-based metrics, each of them with a slightly different (although clearly defined) biological meaning, allowed me not only to test for the presence of convergence, but also to distinguish between episodes of convergent evolution and conservatism, that are the most common processes leading to trait similarity (Moen et al. 2013; Chapter 5). Being able to assess the occurrence/absence of these patterns has been suggested to potentially improve inferences in the paleoecological and taxonomic fields (Hunter 2021). The adoption of pattern-based methods for the study of evolutionary trends in morphological evolution is in line with the use of similar techniques that were recently employed for the study of evolution in wild populations (e.g., Langerhans 2018), pathogens (e.g., Ramiro et al. 2016), and applied contexts such as cancer research (e.g., Tegze et al. 2012), and allowed researchers to make inferences concerning the predictability of evolution (see Bolnick et al. 2018 for a focus on the concept of “(non) parallel evolution”).

Negative results are disappearing from many scientific fields as a consequence of a worsening of positive-outcome bias (Fanelli 2012), despite they provide useful information concerning previous failed experiments and often describe exceptions to persistent patterns (Mehta 2019). The present Thesis highlights the importance of including negative results as shown in Chapter 5 (i.e., absence of convergent evolution in

many tested dietary categories and textbook examples) and Chapter 7 (i.e., absence of craniofacial evolutionary allometry in pantherines and sabertoothed cats), since evidences deriving from these outcomes allowed me to formulate hypotheses concerning the existence of a complex interplay of one-to-many, many-to-one, and many-to-many relationships taking place between ecology, biomechanics, and morphology in the craniomandibular evolution of carnivorans.

This interplay of evolutionary factors that determines the craniomandibular evolution of carnivorans was also suggested to occur in previous research that highlighted a role of diet, locomotion, aquatic vs terrestrial habitat, evo-devo constraints, and phylogeny in morphological evolution within this clade (e.g., Meloro and O'Higgins 2011; Meloro and Slater 2012; Jones et al. 2015). In this sense, the adoption of theoretical frameworks that heavily rely on morphodynamics and include multidisciplinary analyses will surely be extremely helpful for studying further episodes of directional evolution. For instance, future advances in research on phenotypic evolutionary trends, and macroevolutionary pattern in general, are expected from the implementation of a complex ecological modelling in the study of morphological evolution. Linking these biological fields is also suggested to potentially provide useful information for investigations on conservation prioritization (Zizka et al. 2021), phenotypic diversity (Higham et al. 2021), and predictability of evolution (Chapter 1) in the near future. As discussed in Chapter 1, the inclusion of spatially structured variation in evolutionary models would allow the distinction between patterns produced by spatial processes, like drift and habitat-specific selection, and the ones associated with non-neutral and directional evolutionary regimes through time. Similarly, combining modern techniques of morphological quantification (e.g., geometric morphometrics and finite element analysis) with advanced methods in ecological niche evaluation (e.g., species distribution modelling) is supposed to be a promising way to bring deep insights in the understanding of ecomorphological pattern and processes (e.g., Maestri et al. 2018).

The use of data describing the biological function (e.g., loadings obtained from finite element analysis) in geometric morphometrics is also fundamental to point out the existing biomechanical constraints that shape morphological evolution and to shed light on the interaction between phenotypes and ecological variables (e.g., Tseng and Flynn 2018). In this sense, evolutionary landscapes are a key tool in order to visually represent the selective advantage intrinsic to specific combinations of morphologies and resulting biomechanical performances (Chapter 1). Methods that combine multiple performance surfaces (e.g., Pareto front) to assess the optimal morphologies that are able to carry out specific sets of biomechanical functions are expected to innovate the study of evolutionary patterns in the foreseeable future (e.g., Polly et al. 2016; Jones et al. 2021), and research on phenotypic evolutionary trends makes no exception.

Hopefully, the operative definition of “evolutionary trend” provided in Chapter 1 and the analytical approaches adopted throughout the present Thesis will represent a good starting point for future pattern-based studies on directional evolution, and macroevolution in general, enabling in such a fascinating topic of evolutionary biology, figuratively speaking, “new avenues for old travellers”.

References

- Adams, D. C. 2016. Evaluating modularity in morphometric data: challenges with the RV coefficient and a new test measure. *Methods Ecol. Evol.* 7:565–572.
- Adams, D. C., F. J. Rohlf, and D. E. Slice. 2013. A field comes of age: geometric morphometrics in the 21st century. *Hystrix It. J. Mamm.* 24:7–14.
- Adams, D. C., F. J. Rohlf, and D. E. Slice. 2004. Geometric morphometrics: ten years of progress following the ‘revolution.’ *Ital. J. Zool.* 71:5–16.
- Adams, J. W., A. Olah, M. R. McCurry, and S. Potze. 2015. Surface model and tomographic archive of fossil primate and other mammal holotype and paratype specimens of the Ditsong National Museum of Natural History, Pretoria, South Africa. *PLoS ONE* 10:e0139800.
- Allen, J. A. 1877. The influence of physical conditions in the genesis of species.
- Alroy, J. 2000. Understanding the dynamics of trends within evolving lineages. *Paleobiology* 26:319–329.
- Arthur, W. 2006. D’Arcy Thompson and the theory of transformations. *Nat. Rev. Genet.* 7:401–406.
- Bergmann, C. 1847. Über die verhältnisse der wärmeökonomie derthiere zu ihrer größe.
- Berta, A., M. Churchill, and R. W. Boessenecker. 2018. The origin and evolutionary biology of pinnipeds: seals, sea lions, and walruses. *Annu. Rev. Earth Planet. Sci.* 46:203–228.
- Bolnick, D. I., R. D. H. Barrett, K. B. Oke, D. J. Rennison, and Y. E. Stuart. 2018. (Non)parallel evolution. *Annu. Rev. Ecol. Evol. Syst.* 49:303–330.
- Castiglione, S., C. Serio, A. Mondanaro, M. D. Febbraro, A. Profico, G. Girardi, and P. Raia. 2019. Simultaneous detection of macroevolutionary patterns in phenotypic means and rate of change with and within phylogenetic trees including extinct species. *PLoS ONE* 14:e0210101.
- Castiglione, S., G. Tesone, M. Piccolo, M. Melchionna, A. Mondanaro, C. Serio, M. D. Febbraro, and P. Raia. 2018. A new method for testing evolutionary rate variation and shifts in phenotypic evolution. *Methods Ecol. Evol.* 9:974–983.
- Chemisquy, M. A., S. D. Tarquini, C. O. Romano Muñoz, and F. J. Prevosti. 2021. Form, function and evolution of the skull of didelphid marsupials (Didelphimorphia: Didelphidae). *J. Mammal. Evol.* 28:23–33.
- Diniz-Filho, J. A. F., L. M. Bini, M. Á. Rodríguez, T. F. L. V. B. Rangel, and B. A. Hawkins. 2007. Seeing the forest for the trees: partitioning ecological and phylogenetic components of Bergmann’s rule in European Carnivora. *Ecography* 30:598–608.
- Diniz-Filho, J. A. F., M. Á. Rodríguez, L. M. Bini, M. Á. Olalla-Tarraga, M. Cardillo, J. C. Nabout, J. Hortal, and B. A. Hawkins. 2009. Climate history, human impacts and global body size of Carnivora (Mammalia: Eutheria) at multiple evolutionary scales. *J. Biogeogr.* 36:2222–2236.
- Dumont, M., C. E. Wall, L. Botton-Divet, A. Goswami, S. Peigné, and A.-C. Fabre. 2016. Do functional demands

- associated with locomotor habitat, diet, and activity pattern drive skull shape evolution in musteloid carnivorans? *Biol. J. Linn. Soc.* 117:858–878.
- Evans, K. M., L. Y. Kim, B. A. Schubert, and J. S. Albert. 2019. Ecomorphology of Neotropical electric fishes: an integrative approach to testing the relationships between form, function, and trophic ecology. *Integr. Org. Biol.* 1:obz015.
- Ewer, R. F. 1973. *The carnivores*. Cornell University Press, Ithaca, N.Y.
- Falkingham, P. L. 2012. Acquisition of high resolution three-dimensional models using free, open-source, photogrammetric software. *Palaeontol. Electron.* 15:1–15.
- Fanelli, D. 2012. Negative results are disappearing from most disciplines and countries. *Scientometrics* 90:891–904.
- Figueirido, B., P. Palmqvist, and J. A. Pérez-Claros. 2009. Ecomorphological correlates of craniodental variation in bears and paleobiological implications for extinct taxa: an approach based on geometric morphometrics. *J. Zool.* 277:70–80.
- Figueirido, B., F. J. Serrano-Alarcón, G. J. Slater, and P. Palmqvist. 2010. Shape at the cross-roads: homoplasy and history in the evolution of the carnivoran skull towards herbivory. *J. Evol. Biol.* 23:2579–2594.
- Figueirido, B., and L. H. Soibelzon. 2010. Inferring palaeoecology in extinct tremarctine bears (Carnivora, Ursidae) using geometric morphometrics. *Lethaia* 43:209–222.
- Figueirido, B., Z. J. Tseng, and A. Martín-Serra. 2013. Skull shape evolution in durophagous carnivorans. *Evolution* 67:1975–1993.
- Finarelli, J. A., and J. J. Flynn. 2006. Ancestral state reconstruction of body size in the Caniformia (Carnivora, Mammalia): the effects of incorporating data from the fossil record. *Syst. Biol.* 55:301–313.
- Gittleman, J. L. 1986. Carnivore life history patterns: allometric, phylogenetic, and ecological associations. *Am. Nat.* 127:744–771.
- Higham, T. E., L. A. Ferry, L. Schmitz, D. J. Irschick, S. Starko, P. S. L. Anderson, P. J. Bergmann, H. A. Jamniczky, L. R. Monteiro, D. Navon, J. Messier, E. Carrington, S. C. Farina, K. L. Feilich, L. P. Hernandez, M. A. Johnson, S. M. Kawano, C. J. Law, S. J. Longo, C. H. Martin, P. T. Martone, A. Rico-Guevara, S. E. Santana, and K. J. Niklas. 2021. Linking ecomechanical models and functional traits to understand phenotypic diversity. *Trends Ecol. Evol.* 36:860–873.
- Hipsley, C. A., and J. Müller. 2017. Developmental dynamics of ecomorphological convergence in a transcontinental lizard radiation. *Evolution* 71:936–948.
- Hunter, L. E. 2021. Digest: Taxonomically inclusive and quantitative tests for convergence*. *Evolution* 75:1900–1901.
- Jones, K. E., B. V. Dickson, K. D. Angielczyk, and S. E. Pierce. 2021. Adaptive landscapes challenge the “lateral-to-sagittal” paradigm for mammalian vertebral evolution. *Curr. Biol.* 31:1–10.
- Jones, K. E., J. B. Smaers, and A. Goswami. 2015. Impact of the terrestrial-aquatic transition on disparity and rates

- of evolution in the carnivoran skull. *BMC Evol. Biol.* 15:8.
- Klingenberg, C. P. 2013. Cranial integration and modularity: insights into evolution and development from morphometric data. *Hystrix It. J. Mamm.* 24:43–58.
- Kratsch, C., and A. C. McHardy. 2014. RidgeRace: ridge regression for continuous ancestral character estimation on phylogenetic trees. *Bioinformatics* 30:i527–i533.
- Langerhans, R. B. 2018. Predictability and parallelism of multitrait adaptation. *J. Hered.* 109:59–70.
- Maestri, R., L. R. Monteiro, R. Fornel, T. R. O. de Freitas, and B. D. Patterson. 2018. Geometric morphometrics meets metacommunity ecology: environment and lineage distribution affects spatial variation in shape. *Ecography* 41:90–100.
- Marcé-Nogué, J., T. A. Püschel, and T. M. Kaiser. 2017. A biomechanical approach to understand the ecomorphological relationship between primate mandibles and diet. *Sci. Rep.* 7:8364.
- McKinney, M. L. 1990. Classifying and analysing evolutionary trends. Pp. 28–58 *in* K. J. McNamara, ed. *Evolutionary trends*. University of Arizona Press.
- Mehta, D. 2019. Highlight negative results to improve science. *Nature*, doi:10.1038/d41586-019-02960-3.
- Meloro, C., M. Clauss, and P. Raia. 2015. Ecomorphology of Carnivora challenges convergent evolution. *Org. Divers. Evol.* 15:711–720.
- Meloro, C., and P. O’Higgins. 2011. Ecological adaptations of mandibular form in fissiped Carnivora. *J. Mammal. Evol.* 18:185–200.
- Meloro, C., and G. J. Slater. 2012. Covariation in the skull modules of cats: the challenge of growing saber-like canines. *J. Vertebr. Paleontol.* 32:677–685.
- Michaud, M., G. Veron, S. Peigné, A. Blin, and A.-C. Fabre. 2018. Are phenotypic disparity and rate of morphological evolution correlated with ecological diversity in Carnivora? *Biol. J. Linn. Soc.* 124:294–307.
- Mihlbachler, M. C. 2008. Species taxonomy, phylogeny and biogeography of the Brontotheriidae (Mammalia, Perissodactyla). *Bull. Am. Mus. Nat. Hist.*
- Moen, D. S., D. J. Irschick, and J. J. Wiens. 2013. Evolutionary conservatism and convergence both lead to striking similarity in ecology, morphology and performance across continents in frogs. *Proc. R. Soc. B* 280:20132156.
- Moss, M. L., and R. W. Young. 1960. A functional approach to craniology. *Am. J. Phys. Anthropol.* 18:281–292.
- Muñoz-Muñoz, F., M. Quinto-Sánchez, and R. González-José. 2016. Photogrammetry: a useful tool for three-dimensional morphometric analysis of small mammals. *J. Zool. Syst. Evol. Res.* 54:318–325.
- O’Higgins, P., S. N. Cobb, L. C. Fitton, F. Gröning, R. Phillips, J. Liu, and M. J. Fagan. 2011. Combining geometric morphometrics and functional simulation: an emerging toolkit for virtual functional analyses. *J. Anat.* 218:3–15.
- Osborn, H. F. 1929. *The titanotheres of ancient Wyoming, Dakota, and Nebraska*, Vol. 1. Government Printing

Office.

- Piras, P., D. Silvestro, F. Carotenuto, S. Castiglione, A. Kotsakis, L. Maiorino, M. Melchionna, A. Mondanaro, G. Sansalone, C. Serio, V. A. Vero, and P. Raia. 2018. Evolution of the sabertooth mandible: a deadly ecomorphological specialization. *Palaeogeogr. Palaeoclimatol. Palaeoecol.* 496:166–174.
- Polly, P. D., C. T. Stayton, E. R. Dumont, S. E. Pierce, E. J. Rayfield, and K. D. Angielczyk. 2016. Combining geometric morphometrics and finite element analysis with evolutionary modeling: towards a synthesis. *J. Vertebr. Paleontol.* 36:e1111225.
- Radinsky, L. B. 1981a. Evolution of skull shape in carnivores: 1. Representative modern carnivores. *Biol. J. Linn. Soc.* 15:369–388.
- Radinsky, L. B. 1981b. Evolution of skull shape in carnivores: 2. Additional modern carnivores. *Biol. J. Linn. Soc.* 16:337–355.
- Radinsky, L. B. 1982. Evolution of skull shape in carnivores. 3. The origin and early radiation of the modern carnivore families. *Paleobiology* 8:177–195.
- Ramiro, R. S., H. Costa, and I. Gordo. 2016. Macrophage adaptation leads to parallel evolution of genetically diverse *Escherichia coli* small-colony variants with increased fitness in vivo and antibiotic collateral sensitivity. *Evol. Appl.* 9:994–1004.
- Serrano-Fochs, S., S. D. Esteban-Trivigno, J. Marcé-Nogué, J. Fortuny, and R. A. Fariña. 2015. Finite element analysis of the Cingulata jaw: an ecomorphological approach to armadillo's diets. *PLoS ONE* 10:e0120653.
- Stayton, C. T. 2015a. The definition, recognition, and interpretation of convergent evolution, and two new measures for quantifying and assessing the significance of convergence. *Evolution* 69:2140–2153.
- Stayton, C. T. 2015b. What does convergent evolution mean? The interpretation of convergence and its implications in the search for limits to evolution. *Interface Focus* 5:20150039.
- Stynder, D. D., P. S. Ungar, J. R. Scott, and B. W. Schubert. 2012. A dental microwear texture analysis of the Mio-Pliocene hyaenids from Langebaanweg, South Africa. *Acta Palaeontol. Pol.* 57:485–496.
- Tamagnini, D., C. Meloro, and A. Cardini. 2017. Anyone with a long-face? Craniofacial evolutionary allometry (CREA) in a family of short-faced mammals, the Felidae. *Evol. Biol.* 44:476–495.
- Tegze, B., Z. Szállási, I. Haltrich, Z. Péntváltó, Z. Tóth, I. Likó, and B. Györffy. 2012. Parallel evolution under chemotherapy pressure in 29 breast cancer cell lines results in dissimilar mechanisms of resistance. *PLoS ONE* 7:e30804.
- Terhune, C. E., S. B. Cooke, and E. Otárola-Castillo. 2015. Form and function in the platyrrhine skull: a three-dimensional analysis of dental and TMJ morphology. *Anat. Rec.* 298:29–47.
- Thompson, D. W. 1917. *On growth and form*. Cambridge University Press, Cambridge.
- Tseng, Z. J., and J. J. Flynn. 2018. Structure-function covariation with nonfeeding ecological variables influences evolution of feeding specialization in Carnivora. *Sci. Adv.* 4:eaao5441.

- Tseng, Z. J., C. Grohé, and J. J. Flynn. 2016. A unique feeding strategy of the extinct marine mammal *Kolponomos*: convergence on sabretooths and sea otters. *Proc. R. Soc. B* 283:20160044.
- van Heteren, A. H., A. MacLarnon, C. Soligo, and T. C. Rae. 2016. Functional morphology of the cave bear (*Ursus spelaeus*) mandible: a 3D geometric morphometric analysis. *Org. Divers. Evol.* 16:299–314.
- Watanabe, A., A.-C. Fabre, R. N. Felice, J. A. Maisano, J. Müller, A. Herrel, and A. Goswami. 2019. Ecomorphological diversification in squamates from conserved pattern of cranial integration. *Proc. Natl. Acad. Sci. USA* 116:14688–14697.
- Zizka, A., C. D. Barratt, C. D. Ritter, T. Joerger-Hickfang, and V. M. A. Zizka. 2021. Existing approaches and future directions to link macroecology, macroevolution and conservation prioritization. *Ecography*.

Appendix 1 – Cranial 3D sample

As also detailed in Chapters 3 and 7, the present PhD thesis included 3D morphological data describing the crania of living and extinct species of felids (plus a small number of barbourofelids and nimravids) that were used to perform macroevolutionary analyses in order to assess the presence of different evolutionary trends (i.e., convergent evolution and craniofacial evolutionary allometry) in these clades. The cranial sample is detailed in Table 1. The vast majority of 3D models included in this morphological sample was obtained by means of a technique of 3D digitalisation named photogrammetry. In particular, a set of 150-200 high resolution images was collected for each cranium using a Nikon D3100 camera with an AF-S DX Micro Nikkor 40 mm f2.8G macro lens following an acquisition protocol similar to those proposed in Falkingham (2012) and Muñoz-Muñoz et al. (2016). Then, these images were processed by means of a software for photogrammetric reconstruction (Agisoft PhotoScan) in order to generate 3D surface models of the sampled crania (in .ply format) suitable for the extraction of morphological data by means of 3D geometric morphometrics. Almost all the photogrammetric 3D models included in the present sample are from museum collections including: Muséum National d'Histoire Naturelle (MNHN - Paris); Naturhistorisches Museum (NMBS - Basel); Museo Nacional Ciencias Naturales (MNCN - Madrid); Museo di Storia Naturale "La Specola" (MZUF - Florence); Musei di Anatomia Comparata, Zoologia e Antropologia (University of Rome "La Sapienza" – Rome).

The cranial sample was also integrated with digital models that were shared by other researches/institutions (e.g., Drs. Denis Geraads and Nikolai Spassov; Primate Research Institute – Kyoto; Museu de Ciències Naturals - Barcelona), available in online open-access repositories or published in previous papers on carnivorans (e.g., Adams et al. 2015; Tseng et al. 2016). Hopefully, the morphological data deriving from this cranial sample will be soon included in a publication (e.g., data paper) that would allow other researchers of this field to work on these digital specimens by accessing an online open-access repository (e.g., MorphoSource, DigiMorph).

ID	Species	Family
Acinonyx_jubatus_F_MZUF-1831	<i>Acinonyx jubatus</i>	Felidae
Acinonyx_jubatus_M_MZUF-2135	<i>Acinonyx jubatus</i>	Felidae
Acinonyx_pardinensis_U_NMBS.St.V.975	<i>Acinonyx pardinensis</i>	Felidae
Barbourofelis_fricki_U_MNCN.###	<i>Barbourofelis fricki</i>	Barbourofelidae
Caracal_aurata_F_MNHN.CG1939.687	<i>Caracal aurata</i>	Felidae
Caracal_aurata_M_MNHN.CG1940-1213	<i>Caracal aurata</i>	Felidae
Caracal_caracal_F_MNHN.CG2015-2093	<i>Caracal caracal</i>	Felidae
Caracal_caracal_M_MZUF-1752	<i>Caracal caracal</i>	Felidae
Catopuma_temminckii_F_MNHN.CG1939.2152	<i>Catopuma temminckii</i>	Felidae
Catopuma_temminckii_M_MNHN.CG1962-2927	<i>Catopuma temminckii</i>	Felidae
Dinofelis_barlowi_U_DNMNH.BF55-22	<i>Dinofelis barlowi</i>	Felidae
Dinofelis_piveteaui_U_DNMNH.KA61	<i>Dinofelis piveteaui</i>	Felidae

<i>Eusmilus sicarius</i> _U_CB-07	<i>Eusmilus sicarius</i>	Nimravidae
<i>Felis bieti</i> _U_MNHN.CG1893-151	<i>Felis bieti</i>	Felidae
<i>Felis chaus</i> _F_MNHN.CG2015-1302	<i>Felis chaus</i>	Felidae
<i>Felis chaus</i> _U_MZUF-12308	<i>Felis chaus</i>	Felidae
<i>Felis concolor</i> _U_PRIZ891	<i>Puma concolor</i>	Felidae
<i>Felis margarita</i> _U_IMNH.R-938	<i>Felis margarita</i>	Felidae
<i>Felis serval</i> _U_ac0141	<i>Leptailurus serval</i>	Felidae
<i>Felis silverstris</i> _F_MNHN.CG1995-448	<i>Felis silvestris</i>	Felidae
<i>Felis silvestris</i> _M_SAP.ZOO.84	<i>Felis silvestris</i>	Felidae
<i>Felis silvestris</i> _U_ha0066	<i>Felis silvestris</i>	Felidae
<i>Herpailurus jaguaroundi</i> _F_MNHN.CG2001-1292	<i>Herpailurus yagouaroundi</i>	Felidae
<i>Herpailurus jaguaroundi</i> _M_MNHN.CG1966-7	<i>Herpailurus yagouaroundi</i>	Felidae
<i>Homotherium serum</i> _U_TMM.933-3444	<i>Homotherium serum</i>	Felidae
<i>Hoplophoneus dakotensis</i> _U_CB-15	<i>Hoplophoneus dakotensis</i>	Nimravidae
<i>Hoplophoneus occidentalis</i> _U_CB-18	<i>Hoplophoneus occidentalis</i>	Nimravidae
<i>Hoplophoneus primaevus</i> _U_USNM.V99	<i>Hoplophoneus primaevus</i>	Nimravidae
<i>Leopardus colocolo</i> _F_MNHN.CG1897-1261	<i>Leopardus colocolo</i>	Felidae
<i>Leopardus geoffroyi</i> _F_MNHN.CG1912-748	<i>Leopardus geoffroyi</i>	Felidae
<i>Leopardus jacobita</i> _U_MNHN.CG2006-546	<i>Leopardus jacobita</i>	Felidae
<i>Leopardus pajeros</i> _F_MLP.1913	<i>Leopardus colocolo</i>	Felidae
<i>Leopardus pardalis</i> _F_MNHN.CG1998-1866	<i>Leopardus pardalis</i>	Felidae
<i>Leopardus pardalis</i> _M_MNHN.CH1902-50	<i>Leopardus pardalis</i>	Felidae
<i>Leopardus pardalis</i> _U_SAP.ZOO.Aula_A	<i>Leopardus pardalis</i>	Felidae
<i>Leopardus tigrina</i> _F_MNHN.CG2006-542	<i>Leopardus tigrinus</i>	Felidae
<i>Leopardus tigrinus</i> _M_MZUF-4054	<i>Leopardus tigrinus</i>	Felidae
<i>Leopardus wiedii</i> _F_IMNH.R-601	<i>Leopardus wiedii</i>	Felidae
<i>Leptailurus serval</i> _F_MNHN.CG1995-452	<i>Leptailurus serval</i>	Felidae
<i>Leptailurus serval</i> _M_MNHN.CG1958-164	<i>Leptailurus serval</i>	Felidae
<i>Lynx canadensis</i> _F_IMNH.R-213	<i>Lynx canadensis</i>	Felidae
<i>Lynx canadensis</i> _M_UWBM80612	<i>Lynx canadensis</i>	Felidae
<i>Lynx issiodorensis</i> _U_MNCN63887	<i>Lynx issiodorensis</i>	Felidae
<i>Lynx issiodorensis</i> _U_NMBS.Prr.200	<i>Lynx issiodorensis</i>	Felidae
<i>Lynx lynx</i> _F_MG-2-2013_852	<i>Lynx lynx</i>	Felidae
<i>Lynx lynx</i> _M_MG-2-2013_839	<i>Lynx lynx</i>	Felidae
<i>Lynx pardina</i> _U_MNCN16784	<i>Lynx pardinus</i>	Felidae
<i>Lynx rufus</i> _F_MNHN.CG2012-1024	<i>Lynx rufus</i>	Felidae
<i>Lynx rufus</i> _M_UV.155	<i>Lynx rufus</i>	Felidae
<i>Lynx rufus</i> _M_UWBM32046	<i>Lynx rufus</i>	Felidae
<i>Lynx rufus</i> _U_IMNH.R-115	<i>Lynx rufus</i>	Felidae
<i>Machairodus aphanistus</i> _U_BAT-105-E6-92	<i>Machairodus aphanistus</i>	Felidae
<i>Machairodus giganteus</i> _U_HD-9196	<i>Amphimachairodus giganteus</i>	Felidae
<i>Mayailurus iriomotensis</i> _M_PRIZ774	<i>Prionailurus bengalensis</i>	Felidae
<i>Megantereon cultridens</i> _U_NMBS.L.P.18	<i>Megantereon cultridens</i>	Felidae
<i>Megantereon cultridens</i> _U_NMBS.Se.311	<i>Megantereon cultridens</i>	Felidae
<i>Megantereon nihowanensis</i> _U_CB-20	<i>Megantereon nihowanensis</i>	Felidae
<i>Neofelis diardi</i> _M_MNHN.CG1879-2133	<i>Neofelis diardi</i>	Felidae
<i>Neofelis nebulosa</i> _F_MNHN.CG1971-86	<i>Neofelis nebulosa</i>	Felidae
<i>Neofelis nebulosa</i> _M_MZUF-1024	<i>Neofelis nebulosa</i>	Felidae
<i>Otocolobus manul</i> _F_MNHN.CG2009.251	<i>Otocolobus manul</i>	Felidae
<i>Otocolobus manul</i> _M_MNHN.CG2010-646	<i>Otocolobus manul</i>	Felidae
<i>Panthera atrox</i> _U_CB2900-3	<i>Panthera atrox</i>	Felidae

Panthera blytheae_U_IVPP.V18788.1	<i>Panthera blytheae</i>	Felidae
Panthera gombaszoegensis_U_NMBS.V.A.1953	<i>Panthera gombaszoegensis</i>	Felidae
Panthera leo_F_MNHN.A12259	<i>Panthera leo</i>	Felidae
Panthera leo_M_MNHN.CG1938-632	<i>Panthera leo</i>	Felidae
Panthera leo_U_ab0030	<i>Panthera leo</i>	Felidae
Panthera leo_U_ab0031	<i>Panthera leo</i>	Felidae
Panthera leo_U_DUNUC2021	<i>Panthera leo</i>	Felidae
Panthera leo_U_MVZ.117849	<i>Panthera leo</i>	Felidae
Panthera leo_U_SAP.ZOO.Sala_lettura	<i>Panthera leo</i>	Felidae
Panthera onca_F_MNHN.CG1962-2880	<i>Panthera onca</i>	Felidae
Panthera onca_M_MZUF-501	<i>Panthera onca</i>	Felidae
Panthera onca_U_MZB2003-1528	<i>Panthera onca</i>	Felidae
Panthera onca_U_PRIZ890	<i>Panthera onca</i>	Felidae
Panthera onca_U_WML.D.2-1.11.1853	<i>Panthera onca</i>	Felidae
Panthera pardus_F_MZUF-1221	<i>Panthera pardus</i>	Felidae
Panthera pardus_M_MNHN.CG1998-1249	<i>Panthera pardus</i>	Felidae
Panthera pardus_U_AMNH.113745	<i>Panthera pardus</i>	Felidae
Panthera pardus_U_IMNH.R-2372	<i>Panthera pardus</i>	Felidae
Panthera pardus_U_WML.18.5.97.4	<i>Panthera pardus</i>	Felidae
Panthera spelaea_U_IMNH.###	<i>Panthera spelaea</i>	Felidae
Panthera tigris_F_MNHN.CG1895-355	<i>Panthera tigris</i>	Felidae
Panthera tigris_M_MNHN.CG1985-1860	<i>Panthera tigris</i>	Felidae
Panthera tigris_U_SAP.ANTRO.2954	<i>Panthera tigris</i>	Felidae
Panthera uncia_F_MNHN.CG2016-1664	<i>Panthera uncia</i>	Felidae
Panthera uncia_M_MNHN.CG1998-1248	<i>Panthera uncia</i>	Felidae
Panthera zdanskyi_U_BC-294	<i>Panthera zdanskyi</i>	Felidae
Pardofelis marmorata_U_MNHN.CG1886-25	<i>Pardofelis marmorata</i>	Felidae
Prionailurus bengalensis_F_MNHN.CG1954-293	<i>Prionailurus bengalensis</i>	Felidae
Prionailurus planiceps_U_MNHN.CG1873-228	<i>Prionailurus planiceps</i>	Felidae
Prionailurus rubiginosus_U_MNHN.CG1872-70	<i>Prionailurus rubiginosus</i>	Felidae
Prionailurus viverrinus_F_MNHN.CG2015-1300	<i>Prionailurus viverrinus</i>	Felidae
Puma concolor_F_UV.4117	<i>Puma concolor</i>	Felidae
Puma concolor_M_MNHN.CG1926-250	<i>Puma concolor</i>	Felidae
Puma concolor_U_IMNH.R-27	<i>Puma concolor</i>	Felidae
Puma concolor_U_ISM.ZOO.693928	<i>Puma concolor</i>	Felidae
Puma concolor_U_MZB2003-1534	<i>Puma concolor</i>	Felidae
Smilodon fatalis_U_F.AM.14349	<i>Smilodon fatalis</i>	Felidae
Smilodon neogaeus_U_MSMN.V371	<i>Smilodon populator</i>	Felidae
Smilodon populator_U_MNHN-P-957	<i>Smilodon populator</i>	Felidae
Therailurus diastemata_U_NMBS.Rss83	<i>Dinofelis diastemata</i>	Felidae
Xenosmilus hodsonae_U_BC-113	<i>Xenosmilus hodsonae</i>	Felidae
Yoshi_garevskii_U_MMNH-Sk-69	<i>Yoshi garevskii</i>	Felidae

Table 1: IDs, species and family of the specimens included in 3D cranial sample of living and fossil felids, nimravids, and barbourfelids used for many ecomorphological analyses in the present PhD thesis (e.g., Chapters 3 and 7).

Appendix 2 – Electronic supplementary material of Chapter 4

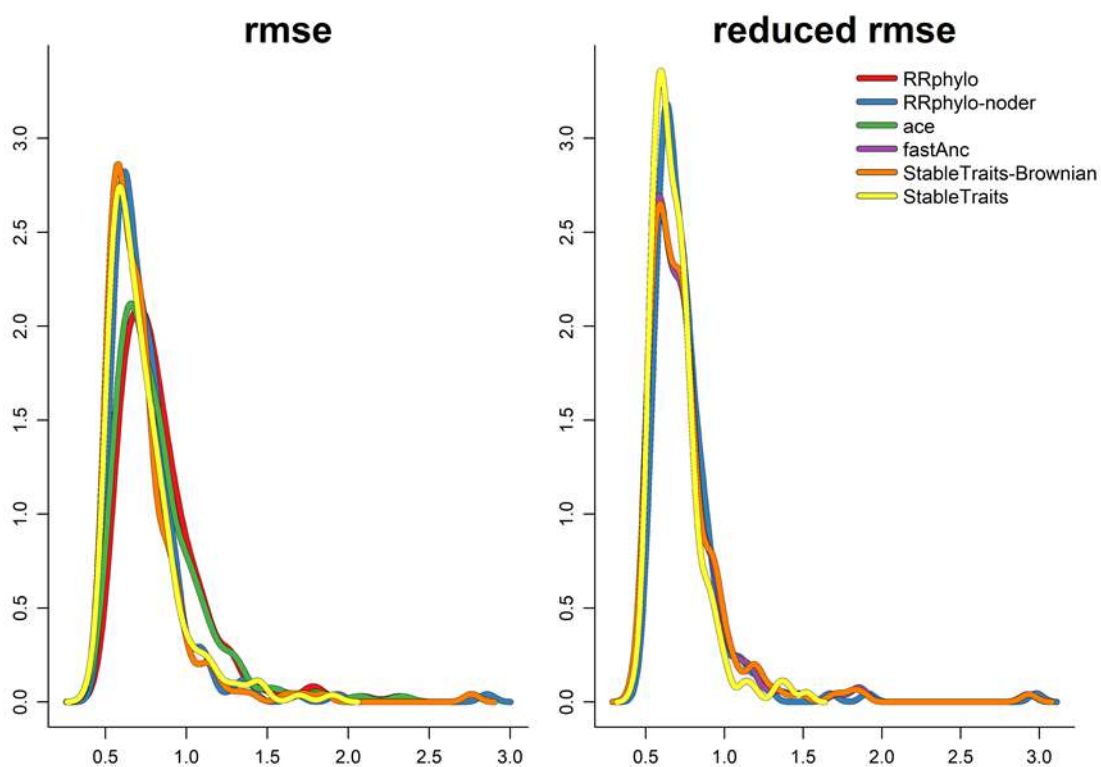
Online Resource 1. Supplementary results in “Ancestral State Estimation with Phylogenetic Ridge Regression” from S. Castiglione, C. Serio, A. Mondanaro, M. Melchionna, F. Carotenuto, M. Di Febbraro, A. Profico, D. Tamagnini, P. Raia, submitted to Evolutionary Biology. (Prof. Raia P., University of Naples, Federico II, pasquale.raia@unina.it)

Supplementary results

Effect of a phenotypic drift in the mean phenotype

To assess the importance of the starting phenotype (either BM or BM with a phenotypic drift in the mean over time), we took those subsets of the simulations designed as starting with either phenotypic evolutionary model.

ANOVA indicated 16 times out of 40 phenotypes there are significant *rmse* difference among methods. When the starting phenotype was BM, post-hoc Tuckey on *rmse* indicated *StableTraits-Brownian* and *StableTraits* were the best method 7 times, *RRphylo-noder* and 6 times and *ace* once. With the *reduced rmse* we found no significant difference among



methods for any of the phenotypes as per ANOVA.

Figure S1. Density plot of root mean square error (*rmse*, left) and reduced root mean square error (right) for simulations designed to start with a phenotype evolving according to Brownian motion.

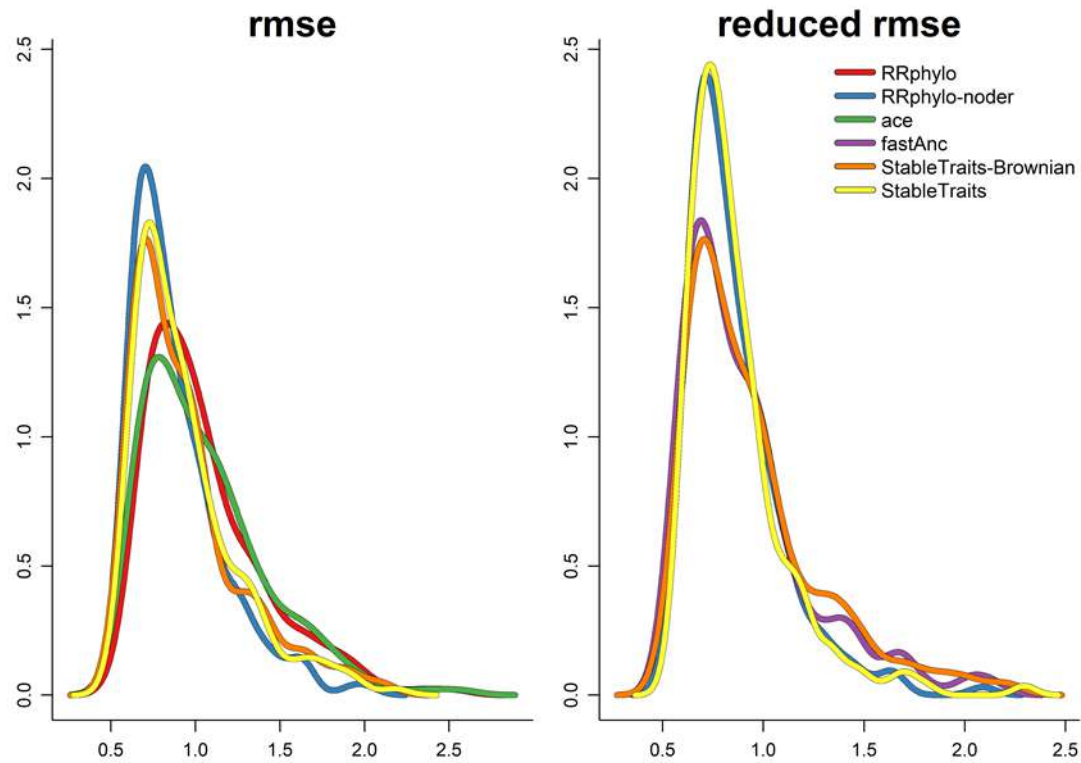
		intercept	slope	r.squared	rmse	red.rmse
RRphylo	mean	0.026	0.944	0.843	0.840	0.674
	2.5%	-0.352	0.752	0.571	0.543	0.531
	97.5%	0.730	1.073	0.969	1.561	0.895
RRphylo - noder	mean	-0.034	0.991	0.877	0.746	0.742
	2.5%	-0.495	0.882	0.660	0.509	0.529
	97.5%	0.406	1.095	0.976	1.351	1.195
ace	mean	0.007	0.959	0.849	0.822	0.650
	2.5%	-0.492	0.764	0.599	0.522	0.504
	97.5%	0.812	1.092	0.975	1.524	0.904
fastAnc	mean	-0.033	0.995	0.889	0.708	0.738
	2.5%	-0.423	0.894	0.675	0.484	0.506
	97.5%	0.304	1.085	0.978	1.300	1.375
StableTraits - Brownian	mean	-0.038	0.995	0.885	0.720	0.742
	2.5%	-0.521	0.898	0.663	0.489	0.498
	97.5%	0.286	1.096	0.978	1.312	1.355
StableTraits	mean	-0.013	0.981	0.883	0.726	0.692
	2.5%	-0.539	0.859	0.698	0.500	0.507
	97.5%	0.377	1.091	0.979	1.340	1.142

Table S1. Summary of regression parameters (slope, intercept, and r^2), root mean square error (*rmse*) and *reduced rmse* as derived by each method, for simulations designed to start with a phenotype evolving according to Brownian motion.

The function *seach.trend* finds a significant phenotypic trend for the entire tree in 7% of the cases by specifying and 8% of the cases not specifying the *aces* (since these are BM models the basic expectation is to find no issue of significant phenotypic drift for the entire

tree). The power of *search.trend* to find significant phenotypic drift at specified nodes which were designed to be so increases 96% when *aces* are specified.

When the starting phenotype was produced according to the Brownian motion with a phenotypic drift (usually referred at as the Brownian motion with trend model), *StableTraits-*



Brownian (9) and *RRphylo-noder* (9) are the best method in terms of *rmse*. Ape's *ace* and *RRphylo* were selected two and one time respectively. We found no difference between methods in terms of *reduced rmse*.

Figure S2. Density plot of root mean square error (*rmse*, left) and reduced root mean square error (right) for simulations designed to start with a phenotype evolving according to Brownian motion with a phenotypic drift.

The function *seach.trend* finds a significant phenotypic trend for the entire tree in 84% of the cases by specifying and 82.5% of the cases not specifying the *aces* (since these

are BM with drift models the basic expectation is to always find evidence for significant phenotypic drift for the entire tree). The power of *search.trend* to find significant phenotypic drift at specified nodes which were designed to be so increases 82% when *aces* are specified.

		intercept	slope	r.squared	rmse	red.rmse
RRphylo	mean	-0.728	1.001	0.852	1.056	0.826
	2.5%	-3.512	0.809	0.606	0.662	0.612
	97.5%	0.469	1.281	0.966	1.899	1.254
RRphylo - noder	mean	-0.684	1.021	0.896	0.884	0.858
	2.5%	-2.383	0.906	0.731	0.584	0.589
	97.5%	0.136	1.157	0.974	1.614	1.442
ace	mean	-0.847	1.011	0.852	1.051	0.824
	2.5%	-3.696	0.815	0.618	0.618	0.597
	97.5%	0.575	1.262	0.970	1.853	1.239
fastAnc	mean	-0.613	1.008	0.892	0.893	0.912
	2.5%	-1.882	0.905	0.688	0.558	0.570
	97.5%	0.124	1.123	0.978	1.676	1.717
StableTraits - Brownian	mean	-0.837	1.028	0.879	0.942	0.944
	2.5%	-2.983	0.916	0.647	0.591	0.598
	97.5%	0.021	1.212	0.973	1.852	1.876
StableTraits	mean	-0.727	1.009	0.881	0.939	0.862
	2.5%	-2.878	0.878	0.681	0.597	0.602
	97.5%	0.228	1.193	0.972	1.748	1.519

Table S2. Summary of regression parameters (slope, intercept, and r^2), root mean square error (*rmse*) and *reduced rmse* as derived by each method, for simulations designed to start with a phenotype evolving according to Brownian motion with a phenotypic drift.

Effect of phenotypic drift at specific nodes within the trees

To assess the importance of complicating the tree phenotypic vector by imposing a drift to specific nodes only, we selected from all simulations those without and those with such clade-wise drifts.

When no drift is imposed at any node, *StableTraits-Brownian* (7) and both *RRphylo-noder* and *StableTraits* (6) perform best in terms of *rmse*, outperforming *ace* (3). By looking at *reduced rmse*, the best performance was for *StableTraits-Brownian* (2) *StableTraits* (2) and *fastAnc* (2).

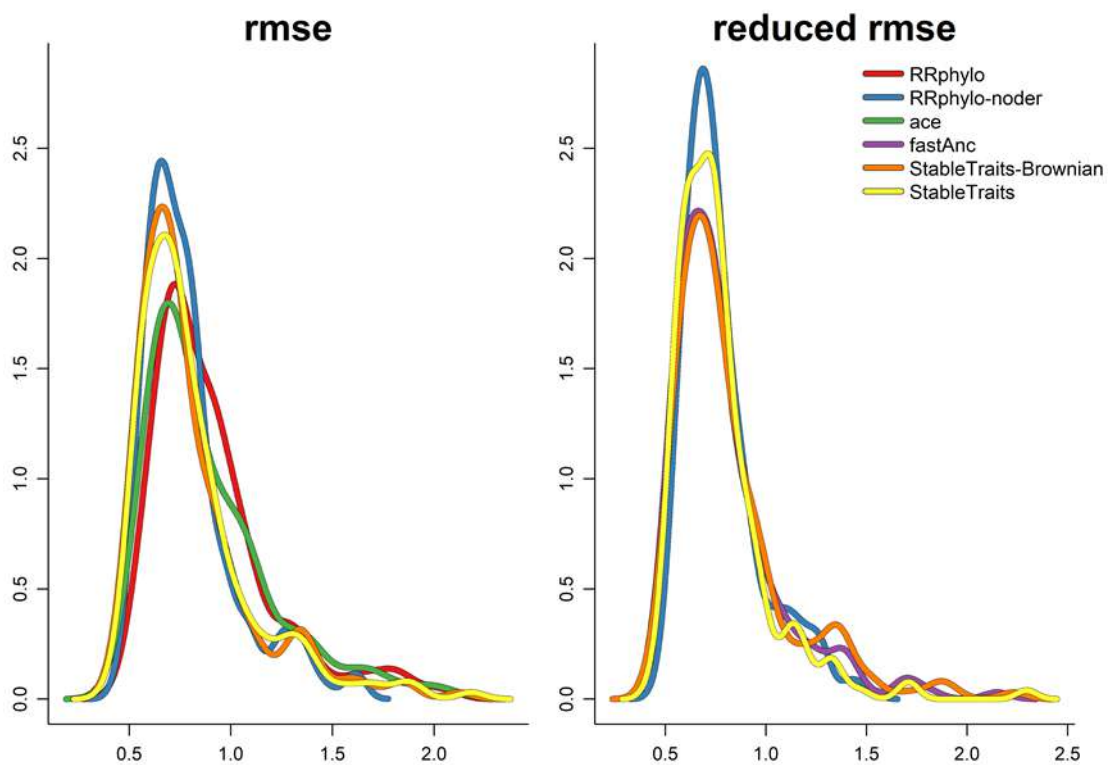


Figure S3. Density plot of root mean square error (*rmse*, left) and reduced root mean square error (right) for simulations where no clade-wise drift was applied.

The function *seach.trend* finds a significant phenotypic trend for the entire tree in 46.5% of the cases by specifying and 44.5% of the cases not specifying the *aces* (the basic expectation is 50% since half of the phenotypes were derived from BM and the other half

from BM with drift). The power of *search.trend* to find significant phenotypic drift at specified nodes which were designed to be so increases 121% when *aces* are specified.

		intercept	slope	r.squared	rmse	red.rmse
RRphylo	mean	-0.437	0.990	0.850	0.908	0.736
	2.5%	-3.512	0.779	0.598	0.549	0.531
	97.5%	0.428	1.281	0.968	1.805	1.177
RRphylo - noder	mean	-0.372	1.012	0.885	0.792	0.777
	2.5%	-1.693	0.894	0.680	0.518	0.537
	97.5%	0.239	1.149	0.974	1.362	1.269
ace	mean	-0.482	1.002	0.855	0.889	0.716
	2.5%	-3.587	0.825	0.618	0.528	0.514
	97.5%	0.571	1.254	0.971	1.732	1.185
fastAnc	mean	-0.349	1.008	0.891	0.773	0.796
	2.5%	-1.518	0.900	0.688	0.484	0.506
	97.5%	0.206	1.122	0.976	1.436	1.492
StableTraits - Brownian	mean	-0.458	1.018	0.880	0.808	0.818
	2.5%	-2.153	0.903	0.647	0.489	0.498
	97.5%	0.195	1.153	0.974	1.620	1.534
StableTraits	mean	-0.403	1.004	0.878	0.817	0.770
	2.5%	-1.959	0.880	0.658	0.503	0.512
	97.5%	0.250	1.143	0.972	1.680	1.333

Table S3. Summary of regression parameters (slope, intercept, and r^2), root mean square error (*rmse*) and *reduced rmse* as derived by each method, for simulations where no clade-wise drift was applied.

When specific clades are selected as to exhibit a phenotypic drift, *StableTraits-Brownian*, *RRphylo-noder* and *StableTraits* are all selected 9 times, and *RRphylo* once in terms of *rmse*. In terms of *reduced rmse* only *StableTraits* and *RRphylo-noder* are selected twice each.

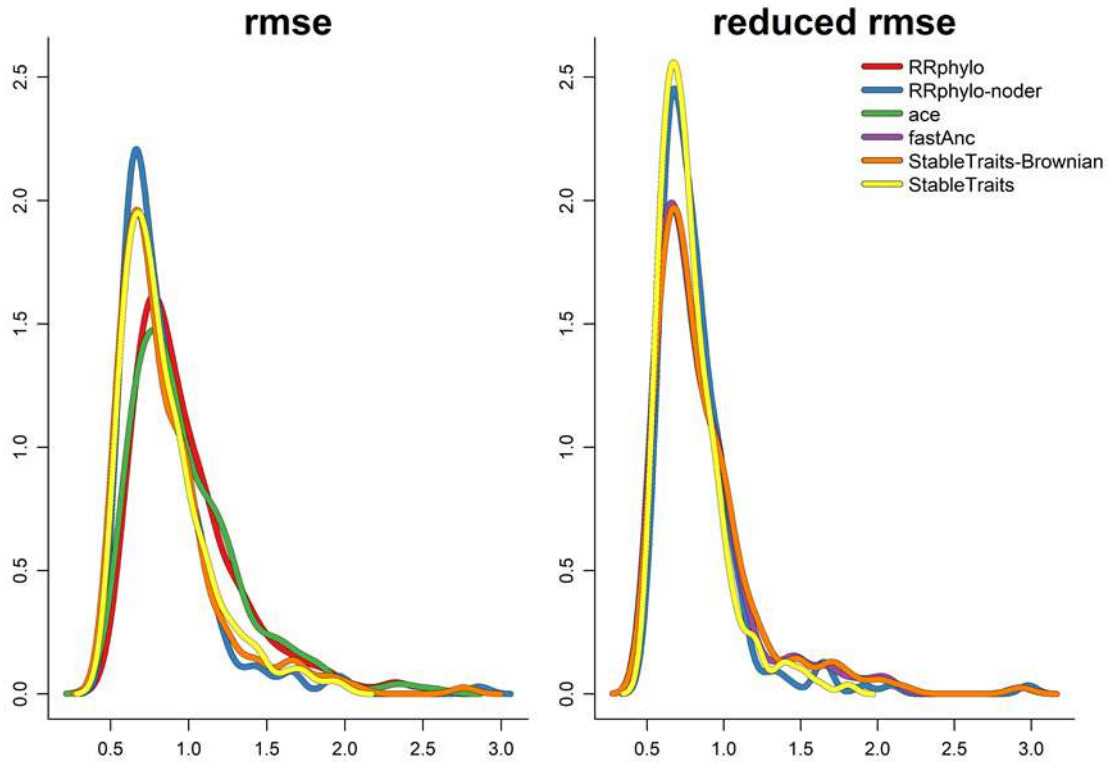


Figure S4. Density plot of root mean square error (*rmse*, left) and reduced root mean square error (right) for simulations where a clade-wise drift was applied.

The function *seach.trend* finds a significant phenotypic trend for the entire tree in 44.5% of the cases by specifying and 46% of the cases not specifying the *aces* (the basic expectation is 50% since half of the phenotypes were derived from BM and the other half from BM with drift). The power of *search.trend* to find significant phenotypic drift at specified nodes which were designed to be so increases 71.5% when *aces* are specified.

		intercept	slope	r.squared	rmse	red.rmse
RRphylo	mean	-0.265	0.955	0.845	0.988	0.764
	2.5%	-2.243	0.793	0.578	0.597	0.551
	97.5%	0.826	1.112	0.967	1.876	1.123
RRphylo - noder	mean	-0.346	1.000	0.889	0.838	0.823
	2.5%	-2.020	0.897	0.660	0.525	0.539
	97.5%	0.406	1.137	0.977	1.661	1.641
ace	mean	-0.358	0.968	0.846	0.984	0.759

	2.5%	-2.740	0.772	0.582	0.571	0.525
	97.5%	0.824	1.153	0.971	1.850	1.166
	mean	-0.296	0.994	0.890	0.829	0.854
fastAnc	2.5%	-1.412	0.905	0.675	0.511	0.524
	97.5%	0.314	1.095	0.978	1.740	1.837
	mean	-0.417	1.006	0.883	0.854	0.868
StableTraits	2.5%	-2.347	0.898	0.663	0.513	0.526
- Brownian	97.5%	0.286	1.158	0.978	1.730	1.809
	mean	-0.337	0.986	0.886	0.848	0.785
StableTraits	2.5%	-1.972	0.857	0.725	0.522	0.532
	97.5%	0.293	1.098	0.978	1.622	1.410

Table S4. Summary of regression parameters (slope, intercept, and r^2), root mean square error (*rmse*) and *reduced rmse* as derived by each method, for simulations where a clade-wise drift was applied.

Effect of shuffling known phenotypic values at nodes

To assess shuffling phenotypic values at nodes whose phenotype is known in advance, we selected from all simulations performed according to the shuffling procedure or without it. In terms of *rmse* *RRphylo-noder* and the two *StableTraits* model perform best (all three methods were selected 3 times). With *reduced rmse*, only *RRphylo-noder* and *StableTraits* were selected (twice each).

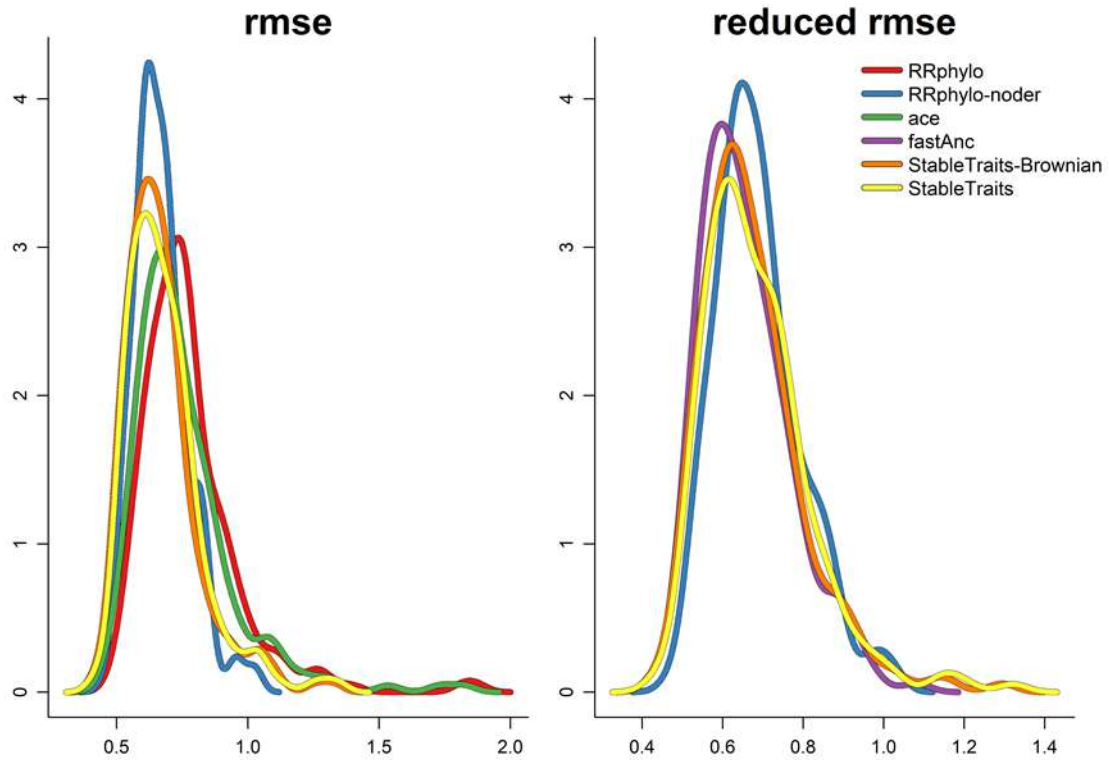


Figure S5. Density plot of root mean square error (*rmse*, left) and reduced root mean square error (right) for simulations where known phenotypic values at nodes are designed to evolve according to Brownian motion (not shuffled).

The function *seach.trend* finds a significant phenotypic trend for the entire tree in 46.5% of the cases by specifying and 42% of the cases not specifying the *aces* (the basic expectation is 50% since half of the phenotypes were derived from BM and the other half from BM with drift). The power of *search.trend* to find significant phenotypic drift at specified nodes which were designed to be so increases 100% when *aces* are specified.

		intercept	slope	r.squared	rmse	red.rmse
RRphylo	mean	-0.527	1.008	0.899	0.775	0.755
	2.5%	-3.501	0.867	0.722	0.543	0.533
	97.5%	0.321	1.279	0.970	1.261	1.140
RRphylo - noder	mean	-0.273	0.996	0.925	0.668	0.688
	2.5%	-1.456	0.897	0.831	0.509	0.529

	97.5%	0.322	1.120	0.977	0.941	0.950
	mean	-0.544	1.017	0.904	0.752	0.730
ace	2.5%	-3.587	0.873	0.691	0.522	0.515
	97.5%	0.455	1.254	0.976	1.227	1.168
	mean	-0.313	1.004	0.932	0.641	0.658
fastAnc	2.5%	-1.408	0.924	0.837	0.484	0.506
	97.5%	0.220	1.109	0.980	0.913	0.908
	mean	-0.439	1.016	0.925	0.671	0.674
StableTraits - Brownian	2.5%	-2.171	0.919	0.813	0.489	0.498
	97.5%	0.199	1.153	0.980	1.048	0.995
	mean	-0.405	1.008	0.922	0.681	0.685
StableTraits	2.5%	-1.980	0.903	0.811	0.500	0.507
	97.5%	0.228	1.148	0.979	1.050	1.012

Table S5. Summary of regression parameters (slope, intercept, and r^2), root mean square error (*rmse*) and *reduced rmse* as derived by each method, for simulations where known phenotypic values at nodes are designed to evolve according to Brownian motion (not shuffled).

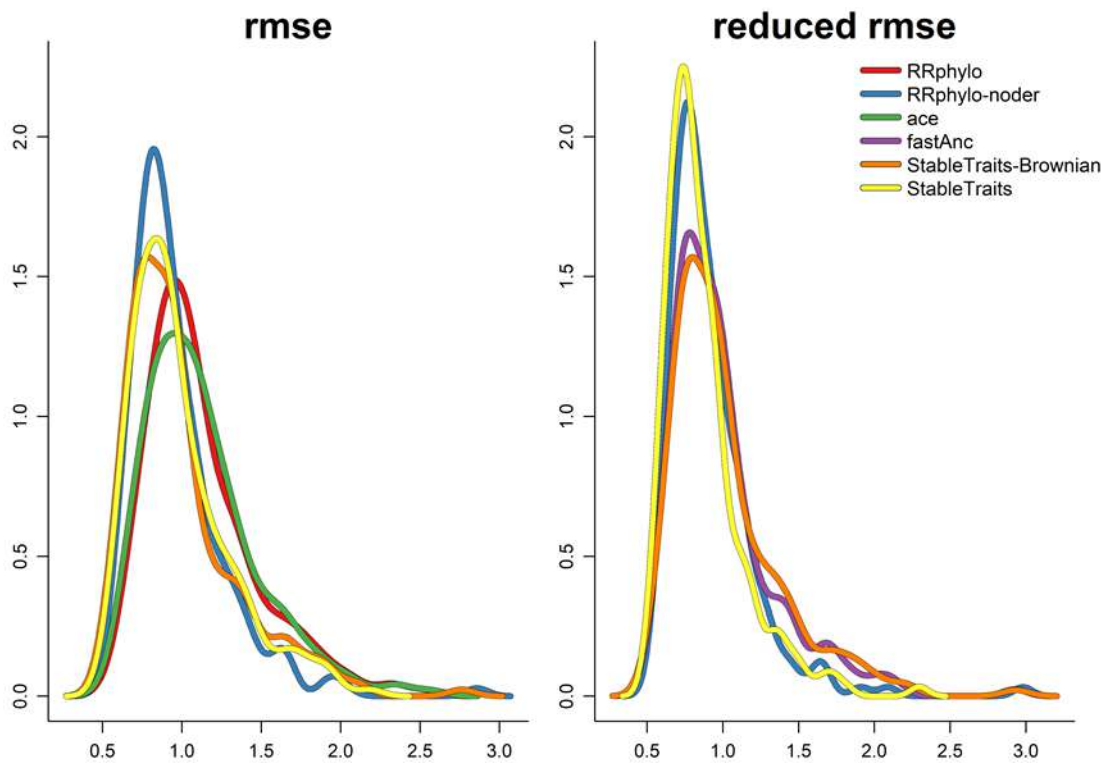


Figure S6. Density plot of root mean square error (*rmse*, left) and reduced root mean square error (right) for simulations where known phenotypic values at nodes do not evolve according to Brownian motion (shuffled).

		intercept	slope	r.squared	rmse	red.rmse
RRphylo	mean	-0.176	0.937	0.797	1.121	0.744
	2.5%	-1.578	0.742	0.557	0.687	0.566
	97.5%	0.819	1.089	0.932	1.983	1.159
RRphylo - noder	mean	-0.445	1.016	0.849	0.962	0.912
	2.5%	-2.020	0.896	0.650	0.607	0.598
	97.5%	0.336	1.175	0.951	1.661	1.641
ace	mean	-0.296	0.952	0.796	1.121	0.744
	2.5%	-1.958	0.762	0.566	0.647	0.526
	97.5%	0.863	1.097	0.939	1.973	1.182
fastAnc	mean	-0.333	0.999	0.849	0.960	0.993
	2.5%	-1.522	0.875	0.618	0.563	0.579
	97.5%	0.304	1.118	0.954	1.774	1.875
StableTraits - Brownian	mean	-0.436	1.008	0.839	0.991	1.012
	2.5%	-2.264	0.860	0.595	0.564	0.579
	97.5%	0.275	1.158	0.954	1.877	1.918
StableTraits	mean	-0.335	0.981	0.842	0.983	0.870
	2.5%	-1.958	0.847	0.652	0.584	0.561
	97.5%	0.316	1.135	0.955	1.823	1.522

Table S6. Summary of regression parameters (slope, intercept, and r^2), root mean square error (*rmse*) and *reduced rmse* as derived by each method, for simulations where known phenotypic values at nodes do not evolve according to Brownian motion (shuffled).

Effect of sampling intensity and bias

To assess the importance of sampling effects, we took those subsets of the simulations designed as starting with sampling either 90% or 50% of the species originally in the tree.

With mild sampling effects (i.e. removing 10% of the species from the tree)

StableTraits-Brownian (6), *RRphylo-noder* (6) and *StableTraits* (6) perform best in terms of

rmse. Ape's *ace* (2) and *RRphylo* (1) were also selected. With *reduced rmse* *StableTraits-Brownian* (2), *RRphylo-noder* (1), *StableTraits* (1) and *fastAnc* (1).

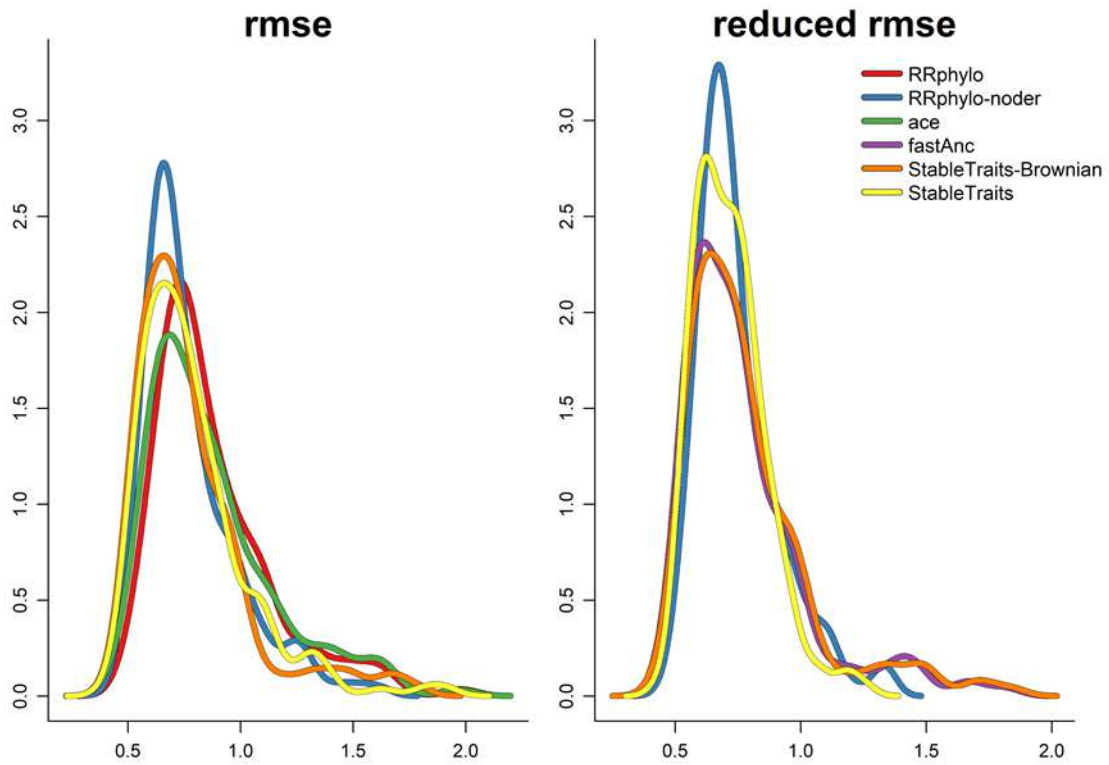


Figure S7. Density plot of root mean square error (*rmse*, left) and reduced root mean square error (right) for simulations designed as starting with sampling 90% of the species originally in the tree.

The function *seach.trend* finds a significant phenotypic trend for the entire tree in 44.4% of the cases by specifying and 43.1% of the cases not specifying the *aces* (the basic expectation is 50% since half of the phenotypes were derived from BM and the other half from BM with drift). The power of *search.trend* to find significant phenotypic drift at specified nodes which were designed to be so increases 82.9% when *aces* are specified.

		intercept	slope	r.squared	rmse	red.rmse
RRphylo	mean	-0.179	0.969	0.879	0.875	0.697

	2.5%	-1.173	0.871	0.705	0.543	0.545
	97.5%	0.438	1.062	0.969	1.598	0.920
RRphylo - noder	mean	-0.270	1.002	0.905	0.773	0.749
	2.5%	-1.095	0.922	0.796	0.517	0.529
	97.5%	0.239	1.094	0.977	1.292	1.140
	mean	-0.199	0.978	0.881	0.867	0.689
ace	2.5%	-1.187	0.854	0.709	0.528	0.520
	97.5%	0.724	1.078	0.976	1.622	0.998
	mean	-0.271	1.002	0.911	0.754	0.772
fastAnc	2.5%	-1.021	0.934	0.802	0.499	0.516
	97.5%	0.157	1.070	0.979	1.413	1.457
	mean	-0.333	1.009	0.905	0.775	0.784
StableTraits - Brownian	2.5%	-1.195	0.937	0.787	0.505	0.518
	97.5%	0.182	1.080	0.979	1.528	1.489
	mean	-0.256	0.990	0.902	0.785	0.717
StableTraits	2.5%	-1.017	0.900	0.769	0.506	0.515
	97.5%	0.285	1.070	0.979	1.349	1.063

Table S7. Summary of regression parameters (slope, intercept, and r^2), root mean square error (*rmse*) and *reduced rmse* as derived by each method, for simulations designed as starting with sampling 90% of the species originally in the tree.

With more important sampling effects (i.e. removing 50% of the tips from the tree), these figures remain almost the same, with *StableTraits-Brownian* (6), slightly preferred over *RRphylo-noder* (5) and *StableTraits* (5). No significant difference among methods was found as per *reduced rmse*.

The function *seach.trend* finds a significant phenotypic trend for the entire tree in 46.2% of the cases by specifying and 46.9% of the cases not specifying the *aces*. The power of *search.trend* to find significant phenotypic drift at specified nodes which were designed to be so increases 81.4% when *aces* are specified.

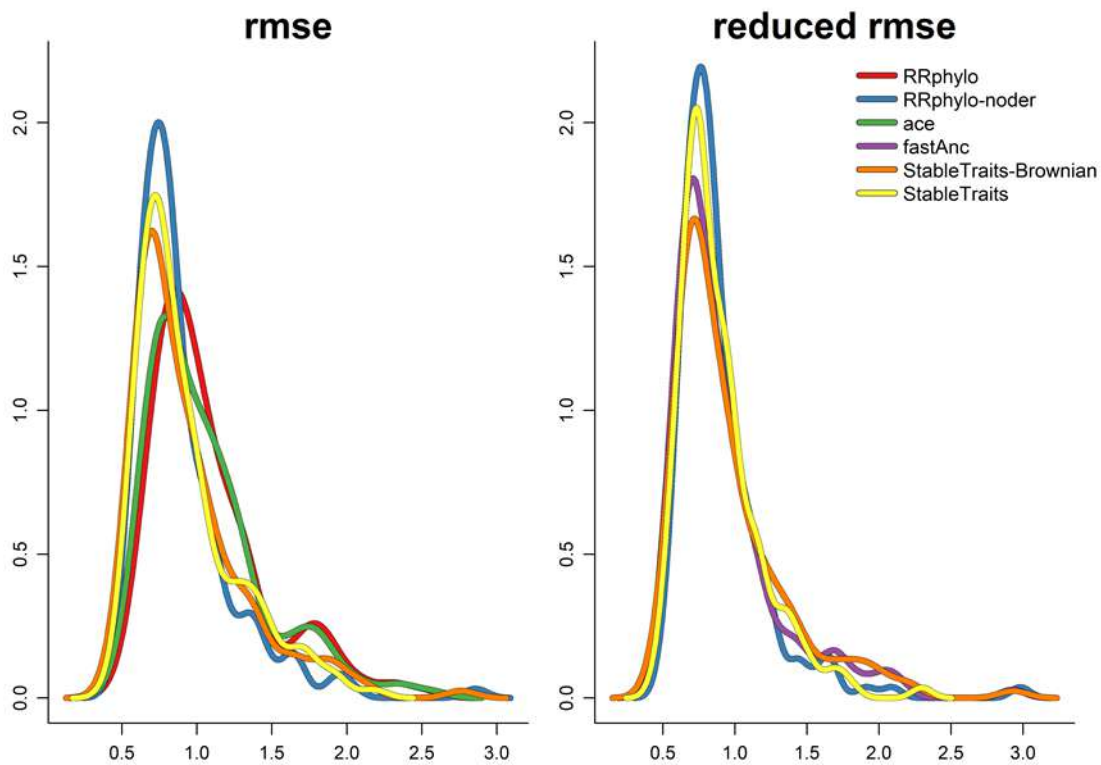


Figure S8. Density plot of root mean square error (*rmse*, left) and reduced root mean square error (right) for simulations designed as starting with sampling 50% of the species originally in the tree.

		intercept	slope	r.squared	rmse	red.rmse
RRphylo	mean	-0.599	0.975	0.794	1.076	0.840
	2.5%	-3.792	0.734	0.555	0.625	0.553
	97.5%	0.804	1.306	0.960	2.076	1.260
RRphylo - noder	mean	-0.502	1.013	0.853	0.899	0.894
	2.5%	-2.475	0.879	0.638	0.541	0.549
	97.5%	0.406	1.175	0.967	1.679	1.663
ace	mean	-0.744	0.995	0.799	1.057	0.818

	2.5%	-3.833	0.762	0.558	0.587	0.531
	97.5%	0.684	1.269	0.960	2.070	1.239
	mean	-0.400	0.999	0.855	0.888	0.923
fastAnc	2.5%	-1.940	0.863	0.568	0.497	0.525
	97.5%	0.314	1.139	0.966	1.901	2.009
	mean	-0.601	1.018	0.840	0.936	0.952
StableTraits - Brownian	2.5%	-3.149	0.846	0.571	0.524	0.531
	97.5%	0.286	1.213	0.967	1.904	2.009
	mean	-0.541	1.001	0.845	0.927	0.891
StableTraits	2.5%	-3.140	0.845	0.630	0.546	0.546
	97.5%	0.316	1.207	0.964	1.750	1.629

Table S8. Summary of regression parameters (slope, intercept, and r^2), root mean square error (*rmse*) and *reduced rmse* as derived by each method, for simulations designed as starting with sampling 50% of the species originally in the tree.

When species are removed randomly, *StableTraits-Brownian* and *StableTraits* (6) perform slightly better than *RRphylo-noder* (5) in terms of *rmse*. Only the two latter were selected (once), in terms of *reduced rmse*. When sampling probability is inversely proportional to the phenotypic value, *StableTraits-Brownian* and *RRphylo-noder* (6) perform equally well and slightly better than *StableTraits* (5).

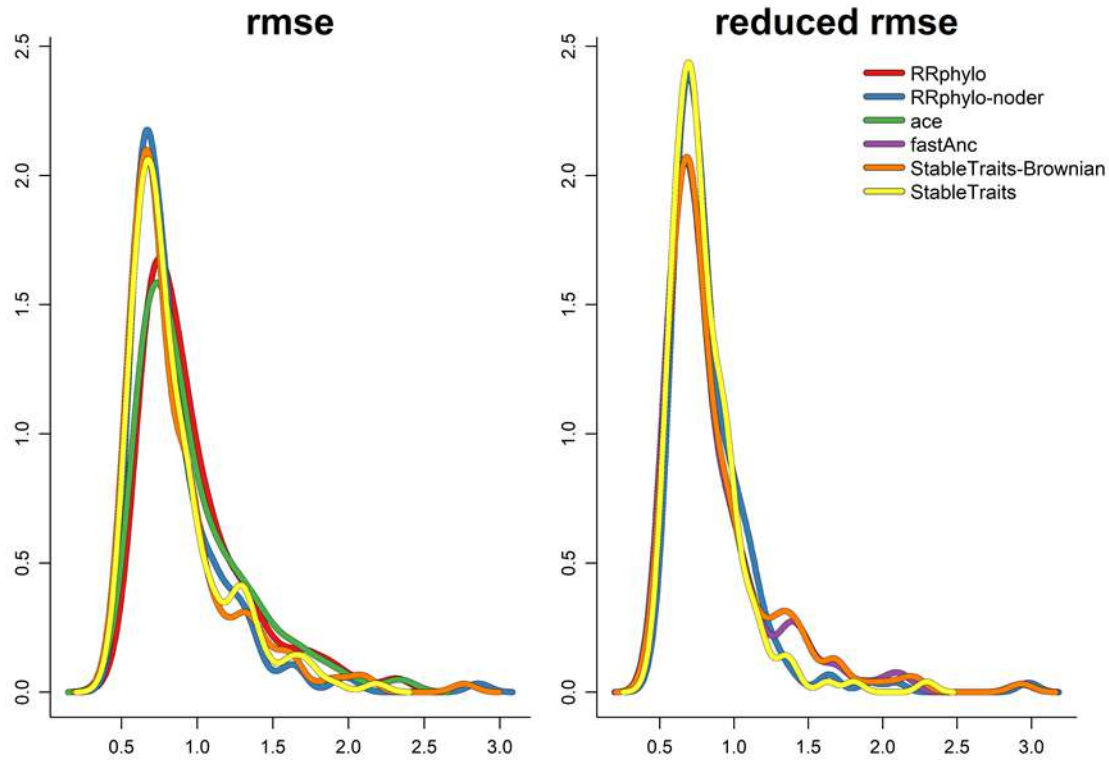


Figure S9. Density plot of root mean square error (*rmse*, left) and reduced root mean square error (right) for simulations designed to remove a random sample of species from the original tree.

The function *seach.trend* finds a significant phenotypic trend for the entire tree in 41.9% of the cases by specifying and 43.1% of the cases not specifying the *aces* (the basic expectation is 50% since half of the phenotypes were derived from BM and the other half from BM with drift). The power of *search.trend* to find significant phenotypic drift at specified nodes which were designed to be so increases 73.5% when *aces* are specified.

		intercept	slope	r.squared	rmse	red.rmse
RRphylo	mean	-0.186	0.945	0.837	0.969	0.741
	2.5%	-1.426	0.734	0.555	0.584	0.545
	97.5%	0.466	1.066	0.963	1.721	1.008
RRphylo - noder	mean	-0.274	0.993	0.876	0.850	0.835
	2.5%	-1.301	0.881	0.660	0.518	0.537
	97.5%	0.241	1.078	0.967	1.363	1.269
ace	mean	-0.270	0.959	0.839	0.961	0.730

	2.5%	-1.650	0.762	0.558	0.570	0.515
	97.5%	0.558	1.088	0.961	1.706	0.970
	mean	-0.245	0.990	0.880	0.831	0.861
fastAnc	2.5%	-1.021	0.863	0.651	0.485	0.517
	97.5%	0.273	1.053	0.970	1.520	1.581
	mean	-0.342	0.998	0.872	0.859	0.876
StableTraits - Brownian	2.5%	-1.303	0.860	0.641	0.503	0.515
	97.5%	0.245	1.086	0.970	1.596	1.645
	mean	-0.259	0.980	0.874	0.852	0.796
StableTraits	2.5%	-1.172	0.847	0.662	0.506	0.520
	97.5%	0.250	1.055	0.969	1.466	1.183

Table S9. Summary of regression parameters (slope, intercept, and r^2), root mean square error (*rmse*) and *reduced rmse* as derived by each method, for simulations designed to remove a random sample of species from the original tree.

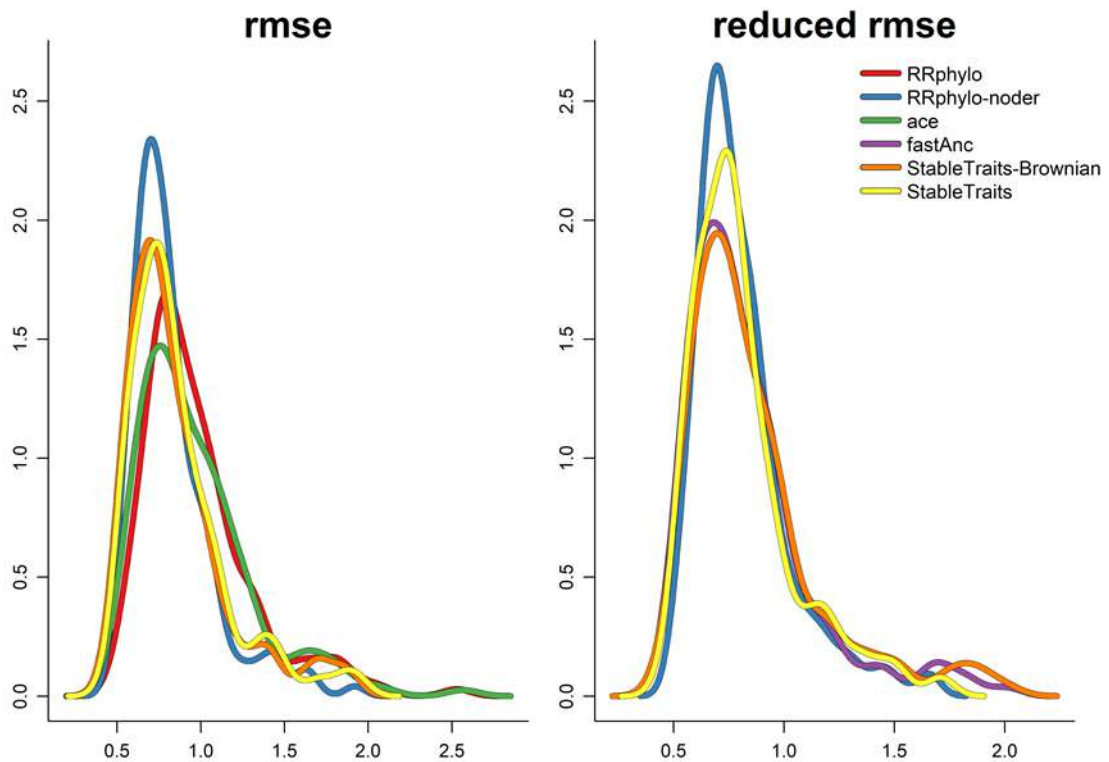


Figure S10. Density plot of root mean square error (*rmse*, left) and reduced root mean square error (right) for simulations designed to have sampling probability inversely proportional to the phenotypic value.

The function *seach.trend* finds a significant phenotypic trend for the entire tree in 48.7% of the cases by specifying and 46.9% of the cases not specifying the *aces* (the basic expectation is 50% since half of the phenotypes were derived from BM and the other half from BM with drift). The power of *search.trend* to find significant phenotypic drift at specified nodes which were designed to be so increases 91.1% when *aces* are specified.

		intercept	slope	r.squared	rmse	red.rmse
RRphylo	mean	-0.592	0.999	0.836	0.981	0.795
	2.5%	-3.792	0.812	0.599	0.577	0.547
	97.5%	0.593	1.306	0.960	1.820	1.260
RRphylo - noder	mean	-0.498	1.022	0.883	0.821	0.808
	2.5%	-2.475	0.908	0.681	0.520	0.538
	97.5%	0.323	1.186	0.970	1.476	1.437
ace	mean	-0.673	1.014	0.841	0.964	0.777
	2.5%	-3.833	0.815	0.614	0.548	0.525
	97.5%	0.597	1.269	0.963	1.824	1.247
fastAnc	mean	-0.426	1.012	0.885	0.811	0.834
	2.5%	-1.884	0.918	0.679	0.499	0.525
	97.5%	0.219	1.139	0.972	1.628	1.700
StableTraits - Brownian	mean	-0.592	1.028	0.874	0.852	0.860
	2.5%	-3.149	0.921	0.662	0.513	0.527
	97.5%	0.199	1.213	0.968	1.728	1.808
StableTraits	mean	-0.538	1.011	0.873	0.860	0.812
	2.5%	-3.140	0.885	0.653	0.525	0.524
	97.5%	0.293	1.207	0.965	1.719	1.469

Table S10. Summary of regression parameters (slope, intercept, and r^2), root mean square error (*rmse*) and *reduced rmse* as derived by each method, for simulations to have sampling probability inversely proportional to the phenotypic value.

StableTraits - Brownian				
mean values	intercept		slope	
	random	bias	random	bias
100%	-0.321	-0.321	1.007	1.007
90%	-0.315	-0.350	1.007	1.010
50%	-0.369	-0.833	0.990	1.046
p-values	100%		90%	50%
intercept	100%	-	0.957	<0.01
	90%	0.996	-	<0.01
	50%	0.785	0.736	-
slope	100%	-	0.949	<0.01
	90%	1.000	-	0.001
	50%	0.096	0.100	-
error	100%	-	0.623	0.984
	90%	0.999	-	0.520
	50%	0.668	0.670	-

StableTraits				
mean values	intercept		slope	
	random	bias	random	bias
100%	-0.256	-0.256	0.993	0.993
90%	-0.235	-0.277	0.989	0.991
50%	-0.283	-0.800	0.971	1.031
p-values	100%		90%	50%
intercept	100%	-	0.979	<0.01
	90%	0.940	-	<0.01
	50%	0.905	0.727	-
slope	100%	-	0.979	<0.01
	90%	0.867	-	<0.01
	50%	0.024	0.087	-
error	100%	-	0.616	0.983
	90%	0.999	-	0.511
	50%	0.701	0.698	-

RRphylo - noder				
mean values	intercept		slope	
	random	bias	random	bias
100%	-0.250	-0.250	1.000	1.000
90%	-0.286	-0.255	1.002	1.002
50%	-0.263	-0.741	0.984	1.042
p-values	100%		90%	50%
intercept	100%	-	0.999	<0.01
	90%	0.840	-	<0.01

slope	50%	0.979	0.929	-
	100%	-	0.988	<0.01
	90%	0.955	-	<0.01
	50%	0.121	0.062	-
	100%	-	0.611	0.988
	90%	0.616	-	0.524
error	50%	0.983	0.511	-
	ace			
	intercept		slope	
mean values	random	bias	random	bias
100%	-0.214	-0.214	0.978	0.978
90%	-0.178	-0.220	0.974	0.982
50%	-0.363	-1.125	0.944	1.045
p-values		100%	90%	50%
intercept	100%	-	0.999	<0.01
	90%	0.918	-	<0.01
	50%	0.224	0.101	-
slope	100%	-	0.961	<0.01
	90%	0.922	-	<0.01
	50%	0.015	0.046	-
error	100%	-	0.994	0.712
	90%	0.998	-	0.769
	50%	0.688	0.716	-
fastAnc				
mean values	intercept		slope	
	random	bias	random	bias
100%	-0.271	-0.271	1.003	1.003
90%	-0.255	-0.288	1.001	1.004
50%	-0.236	-0.564	0.979	1.020
p-values		100%	90%	50%
intercept	100%	-	0.971	<0.01
	90%	0.955	-	0.001
	50%	0.810	0.942	-
slope	100%	-	0.987	0.061
	90%	0.967	-	0.088
	50%	0.003	0.008	-
error	100%	-	0.624	0.981
	90%	0.999	-	0.512
	50%	0.687	0.691	-
RRphylo				

mean values	intercept		slope	
	random	bias	random	bias
100%	-0.201	-0.201	0.974	0.974
90%	-0.174	-0.183	0.968	0.970
50%	-0.197	-1.001	0.922	1.029
p-values	100%		90%	50%
intercept	100%	-	0.991	<0.01
	90%	0.935	-	<0.01
	50%	0.998	0.953	-
slope	100%	-	0.965	<0.01
	90%	0.902	-	<0.01
	50%	<0.01	<0.01	-
error	100%	-	0.616	0.995
	90%	0.994	-	0.560
	50%	0.712	0.769	-

Table S11. Effect of sampling on prediction performance of each method for ancestral states estimation. For each sampling level (100, 90 or 50% of the original tree), the results represent mean values and p-values of the post hoc Tukey, either for biased (upper triangle) and random (lower triangle) sampling designs.

<i>rmse</i>				
pair	slope		emm	
	contrast	p.value	contrast	p.value
ace-RRphylo	0.001	0.909	-0.008	0.946
ace-RRphylo-noder	0.005	<0.001	0.143	<0.001
ace-StableTraits-Brownian	0.001	0.603	0.117	<0.001
ace-StableTraits	0.003	0.024	0.125	<0.001
RRphylo-RRphylo-noder	0.004	0.000	0.152	<0.001
RRphylo-StableTraits-Brownian	0.001	0.979	0.126	<0.001
RRphylo-StableTraits	0.002	0.201	0.133	<0.001
RRphylo-noder-StableTraits-Brownian	-0.004	0.002	-0.026	0.144
RRphylo-noder-StableTraits	-0.002	0.166	-0.019	0.462
StableTraits-Brownian-StableTraits	0.002	0.511	0.007	0.965
<i>reduced rmse</i>				
pair	slope		emm	
	contrast	p.value	contrast	p.value
fastAnc-RRphylo-noder	0.003	0.070	-0.008	0.912

fastAnc-StableTraits-Brownian	-0.002	0.357	-0.034	0.025
fastAnc-StableTraits	-0.001	0.899	-0.027	0.120
RRphylo-noder-StableTraits-Brownian	-0.004	0.000	-0.026	0.130
RRphylo-noder-StableTraits	-0.003	0.010	-0.019	0.399
StableTraits-Brownian-StableTraits	0.001	0.778	0.007	0.925

Table S12. Differences between methods across all types of phenotypes. ‘slope’

represents the increase in *rmse* or *reduced rmse* either as the phenotype deviates from Brownian motion. ‘emm’ represents the estimated marginal mean *rmse* or *reduced rmse* either per method.

Real Case # 2: Caniforms body size evolution

Materials and methods

The second real case regards the evolution of body size in caniform carnivores. This is a paradigmatic case for ancestral state estimation studies. Finarelli and Flynn (2006) calculated a body size estimate at the root of the caniform tree of 25 kg. This figure reduced to some 5 Kg by including fossil taxa body size estimate as known values at nodes. Slater et al., (2012) developed a Bayesian approach to estimate ancestral states while providing node priors. They feed their method with a 135 species canid phylogeny and 11 different node priors, corresponding to the most recent common ancestors of several tribes and families within the Caniformia suborder. Slater et al., (2012) obtained an interval spanning from 0.89 to 4.5 Kg as the 95% highest posterior density phenotype at the root. We used the same data, tree and node priors under *RRphylo-noder* to compare our results to theirs. We repeated the ancestral state estimation by using *fastAnc* and then *StableTraitsR* with the same set of eleven node priors. Eventually, we further retrieved the 95% highest posterior density interval calculated by using the function *fitContinuousMCMC* in *geiger* (Harmon et al., 2007). As both Finarelli and Flynn (2006) and Slater et al. (2012) found evidence for increasing body

size in caniforms over time (i.e. Cope's rule), we also regressed the *noder* and *fastAnc* and *StableTraits* estimates against their distance from the root. A positive and significant relationship should apply in support of Cope's rule.

Results and discussion

Under the *RRphylo-noder* method, estimates at the specified nodes are very close to the node priors for canids (Supplementary Table S14). Slater et al. (2012) found evidence for a significant increase in body size in caniforms over time (Cope's rule), in keeping with the trend (i.e. phenotypic drift) mode of evolution. By regressing the ancestral states fitted under *RRphylo-noder* against their distance from the root a marginally significant and positive trend in the phenotype applies (slope = 0.028, $p = 0.06$), in keeping with the presence of Cope's rule. Almost the same applies by fitting *fastAnc* and *StableTraits* (slope_{fastAnc} = 0.029, p_{fastAnc} = 0.158; slope_{StableTraits} = 0.030, $p_{\text{StableTraits}}$ = 0.157), although the slope is not significantly different from zero. Eventually, by using *fitContinuousMCMC* taking the mean value calculated over the 95% of the highest posterior density distribution to represent the ancestral states, the pattern of phenotypic drift is not significant (slope = 0.022, $p = 0.298$).

Finarelli and Flynn (2006) obtained a 25 kg body size estimate at the root of the caniforms phylogeny which they deem questionable. Yet, they obtained a much more plausible ca. 5 Kg estimate when fossils were considered in their phylogeny. Slater and colleagues (2012) found a similar estimate by applying *fitContinuousMCMC* (a Bayesian approach) to the same tree and data. They further found substantial but non-definitive evidence for a body size trend (i.e. Cope's rule) for this clade. With *RRphylo-noder* the phenotypic estimate at the tree root (2.11 Kg) is indistinguishable from the prior (Table S14). By regressing *RRphylo-noder* ancestral estimates against their age in canids we found supportive evidence in favor of Cope's rule in caniforms (at $p = 0.06$, see Fig. S12). Although

this result is not a robust indication of Cope's rule per se, it is interesting that the pattern appears even at the level of ancestors with *RRphylo-noder*.

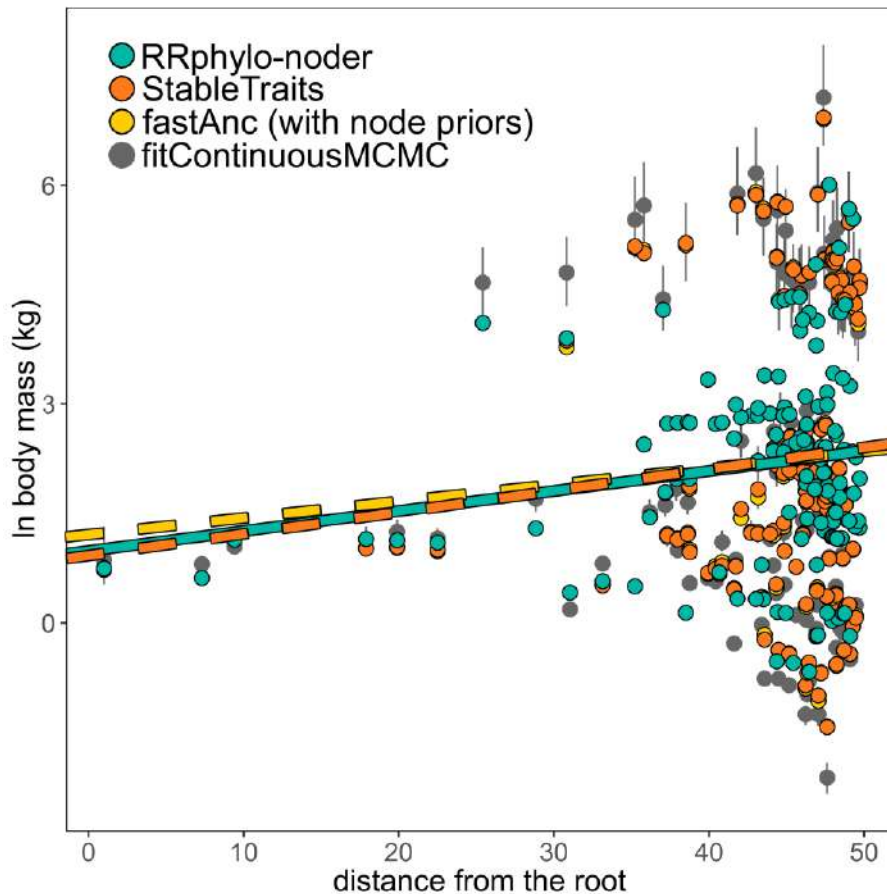


Figure S11. Ancestral body mass estimates caniform carnivores plotted against time. Gray dots and lines represent the mean ancestral estimates and the 95% interval of the highest posterior density distribution derived by *fitContinuousMCMC*. Green dots represent the ancestral states as estimated by *RRphylo - noder*. Orange dots represent ancestral estimates as produced by *StableTraits* (with node priors). Yellow dots

represent ancestral estimates as produced by *fastAnc* (*fanc*, with node priors). The regression of ancestral phenotypes through time for *RRphylo - noder*, *StableTraits*, and *fastAnc* and are drawn (green, orange and yellow lines, respectively).

	Node priors	<i>RRphylo</i> <i>-noder</i>	<i>fastAnc</i> (with node priors)	<i>StableTraits</i>	<i>StableTraits</i> <i>-Brownian</i>
root	0.749	0.746	0.749	0.731	0.742
Caninae	1.451	1.451	1.451	1.452	1.451
Vulpini	1.974	1.974	1.974	1.974	1.974
Vulpes	1.831	1.832	1.831	1.831	1.830
Canini	2.225	2.225	2.225	2.225	2.225
Arctoidea	0.615	0.615	0.615	0.615	0.615
Ursinae/Tremarctinae	4.293	4.293	4.293	4.293	4.293
Ursinae	4.406	4.406	4.406	4.406	4.406
crown Mustelidae	1.296	1.296	1.296	1.296	1.296
crown Procyonidae	0.417	0.417	0.417	0.417	0.417
Pinnipedimorpha+Musteloidea	1.14	1.14	1.14	1.140	1.140
crown Pinnipedia	4.111	4.111	4.111	4.111	4.111

Table S13. Ancestral state estimates according to *RRphylo-noder*, phytools' function *fastAnc*, and *StableTraits* for the corresponding values at nodes (Node priors) for the Caniform tree and data.

References

- Finarelli, J.A. & Flynn, J.J. (2006). Ancestral state reconstruction of body size in the Caniformia (Carnivora, mammalia): The effects of incorporating data from the fossil record. *Systematic Biology*, 55, 301–313. doi:10.1080/10635150500541698
- Harmon, L.J., Weir, J.T., Brock, C.D., Glor, R.E., & Challenger, W. (2007). GEIGER: investigating evolutionary radiations. *Bioinformatics*, 24, 129-131.
- Slater, G.J., Harmon, L.J., & Alfaro, M.E. (2012). Integrating fossils with molecular phylogenies improves inference of trait evolution. *Evolution*, 66, 3931–3944. doi:10.1111/j.1558-5646.2012.01723.x